DAMAGE IDENTIFICATION FROM WAVELET-BASED ACCELERATION RESPONSE SENSITIVITY

Xue Yan, LI

B. Sc., M. Sc.

A Thesis Submitted in Partial Fulfillment for the Degree of

Doctor of Philosophy

Department of Civil and Structural Engineering

The Hong Kong Polytechnic University

February, 2008

To my parents and my husband

CERTIFICATION OF ORIGINALITY

I hereby declare that this thesis is my own work and that, to the best of my knowledge and belief, it reproduces no material previously published or written, nor material that has been accepted for the award of any other degree or diploma, except where due acknowledgement has been made in the text.

_____ (Signed)

Li Xueyan (Name of student)

ABSTRACT

Early detection of damage in engineering systems during their service life has been receiving increasing attention from engineers recently because of its importance. Though vibration-based damage detection has been developed for several decades and there is a large number of literature, there are still many problems refraining it from application. The research in this thesis is on the developments of structural damage detection methods based on acceleration response sensitivity via wavelet transform. The wavelet packet component energy (WPCE) and wavelet coefficients (WC) of acceleration responses, unit impulse response function (UIR) and covariance of acceleration responses from ambient vibration are all used in the damage detection via model updating techniques. Tikhonov regularization and L-curve method are also improved for the proposed damage detection methods to solve the ill-conditioning problem. The propagation of uncertainties in the damage detection procedure is also studied with a sensitivity analysis with respect to random variables and a reliability result is finally obtained for the structure.

To avoid modal extraction via the Fourier Transform which will cause structural information lost, introducing errors in the identified results, in this study, wavelet packet component energy and wavelet coefficients of acceleration responses are adopted to detect damage via sensitivity analysis and model updating techniques. The sensitivity of WPCE with respect to structural parameters has been derived analytical and the distribution and properties of the WPCE are studied. They are adopted for damage detection in a simply supported concrete beam for numerical demonstration and in a steel

beam tested in the laboratory for experimental verification. The WPCE assigns the energy of the acceleration responses to different frequency bandwidth with good tolerance to noise but the associated damage detection algorithm requires more measurement locations especially in a structure with a large number of DOFs. The sensitivity of WC of acceleration response from as few as one sensor with respect to structural parameters under general excitation and support excitation are obtained analytically and computationally, and it is used for damage detection in a one-story plane frame structure and a three-dimensional frame structure for simulation study, and in a simply supported reinforced concrete beam and a three-dimensional frame structure tested in the laboratory. It is noted that time series data with a low sampling frequency also carries damage information for damage identification.

Because most damage detection methods based on the acceleration responses rely on the type and the location of the force excitation, wavelet coefficient of unit impulse response function obtained via discrete wavelet transform (DWT) of the measured accelerations of a structure and the measured excitation force or measured accelerations at its support are used to assess the structural health condition. DWT is employed in the extraction procedure for UIR to avoid the end effects with Fourier transform. The sensitivity of wavelet coefficient of UIR is given numerically. In order to study the noise effect in the UIR-based method, a statistical analysis on the UIRs with measurement noise is conducted and the results compared favorably with those from Monte Carlo Technique (MCT). The proposed methods are demonstrated successfully by a 31-bar plane truss and a nine-bay three-dimensional frame structural system in a simulation study and an experimental verification.

In order to have the identification method completely independent of the external excitation, the covariance of acceleration responses of structures under ambient excitation is numerically computed and its wavelet packet energy is used to identify structural damage such that the damage detection can be performed with the response-only measurement. Covariance of acceleration responses is computed based on the unit impulse response function. Wavelet packet transform is applied to the covariance functions to find the wavelet packet energy. Damage localization is carried out firstly using the elemental modal strain energy approach. A five-bay three-dimensional cantilever truss structure is used to demonstrate the efficiency of the method, and a nine-bay three-dimensional frame structure is tested in the laboratory for verification of the proposed method.

The ill-conditioning phenomenon in the inverse problem is an important factor limiting the application of damage detection methods. Tikhonov regularization and L-curve method are improved in this thesis for a better solution of the ill-conditioned problem in the proposed damage detection methods. The range of percentage damage is limited in the determination of the regularization parameter λ in the regularization method. Because there will be great similarity between the sets of results from two successive iterations, the convergence of results is further ensured by checking on such similarity using a Multiple Parameter Correlation Criteria. Numerical studies with one-story plane frame and thirty-one bar plane truss structure are performed with the proposed improved regularization techniques and satisfactory results are obtained.

Uncertainties in the analytical model and the measured vibration data always exist and they affect the identified results. A statistical method for structural damage detection

based on measured acceleration response is proposed in this thesis. Uncertainties in the system parameters, such as the structural parameters of the finite element model, the excitation force acting on the structure and the measured acceleration response from the perturbed state of the structure are analyzed and the analytical formula are given. The effect of each of these uncertainties on the assessment results is monitored in an updating damage detection algorithm based on the response sensitivity approach. The probability density function of the stiffness parameters in both the intact and perturbed states are compared in a subsequent reliability assessment. A three-dimensional five-bay steel frame structure is studied for illustration.

In summary, the contributions of the thesis to the engineering application include: (a) As few as one accelerometer is required in the vibration measurement and it makes the damage detection be more economical, convenient and practical especially for large scale structure. (b) The study of damage detection based on response-only measurement is very useful for the case where the actual excitations may be very difficult and expensive to be measured and be generated. (c) The identified results obtained from uncertainty analysis have the higher reliability when the measurements are subject to noise and the models used have model errors.

LIST OF PUBLICATIONS

***JOURNAL PAPERS*:**

Law, S.S. and Li, X.Y. (2007), "Wavelet-based sensitivity analysis of the Impulsive Response Function for Damage Detection", *Journal of Applied Mechanics*, ASME. **74**(2), 375-377.

Li, X.Y., and Law, S.S. (2008), "Damage Identification of Structures Including System Uncertainties and Measurement Noise", *AIAA Journal*, 46(1), 263-276.

Li, X.Y. and Law, S.S. (2007), "Inverse problem with noise and model errors for damage detection", *Journal of Engineering Mechanics*, ASCE. (under review).

Li, X.Y. and Law, S.S. (2007), "Condition assessment of structures under ambient excitation", *AIAA Journal* (under review).

Li, X.Y. and Law, S.S. (2007), "Structural damage detection with statistical analysis from support excitation", *Journal of Engineering Mechanics* (under review).

***CONFERENCE PAPERS*:**

Li, X.Y. and Law, S.S. (2006), "Condition assessment of bridges under earthquake loading", *International Conference on Bridge Engineering*, Hong Kong, 1-3, November, (full paper in CD-ROM).

Li, X.Y. and Law, S.S. (2007), "On-line Condition Assessment of Bridges under Ambient Excitations", *IMAC*, Orlando, Florida, USA, 19-22, February, 2007, (full paper in CD-ROM).

Law, S.S. and Li, X.Y. (2004), “Wavelet Packet sensitivity for structural damage detection”, *International Conference on Computational Methods,* ICCM 2004, 15-17 December, National University of Singapore.

Law, S.S. and Li, X.Y. (2007), “Damage quantification of structure under operational conditions”, *12th Asia Pacific Vibration Conference, Sapporo, Japan, 6th-9th August.*

ACKNOWLEDGEMENTS

First of all, I am deeply indebted to my chief supervisor, Dr S.S. Law, for his patient, persistent and beneficial guidance during my whole Ph.D. study period. His open, critical and creative thinking as well as high efficiency all left me deep impressions. I also benefited a lot from his prudent attitude to research. I would like to express my sincere gratitude to Prof. J.K. Liu from Sun Yen-Sat University of China, my chief supervisor of my M.Sc. degree, for his introduction and kind encouragement to my study in Hong Kong.

I am truly grateful to Dr X.Q. Zhu for his beneficial discussion and guidance on my research. His smart thinking and hardworking also left me a deep impression. I would like to thank Dr. Z.R. Lu, Prof. Z.Y. Shi and Mr. J.Q. Bu for their constructive comments and encouraging discussions. Special thanks are extended to Mr. T. T. Wai, Mr. H.Y. Yau, Mr. C.W. Liauw and Mr. C.F. Cheung for their assistance in the laboratory work.

Appreciation is extended to the financial support to my study and research from The Hong Kong Polytechnic University, which makes the graduate study become possible.

Last but not least, I am greatly indebted to my family and Mr. L.X. Wang for their persistent support and encouragement throughout the whole study period.

TABLE OF CONTENTS

Certification of Originality i

Abstract ii

List of Publications vi

Acknowledgements viii

Table of Contents ix

List of Tables xiv

List of Figures xv

Chapter 1 Introduction **1**

1.1 General Remarks for Damage Detection 1

1.2 Vibration-based Damage Detection Techniques 2

1.3 Definition of Structural Damage 4

1.4 Four-Level Damage Identification 6

1.5 Non-Model-based versus Model-based Identification 7

1.6 Frequency versus Time Series-based Methods 8

1.7 Objective and Scope 10

Chapter 2 Literature Review **16**

2.1 Damage Model 17

2.2 Damage Index Method 19

2.2.1 Methods based on Shifts in Modal Frequency 20

2.2.2 Methods based on Mode Shape Changes 25

2.2.3 Methods based on Mode Shape Curvatures/Strain Mode Shapes 28

2.2.4 Methods based on Modal Flexibility Changes 31
2.2.5 Methods based on Modal Strain Energy Changes 33
2.2.6 Methods based on Frequency Response Function 35
2.3 Model Updating Methods 37
2.3.1 Optimal Matrix Updating Method 38
2.3.2 Sensitivity-based Updating Method 41
2.3.3 Eigenstructure Assignment Method 44
2.3.4 Stochastic Model Updating Method 46
2.3.5 Regularization Techniques 49
2.4 Wavelet Transform based Methods 52
2.5 Damage Identification based on Direct Use of Vibration Time Series Responses ..... ……57
2.6 Critical Issues and Shortcomings in Existing Methods 61

Chapter 3 Inverse Problem based on Finite Element Model and Response Sensitivity 68
3.1 Introduction 68
3.2 Forward Problem 71
3.2.1 Computation of Dynamic Responses of the Structure 71
3.2.2 Signal Analysis 73
3.3 Establishment of Damage Model 79
3.4 Sensitivity Analysis 80
3.5 Damage Detection 81
3.5.1 Objective Function 81
3.5.2 Penalty Function Method 83
3.5.3 Updating the Analytical Model and Identifying Local Damages 84
3.6 Regularization Technique 86
3.7 Uncertainty Analysis 88
3.8 Summaries 88

Chapter 4 Damage Detection directly from Time Response via Wavelet and Wavelet Packet Transform 90

4.1 Introduction 90

4.2 Structural Damage Detection from Wavelet Packet Energy of Time Responses 93

4.2.1 Dynamic Response Sensitivity 94

4.2.2 Sensitivity of Wavelet Packet Transform Component Energy 96

4.2.3 Equation for Damage Assessment 98

4.2.4 Numerical Study 99

4.2.5 Experimental Study 104

4.2.6 Conclusions 106

4.3 Structural Damage Detection from Wavelet Coefficient of Time Responses with Model Errors 106

4.3.1 Wavelet Coefficient Sensitivity 107

4.3.2 Damage Identification 111

4.3.3 Simulation 112

4.3.4 Experimental Verification 118

4.3.5 Conclusions 122

4.4 Condition Assessment from Wavelet Coefficients of Acceleration Response in Structures under Support Excitation 123

4.4.1 Response of Structures under Support 123

4.4.2 Sensitivity of Wavelet Packet Transform Coefficients 124

4.4.3 The Sensitivity-based Approach 125

4.4.4 Simulation 126

4.4.5 Experimental Verification 132

4.4.6 Conclusions 135

4.5 Summaries 136

Chapter 5 Structural Damage Detection via Wavelet-based Impulse Response Function 160

5.1 Introduction 160

5.2 Wavelet-based Sensitivity of Impulse Response Function for Damage Detection ..... ……162
5.2.1 Wavelet-based Unit Impulse Response 163
5.2.2 Impulse Response Function via Discrete Wavelet Transform..... 165
5.2.3 Damage Identification Equation 168
5.2.4 Simulation..... 169
5.3 Impulse Response Function from Structures under Support Excitation for Damage Identification..... 173
5.3.1 Unit Impulse Response from Measurement..... 174
5.3.2 Sensitivity Matrix from Analytical Finite Element Model..... 176
5.3.3 Damage Identification..... 178
5.3.4 Statistical Analysis..... 179
5.3.5 Numerical Verification 182
5.3.6 Experimental Verification..... 185
5.3.7 Discussions 190
5.4 Improved Regularization Techniques for IRF-based Damage Detection..... 191
5.4.1 Regularization Method for Identification Equation..... 192
5.4.2 Determination of regularization parameters 196
5.4.3 Noise Reduction prior to Regularization 200
5.4.4 Simulation..... 201
5.5 Summaries..... 205

Chapter 6 Structural Damage Detection under Ambient Excitation..... 221
6.1 Introduction..... 221
6.2 Covariance of Responses under Ambient Excitation..... 223
6.2.1 Covariance of Measured Responses 223
6.2.2 Covariance of Responses based on the Structural System..... 224
6.2.3 Sensitivity of the Cross-Correlation Function 228
6.2.4 Numerical Experiments 229
6.2.5 Conclusions..... 232
6.3 Condition Assessment of Structures under Ambient Excitation..... 232

6.3.1 The Wavelet Packet Energy of Cross-covariance of Acceleration Responses....233
6.3.2 Damage Identification....235
6.3.3 Numerical Study....239
6.3.4 Experimental Verification....243
6.4 Summaries....248

Chapter 7 Structural Damage Detection using Statistical Analysis with Time Series Data....257
7.1. Introduction....257
7.2. Theoretical Formulation....259
7.2.1 Damage Detection Procedure....259
7.2.2 Uncertainties of the System....260
7.2.3 Derivatives of local damage with respect to the uncertainties....262
7.2.4 The Statistical Characteristics of the Damage Vector....267
7.2.5 Statistical Analysis in Damage Detection....269
7.2.6 Reliability of the Identified Damage....270
7.3. Numerical Study....271
7.3.1 The Structure....271
7.3.2 Damage Detection....272
7.3.3 Reliability Assessment....277
7.4. Conclusions....278

Chapter 8 Conclusions and Recommendations....291
8.1 Conclusions....291
8.2 Recommendations....295

References....299

LIST OF TABLES

Table 4.1 - Natural frequencies of the response from the two states of structure.....137

Table 4.2 - Damage Scenarios 138

Table 4.3 - The experimental natural frequencies (Hz) and damping ratio of the steel beam.....139

Table 4.4 - The frequency content of the wavelet coefficients (Hz) 139

Table 4.5 - Comparison of response sensitivity to wavelet sensitivity.....140

Table 4.6 - Error of Identification in percentage. 141

Table 4.7 - The natural frequencies (Hz) and experimental damping ratio of the reinforced concrete beam.....141

Table 4.8 - Material and geometrical properties.....142

Table 4.9 - Damage scenario. 142

Table 5.1 - Damage scenarios.....207

Table 5.2 - Identified percentage reduction in the modulus of elasticity.....207

Table 5.3 - The natural frequencies (Hz) and damping ratio of the frame structure..208

Table 5.4 - Damage scenarios.....209

Table 6.1 - Damage scenarios.....249

Table 6.2 - The experimental natural frequencies (Hz) and damping ratio of the frame structure. 249

Table 6.3 - The identified results on the suspected damaged elements.....250

Table 7.1 - Identified Damage Probability and Mean Value (%).....279

LIST OF FIGURES

Figure 4.1 - Simply supported concrete beam. 143

Figure 4.2 - The Wavelet Packet Transform Component Energy. 143

Figure 4.3 - Variation of Wavelet Packet Transform Component Energy under impulsive excitation. 144

Figure 4.4 - Variation of Wavelet Packet Transform Component Energy under sinusoidal excitation. 145

Figure 4.5 - Identified results for Scenarios 1 to 12. 146

Figure 4.6 - Identified results for Scenarios 13 to 15. 146

Figure 4.7 - Dynamic test set-up of a steel beam and its finite element model. 147

Figure 4.8 - The measured and computed strain responses and the identified result. .147

Figure 4.9 - The one-story plane frame structure. 148

Figure 4.10 - Identified results for Scenarios 3 to 5. 148

Figure 4.11 - Identified results for Scenarios 6 to 8. 149

Figure 4.12 - Identified results for Scenarios 9 to 12. 150

Figure 4.13 - Identified results for Scenarios 13 to 15. 151

Figure 4.14 - Dynamic test set-up of a RC beam and its finite element model. 152

Figure 4.15 - Experimental Identified result. 152

Figure 4.16 - Acceleration responses from the second accelerometer. 153

Figure 4.17 - A five-bay three-dimensional frame structure. 153

Figure 4.18 - The excitation at the support of the structure. 154

Figure 4.19 - Sensitivities of the response and the WPT coefficients with respect to the elemental stiffness. 155

Figure 4.20 - Identified results for Scenarios 1 to 6. 156

Figure 4.21 - The experimental set up and the damaged elements of the nine-bay frame structure. 157

Figure 4.22 - A nine-bay three-dimensional frame structure. 158

Figure 4.23 - Support acceleration and comparison of the measured and the computed accelerations. 158

Figure 4.24 - Identified results from experiment. 159

Figure 5.1 - Thirty-one bar plane truss structure. 210

Figure 5.2 - The Impulsive response functions from different excitations. 210

Figure 5.3 - Identified results for Scenarios 1 to 4. 211

Figure 5.4 -Identified results for Scenarios 5 to 10. 212

Figure 5.5 - The support acceleration and UIRs obtained at Node 7. 213

Figure 5.6 - Identified results from response with 15% noise level. 214

Figure 5.7 - The measured mode shapes of the intact steel frame structure. 215

Figure 5.8 - Measured support acceleration and UIR at Node 6. 216

Figure 5.9 - Identified experimental results. 217

Figure 5.10 - The L-Curve. 217

Figure 5.11 - Identified results for Scenarios 1 to 4. 218

Figure 5.12 - Identified results for Scenarios 5 to 10. 219

Figure 5.13 - The convergence norm and MPCC. 220

Figure 6.1 - The one-story frame structure. 250

Figure 6.2 - Comparison of auto- and cross- correlation of accelerations from analytical and experimental. 251

Figure 6.3 - Thirty-one-bar truss structure..... 251

Figure 6.4 - Comparison of auto- and cross- correlation of acceleration from analytical and experimental. 252

Figure 6.5 - Identified results for Damage Scenario 1..... 253

Figure 6.6 - Identified results for Damage Scenarios 2 and 3. 254

Figure 6.7 - Auto-covariance of accelerations at support and structure. 255

Figure 6.8 - Identified results for the experimental structure. 256

Figure 7.1- the PDFs of the structural parameter under two states..... 280

Figure 7.2 - A five-bay three-dimensional frame structure. 280

Figure 7.3 - the mean values of all elements, 7th and 26th elements for all iterations 281

Figure 7.4 - the standard deviation of all elements due to noise in density..... 282

Figure 7.5 - the standard deviations for 10 iterations due to noise in mass density. . 283

Figure 7.6 - the standard deviation of all elements due to noise in stiffness. 284

Figure 7.7 - the standard deviations for 10 iterations due to noise in stiffness..... 285

Figure 7.8 - the standard deviation of all elements due to noise in excitation..... 286

Figure 7.9 - the standard deviations for 10 iterations due to noise in measured force excitation..... 287

Figure 7.10 - the standard deviation of all elements due to noise in measured acceleration. 288

Figure 7.11 - the standard deviations for 10 iterations due to noise in measured acceleration. 289

Figure 7.12 - the identified results with all types of noise..... 290

CHAPTER 1 INTRODUCTION

1.1 General Remarks for Damage Detection

Early detection of damage in engineering systems during their service life is receiving increasing attention from researchers in the last few decades. The problem of detecting structural damage in mechanical, aeronautical and civil engineering systems has been the subject of numerous research papers and conferences over the past few years. The increasing interest in detecting damage as early as possible comes from the past catastrophic failures with great loss of life and property (Lancaster, 2000; Jones, 1998, 2001). Catastrophes due to structural failures, such as the series of Comet I aircraft failures in the 1950s caused by fatigue cracks of the cabin, the capsizing of the Alexander L Kielland rig in 1980 started from fatigue fracture of a brace and the air crash due to in-flight loss of the exterior skin on an Aloha Airlines flight in Hawaii in 1988, draw the public attention on the safety of structural and mechanical systems. The public concerns, in turn, urge the government for the need of health monitoring on the existing but ageing infrastructures. With the huge number of structures, such as bridges, built in the past century in the world, it is a real challenge for the technology and the economy to monitor them and carry out proper repair if it is needed. In another aspect, the development of technology in many areas, such as the increase in computer memory and the speed of scientific computation, advances in sensor and experimental techniques, and the development of finite element methods, has contributed to the development of damage detection methods. Information on the location and extent of damages obtained by early

damage detection could assist in the diagnosis of the structural health conditions and in the recommendation on associated maintenance work, allowing maintenance and repair work to be properly carried out and thus minimizing the maintenance cost.

1.2 Vibration-based Damage Detection Techniques

Visual inspection by an expert has been the only available means of damage detection and structural maintenance in the early years. However, many modern structures, such as offshore platforms, long-span bridges and space structures are inaccessible during their service life.

Moreover, many failures start from the inside of structural components, thus they cannot be detected by naked eyes at an early damage stage. Therefore, non-destructive evaluation (NDE) techniques are developed and introduced. Traditional non-destructive damage detection techniques are local experimental methods, such as acoustic or ultrasonic methods, magnetic field methods, radiography, eddy-current methods, or thermal field methods (Doherty, 1993). All of these experimental techniques require that the location of the damage be known a *priori* and be readily accessible and they usually require that the structure/system under investigation be taken out of service for inspection at prescribed time intervals. The inspection procedure can be very tedious and time consuming, especially when it involves components at inaccessible locations. Due to these limitations, the application of these methods is far from satisfactory since we are limited to detect local damage on the surface of the structure and the size of the structure is also practically limited. There is a great need for local damage identification methods that can be applied to complex and large-scale structures. This has motivated the research

of new NDE techniques that can be applied to in-service structures, reducing maintenance costs and improving safety as well as system performance. Vibration-based damage methods then came into being and have been developed by many researchers.

The structural damage may be caused by various reasons such as operating loads, impact, fracture, fatigue, corrosion, manufacturing fault etc., in general, producing changes in the structural physical properties (i.e., stiffness, mass, and damping), and these changes will lead to changes in the dynamic characteristics of the structure. This fact has been widely noticed and used by structural engineers for damage detection or health monitoring of a structure. The vibration-based damage detection is found on the basis that the dynamic characteristics (namely frequencies, mode shapes and/or transfer functions, modal damping, and dynamic response and so on) are functions of the physical properties of the structure (mass, damping, and stiffness).

In general, the vibration-based damage assessment is an inverse problem to identify the location, pattern and quantity of the loss in structural physical properties from the measured structural vibration data. With the discovery of the Fast Fourier Transform (FFT) algorithm (Cooley and Tukey, 1965) and the use of digital computers in laboratory test systems, the development of techniques such as digital signal processing, modal testing and analysis are notably boosted. The advances in these areas in turn allowed researchers to investigate the possibilities for quantitatively identifying the state of a structure by inspecting its vibration data. This encouraging technique has received wide attention throughout the civil, mechanical and aerospace engineering communities due to its potential for solving the aforementioned inaccessibility problem of localized

experimental inspection methods. Doebling et al. (1998) provided an excellent summary of the development of the technique over the last three decades.

A typical scheme of vibration-based frequency-domain methods is summarized as follows: firstly, the vibration response of the structure is measured. For an ambient vibration test, only the output response of the structure aroused from ambient excitation sources such as wind loads, normal traffic and wave loads is measured. For a forced vibration test, both the input excitation force and output structural response are measured. Secondly, modal analysis is performed to obtain modal parameters such as natural frequencies, mode shapes and damping ratios from the measured time histories. Thirdly, a non-destructive damage detection algorithm is applied to identify damage using the previously estimated modal parameters. An analytical model of the structure and/or its predicted response may also be used as a baseline in the detection process if necessary. Lastly, structural safety and reliability analysis are carried out to guide the future usage of the structure according to the identified results.

1.3 Definition of Structural Damage

Damage may be defined as a change introduced into a system that adversely affects the current or future performance of the system (Doebling et al. 1998). In the past three decades, research work is focused on identification of damage in the civil, mechanical, and aerospace engineering systems. Thus, the definition of damage will be confined to the changes of the material and/or geometric properties of these systems, including changes to the boundary conditions and system connectivity, which adversely

affect the performance of the systems (Farrar et al., 2001). In many existing research literatures, damage is mainly in the form of a loss of the stiffness of the structure.

Damage may be classified as linear or non-linear according to its effects on the dynamic response of a structure. A linear damage is defined as the case in which the structure retains its initial linear-elastic property after damage occurrence (Doebling et al., 1998). The damage, in terms of changes in the geometry and/or material properties of the structure, changes the dynamic properties of the structure in a linear or a linear combination manner. Therefore, the response of the damaged structure can still be modeled under linear assumptions. Up to now, the majority of research work published in the technical literature addresses only the linear cases of damage detection.

Non-linear damage is defined as the case when the initially linear-elastic structure behaves in a non-linear manner after the damage has been introduced (Doebling et al., 1998). These non-linear behaviors in structural response are also attributed to the changes in geometry and/or material properties caused by the damage. One example of the geometrically non-linear damage is a crack that opens and closes under the operating load. If a structure exhibits moderate or severe nonlinearities, conventional damage identification approaches will give results with large error or even wrong prediction. Some researchers (Topole and Tzvetkova, 1996) try to directly obtain the equations on the system physical properties based on the first law of thermodynamics rather than use modal analysis techniques for structural nonlinear damage prediction. Jin et al. (2000) investigates the possibility of applying an energy index approach in nonlinear finite element analysis for damage detection in highway bridge structures. The nonlinear behaviors of the bridges under dynamic loading conditions due to inelastic deformation

of the material and crack damages have been studied. In another study, nonlinear analysis and chaos theory were applied in structural health monitoring (Livingston et al., 2001). Chaotic behavior was observed in the bridge model. They found that the natural frequencies of the structure are not fixed, but wander in time in a characteristic pattern around a central value.

1.4 Four-Level Damage Identification

The vibration-based damage detection approaches can be categorized according to various criteria. A well known classification for damage detection methods, proposed by Rytter (1993), defines the following four levels.

- Level 1(Damage Detection): Determination of the presence of damage in the structure;
- Level 2(Damage Localization): Level 1 plus determination of the damage location;
- Level 3(Damage Quantification): Level 2 plus quantification of severity of damage;
- Level 4(Life Prediction): Level 3 plus prediction of the remaining useful life of the structure.

The four-level damage identification method provides a sequence to assess the structural damage. Since prediction in Level 4 requires knowledge of other fields such as structural design, fracture mechanics, materials aging studies, and damage mechanism, it is therefore not included in this research. This thesis will address only the vibration-based damage identification methods that focus on the first three levels.

1.5 Non-Model-based versus Model-based Identification

Among the different vibration-based structural health monitoring techniques, one may find two distinct classes of methods: model-based techniques and non-model-based techniques. Each approach has its own advantages and limitations. Non-model-based methods have the advantage of avoiding modeling errors and computational costs involved in numerical simulations, which can pose severe limitations when iterative identification schemes are used. However, most non-model-based methods developed to date can only provide Level 1 and limited Level 2 damage identification. Furthermore, attempts of Level 2-3 diagnostics by means of non-model-based methods imply a considerable increase in the number of sensors and subsequent amount of signal processing. This indicates that, in order to achieve Level 3 identification, a mathematical model of the structure is necessary. The level of model refinement needed to describe small flaws, as in the case of fatigue cracks, can be a considerable restriction. However, the use of a theoretical model can be advantageous in many aspects. (1) The use of a mathematical structure describing the dynamic system permits the application of model-based parameter identification methods, possibly reducing the amount of experimental data required. (2) It allows inexpensive off-line simulations of slight variations in the system, such as changes in physical parameters, boundary conditions, external influences, etc. These simulations can provide valuable information for pre-test procedures. (3) The model can be used in the test design phase to optimize the number and location of sensors, actuators, and excitation/measurement cycles. (4) The model can be used to easily generate extensive amounts of data, as needed for example, in the training phase of

neural-network-based monitoring schemes. (5) In addition, modeling errors inherent to theoretical models can be reduced by using well-established model updating techniques. A good compromise between the requirements of accuracy and simplicity is a desired characteristic of a model used in any on-line health monitoring procedure.

The next important question now becomes how to find the suitable model for the method we envision. Most of the work on dynamics of cracked members deals with the forward problem, either quantifying the effects of a certain damage of known extent on the dynamic characteristics of the structure or predicting a nonlinear signature spectrum that would indicate the presence of damage. The computational cost is usually not a concern when dealing with the forward problem. Investigations on solving the inverse problem (localizing and quantifying a crack from the responses) are usually based on simplified linear models where the effect of the damage is represented by a local reduction in stiffness.

1.6 Frequency versus Time Series-based Methods

A very important aspect to consider is the choice of dynamic quantities used in the monitoring process. Friswell (1994) presents a discussion of damage detection methods in terms of the measured data used, which can basically be in three forms: time series, frequency response functions (FRR's), and modal parameters. Time series are digitalized responses from sensors such as accelerometers, strain gauges, PZT sensors and other measuring devices. Frequency responses are obtained from time series by nonparametric estimation and signal processing techniques, usually through numerical Fourier transform. The FRF's are then used as the data source to the estimation of modal parameters through

curve fitting methods of varying complexity level, depending on the amount of data in hand. Time series and FRF's are the main components of a typical modal test, a very well established experimental tool for the dynamic analysis of structures. Some potentially useful information is lost during each step of data reduction. In some cases, modal parameters can be directly estimated from time responses, but the extent of data compression remains the same. For a linear system, it is possible to accomplish intensive data reduction, from time series to a modal model, without significant loss of relevant information in the frequency range of interest.

Friswell and Penny (1997a) also note that the use of FRF's and modal parameters is equivalent for most linear cases. Although FRF data might contain some information from out of range modes, or from modes not captured during the curve fitting procedure, these advantages will disappear provided the modal parameter estimation phase is careful and thorough. This is the main reason why the vast majority of technical papers published recently focus on diagnosis methods based on modal parameters such as natural frequencies, mode shapes, modal strain energy, strain mode shapes, etc., which have the appealing advantage of dealing with a reduced volume of data. However, there are two main reasons to explain why the use of modal parameters may be a serious limitation for the case of crack-type damage: firstly, the effect of small flaws on modal quantities, such as natural frequency shifts and local changes in the mode shapes, are usually very small and likely to be masked by experimental uncertainties and data reduction; and secondly, the assumption of linearity inherent in modal methods may introduce errors in the identification procedure. Frequency domain data may provide a quick, qualitative assessment of the presence of cracks, since the nonlinearity introduces peaks due to

harmonics of the natural frequencies or combinations of those frequencies and the excitation frequency. This crack-signature analysis is limited to a Level 1 diagnostic, and the extension to Levels 2 and 3 would require complex nonlinear models in the frequency domain.

A promising alternative is the direct use of time responses in a model-based, iterative parametric identification procedure proposed by Banks, Inman and co-workers (1996, 1998) which is proven to be capable of detecting fairly small defects modeled as geometrical imperfections in the cross section of beams. The methodology involves a theoretical model based on a B-spline Galerkin approximation of the differential equations of equilibrium that provides both the accuracy and the simplicity required for a successful damage diagnosis. The use of time responses is less likely to be limited by data reduction problems, since the only differences from raw, analog data are due to the digital data acquisition process. Besides, the nonlinear behavior is also preserved, increasing the chances of a more realistic characterization of small crack-type damage.

1.7 Objective and Scope

The primary goal of this research thesis aims to develop a simple, economical and yet technological feasible vibration-based evaluation procedure to assess local damage in existing structures using the measured structural time series data. The specific objectives of this research are:

1) To develop damage detection methods using directly the measured acceleration via wavelet transform. The wavelet packet energy and the wavelet coefficients of acceleration responses of the structure under general excitation and support

excitation are used to identify the location and extent of local structural damage via a model updating and sensitivity analysis.

2) A damage detection method based on the impulsive response function is proposed. The impulsive response function is computed from the measured acceleration responses via wavelet transform and its wavelet coefficients are used to identify local damage in the structure under general excitation and support excitation.
3) To propose a method making use of the wavelet packet energy of covariance of acceleration responses of a structure under ambient excitation to identify structural damage such that the damage detection can be done with the response-only measurement.
4) To investigate the regularization methods for treatment of the ill-conditioning in the damage identification equations based on measured acceleration responses. Tikhonov regularization technique is improved in the inverse problem of the damage detection using the time domain data.
5) To develop a technique to include the effect of uncertainties in the damage identification procedure with subsequent structural reliability analysis. The uncertainties are assumed to exist in the system parameters, the excitation force and the measured acceleration response.

This dissertation comprises eight chapters and is organized as follows.

Chapter 1 introduces the motivation for the present research and lists the objectives to be achieved in this research thesis.

Chapter 2 gives a literature review on five topics associated with the present research: damage model, damage index method, model updating methods, wavelet transform-based methods and damage diagnosis based on vibration responses. After introducing the general concept and an overview of the structural damage detection methods, damage index methods that utilize modal properties before and after the damage occurrence to generate damage indices for damage detection are discussed. Subsequently various model updating methods for both model refinement and damage detection applications are reviewed. These methods include optimal matrix updating methods, sensitivity-based updating methods, eigenstructure assignment methods and statistical methods for model updating. The regularization techniques for mode updating are reviewed. Then the damage detection methods based on wavelet transform are investigated. The damage detection methods using time series data are also investigated specifically. A discussion on the critical issues and shortcomings related to existing methods is provided at the end of the chapter.

Chapter 3 presents the general procedure of damage detection based on time series data. Firstly, the forward problem including the computation of time responses from an analytical model using numerical methods and signal analysis is introduced. Secondly, a simple model of damage is established for demonstration of the damage detection method. Thirdly, the sensitivities of time series data with respect to the structural parameters are computed numerically. Fourthly, the damage identification based on the model updating and output-error matrix was described. Fifthly, regularization technology is used to treat

the ill-conditioning problem and its basic theory was presented. Finally, the modeling of uncertainty is presented.

Chapter 4 presents the damage detection methods based on model updating techniques using measured acceleration responses via wavelet transform. Wavelet packet energy of acceleration responses are computed analytically and applied to identify damage via a sensitivity analysis. The wavelet coefficient of acceleration responses of the structures under general excitation and support excitation are numerically computed and adopted for damage detection where the effects of model errors and noise in the coefficients from different frequency bands are studied and the use of subsets of the measured response at different resampling rates is discussed. Numerical studies and experimental verifications are performed for each method with satisfactory results.

In Chapter 5, wavelet coefficients of the unit impulse response function of the structures under general excitation and support excitation are obtained from the measured acceleration responses via wavelet transform, and they are applied to identify damage via a sensitivity analysis and model updating techniques. Regularization techniques and L-curve method with improvements are used to solve the identification equation. Numerical studies and experimental verifications are performed for the proposed methods and improved techniques.

Chapter 6 extends the method developed in Chapter 5 to the damage identification of a structure under ambient excitation as experienced by most of the large-scale structures.

Firstly, covariance of acceleration responses is computed based on the unit impulse response function. Then, the wavelet packet energy of covariance of measured acceleration responses of structures under ambient excitation is used for damage detection assuming that the ambient excitation is of white noise distribution. To reduce the number of unknowns involved in the inverse problem, damage localization is carried out firstly with the elemental modal strain energy. A five-bay three-dimensional cantilever truss structure is used to demonstrate the efficiency of the method with three damage cases, and a nine-bay three-dimensional frame structure is test in the laboratory for verification of the proposed method.

In Chapter 7, a statistical model updating method for the structural damage detection based on measured acceleration response and a reference model of the structure is proposed. Uncertainties in the system parameters, such as the structural parameters of the finite element model, the excitation force acting on the structure and the measured acceleration response from the perturbed state of the structure are analyzed. Analytical formula are given and they are included in the study for the damage detection. The effect of each of these uncertainties on the assessment results is studied separately in an updating damage detection algorithm based on the response sensitivity approach. The probability density function of the stiffness parameters in both the intact and perturbed states are compared in a subsequent reliability assessment. A three-dimensional five-bay steel frame structure is studied for illustration.

Chapter 8 summarizes the contributions, findings and conclusions achieved in both the theoretical and experimental studies in this project. Recommendations for future work are also given.

CHAPTER 2 LITERATURE REVIEW

Damage detection based on vibration information first appeared in the 1970s. In the early 1980s the subject of damage detection using vibration data has received enormous attention from the engineering and research communities, with emphasis on turbomachinery, civil engineering, and aerospace applications. A great deal of research has been carried out in the last two decades on the development of analytical techniques of vibration-based damage detection. Since vibration-based structural health monitoring (SHM) found its early application in aerospace and mechanical engineering, much research has been carried out in these fields. Research studies on the application of vibration-based assessment in the health monitoring of civil engineering structures are more recent. Doebling et al. (1996a, 1998) provide an extensive bibliography related to this subject. Farrar et al. (1994) have reviewed the literature on vibration testing and damage detection in bridges. More recent studies have been reported in the proceedings of a series of conferences and workshops on structural health monitoring. These include the 2nd, 3rd, and 4th International Workshops on Structural Health Monitoring at Stanford, USA (Chang, 1999, 2001, 2003), the 1st (Cachan, France) and 2nd (Munich, Germany) European Workshops on structural health monitoring (Balageas, 2002, Boller and Staszewski, 2004), the 2nd International Workshop on Structural Health Monitoring of Innovative Civil Engineering Structures, Winnipeg, Canada (Mufti and Ansari, 2004), and the 1st International Workshop on Structural Health Monitoring and Intelligent Infrastructure, Tokyo, Japan (Wu and Abe, 2003).

This chapter aims to provide a review on recent research on vibration-based damage diagnostics. A complete procedure for damage diagnostics includes establishment of damage model of the structure, choice of vibration types (i.e linear or non linear vibration), using model or non-model-based damage detection methods, using modal methods or non-modal methods, and finally choosing corresponding vibration characteristics (i.e natural frequency, mode shape, modal strain energy, flexibility matrix, strain mode shape, modal damping, time responses, FRF and covariance of response and etc.) with effective signal processing techniques and numerical methods such as iteration, regularization, optimization and so on for damage detection. The literature review mainly covers the following topics. Firstly, a general review of damage model for the detection is given. Secondly, a survey of the investigations on damage index method is presented. Thirdly, the survey of model updating methods is investigated. Fourthly, wavelet transform based methods and regularization techniques are explored. Fifthly, the development of damage diagnostics based on direct use of vibration responses is discussed. Finally, critical issues and shortcomings in existing methods are discussed.

2.1 Damage Model

There are a number of approaches to model damage in structures in the literature. Generally, these methods can be classified into two main groups: the first group is linear model which is often used for open crack which is the most common damage type, in which the crack is assumed to be permanently opened. This crack model also takes up different forms and there are many existing technical literature on the three categories of: local stiffness reduction, discrete spring models, and crack functions. The second group is non-linear model for an opening and closing crack or breathing crack, in which the crack

opens and closes alternately during vibration. Damage model can also be sorted into discrete and continuous models. Discrete model is often in the form of lumped flexibility model including a compliance matrix, discrete spring model and finite element model and etc.

There are many literatures on damage models since the emphasis of the thesis is not on the models, only typical work on damage model are listed in the section.

The first investigation on damage model is attributed to Kirmser (1944) and Thomson (1949). They represented the effect of a notch by equivalent forces and moments at the location of the geometrical discontinuity. Among the most referred publications in the literature we must cite the investigations by Dimarogonas (1976), who was arguably the first to propose the derivation of compliance constants from fracture mechanics for vibration analysis.

The typical use of finite element model was done by Thyagarajan et al. (1998) who used a finite element model of a bridge to calculate the nodes at which damage may be present. Firstly, the model was adjusted so that the measured undamaged frequencies matched the predicted ones. Then using the mass, stiffness and damping matrices of the undamaged model and the damaged mode shapes, a damage vector was calculated.

Continuous models were developed more recently in an attempt to explicitly incorporate the relevant damage parameters, i.e., location and extent, as part of the equation of motion of the damaged structure. Christides and Barr (1984, 1986) initially developed models for the transverse vibration of a symmetric, double-edge cracked Euler-Bernoulli beam and for the torsional vibration of a cracked bar. Both models rely on the characterization of the stress concentration due to the crack by means of a decay

function introduced in the kinematic assumptions used in a variational derivation of the equations of motion.

Because of the complexity of failure in structures, damage models are often established for specific structures. Ang (1988) developed a seismic damage model for reinforced concrete structures in which the structural damage is expressed as a linear combination of the maximum deformation and the hysteretic energy dissipation. From an extensive damage analysis of various reinforced concrete buildings, an intensity scale is derived to describe the potential destructiveness of ground motion. Wu and Law (2004a) proposed an anisotropic damage model for a thick plate element with an inclined crack. The cracked plate element is represented by an effective plate element with anisotropic material properties expressed in terms of the virgin material stiffness and a vector of damage variables. The orientation of the crack is directly indicated by the geometric parameter and the damage severity can be estimated from other variables representing the relative stiffness reduction along the local axes. The validity of the methodology is demonstrated by numerical examples and experiment results.

2.2 Damage Index Method

Damage index method is the earliest appearing method because it is relatively simple and straightforward. Damage index method is a detection approach which adopts modal parameters as indicators to identify the structural damage location and extent. The test modal data from the damaged and the intact structures, such as natural frequencies, mode shape, etc. are required in this approach to correlate with the corresponding

parameters of the analytical model or the baseline model to obtain information on the damage location and even the extent. Though damage index methods are applied simply in engineering structures, generally they do not provide quantitative information about the structural damage. Existing approaches may be classified into the following categories based on the parameters used in the damage detection: (1) methods using natural frequency shifts; (2) methods using mode shape changes; (3) methods using mode shape curvatures/strain mode shapes; (4) methods using modal flexibility changes; (5) methods using modal strain energy changes; and (6) methods using frequency response function.

2.2.1 Methods based on Shifts in Modal Frequency

Natural frequency is the vibration characteristics which are firstly used for structural health monitoring, because it is the basic vibration parameters of the structure and can be measured easily and reliably, especially in the early days when the vibration testing techniques are not fully developed and other vibration parameters can not be obtained with satisfactory accuracy. Relevant literature for methods using modal frequency is plenty.

The earliest work published to use frequency changes for damage detection was done by Lifshiz and Rotem (1969) who treated the damage detection as an inverse problem so that the damage parameters are calculated directly from measured frequency changes via vibration measurements. They found the change in the dynamic modulus, which is related to the frequency change, could be used as an indicator of damage in

particle-filled elastomer. The dynamic modulus is computed by using curve fitting of the measured stress-strain relationships at various levels of filling.

Natural frequencies can be directly compared between those from the inspected structure and the intact structure. When the difference exists, damage has occurred in the structure. Vandiver (1975, 1977) detected structural failure on fixed platforms by examining the change in the frequencies associated with the first two bending modes and first torsional mode of an offshore light station tower. Wojnarowski, et al (1977) evaluated structural integrity of a fixed offshore lighthouse platform by examining the effects of eleven different parameters on the dynamic properties of the structure using finite element analysis. Foundation modeling assumptions, entrained water, marine growth, corrosion, variation in deck loads, and failed structural members are examined.

Direct comparison of natural frequency is limited for damage detection. Cawley and Adams (1979) used the ratio of natural frequency shifts between different modes to detect the possible damage location in composite materials. The ratio between frequency shifts for modes *i* and *j* can be denoted by $\delta\omega_i / \delta\omega_j$. Because the change in the natural frequency of a structure is a function of the damage position vector only, but not the damage extent, when the analytical ratio $\delta\omega_i / \delta\omega_j$ from the simulated damage case equals the ratio from the measured data, the damage location is determined. However, the method is limited to single damage scenarios. The work was further developed via the error function for each mode and for each structural member based on sensitivity analysis of modal frequency to damage parameters by Stubbs and Osegueda (1990). Penny et al (1993) presented a method to determine the damage case by comparing the measured frequencies from the inspected structure with the computing frequency for all simulated

damage cases considered in a least-squares sense. Finally the possible damage case is determined with the minimal error. They also found that the frequency damage detection method is sensitive to measurement errors.

Ratios of frequency changes for damage detection are also adopted by Friswell et al (1994) who used frequencies and statistical measures to locate damage in structures. The damage detection method is based on a known catalogue of likely damage scenarios, where it is assumed that there exists a precise model of the structure and the ratios of the frequency changes for several lower modes using the model of the intact state and all the simulated damage scenarios are computed. The same ratios are also calculated for the inspected structure. The relationship between the two sets of values is established by a power law relation. When damage scenario of the structure lies in the set of assumed damages, the correct type of damage will produce a good fit plotted by a unity-slope line. For all other types of damage, the fit will be inexact.

Patterns of shifts in a set of modal frequencies are examined alternatively and applied for detecting structural parameters changes. Messina et al (1996) proposed an assurance criterion for detecting single damage sites from natural frequency change by defining the Damage Location Assurance Criterion "DLAC" for location *j*,

$$DLAC(j) = \frac{\left|\Delta\mathbf{f}^T \cdot \delta\mathbf{f}_j\right|^2}{(\Delta\mathbf{f}^T \cdot \Delta\mathbf{f}) \cdot (\delta\mathbf{f}_j^T \cdot \delta\mathbf{f}_j)} \qquad (2.1)$$

where $\Delta\mathbf{f}$ is the measured frequency change vector for a structure with a single defect, and $\delta\mathbf{f}_j$ is the theoretical frequency change vector for a damage with a known size at known location *j*. The location *j* with the highest *DLAC* value is regarded as the possible

damage site because it best matches the measured frequency change. The method is also extended for multiple damage detection known as the multiple damage location assurance criterion (*MDLAC*) and the algorithms for estimating the size of the defects are also introduced by Messina et al. (1998). The MDLAC is formulated as,

$$MDLAC(j) = \frac{\left|\Delta\mathbf{f}^T \cdot \delta\mathbf{f}(\delta\mathbf{D})\right|^2}{(\Delta\mathbf{f}^T \cdot \Delta\mathbf{f}) \cdot (\delta\mathbf{f}(\delta\mathbf{D})^T \cdot \delta\mathbf{f}(\delta\mathbf{D}))} \qquad (2.2)$$

The MDLAC approach offers the practical attraction of only requiring measurements of the changes in a few of the structure's natural frequencies between the undamaged and damaged states and is shown to provide good predictions of both the location and absolute size of damage at one or more sites.

Modal frequencies combined with sensitivity analysis are also found for damage detection in the literature. Stubbs and Osegueda (1990) developed a method for damage detection that relates changes in the resonant frequencies to changes in member stiffness using a sensitivity relation. They assumed that damage occurs at only one member of the structure, and computed an error function for each mode and each structural member based on sensitivity analysis of modal frequency to damage. The authors illustrated that this sensitivity method has difficulty when the number of modes is much fewer than the number of damage parameters. Sophia and Garrett (1995) presented a technique for identifying localized reductions in the stiffness of a structure using measurements of natural frequency. The sensitivities of the eigenvalues to localized changes in the stiffness are developed as a set of under-determined equations. The method is also verified using test data from an aluminum cantilever beam. Williams et al (1996) proposed a method for damage detection and localization by means of using natural

frequency sensitivity and satisfactory results are obtained. Other examples of inverse methods for detecting damage via modal frequency changes were reported by Adams et al (1978), Wang and Zhang (1987), Hearn and Testa (1991), Koh et al (1995), Morassi and Rovere (1997) and Salawu (1997a, 1997b).

There are several advantages associated with the application of frequency-based approaches, such as frequency information being independent of the sensor position, few measuring points required; the natural frequency being less contaminated by measurement noise than other modal parameters; the ability to be implemented to continuously health monitoring a structure, since ambient vibration induced by inputs of low energy level, such as normal traffic, are sufficient for the extracting of the resonant frequencies.

On the other hand, limitations also exist with frequency-based damage detection. Because modal frequencies are the global dynamic characteristics of the structure, they are usually not sensitive enough to identify the local changes in the structural parameters. The frequencies generally cannot provide spatial information on the structural changes. In the case of a symmetrical structure, the changes in natural frequencies due to damage at two symmetric locations are exactly the same. So the frequency method often fails in this case. One may expect that higher modal frequencies are associated with local responses, or that multiple frequency shifts can provide spatial damage information because structural changes at different locations will cause different combination of frequency changes. Unfortunately, there is often insufficient number of frequencies with significant changes to uniquely determine the damage location because of the practical limitations in modal test and analysis involved with excitation, modal density, etc.

2.2.2 Methods based on Mode Shape Changes

Mode shapes inherently contain the spatial information about structural changes. Then mode shape is more potential for the identification of damage which is the local change of the structure condition. With the development of modal testing techniques especially in sensor technology and computing speed, many researchers devoted their efforts in detecting damage using measured mode shape information.

West (1984), who possibly published the first systematic use of mode shape information for locating structural damages, proposed the Modal Assurance Criteria (MAC) to determine the level of correlation between the modes measured from undamaged and damaged structures. The MAC, generally, is defined as

$$MAC(\varphi_r, \varphi_s) = \frac{\left|\varphi_r^T \varphi_s\right|^2}{\varphi_r^T \varphi_r \varphi_s^T \varphi_s} \tag{2.3}$$

where φ_r and φ_s are any two eigenvectors of a structural system. The value stands for the correlation level between the two modes in the range of 0.0 to 1.0, with a value of 1.0 indicating identical mode shapes and 0.0 for orthogonal ones. For the application of damage detection, the eigenvectors φ_r and φ_s often denotes a pair of mode shape vectors measured from the structure before and after damage occurs. In model updating cases, however, the mode shape pairs from a tested structure and its corresponding analytical model respectively are used instead to calculate the MAC values. The mode shapes often need to be partitioned using various schemes, and the change in MAC across the different partitioned schemes is used to localize the structural damage.

Yuen (1985) presented a systematic study of the relationship between damage location, damage size and the changes in the eigenvalues and eigenvectors of a cantilever beam when subjected to damage in a numerical study using a finite element model of a uniform cross-sectioned cantilever, and it shows that the changes in the eigenvectors follow a definite trend in relation to the location and extent of damage.

Fox (1992) proposed and found that a node-line MAC, a MAC based on measurement point close to a node point for a particular mode, is a more sensitive indicator of mode shape changes due to damage. He experimentally found that the measurement of mode shape changes for single vibration mode, such as MAC, were relatively insensitive to damage in a beam with saw cut. To locate the damage, the relative mode shape changes at node points (in modes that show little change in natural frequencies) are related with the corresponding peak amplitude points (in modes that show relatively large changes in natural frequencies) by a simply graphical comparison method. He also proposed a method of scaling the relative changes in mode shapes to better identify the damage location. Mayes (1992) developed a method known as structural translational and rotational error checking (STREC) based on the changes in mode shapes. By using the ratios of relative modal displacements, STREC assessed the difference of structural stiffness between two different sets of degrees-of-freedom (DOFs).

Based on the concept of MAC, Lieven and Ewins (1988) proposed COMAC for damage localization, which is defined as,

$$COMAC(i) = \frac{(\sum_{r=1}^{m} \phi_{Dr}^{i} \phi_{Ur}^{i})^2}{(\sum_{r=1}^{m} \phi_{Dr}^{i} \phi_{Dr}^{i})(\sum_{r=1}^{m} \phi_{Ur}^{i} \phi_{Ur}^{i})} \qquad (2.4)$$

where ϕ_{Dr}^{i} and ϕ_{Ur}^{i} are modal component of the *r*th mode shape at measurement location *i* for the damaged state and the undamaged state of the structure, respectively; and *m* is the number of measured modes. The location where a COMAC value is close to zero is the possible damage location. The correlation value is related to structural degrees-of-freedom (DOFs) rather than to mode indices, and obviously more helpful to show where are the defects in the structure than the MAC.

Ko *et al.* (1994) presented a method that uses a combination of MAC, COMAC, and sensitivity analysis to detect damage in steel-framed structures. The sensitivities of the analytically derived mode shapes to particular damage locations were first computed to determine which DOFs are the most relevant. The results demonstrated that particular mode pairs could indicate damage; but when all mode pairs were used, the indication of damage might be masked by modes that were not sensitive to the damage. Shi et al (2000a) presented a sensitivity- and statistical-based method to localize structural damage by direct use of incomplete mode shapes. Messina et al. (1998) developed a method which is an extension of the multiple damage location assurance criterion (MDLAC) by using incomplete mode shape instead of modal frequency. A plane truss structure is analyzed as a numerical example to compare the performance of the proposed method with the multiple damage location assurance criterion. Results indicate that the new method is more accurate and robust in damage localization with or without noise effect.

Mode shapes combined with other parameters are also adopted to identify damage. Skjaeraek et al (1996) presented a method for the localization of structural damage in seismically excited reinforced concrete (RC) structures using the two lowest smoothed eigenfrequencies and mode shape coordinates which are used as an input via a substructure iteration technique. The optimal sensor placement issue for the method is also examined. Cobb and Liebst (1997) presented a method of identifying damaged structural elements from measured modal data using an incomplete measurement set. The method uses a mathematical optimization strategy to minimize deviations between measured and analytical modal frequencies and partial mode shapes. Damage is identified by determining the stiffness change to a finite element model required to match the measured data of the damaged structure. Ratcliffe (1997) develops and presents a technique for identifying the location of structural damage in a beam by applying a finite difference approximation of Laplace's differential operator to the mode shape, when damage is less severe, further processing of the Laplacian output is required before the location can be determined. The procedure operates solely on the mode shape from the damaged structure, and does not require *a priori* knowledge of the undamaged structure. Parloo et al (2003) used mode shape sensitivities to damage detection. Since the sensitivities are calculated on the basis of the experimentally determined mode shapes, there is no need for a prior finite element model of the test structure. Pascual et al (2005) introduces a new general procedure to the expansion of mode shape for damage assessment process using an optimised choice and he obtained satisfactory results.

2.2.3 Methods based on Mode Shape Curvatures/Strain Mode Shapes

In theory, changes in the mode shapes could be used to detect damage, however, the change is usually so small that detection of damage is of difficulty. An alternative to using mode shapes is to adopt mode shape derivatives such as curvatures for damage detection which still contain spatial information about changes in structural vibration characteristics. The mode shape curvature of a structure can be computed from the modal displacement or accelerations. For beams, plates, and shells, there is a direct relationship between curvature and bending strain, and some researchers also examine the practical possibility to obtain the curvature by measuring strain directly.

Pandey et al (1991) suggested the application of mode shape curvature for detecting damage. By using an analytical cantilever and a simply supported beam model, it is shown here that the absolute changes in the curvature mode shapes are localized in the region of damage and hence can be used to detect damage in a structure. Finite element analysis was used to obtain the displacement mode shapes of the two models. By using a central difference approximation, curvature mode shapes were then calculated from the displacement mode shapes as,

$$\phi''_{q,i} = \frac{\phi_{q-1,i} - 2\phi_{q,i} + \phi_{q+1,i}}{h^2} \qquad (2.5)$$

where h is the length of each of the two elements between the DOF (q-1) and (q). An advantage in using Equation (2.5) is that when healthy mode shapes are also obtained from measurement, there is no need to develop an analytical model of the structure. In addition, rotational components of the mode shapes need not be measured, and the mode shapes can be normalized in any arbitrary manner, as long as the same procedure is used in the normalization for both healthy and damaged structures.

Chance et al (1994) found that numerically calculated curvature for mode shapes could introduce unacceptable errors. Instead of measuring or computing curvature directly, they used measured strains and achieved dramatic improvement in the results of damage identification. Nwosu et al (1995) evaluated strain changes with the introduction of a crack in a tubular T-joint. They found these changes to be much greater than any frequency shifts and they can be measured even at a relatively large distance from the crack.

Though measuring the rotation of mode shapes is more difficult than measuring the translational mode shapes, Abdo and Hori (2002) forecasted that the rotation of mode shapes may be feasible to be measured in the near future and found that the rotation of mode shape is a sensitive indicator of damage in a numerical study where the results show that the rotation of mode shape has the characteristic of localization at the damaged region even though the displacement modes are not localized. Also, the results illustrate that the rotational mode shapes are robust in locating multiple damage locations with different sizes in a structure. Furthermore, using the changes in the rotation of mode shape does not need very fine grid of measurements to detect and locate damage effectively.

Despite the advantage of providing spatial information on the structural damage, methods using mode shapes and their derivatives suffer from several drawbacks in practical applications: 1) a large number of measuring points are needed in order to obtain the mode shapes for a complex structure; 2) mode shape measurements are sensitive to random errors and show more statistical variation than resonant frequencies; 3) rotational mode shapes, though more sensitive to structural changes than translational

mode shapes, are still difficult to obtain with current modal test techniques; 4) the mode shape based methods, especially the curvature techniques, are not generally applicable to a structure of any shape.

2.2.4 Methods based on Modal Flexibility Changes

In general, higher modes contain more information of local changes of structures than lower modes. However, it is increasingly difficult to measure higher frequency response data due to practical limitations in experimental modal test. To overcome this difficulty, another class of damage detection methods using the flexibility matrix to estimate changes in structural stiffness appeared. Generally the flexibility matrix can be estimated from the mass-normalized measured mode shapes and frequencies. The formulation of the flexibility by this method is called modal flexibility. A commonly accepted feature of modal flexibility, related to vibration-based damage detection, is the fact that modal flexibility can be approximately estimated from a few lower modes of the structure. As this feature inherently overcomes the shortcoming of mode incompleteness of measured modal data, many research efforts have been conducted on this subject.

Raghavendrachar and Aktan (1992) examined the application of modal flexibility for a three span concrete bridge. In their comparison, the modal flexibility is found to be more sensitive to local damages than natural frequencies or mode shapes. Aktan et al (1994) proposed the use of measured flexibility as a “condition index” to indicate the relative integrity of a bridge. They applied this technique to two bridges and compare the measured flexibility with the static deflections induced by a set of truck-load tests. Pandey and Biswas (1994) presented evaluation of changes in the flexibility matrix of a

structure as a candidate method not only for identifying the presence of the damage but also locating the damage. It is shown that the flexibility matrix can be easily and accurately estimated from a few of the lower frequency modes of vibration of the structure, which can be easily measured. Lu et al. (2002) pointed out that Pandey and Biswas's method is difficult to locate multiple damages, and recommended the modal flexibility curvature for multiple damage localization due to its high sensitivity to closely distributed structural damages.

Toksoy and Aktan (1995) measured the flexibility of a bridge and examined the cross-sectional deflection profiles with and without a baseline data set. Mayes (1995) used measured flexibility to locate damage from the results of a modal test on a bridge. He also proposed a method for using measured flexibility as the input for a damage-detection method (STRECH) which evaluates changes in the load-deflection behavior of a spring-mass model of the structure. Doebling et al (1996b) proposed a technique to estimate unmeasured residual flexibility matrix. The residual flexibility matrix represents the difference between the exact flexibility matrix and the measured dynamic flexibility matrix, which is contributed from modes outside the measured bandwidth. Zhao and Dewolf (1999) presents a sensitivity study comparing the use of natural frequencies, mode shapes, and modal flexibilities for monitoring. The results demonstrate that modal flexibilities are more likely to indicate damage than either natural frequencies or mode shapes.

Zhang and Aktan (1995 and 1998) analyzed the modal flexibility and its derivative, called uniform load surface (ULS), which is defined as the deformed shape of the structure when subjected to a uniform unit load. The ULS is found to have much less

truncation effect and is least sensitive to experimental error. They also discuss how to utilize pre-test analysis to determine the test frequency band that will lead to the least truncation error. Wu and Law (2004b) developed a damage localization method based on changes in uniform load surface (ULS) curvature for two-dimensional plate structures. A new approach to compute the ULS curvature is proposed based on the Chebyshev polynomial approximation, instead of the central difference method.

The main advantage of the methods using modal flexibility attributes to the fact that the flexibility matrix can be approximately synthesized from a few lower natural frequencies and mode shapes. Furthermore, the flexibility matrix is insensitive to mass changes compared to the stiffness matrix (Berman and Flannelly, 1971). Computation of damage index based on modal flexibility is simple, fast and inexpensive through direct comparison of difference in modal flexibility before and after damage without the requirement of an analytical model of the structure. The disadvantage lies in that modal mass or mass-normalized mode shapes are required to estimate the modal flexibility. Thus, for ambient vibration tests from which the mass-normalized mode shapes cannot be extracted, there is no way to estimate the modal flexibility from the output-only measurements without certain assumptions or approximations.

2.2.5 Methods based on Modal Strain Energy Changes

To further seek an effective approach to identify structural damage, some researchers start to make use of mode shapes combined with structural finite element model to produce a new damage indicator such as the modal strain energy. The general

definition of modal strain energy of a structure with respect to the *ith* mode can be expressed as,

$$MSE_i = \frac{1}{2}\phi_i^T \mathbf{K} \phi_i \qquad (2.6)$$

where ϕ_i is the modal displacement shape of the *ith* mode, and **K** is the stiffness matrix of a structure. Chen and Garba, (1988) and Kashangaki et al., (1992) pointed out that the strain energy can be used for identifying structural damage.

This method as originally developed by Stubbs et al (1992) is applicable to beam type structures and is based on examining the decrease in modal strain energy between two structural DOFs, as defined by the curvature of the measured mode shapes. Topole and Stubbs (1995) adopted matrix structural analysis for obtaining a system of equations which relates the relative change of stiffness of structural members to a load vector generated from limited modal parameters of the damaged structure to perform damage evaluation. Stubbs and Kim (1996) improved the method by using the modal strain energy to localize and estimate the severity of the damage without baseline modal parameters.

Another development on the use of modal strain energy is presented by Law et al. (1998), named Elemental Energy Quotient (EEQ). The EEQ of the *j* th element and the *r* th mode is defined as,

$$EEQ_{rj} = \frac{\phi_r^T \mathbf{K}_j^e \phi_r}{\phi_r^T \mathbf{M}_j^e \phi_r} \qquad (2.7)$$

where $\mathbf{K}_j^e$ is the *j*th elemental stiffness matrix, $\mathbf{M}_j^e$ is the *j*th mass matrix.

Shi et al. (1998) proposed the concept of the Elemental Modal Strain Energy (EMSE) and the Modal Strain Energy Change Ratio (MSECR) which could be a

meaningful indicator for damage localization. The authors also presented two damage quantification algorithms based on sensitivity analysis of modal strain energy (Shi et al., 2000b; Shi et al., 2002).

2.2.6 Methods based on Frequency Response Function

Since indirectly measured modal data contain accumulative errors caused in modal parameter extraction and provide much less information than FRF data, it is more reasonable and reliable to use directly measured FRF data for structural damage detection.

Samman et al (1991) used a scaled model of a typical highway bridge to investigate the change in FRF signals caused by the development of cracks in its girders by a pattern recognition method which utilized the integer slope and curvature values of FRF wave forms, rather than peak magnitude. Only one FRF reading per girder is required to detect relatively minor cracks and locate crack approximately. Wang and Liou (1991) presented a new method to identify joint parameters by using the two sets of measured FRFs of a substructure with and without the effect of joints. Some strategies are applied to overcome the measurement noise problem that may result in false identification. Law et al (1992) developed the sensitivity from a formulation based on the change in the FRF at any point, rather than just at the resonances. In practice, many points of the FRF around the resonances are taken, and a least squares fit is used to determine the changes in the physical parameters.

Biswas et al (1994) utilized the frequency response function obtained by exciting the structure at a selected reference point as the preferred form of vibration signature for interrogation. The chain code computer vision technique is modified to evaluate the

frequency response function signature as a waveform from a ribbed plate in the laboratory, similarly a highway bridge. Successful performance of the technique in the presence of noise indicates the potential for fault diagnosis of large outdoor structures. Chaudhry and Ganino (1994) used frequency response data obtained from a pieoelectric actuator/sensor pair bonded to a composite/aluminum beam structure with a debond between the interface to train an artificial neural network by back propagation to identify the severity and presence of delamination with substantial accuracy. Juan and Dyke (2000) presented and experimentally verified a new technique to identify damage based on changes in the component transfer functions in the floors of a structure. Multiple locations of damage can be identified and quantified using this approach.

The application of FRFs has been done by many other researchers. Park and Park (2003) suggested a damage detection method not based on an accurate analytical finite element model but based upon incompletely measured frequency responses, noting that the reduced dynamical system is an inverse of incompletely measured frequency responses. Hwang and Kim (2004) presented methods to identify the locations and severity of damage in structures using frequency response function (FRF) data where the preferred technique used only a subset of vectors from the full set of FRFs for a few frequencies, and it calculates the stiffness matrix and reductions in explicit form. Huynh et al (2005) presented a method for structural damage detection using frequency response functions (FRF) obtained from non-destructive vibration tests and they showed that this method can overcome the problems of coordinate incompatibility and noise and deliver encouraging results on damage detection. Ni et al (2006) presented an experimental

investigation of seismic damage identification of a 38-storey tall building model using measured frequency response functions (FRFs) and neural networks (NNs).

2.3 Model Updating Methods

Another large class of damage identification methods is model updating methods whose basic idea is the modification of a structural model to reproduce as closely as the measured static or dynamic responses from the damaged structure. Model updating algorithms are the algorithms to obtain the updated matrices (or perturbations to the original model that produce the updated matrices) based on the governing equations of structural motion, the original model and the measured data. The model is usually constructed by the stiffness, mass, and/or damping matrices assembled based on finite element theory. Comparisons of the updated matrices to the original model correlated to the intact structure provide an indication of the location and extent of damage.

In application, the model updating algorithms are usually applied in both damage detection applications and model improvement applications with similar purposes, i.e. to seek an analytical model that is as close to the real structure as possible. However, there are the differences in application objectives between model improvement and damage detection, and one should pay attention to some particular issues for discriminating and relating the usage to model updating methods in these two categories.

The purpose of model improvement is to seek an accurate model correlated to the real structure for predicting the response of the structure to disturbances and suggesting the modifications in the structural configuration for performance improvements. In the

construction of the original finite element model it is usual to make some simplifying assumptions. Often there are detailed features in the geometric representation of the structure that can not be modeled by a computationally economical finite element mesh, or the boundary conditions and joints between components are seldom fully understood. In such cases the analyst may, according to experienced engineering judgments, manage to find a compromise which acceptable results.

The damage detection applications aim to identify changes in stiffness, mass and damping matrices due to damage excluding the modeling errors. The major differences between the model updating and damage detection can be briefly explained as: the objective of the model updating is to obtain an improved finite element model so that model predictions match the measured data in an optimal way, while the damage detection is the process of locating areas of local stiffness or strength degradation in this context.

In general, the damage detection or finite element refinement approaches can be further classified into the following four categories: (1) Optimal matrix updating method, (2) Sensitivity-based updating method, (3) Eigenstructure assignment method, (4) Stochastic model updating method.

2.3.1 Optimal Matrix Updating Method

Optimal matrix updating algorithms are the methods which try to find an updated matrix (stiffness and/or mass) that is as close as possible to the original matrix that produces the measured frequencies and mode shapes by using optimization of functions.

Smith and Beattie (1991) and Zimmerman and Smith (1992) have done relevant review of these methods.

Rodden (1967) did the early work in optimal matrix updates using measured test data by using ground vibration test data to determine the structural influence coefficients of a structure. Brock (1968) examined the problem of determining a matrix that satisfied a set of measurements as well as ensuring its symmetry and positive definiteness. Hall (1970) presented an approach to optimize the stiffness matrix by minimizing the least-squares difference formed between the analytical modes and experimental modes with the assumption that the mass matrix is exact.

Constrained minimization theory has also been applied to the optimal matrix updating algorithms. Berman and Flannelly (1971) presented the theory of incomplete models of dynamic structures and discussed the computation of system matrices using incomplete data. Baruch (1978) proposed a method by which a given stiffness matrix can be corrected optimally by using corrected mode shapes and natural frequencies obtained from vibration tests with a proper constraint, and a similar method is applied to correct optimally a given flexibility matrix. Berman (1979) questioned the assumption of the exact mass matrix, and established a so-called analytical model improvement (AMI) procedure to adjust the stiffness and mass matrix simultaneously. Berman and Nagy (1983) developed a method that uses measured normal modes and natural frequencies to improve an analytical mass and stiffness matrix model of a structure. The method directly identifies, without iteration, a set of minimum changes in the analytical matrices which force the eigensolutions to agree with the test measurements.

Optimal matrix updating techniques for damage detection were further developed by Kabe (1985) who introduced a procedure to use, in addition to mode data, structural connectivity information to optimally adjust deficient stiffness matrices. The adjustments are performed such that the percentage change to each stiffness coefficient is minimized. The physical configuration of the analytical model is preserved and the adjusted model will exactly reproduce the modes used in the identification. McGowan et al (1990) also used structural connectivity information in their stiffness adjustment algorithms for damage identification, in which mode shape expansion algorithms are employed to extrapolate the incomplete measured mode shapes to be comparable with analytical predicted modes.

Later, iterative techniques are adopted in optimal matrix updating methods. Mottershead and Shao (1991) utilized a cost function minimizing output errors to tune an analytical model. The output errors include frequency changes and response displacement changes. Gauss-Newton iterative approach is applied to solve the least squares problem. Smith (1992) presented an iterative technique to the optimal update problem that enforces the sparsity of the matrix at each iteration step. The sparsity is enforced by multiplying each entry in the stiffness update by either one or zero, depending on the correct sparsity pattern. The minimum rank perturbation theory is also proposed to apply in the matrix updating methods. Zimmerman and Kaouk (1994) revealed that perturbation matrices tend to be of small rank because damage is usually located in a few structural members rather than distributed all over the structure. They presented an algorithm based on the basic minimum rank perturbation theory that a unique minimum rank matrix solution for an under-determined structure exists. Further research is subsequently conducted by them

and their colleagues. Kaouk and Zimmerman (1994, 1995) adopted the concept of the minimum rank perturbation theory (MRPT) to determine the damage extent on the mass properties of an undamped structure and proportionally damped structures. For proportionally damped structures, the MRPT is used to find the damage extent in any two of the three structural property matrices (mass, damping, or stiffness). Doebling (1996) presented a method to compute a minimum-rank update for the elemental parameter vector, rather than for global or elemental stiffness matrices.

Although the optimal matrix update method, with constraints based on structural vibration mechanics and physical connectivity, may be useful in an engineering sense for the model refinement problem, its applicability for damage detection is doubtful. It is because the damage typically causes local changes in the stiffness matrix only at some locations, whereas the optimal matrix update would tend to have the changes throughout the entire stiffness matrix and it could not identify the damage location.

2.3.2 Sensitivity-based Updating Method

The sensitivity-based method is another class of model updating method which is based on the solution of first-order Taylor series that minimizes a function of residual errors caused by structural matrices perturbations. The residual r_i characterizing the differences between the damaged and intact state can be formulated for modal parameters such as real eigenvalues λ_i, mode shape ϕ_i and so on, frequency response functions (FRFs) and time response $d(t)$ and so on. A linear or sequentially linearized relation is required of the form as,

$$\mathbf{S} \cdot \delta\mathbf{p} = \mathbf{r} \tag{2.8}$$

$\delta\mathbf{p}$ is the perturbation in the unknowns. Equation (2.8) expresses the effects of parameter changes due to changes of the measured vibration data included in the residual vector $\mathbf{r}$. $\mathbf{S}$ is the sensitivity matrix, which is used here in general use.

An exhaustive classification of various sensitivity-based updating techniques was given by Hemez (1993). Going back to the earlier work, Jahn (1948) derived the complete formulae for eigenvalue and eigenvector sensitivities in a first-order Taylor series for a standard eigenproblem. Fox and Kappor (1968) present the exact expressions for the rates of change of eigenvalues and eigenvectors with respect to the design parameters of the actual structure, and indicates that these derivatives can be used successfully to approximate the analysis of new structural designs. To essentially avoid such difficulties, Nelson (1976) presented a simplified procedure for the determination of the derivatives of eigenvectors of *nth* order algebraic eigensystems which can be applicable to symmetric or nonsymmetric systems, and requires knowledge of only one eigenvalue and its associated right and left eigenvectors. Ting (1992) developed an accelerated subspace iteration method for calculating eigenvector derivatives by identifying factors affecting the effectiveness and the reliability of the subspace iteration, and presented effective strategies concerning these factors.

The earliest application of eigen-sensitivity analysis to finite element model updating is proposed by Collins et al. (1974). Based on the work of Collins et al, Chen and Garba (1980) proposed a matrix perturbation method to calculate the Jacobian matrix and to compute the new eigendata for the parameter estimation procedure with the advantages of the applicability to large complex structures without knowing the analytical expressions for the mass and stiffness matrices and the need of a cost effective

approach for the recomputation of the eigendata. Hajela and Soeiro (1990) used the sensitivity method and nonlinear optimization technique to study the damage detection problem. Lin et al (1995) suggested employing both analytical and experimental modal data to calculate the eigen-sensitivities. Such accurately determined eigensensitivity coefficients are then used in the classical model updating procedure to overcome the existing difficulties of identifying small magnitude model errors and slow convergence.

Zhang et al. (1987) further improved the solution condition of the inverse problem by reducing the number of unknowns through early localization of the significant model errors. Jung and Ewins (1992) suggested dividing the model updating procedure into two sessions, with the first session to locate major errors in grouped macro elements, then to refine the analytical model in the second session. Law et al (2001) applied the super-element modeling technique to improve the finite element model of a bridge deck structure based on a similar consideration. The large number of DOFs in the original analytical model is dramatically reduced and the solution condition is improved.

In addition to the most popular natural frequencies and mode shapes adopted to estimate the sensitivity matrix, other types of data, e.g., FRF, time histories of responses, or combination of these, can also be used in the sensitivity-based model updating methods. Ziaei-Rad (1997) developed a FRF-based model updating by expanding the inverse matrix of FRF as a Taylor series function with respect to structural parameters. Numerical examples and experimental examples are applied to update the analytical model so that the FRFs match those obtained in testing. Ziaei-Rad and Imregun (1996) further discussed the experimental error bounds for convergence of this updating algorithm. The sensitivity of the modal strain energy (MSE) to damage is also derived

and used in damage identification (Shi et al., 2000b). Abdel (2001) studied the application using the sensitivity-based updating approaches, in which the sensitivity of the natural frequencies, mode shapes and modal curvatures to damage are combined to construct the sensitivity matrix.

A structural damage detection method through the sensitivity-based finite element model updating procedure was presented by Hemez and Farhat (1995). They formulated the sensitivities at the element level. This allows the identification to focus on the structural members susceptible to damage, and also improves the computational efficiency comparing with the sensitivity analysis in system level. Lu et al (2007) proposed a method directly using sensitivity of acceleration response with respect to structural parameters for damage detection. The merits of the method lie in the use of a few sensors in the measurement.

2.3.3 Eigenstructure Assignment Method

Eigenstructure assignment method is another typed matrix updating method which is based on the design of a fictitious controller that would minimize the modal force error. The controller gains are then interpreted as parameter matrix perturbations to the undamaged structural model. Andry et al. (1983) presented an excellent overview of eigenstructure assignment theory and applications. This procedure for eigenstructure assignment methods will result in modifications to the stiffness and damping matrices but the mass matrix remains unchanged. The updated stiffness and damping matrices are given by

$$\mathbf{K} = \mathbf{K}_A + \mathbf{B} \cdot \mathbf{G} \cdot \mathbf{C}_o, \quad \mathbf{C} = \mathbf{C}_{\mathrm{A}} + \mathbf{B} \cdot \mathbf{G} \cdot \mathbf{C}_{\mathrm{s}} \tag{2.9}$$

where $\mathbf{G}$ is the feedback gain matrix determined by the eigenstructure assignment method. $\mathbf{B}$ is an input distribution matrix which may be chosen arbitrarily. $\mathbf{K}$ and $\mathbf{C}$ are the updated stiffness and damping matrices respectively, $\mathbf{K}_A$ and $\mathbf{C}_A$ are the original stiffness and damping matrices respectively. $\mathbf{C}_o$ and $\mathbf{C}_s$ are the matrices relating the outputs and states. Because the obtained correction matrix $\mathbf{B}\cdot\mathbf{G}\cdot\mathbf{C}_o$ and $\mathbf{B}\cdot\mathbf{G}\cdot\mathbf{C}_s$ are generally non-symmetric, a further process of determining the matrices $\mathbf{C}_o$ and $\mathbf{C}_s$ iteratively may be needed until symmetric correction matrices are acquired.

Minas and Inman (1990) proposed two techniques for FEM refinement. The first one assigns both eigenvalue and eigenvector to produce updated damping and stiffness matrices. An unconstrained numerical nonlinear optimization problem is posed to enforce symmetry of the resulting model. The second approach uses only the eigenvalue information in which a state-space formulation is used to determine the state matrix that has the measured eigenvalues closest to the original state matrix. Zimmerman and Widengren (1990) developed a symmetric eigenstructure assignment algorithm to improve structural models by incorporating measured structural modal parameters from a control aspect for linear structures with non-proportional damping. Residual damping and stiffness matrices are determined such that the improved analytical model eigenstructure matches more closely to that obtained experimentally.

Eigenstructure assignment methods were directly used in the area of structural dynamics firstly by Zimmerman and Kaouk (1992) who utilize a symmetric eigenstructure assignment algorithm to perform the partial spectral assignment for detecting and locating structural damage by incorporating measured modal data into an existing refined finite element model. The algorithm can enhance mode shape

assignability and to preserve sparsity in the damaged FEM are developed. Lindner and Goff (1993) used an eigenstructure assignment technique to identify the damage coefficient defined for each structural member and demonstrated by a numerical simulation with the finite element model of a ten-bay truss structure for detecting damage.

Lim (1994, 1995) applied a constrained eigenstructure assignment technique to process the measured incomplete modal data from a twenty bay planar truss. The feedback gain matrix is diagonalized, and the diagonal members are interpreted as element-level perturbations to the stiffness matrix so that the damage is localized directly. Lim and Kashangaki (1994) presented a method by computing the Euclidean distances between the measured mode shapes and the best achievable eigenvectors to determine the location and magnitude of damage in a space truss structure. The best achievable eigenvectors are the projection of the measured mode shapes onto the subspace defined by the refined analytical model of the structure and the measured frequencies. A technique similar to eigenstructure assignment known as FRF assignment was presented by Schultz et al (1996) who formulated the problem as a linear solution for element-level stiffness and mass perturbation factors and illustrated that using FRF measurements directly to solve the problem is more straightforward than extracting mode shapes. Cobb and Liebst (1997) made use of the cost-function minimization which is based on an assigned partial eigenstructure algorithm to obtain damaged elements from measured modal data using an incomplete measurement set.

2.3.4 Stochastic Model Updating Method

The efficiency of the damage identification algorithm relies on accuracy of the analytical model and the measured vibration data. Most studies assume that the analytical model is precise enough to represent the vibration properties of the structure and the measurements are accurate as well. In practice, however, there are many uncertainties during model updating procedure such as the FE modeling error and measurement noise (Friswell et al, 1997b). Uncertainties in the analytical model exist due to inaccurate physical parameters, non-ideal boundary conditions and structural non-linear properties. The corruption of the measured vibration data is inevitable no matter how precise the instrumentation is, whereby the measurement noises are generally characterized to have a zero mean and their magnitude depend on the experimental equipment. So it is necessary to study the effects on damage detection by model updating, as well as to estimate the resulting statistics of the identified results. For simplicity, the stochastic model updating or statistical system identification can be described as follows: If the statistics of measured vibration data were given, then determine the statistics of structural parameters in the updated FE model and assess the reliability of the structural safety.

Collins et al (1974) first derived a statistical identification procedure by treating the initial structural parameters as normally distributed random variables with zeros means and specified covariance and used experimental measurements of the natural frequencies and mode shapes of a structure to modify stiffness and mass characteristics of a finite element model and they demonstrated the convergence and versatility of the method by numerical examples. Using the sensitivity analysis of Collins et al, Ricles and Kosmatka (1992) utilized mass and stiffness uncertainties to locate potential damaged regions and evaluate the estimate of the damage. Tavares et al (1993) validated the work

of Ricles and Kosmatka using experimentally obtained modal data from a three-dimensional four-bay truss.

The commonly developed approach for uncertainty propagation is the Monte Carlo Simulation (MCS) method which first generates large amounts of samples following the predefined probability density functions (PDFs) or the joint PDFs of modal properties. Then, model updating algorithm is repeatedly carried out for these samples to obtain the corresponding solution samples of updating parameters. The PDFs of updating parameters are finally determined based on the solution samples. Agbabian et al (1988) employed the MCS method to identify the statistical properties of stiffness coefficients in a linear system and generated the time histories of the applied excitation as well as the accelerations, velocities, and displacements of a system. By separately applying the model updating procedure to different time segments, ensembles of stiffness coefficients were identified. Their work has been later extended to statistical identification of a nonlinear system approximated by an equivalent linear system (Smyth et al., 2000). Banan et al (1994a, b), Sanayei and Saletnik (1996a, b), Yeo et al (2000) and Zhou et al (2003) adopted similar approaches for studying the effects of measurement noise on identification results. However, the MCS method is by itself computationally intensive as it requires a large number of simulations to obtain accurate and valid statistics.

Another technique for uncertainty propagation is perturbation method. It has been applied very successfully in the discipline of stochastic structural analysis where the perturbation technique in conjunction with the FE analysis is applied to evaluate the response variability and failure probabilities associated with prescribed limit states (Kleiber and Hien 1992). Perturbation method expands the nonlinear function in terms of

random variables either by a linear function or by a quadratic one at a particular point. Second moment technique is then applied to evaluate the mean and standard deviation of the response, or to evaluate the failure probabilities. Liu (1995) considered the measurement noise effect on the damage detection with the perturbation method and Monte Carlo Simulation algorithm by describing the identification of structural parameters as a linear least squares problem with each term expanded in a system of linear equations in terms of random modal properties. Papadopoulas and Garcia (1998) presented a two-step probabilistic method for damage assessment to determine the statistics of stiffness coefficients (SC) of the damaged structure. They first used the measured statistical changes in modal frequencies and mode shapes to obtain the statistics of stiffness reduction factor (SFR). These statistics of SFR along with the statistics of SC corresponding to healthy structure are then combined to determine the statistics of SC of the damaged structure. A set of graphical and statistical probability damage quotients was then used to assess the existence of damage by the comparison of statistics of SC before and after damage. Later, Xia et al (2002, 2003) developed a statistical damage identification algorithm based on changes of frequency and mode shape to account for the effects of random noise on both the vibration data and finite element model. The statistics of the parameters are estimated by the perturbation method and verified with Monte Carlo technique. Other researches addressing the statistical parameter estimation using uncertain modal data include the work of Katafygiotis and Beck (1998), Li and Roberts (1999a, b), and Yuen and Katafygiotis (2005).

2.3.5 Regularization Techniques

Model updating is usually adopted for damage detection. However, model updating is an inverse problem, and the characteristic feature of an inverse problem is that it may be ill-posed. A problem is well-posed if its solution exits, is unique, and continuously depends on errors present in problem formulation. If the problem fails to fulfill any of these conditions, then it is said to be ill-posed. The existence and uniqueness is often assured by the introduction of additional assumptions, leading to some generalized solution of the problem, such as the normal pseudosolution (Yagola et al., 2002), i.e. a minimum norm solution. The solution stability, that is the dependence of the solution on perturbations in the data, can be violated even when the solution exists and is unique (Phillips, 1962).

Research in this area has built on the early work of Tikhonov (1977), who defined the regularized solution $x(\lambda)$ as the minimization of the weighted combination of the residual norm and the side constraint (quadratic cost function)

$$\left\|\mathbf{Ax}-\mathbf{b}\right\|_2^2+\lambda\left\|\mathbf{Lx}-\mathbf{d}\right\|_2^2 \qquad (2.10)$$

The basic idea is to minimize the cost function in Equation (2.10) by searching for a solution $\mathbf{x}(\lambda)$ which at the same time produces a small residual $\left\|\mathbf{Ax}-\mathbf{b}\right\|_2^2$ and a moderate value of the side constraint $\left\|\mathbf{Lx}-\mathbf{d}\right\|_2^2$. The way in which these two terms are balanced depends on the size of the regularization parameter λ.

Early work on the application of Tikhonov method to system identification and model updating includes those of Rothwell and Drachman (1989), Ojalvo and Ting (1990), Mottershead and Foster (1991), and Fregolent *et al.* (1996). In these studies the Tikhonov parameter was determined through trial-and-error. Busby and Trujillo (1997)

studied the effect of Tikhonov regularization in the reconstruction of dynamic loadings from the strain measurement. They applied both the L-curve method (LCM) and generalized cross validation (GCV) to choose the optimal regularization parameter. Ahmadian et al (1998) investigated the ill-posed problem of selecting a side constraint and determining the regularization parameter in model updating by determining the weight attached to the constraint by the regularization parameter. The authours found that the method of cross validation can be used reliably to truncate the small generalized singular values which contain the measurement noise. The L-curve approach is similarly robust in locating the regularization parameter, and this is demonstrated in a physical experiment. Ziaei-Rad and Imregun (1999) summarized the existing regularization methods applied to model updating. They further examined the performance of Tikhonov regularization, truncated SVD, total least squared method, and the maximum entropy method for FRF-based model updating technique. Mares *et al.* (2002) explored the robust estimation technique and Tikhonov regularization method for the output-error-based model updating using measured modal frequencies, and applied an uncertainty bound model and LCM to determine the regularization parameters.

Truncated SVD is another form of regularization by truncating the last several smallest SVs to improve the conditioning of matrix. Likewise, the difficulty existing in this type of regularization is the determination of the truncation parameter. A trial-and-error procedure is used by Mottershead and Foster (1991) to determine the truncation parameter. D'Ambrogio and Fregolent (1998) determined the truncation parameter by simultaneous minimization of the natural frequency error and the response residual error. Ren (2005) presented a method for determination of the truncation level. In his method,

those SVs, the ratios of which to residual norm are smaller than a prescribed value, are disregarded. However, the success of the method depends on the choice of the prescribed value which was not discussed in the study. A small value could cause the divergence in the computation, while a large value would lead to a low convergence rate.

Other work on regularization techniques was done by Natke (1992a, 1992b) who advocated the application of regularization techniques in model updating. Fregolent et al (1996) considered a variety of methods for determining the regularization parameter in the equation error problem. Friswell et al (1995) pointed out that the regularization has become a central issue in system identification, because the dynamic behavior is observed in a narrow knowledge space and, consequently, the systems of equations are strongly under-determined. Yeo et al (2000) presented a damage assessment algorithm for framed structures based on a system identification scheme with a regularization technique by proposing a new regularization function based on the Frobenius norm of the difference between the estimated and the baseline stiffness matrix.

2.4 Wavelet Transform based Methods

All dynamic response based approaches require modal properties with the aids of the traditional Fourier transform (FT). In fact, there are a few inherent characteristics of FT that might affect the accuracy of damage identification. First, the FT is in fact a data reduction process and information about structural health might be lost during the process (Gurley and Kareem 1999). Then, FT is a global analysis. The basis functions are global functions. Any perturbations of the function at any point in the time domain will influence every point in the frequency domain. So it means that the FT cannot present the

time dependency of signals and it cannot capture the evolutionary characteristics that are commonly observed in the signals measured from naturally excited structures. Damage is typically a local phenomenon which tends to be captured by higher frequency modes (Doebling et al., 1998). These higher frequencies normally are closely spaced but poorly excited. All these factors add difficulty to the implementation of FT-based damage detection techniques.

There has been increasing interest in the wavelet-based approach in recent years due to successes of the wavelet-based methods in several applications. The wavelets decompose a signal using a short-duration wave allowing a refined decomposition rather than decomposition with infinite-duration sinusoids as with Fourier transforms. The short-duration wave, known as the wavelet basis, generally has a higher energy density than the sinusoid in Fourier transforms. Therefore, the wavelets would require fewer coefficients than Fourier transforms to describe a signal in many cases. The wavelet transform is a two-parameter transform. For time signals, the two domains of the wavelet transform are time t and scale a. The scale a can be approximately related to the frequency w. The main advantage gained by using wavelets is the ability to perform local analysis of a signal, i.e. to zoom on any interval of time or space. Wavelet analysis is thus capable of revealing some hidden aspects of the data that other signal analysis techniques fail to detect. This property is particularly important for damage detection applications. The wavelet transform is becoming as a promising new tool for damage identification in structural system.

Reda Taha et al (2006) wrote an exposition on the application of the current WT technologies in structural health monitoring (SHM). They discussed the specific needs of

SHM addressed by WT, classified WT for damage detection into various fields, and described features unique to WT that lend itself to SHM.

The mathematical foundation of wavelets was developed by Meyer (1992). Daubechies (1992) and Mallat (1998) pushed the application of wavelet from pure mathematical theory by defining the connection between wavelets and digital signal processing. Wavelets have been applied to a number of areas, including data compression, image processing and time-frequency spectral estimation. The earliest work on applying wavelet analysis in structural damage detection dates back to the work of Yamamato and his group in 1995, in Kyoto, Japan. The research group of Yamamato and a group at Worcester Polytechnic Institute (WPI), headed by Noori and Hou, collaborated in advancing this new technique further in 1996.

The application of wavelet analysis in damage detection includes many aspects such as time-frequency analysis, wavelet spectrum, orthogonal or discrete wavelet decomposition, wavelet-based data compression, denoising and feature extraction, linear and nonlinear system identification and image processing. In damage detection, WT applications can be classified into four areas: composite plates, large-scale structures like bridges, civil infrastructure and mechanical systems.

Kumara et al. (1999) and Sohn et al. (2003) suggested using continuous wavelet transform (CWT) to detect delamination of composite structures. The system is designed to analyze the responses of an active SHM system using piezoelectric sensors. Damage detection is performed by observing the signal energy in a wavelet scalogram. Rus et al. (2004) showed that the CWT can be used to discriminate between degraded and intact composite. Damage occurrence in thin walled composite structures, ‘sandwich panels’,

can be detected using a combined WT and finite element algorithm. Qi et al. (1997) showed that wavelet multi-resolution analysis (WMRA) can not only detect damage but also detect particular levels of damage. They demonstrated that the energy computed from decomposed signals at three specific frequency ranges was related to three different damage modes in a carbon fiber reinforced polymer (CFRP) composite. Dawood et al. (2002) showed successful WMRA de-noising of signals with Bragg grating sensors contaminated with noise from thermal effects of a structural composite. Yan and Yam (2004) used the energy spectrum and wavelet packet analysis with an index vector to detect small structural damage. Their index vector is used in a non-dimensional comparison of intact and delaminated plates. The maximum value of the index vector at a particular wavelet decomposition level indicates damage due to an excited and damaged mode.

Wang and Deng (1999) discuss a structural damage detection technique based on wavelet analysis of spatially distributed structural response measurements. The premise of the technique is that damage (e.g. cracks) in a structure will cause structural response perturbations at damage sites. Such local perturbations, although they may not be apparent from the measured total response data, are often discernible from component wavelets. Wang and McFadden (1995) discussed the use of the orthogonal wavelet transform to detect abnormal transients generated by early gear damage from the vibration signal of a gearbox casing. Orthogonal wavelets, such as Daubechies 4 and harmonic wavelets, are used to transform the time domain synchronous vibration signal into the time-scale domain. Staszewski and Tomlinson (1997) presents an application of

the wavelet transform in the detection of a damaged tooth in a spur gear based on a similarity analysis of patterns obtained from the modulus of the wavelet transform.

One possible drawback of the WT is that the frequency resolution is quite poor in the high frequency region. The wavelet packet transform (WPT) is one extension of the WT that provides complete level-by-level decomposition. The wavelet packets are alternative bases formed by linear combinations of the usual wavelet functions (Coifman, 1992). As a result, the WPT enables the extraction of features from signals that combine stationary and nonstationary characteristics with arbitrary time-frequency resolution. Learned and Willsky (1995) contributes to this ongoing investigation through the development of a non-parametric wavelet packet feature extraction *procedure* which identifies features to be used for the classification of transient signals for which explicit signal models are not available or appropriate. Wu and Du (1996) introduces a new method of feature extraction and feature assessment using a wavelet packet transform for the monitoring of machining processes. Four criteria are proposed To assess the effectiveness of the selected features in both time and frequency domains. Accordingly an automatic feature extraction procedure is developed. Sun et al (2002a, 2002b) proposed a WPT based method for the damage assessment of structures. Dynamic signals measured from a structure are first decomposed into wavelet packet components. Component energies are then calculated and used as inputs into neural network models for damage assessment. Chang and Sun (2005) proposed a wavelet packet based method for identifying damage occurrence and damage location for beam-like structures by calculating the wavelet packet signature (WPS) that consists of wavelet packet component signal energies. One advantage of the proposed method is that it does not

require any mathematical model for the structure being monitored and hence can potentially be used for practical application.

2.5 Damage Identification based on Direct Use of Vibration Time Series Responses

All damage detection methods reviewed above make use of modal parameters. Modal extraction procedure is needed to obtain the modal parameters and it will cause the loss of some important structural information which affects the results of damage identification. There are also many publications on damage detection based on direct use of structural time series response without the need of modal extraction procedure.

Time histories of the vibration response of the structure are used to identify the presence of damage by Cattarius and Inmanm (1997) who presented a non-destructive approach based on acceleration responses to examine structural damage. They constructed two simple finite element models to examine axial as well as transverse vibrations. The knowledge gained from simulations led to a series of experiments which substantiated the potential of the proposed method. Comparison of time responses, e.g., displacement of velocity, due to different material defects revealed the existence of damage in cases where measured frequency shifts were minimal.

Earlier, Seibold and Weinert (1996) proposed a method to localize cracks in rotating machinery based on measured vibrations. This method used a time domain identification algorithm: the Extended Kalman Filter (EKF). The localization is performed by designing a bank of EKFs, in which each filter is tuned to a different

damage hypothesis. By calculating the probabilities of different hypotheses, the crack can be localized and its depth can be determined.

Recently, Shi et al. (2000) and Chen and Li (2004) presented methods to identify structural parameters and input time history simultaneously from output-only measurements. The structural parameters and the input time history are obtained in an iterative manner. Zhu and Law (2007) proposed an approach for damage detection in a concrete bridge structure in time domain. Both the damage and moving vehicular loads are identified successfully.

Majumder and Manohar (2003) proposed a time domain approach for damage detection in bridge structures using ambient vibration data. The force actuator induced by a moving vehicle on the bridge is taken to be the excitation force. It was assumed that a validated finite element model for the bridge structure in its undamaged state is available. Alterations made to this initial model, simulating damages which cause changes in bridge behavior, are determined using a time domain approach. Based on the work, Majumder and Manohar (2004) developed the time domain damage detection scheme with time varying structural matrices, structural nonlinearities and spatial incompleteness of measured data, within the finite element modeling framework. The damage parameters associated with changes in structural stiffness are shown to be governed by a set of over-determined nonlinear equations which are solved iteratively. Illustrative examples on a geometrically nonlinear Euler–Bernoulli beam carrying a moving single degree-of-freedom oscillator are provided.

Ling and Haldar (2004) proposed a system identification procedure for nondestructive damage detection of structures, which is a finite element based time-

domain linear system identification technique capable of identifying structures at element level. The proposed algorithm can identify a structure without using input excitation information and can consider both viscous and Rayleigh type proportional damping in the dynamic model. Choi and Stubbs (2004) formed the damage index directly from the time response to locate and quantify damage in a structure. The measured response in the time domain is spatially expanded over the structure and the mean strain energy for a specified time interval is obtained for each element of the structure. The mean strain energy for each element is, in turn, used to build a damage index that represents the ratio of the stiffness parameter of the pre-damaged to the post-damaged structure. The damage indices are used to identify possible locations and corresponding severities of damage in the structure. Kang et al. (2005) presented a system identification scheme in time domain to estimate stiffness and damping parameters of a structure using measured accelerations, and the method is demonstrated with numerical simulation study on a two-span truss bridge and an experimental laboratory study on a three-story shear building model.

Besides the traditional means for time series damage detection, time responses are usually used with the aid of new techniques such as ARMA family models, genetic algorithm, neural network, wavelet transform etc. Sohn and Farrar (2000) applied statistical process control techniques to vibration based damage diagnosis. Firstly, an AR mode is fit to the measured acceleration time histories from an undamaged structure. Then, the AR coefficients obtained from subsequent new data are monitored relative to the baseline AR coefficients. Any significant deviation from the baseline of AR coefficients would indicate either a change in environmental conditions or damage. The statistical procedure combined with the AR time prediction model is applied to vibration

test data acquired from a concrete bridge column as the column is progressively damaged. Loh and Wu (2000) presented an experimental investigation of the Fei-Tsui arch dam through forced vibration tests and the analysis of seismic response data. In the identification of dam properties from seismic response data, the multiple input/multiple output discrete-time ARX model with least squares estimation was applied to consider the nonuniform excitation of the seismic input and the global behavior of the dam. To verify the accuracy of the identification results, comparisons between the discrete-time ARX model and a frequency domain conditioned spectral analysis were made.

Liu and Chen (2001) proposed an inverse identification technique to assess the presence, location, size and degree of flaw in the core layer of sandwich plates, where the time-harmonic response was used as the input for inverse analysis and the genetic algorithm (GA) is applied to search the parameters. Ishak et al (2001) described the application of Strip Element Method and adaptive Multilayer Perceptron Networks for inverse identification of interfacial delaminations in carbon/epoxy laminated composite beams. Further Ishak et al (2002) performed non-destructive evaluation of crack detection in beams using transverse impact with the aid of the beam model of wave propagation and adaptive multilayer perceptron networks. Examples showed that the procedure performs well for the determination of a wide range of location, depth and length of the crack.

A novel neural network-based strategy is proposed and developed for the direct identification of structural parameters from the time series dynamic responses of a structure without any eigenvalue analysis and extraction and optimization process by Xu et al (2004). Lu and Gao (2005) proposed a new method for damage diagnosis using

time-series analysis of vibration signals which is formulated in a novel form of ARX model with acceleration response signals.

With the help of the new mathematical tool-wavelet transform, Law et al. (2005) developed the sensitivity-based damage detection method basing on the wavelet packet energy of the measured accelerations and the method can identify damage of a structure from a few measurement locations. More recently the sensitivity matrix of response with respect to a system parameter is derived analytically (Lu et al 2007). But the damage detection results are subject to the effect of measurement noise and model error. Further, Law and Li (2006) used the wavelet coefficient sensitivity of structural response with respect to a system parameter for structural condition assessment. This sensitivity is shown to be more sensitive to local structural changes than the response sensitivity and it has the advantage in handling problem with model errors in the initial finite element model of the system. This is because the wavelet transform extracts separately different frequency component information from the response.

Method from direct use of acceleration responses is a promising tool for damage detection. There are many advantages over conventional modal methods. That is also one of the research focuses in the thesis.

2.6 Critical Issues and Shortcomings in Existing Methods

Vibration-based damage detection is promising in recent years and has drawn much research attention. However, due to many reasons, it is still difficult, and sometimes even impossible to apply many of these approaches for damage detection with practical engineering structures, especially for large-scale or complex engineering

structures. The primary difficulty for reliable damage detection includes the insensitivity of modal properties to local damage, the uncertainty in the measured vibration data and in the analytical model, the incompleteness of measurement data, the ill-conditioning in inverse problem, the effect of the varying operational and environmental conditions.

The first obstacle to restrict the general application of vibration-based damage detection is that the global dynamic properties of the structure may not be sensitive enough to the local changes in stiffness or mass properties. Kashangaki et al. (1992) indicated that damage detection is more feasible for the structural members that contribute significantly to the strain energy of the measured modes, but most structural members have only small contributions to the strain energy of a structure. Thus it is difficult to detect local damage in its early stage or localize small model errors. For example, Creed (1987) shows that it would be necessary for natural frequency to change by about 5% for damage to be detected with confidence. However, even if the change of natural frequency is enough, the damage detection can not be performed successfully because statistical uncertainties in the measured vibration data exist. It is commonly acknowledged that modal frequencies are measured more accurately than mode shapes. Typical resolution for the modal frequencies of a lightly damped structure is 0.1%; whereas typical mode shape error is 10% or more (Friswell and Penny 1997b). It is presumable that these synthesized damage indices could have more uncertainty than those associated with mode shapes. A study by Worden *et al.* (2005a) indicated that those indices sensitive to local damage are also sensitive to environmental conditions and measurement noise. This severely hinders the efforts to improve identification accuracy.

The second obstacle is the uncertainty associated with measured vibration data which also impedes reliable implementation of FE model updating algorithms. It requires that the damage detection methods have the ability to discriminate changes in the modal properties resulting from occurrence of damage from those resulting from variations in measurements due to changing environmental and/or test conditions and from the repeatability of the test. High level of uncertainty in the measurements will prevent early damage detection when the damage in the structure is small. As uncertainty is inevitable in the measurement data, it seems more natural to pursue the model updating in a framework of probability and statistics. However, most current investigations on system identification and model updating aim at developing methods for deterministic estimation of structural parameters on the assumption that all information on the structures (material properties, modal frequencies, and mode shapes, and so forth) is considered to be fixed quantities. These methods are incapable of accommodating the stochastic nature of measured modal properties and they lack robustness in dealing with uncertainties in the measured modal properties. In contrast to the myriad of literature addressing deterministic FE model updating, there is a long list of publications on the statistical identification of structural systems. The application of statistical methods in model updating has been advocated by Collins *et al.* (1974) although their study was originally intended to overcome the ill-conditioning. The necessity to incorporate statistical methods into model updating algorithms has been recognized by several researchers (Liu, 1995; Papadopoulas and Garcia, 1998; Araki and Hjelmstad, 2001; Xia *et al*, 2002; Fonseca *et al*, 2005; Zimmerman, 2006). The current application of probabilistic methods in model refinement and damage detection is immature. More development and

exploration are needed in the direction of stochastic model updating and probabilistic damage detection.

Another major problem in damage detection is the requirement of accurate analytical model and the reliance on the model. Many damage detection methods are dependent on prior analytical models and/or prior test data for the damage detection, and there is a need to access a detailed finite element model of the structure, or it is assumed that a data set from the undamaged structure is available. However, uncertainty usually exists in the analytical model. Friswell and Penny (1997b) discussed the limitations of various SHM methods. In their opinion, the most significant limitations of SHM methods are the systematic error between a model and a structure as well as the nonstationarity of the structure. They stated that it is necessary to test any method on both simulated and real data. Uncertainties in the FE model exist due to inaccurate physical parameters, non-ideal boundary conditions and structural non-linear properties. These are very true in civil engineering especially for concrete structures. There will undoubtedly be errors even in the model of the undamaged structure (Xia and Hao, 2003). Thus if the measurements on the damaged structures are used to identify damage locations, the deterministic damage detection methods will have great difficulty in distinguishing between the actual damage sites and the location of errors in the original model.

The incompleteness of measurement data and the measurement location further complicate the reliable damage detection. Many techniques work very well in example cases but perform poorly when subject to the measurement limitations imposed by practical modal testing. These limitations usually arise because of the fact that the number of measurement stations is limited by commercial consideration, and that the

rotational DOFs usually cannot be measured, and that some DOFs in the structures are inaccessible. For the damage detection based on model updating techniques, since the finite element models for modern civil engineering structures, such as long-span bridges and tall buildings, involve a large number of DOFs by assembling all the critical and uncritical structural components, the number of DOFs in the model will be much greater than the number of measured DOFs. To deal with the spatially incomplete modal data, the modal reduction or modal expansion techniques are often used. However, when the measured DOFs are far less than the analytical model DOFs, both techniques lead to remarkable additional errors and seriously degrade the accuracy of damage detection results. Damage detection is also associated with measurement selection strategy including mode selection and optimal sensor placement selection. Lim (1992) presented a method to select optimal actuator and sensor locations based on the degree of effectiveness and versatility of pairs of actuator/senor. Xia and Hao (2000) introduced a concept of damage measurability in terms of two factors, namely the sensitivity of the residual vector to damage and the sensitivity of damage to measurement noise. The modes and measuring points selected corresponding to the larger damage measurability values yield more accurate and reliable damage identification results.

Recently, although there have been attempts to deal with the ill-conditioned and noisy system of equations, these attempts are largely restricted to the linear least squares problem formulated by minimization of the equation error (Ahmadian *et al.*, 1998; Ziaei-Rad and Imregun, 1999; Friswell *et al.*, 2001). However many model updating algorithms, especially those used in civil engineering community, leads to the nonlinear optimization problems in terms of updating parameters. The investigation of regularization methods in

this type of model updating algorithms, in particular the methods to optimize regularization parameters, is still limited and requires further exploration.

There is an issue that has received almost no attention in the previous technical literature when applying model updating methods to damage detection problem, which can be generalized as the ability to differentiate the damage patterns and then identify them. The damage may be caused by different factors such as operating loads, impact, fatigue, corrosion, etc., and therefore various damage patterns may occur. Damage of typical patterns, such as crack, delamination and aging, affects the structure's behaviors very differently. Therefore modeling the damage itself plays a significant role in the detection procedure. Most of the existing approaches simply limit structural damages as isotropic reduction in local stiffness, involving a scalar parameter such as Young's modulus. Subsequently two questions are often asked: where is the location of damage and what is its extent. As this over-simplified model could lead to significantly different modal response from the real damaged structure, additional errors is introduced into the model updating process and the accuracy of the detection results is decreased subsequently. A more satisfactory procedure to detect damage should answer the following questions: where is the location of damage; what kind of damage it is; then what is its extent. Although some efforts have been made to build a more refined model for damage, research work in this area is still limited.

Based on the existing problems and shortcomings in damage detection method, the following aspects deserve further exploration: 1) the time series data are directly adopted to identify damage for avoiding modal extraction procedure which will cause information lost and errors introduced; 2) implementation of vibration-based damage

detection which is independent of external excitation and even ambient vibration; 3) the treatment of ill-conditioning in output-error-based model updating; and 4) the quantification of influence of uncertainty in measurement data and the analytical model on the quality of model updating/damage detection results. The above issues will be addressed in this thesis.

CHAPTER 3 INVERSE PROBLEM BASED ON FINITE ELEMENT MODEL AND RESPONSE SENSITIVITY

This chapter provides an overview on the procedure and existing problems of damage detection method based on finite element model and the sensitivity of time series data with respect to the structural parameter.

3.1 Introduction

Modal method for damage detection is a matured field of study and there are many literatures about them as listed in Chapter 2. However, literatures on condition assessment from direct use of vibration response do not appear until recently and there is only a few of them. Cattarius and Inmanm (1997) presented a non-destructive approach based on acceleration responses to examine structural damage. They constructed two simple finite element models to examine axial as well as transverse vibrations. The knowledge gained from simulations led to a series of experiments which substantiated the potential of the proposed method. Comparison of time responses, e.g., displacement of velocity, due to different material defects revealed the existence of damage in cases where measured frequency shifts were minimal. Majumder and Manohar (2003) proposed a time domain approach for damage detection in bridge structures using vibration data. The force from a moving vehicle on the bridge is taken to be the excitation force. It was assumed that a validated finite element model for the bridge structure in its undamaged state is available. Alterations made to this initial model, simulating damage

which causes the changes in bridge behavior, are determined using a time domain approach. Based on the work, Majumder and Manohar (2004) developed the time domain damage detection scheme that takes account into the time varying structural matrices, structural nonlinearities and spatial incompleteness of measured data, within the finite element modeling framework. The damage parameters associated with changes in the structural stiffness are shown to be governed by a set of over-determined nonlinear equations which are solved iteratively. Illustrative examples on a geometrically nonlinear Euler–Bernoulli beam carrying a moving single degree-of-freedom oscillator are provided.

More recently the simple use of time response for damage detection was proposed by Lu and Law (2007) where the sensitivity matrix of response time history is computed using Newmark method, and it is used directly in an inverse problem for structural damage identification. This method can locate and quantify local damages accurately using a small number of sensors. But the results are subjected to the effect of measurement noise and model error. Law and Li (2006) used the wavelet coefficient sensitivity of structural response with respect to a system parameter for structural condition assessment. This sensitivity is shown to be more sensitive to local structural changes than the response sensitivity and it has the advantage in handling problems with model errors in the initial finite element model of the system. This is because the wavelet transform extracts separately different frequency component information from the response. However, all the above methods rely on the need of an externally applied excitation. This requirement is not possible in the case of a large civil engineering structure where a large amount of energy input is required. For practical applications,

time domain methods are further developed to apply in the structures under ambient excitations by the author in the thesis.

Comparing to modal methods, methods based on direct vibration responses have many advantages and they can be applied more widely. Firstly, modal parameters used in modal methods are global quantities of the structures. They have limited abilities to capture local and instantaneous changes in the systems. Secondly, because modal parameters are usually obtained from the measured time responses with signal processing techniques such as Fourier transform, some information will be lost during the transformation and data reduction, and this will affect the final results. Thirdly, in the time-domain, plenty of measured data can be obtained with increasing period of measurement and the information can be perfectly preserved in the time series without the need of modal identification. Fourthly, time-domain methods can use any sampling frequency in the vibration measurements, however, modal methods require a sampling frequencies to include several modes of the structures. Fifthly, methods based on time series data make use of not only the global characteristics (natural frequency, mode shape and so on) but also the local ones (such as the amplitude attenuation). Sixthly, because the condition of real structures is often time-varying, methods based on time series data will be more appropriate for health assessment. With the development of methods based on time series data, more and more merits will be found. These methods will be employed more widely both in linear and non-linear problems of the engineering structures.

In this chapter, the procedure of damage detection based on time series data was presented. Firstly, the forward problem including the computation of time responses from

an analytical model using numerical methods and signal analysis using Fourier Transform and Wavelet transform are introduced. Secondly, a simple damage model is established for demonstration of the damage detection method. Thirdly, the sensitivities of time series data with respect to the structural parameters are computed numerically. Fourthly, the damage identification based on model updating and the output-error was described. Fifthly, to solve the ill-conditioning in the solution in the inverse problem, regularization theory was used and its basic theory was presented. Finally, the uncertainty analysis is necessary in damage detection, and the uncertainty model was given.

3.2 Forward Problem

Because damage detection is based on the model updating procedure, the dynamic response of one state of the structure needs to be simulated from the finite element model. To give the complete procedure and investigate the possible problems, the forward problem including the computation of the dynamic responses and the corresponding signal analysis are presented briefly. In the thesis, only the linear vibration models are studied.

3.2.1 Computation of Dynamic Responses of the Structure

For a general finite element model of a linear-elastic time-invariant N degrees-of-freedom damped structural system under general excitation, the dynamic governing equation is given by,

$$\mathbf{M}\ddot{\mathbf{x}} + \mathbf{C}\dot{\mathbf{x}} + \mathbf{K}\mathbf{x} = \mathbf{D}F(t) \qquad (3.1)$$

where $\mathbf{M}, \mathbf{C}, \mathbf{K}$ are the $N \times N$ mass, damping and stiffness matrices respectively. **D** is the mapping matrix relating the force excitation location to the corresponding DOFs of the system. $\mathbf{x}, \dot{\mathbf{x}}, \ddot{\mathbf{x}}$ are the $N \times 1$ displacement, velocity, acceleration vectors respectively. $F(t)$ is the force vector which acts on the structure. As we know, Rayleigh damping is the most popular damping model for structural dynamic analysis. In the thesis, Rayleigh damping model is taken, which has the form as: $\mathbf{C} = \alpha_1 \mathbf{M} + \alpha_2 \mathbf{K}$, where α_1 and α_2 are constants to be determined from two given damping ratios that corresponding to two unequal frequencies of vibration. If a more accurate estimation of the actual damping is required, a more general form of Rayleigh damping, the Caughey damping model (Bathe, 1982) can be adopted.

The solution of Equation (3.1) can be obtained by standard techniques such as the Duhamel integral (Meirovitch, 1997). In this thesis, a time-stepping technique, Newmark method was adopted to solve Equation (3.1). The important approximations (or basic principles) in Newmark method can be described as,

$$\dot{x}_{n+1} = \dot{x}_n + (1-\gamma)\ddot{x}_n \cdot \Delta t + \gamma \ddot{x}_{n+1} \cdot \Delta t \qquad (3.2)$$

$$x_{n+1} = x_n + \dot{x}_n \cdot \Delta t + \frac{1-2\beta}{2} \ddot{x}_n \cdot \Delta t^2 + \beta \ddot{x}_{n+1} \Delta t^2 \qquad (3.3)$$

Where the subscripts n and $n+1$ denote the instant point, γ and β are constants. A stable solution can be obtained, when $\gamma \geq 0.5$ and $\beta \geq 0.25(0.5+\gamma)^2$. If $\gamma = 0.5$ and $\beta = 0.25$, the method becomes the averaging acceleration method. Δt is the time step length used in the computation. The computation error can be estimated by comparing the responses

from using different time steps, say, Δt and $\Delta t / 2$. The error is defined by $\frac{\left\| \ddot{\mathbf{X}}_{\Delta t/2} - \ddot{\mathbf{X}}_{\Delta t} \right\|}{\left\| \ddot{\mathbf{X}}_{\Delta t} \right\|}$. If the error is limited to the given value such as 5%, it can be assumed that the acceptable computing responses are obtained. To start this time-stepping method both the displacements and velocities are required at the start time. The dynamic responses computed from Duhamel integral can contains arbitrary modes of the structure since Duhamel integral is performed via mode superposition. However, the number of modes involved in the dynamic responses from Newmark method is determined by the sampling frequency which is equal to $\frac{1}{\Delta t}$ where Δt is the time step in the computation of the responses. The sampling frequency is at least two times the maximum frequency to be considered (the cut-off frequency).

3.2.2 Signal Analysis

Fourier transform is often used to obtain the modal properties such as natural frequency and mode shape. Though many limitations exist in the application of Fourier transform, it is still used widely and it is introduced briefly here. In the thesis, structural response time histories will be directly used for damage detection instead of the modal properties. The properties such as energy distribution, frequency content and amplitude decay and so on are needed to be comprehended more carefully. The powerful signal analysis tools-wavelet transform are also applied to the computed and measured acceleration responses and the resulted wavelet coefficients and energy will be used for

damage detection. The promising wavelet transform and its extension-wavelet packet transform are also presented simply.

Fourier transform

The discrete Fourier transform (DFT) is used to calculate the frequency content of a discrete, finite-length time signal. It assumes that the frequency content remains unchanged during the time span of the signal. Despite this, the DFT may be used to predict the time-frequency properties of a signal by using the moving-window method. The Fourier series (FS) representation of a cyclic signal $x(t)$ with time period T may be written as,

$$x(t) = C_0 + C_1 e^{i2\pi t/T} + C_2 e^{i4\pi t/T} + \cdots = \sum_{m=0}^{\infty} C_m e^{i2m\pi t/T} \tag{3.4}$$

Where the constants C_m are the amplitudes of the sinusoids at each frequency m/T. These values may be found using the equation,

$$C_m = \frac{1}{T}\int_{-T/2}^{T/2} x(t) e^{-i2m\pi t/T} dt \tag{3.5}$$

The Fourier transform (FT) of a continuous infinite signal $x(t)$ may be written as,

$$X(f) = \int_{-\infty}^{\infty} x(t) e^{-i2f\pi t/T} dt \tag{3.6}$$

The signal $x(t)$ can be reconstructed from the Fourier transform coefficients as,

$$x(t) = \frac{1}{2\pi}\int_{-\infty}^{\infty} X(f) e^{i2f\pi t/T} dt \tag{3.7}$$

The finite discrete form of the Fourier transform may be derived from considering either the frequency content of the Fourier series representation, Equation (3.5), or a discretized

version of the Fourier transform, Equation (3.6), multiplied by a finite-length window. (see, for example, Randall, 1987).

Wavelet transform

Wavelet analysis is a method of decomposing the time signal into constituent parts. The shape and magnitude of these constituent parts depends on the selected wavelet (see, for example, Newland, 1993). The wavelet can take any form provided it is localized in time, but for computational simplicity, it tends to be limited to a function which leads the signal being decomposed into orthogonal parts. Daubechies wavelets are adopted to decompose the time signal in the thesis.

A wavelet is a function with two important properties: oscillation and short duration. A function $\psi(t)$ is a wavelet if and only if its Fourier transform $\tilde{\psi}(\omega)$ satisfies

$$\int_{-\infty}^{+\infty} \frac{\left|\tilde{\psi}(\omega)\right|^2}{\left|\omega\right|^2} d\omega < +\infty \qquad (3.8)$$

This condition implies that

$$\int_{-\infty}^{+\infty} \psi(t) dt = 0 \qquad (3.9)$$

And the function $\psi(t)$ has to be oscillatory. For practical purposes it is also required to define the wavelet in a limited interval $[-K, \quad K]$, where K is a scalar.

Because dyadic wavelet is used for the present study in the thesis, the transformation procedure based on dyadic wavelet is provided below. Let $\psi(t)$ be the mother wavelet function, and $\varphi(t)$ be the scaling function. Then they have the following relations as,

$$\varphi(t) = \sqrt{2} \sum_{k=-\infty}^{+\infty} h(k)\varphi(2t-k) \tag{3.10a}$$

$$\psi(t) = \sqrt{2} \sum_{k=-\infty}^{+\infty} g(k)\varphi(2t-k) \tag{3.10b}$$

where $h(k)$ and $g(k)$ are the low-pass and high-pass analysis filters respectively which are all constants related to the wavelet type.

The wavelet function $\psi_{j,k}(t)$ is defined based on the mother wavelet function $\psi(t)$ and the scaling function $\varphi(t)$ as,

$$\psi_{j,k}(t) = 2^{\frac{-j}{2}} \psi(2^{-j}t - k) \tag{3.11}$$

where both j and k are in the integer domain. j is the scale parameter and k is the translation parameter.

Because of the orthogonality on both translation and scale of the Daubechies wavelets, the relationship can be obtained as,

$$\int \psi_{j,k}(t)\psi_{m,n}(t)dt = \delta_{j,m}\delta_{k,n} \tag{3.12}$$

where $\delta_{j,m}, \delta_{k,n}$ are the Dirac delta function and they satisfy the following equation,

$$\delta_{i,j} = 0, \ (i \neq j) \tag{3.13}$$

The forward decomposition of the time signal $f(t)$ by Daubechies wavelets can be expressed as,

$$d_{j,k} = \int_{-\infty}^{+\infty} f(t)\psi_{j,k}(t)dt \tag{3.14}$$

where $d_{j,k}$ is the wavelet coefficient.

On the other hand, the signal can be reconstructed from the wavelet coefficient and the wavelet function.

$$f(t) = \sum_{j,k} d_{j,k} \psi_{j,k}(t) \tag{3.15}$$

Wavelet packet transform

Wavelet packet is a generalization of the wavelet transform where arbitrary time-frequency resolution can be chosen according to the signal. This will be done, of course, within the bounds of Heisenberg uncertainty principle (see Coifman et al, 1992). The idea of separating the signal into packets is to obtain an adaptive partitioning of the time-frequency plane depending on the signal of interest.

The i th wavelet packet $\psi^i(t)$ can be expressed by the low-pass analysis filter $h(n)$ and high-pass analysis filter $g(n)$ as,

$$\psi^0(t) = \sqrt{2} \sum_{k=-\infty}^{+\infty} h(k) \psi^0(2t-k) \tag{3.16}$$

$$\psi^1(t) = \sqrt{2} \sum_{k=-\infty}^{+\infty} g(k) \psi^0(2t-k) \tag{3.17}$$

where $\psi^0(t) = \varphi(t)$, $\psi^1(t) = \psi(t)$. When i is arbitrary, Equations (3.16) and (3.17) become

$$\psi^{2i}(t) = \sqrt{2} \sum_{k=-\infty}^{+\infty} h(k) \psi^i(2t-k) \tag{3.18}$$

$$\psi^{2i+1}(t) = \sqrt{2} \sum_{k=-\infty}^{+\infty} g(k) \psi^i(2t-k) \tag{3.19}$$

and the wavelet packet transform of a time signal $f(t)$ can be defined as,

$$c_{j,k}^{i} = \int_{-\infty}^{+\infty} f(t)\psi_{j,k}^{i}(t)dt \tag{3.20}$$

with $\psi_{j,k}^{i}(t) = 2^{-\frac{j}{2}}\psi^{i}(2^{-j}t-k)$.

The original signal can be reconstructed as,

$$f_{j}^{i}(t) = \sum_{k=-\infty}^{+\infty} c_{j,k}^{i}\psi_{j,k}^{i}(t) \tag{3.21}$$

$$f(t) = \sum_{i=0}^{2^{j}-1} f_{j}^{i}(t) \tag{3.22}$$

The wavelet packet transform coefficients can be computed in detail as,

$$c_{0,k}^{0} = \int_{-\infty}^{+\infty} f(t)\psi_{0,k}^{0}(t)dt \tag{3.23}$$

with $\psi_{0,k}^{0} = \psi^{0}(t-k) = \varphi(t-k)$

or in a more general format, $c_{0,k}^{0} = \int_{-\infty}^{+\infty} f(t)\varphi(t-k)dt$,

$$c_{j+1,k}^{2i} = \sum_{m} h(m-2k)c_{j,m}^{i}\ ,\quad c_{j+1,k}^{2i+1} = \sum_{m} g(m-2k)c_{j,m}^{i} \tag{3.24a}$$

or in matrix form,

$$\mathbf{c}_{j+1}^{2i} = \mathbf{H}^{j+1}\mathbf{c}_{j}^{i}\ ,\quad \mathbf{c}_{j+1}^{2i+1} = \mathbf{G}^{j+1}\mathbf{c}_{j}^{i} \tag{3.24b}$$

where $\mathbf{H}^{j+1} = \begin{bmatrix} h(1-2) & h(2-2) & \cdots & h(l\max-2) \\ \cdots & \cdots & \cdots & \cdots \\ h(1-2k) & h(2-2k) & \cdots & h(l\max-2k) \\ \cdots & \cdots & \cdots & \cdots \end{bmatrix}$,

and $\mathbf{G}^{j+1} = \begin{bmatrix} g(1-2) & g(2-2) & \cdots & g(l\max-2) \\ \cdots & \cdots & \cdots & \cdots \\ g(1-2k) & g(2-2k) & \cdots & g(l\max-2k) \\ \cdots & \cdots & \cdots & \cdots \end{bmatrix}$

$(k = 1,2,\cdots, N/2^{j+1},\quad l = 1,2,\cdots, N/2^{j})$

where N is the number of data points of the finite time signal $f(t)$.

Equation (3.24) can also be simplified as,

$$\mathbf{c}_j^i = \mathbf{D}_j^i \mathbf{c}_0^0 \tag{3.25}$$

with $$\mathbf{c}_{j+1}^{2i} = \mathbf{D}_{j+1}^{2i}\mathbf{c}_0^0 = \mathbf{H}^{j+1}\mathbf{c}_j^i = \mathbf{H}^{j+1}\mathbf{D}_j^i\mathbf{c}_0^0,$$

$$\mathbf{D}_{j+1}^{2i} = \mathbf{H}^{j+1}\mathbf{D}_j^i, \qquad \mathbf{D}_{j+1}^{2i+1} = \mathbf{G}^{j+1}\mathbf{D}_j^i \tag{3.26}$$

where $$\mathbf{D}_1^0 = \mathbf{H}^1, \qquad \mathbf{D}_1^1 = \mathbf{G}^1$$

3.3 Establishment of Damage Model

Damage models can be classified as discrete models (such as finite element model) and continuous models, and also they can be sorted as linear model and non-linear model. Because the author's aims in the thesis are to investigate the techniques for damage detection using time series data and their sensitivities, simple finite element linear models are used in the research.

For an isotropic elastic material, the elemental stiffness matrix is proportional to the elastic modulus of the material and the geometric coefficient such as the length of the element, cross sectional area, etc., which are usually taken as the unknown parameters to be identified in the inverse problem. In the thesis, an approximate model on the local damage is adopted in which the local damage in the structural system is expressed in the form of $\mathbf{\Delta K} = \sum_{i=1}^{ne} \Delta\alpha_i \mathbf{K}_i$, where $\Delta\alpha_i$ is the fractional change in the stiffness of an element,

$\mathbf{K}_i$ is the element stiffness matrix assembled in the global matrix and ne is the number of elements in the structure.

When a more detailed finite element or numerical model is used for modeling the behavior of the cracks, the proposed methods in the thesis still work. However it must be noted that the computation increases with increasing number of degree-of-freedoms of the structure.

3.4 Sensitivity Analysis

From the equation of motion (3.1), the time responses can be computed by Newmark method. In order to investigate the properties of these time series data and perform damage detection, the derivatives of these time series data with respect to the structural parameter need to be derived. For different types of time series data, the method for obtaining the derivatives are different. In this Chapter, only the vibration response sensitivities are presented and the derivatives of their ramifications with respect to structural parameter will be given in later Chapter in details.

The derivatives of the vibration responses with respect to the structural parameters can be obtained in an analytical approach via the sensitivity of the modal properties with respect to structural parameters. This method is complicated and can not avoid the modal extraction from the time responses which also bring errors into the data. Then the direct numerical approach is adopted to compute the sensitivity of the time series data.

We can now derive the vibration response sensitivity with respect to the physical parameters. Performing partial differentiations on both sides of Equation (3.1) with respect to the stiffness parameter of the $i\,th$ element, we have,

$$\mathbf{M}\frac{\partial \ddot{\mathbf{x}}}{\partial \alpha_i}+\mathbf{C}\frac{\partial \dot{\mathbf{x}}}{\partial \alpha_i}+\mathbf{K}\frac{\partial \mathbf{x}}{\partial \alpha_i}=-\frac{\partial \mathbf{K}}{\partial \alpha_i}\mathbf{x}-\frac{\partial \mathbf{C}}{\partial \alpha_i}\dot{\mathbf{x}} \qquad (3.27)$$

The sensitivities $\frac{\partial \mathbf{x}}{\partial \alpha_i}, \frac{\partial \dot{\mathbf{x}}}{\partial \alpha_i}, \frac{\partial \ddot{\mathbf{x}}}{\partial \alpha_i}$ can then be obtained from Equations (3.27) and (3.1). Since the displacement and velocity responses have been obtained from Equation (3.1), the right-hand-side of Equation (3.27) can be treated as the equivalent force input, and similarly, the sensitivities can also be obtained numerically by Newmark method. The dynamic response sensitivities of the initial conditions usually vanish because the initial conditions are independent of the system parameters. In the case when a structure is suddenly released from a static equilibrium state, the sensitivity of the initial displacement to the elemental Young's modulus exists, and thus the sensitivity of initial velocity has a non-zero value. In this case, the sensitivity of initial displacement is obtained from the direct differential of the static equilibrium equation.

3.5 Damage Detection

Damage identification can be performed with the above preparation. We consider a general structure which behaves linearly before and after the occurrence of damage for the illustration of the procedure of damage detection. The study of a non-linear system with time-varying damage model is not included in this study as it involves a different treatment of the identification problem.

3.5.1 Objective Function

In the forward analysis, the dynamic responses and their sensitivity with respect to the structural parameter of a finite element system can be obtained from Equations (3.1) and (3.27) for a given set of parameters α_i (*i=1, 2, …, ne*). In the procedure for damage detection, however, these parameters are required to be identified from the measured responses. In other words, the parameters are chosen to best fit the experiment data. Optimization methods according to different criteria can be used to fit the data. The least-squares techniques are usually adopted to minimize the sum of squared errors by linear approximation or higher order approximation. The sensitivity-based analysis methods which have different formulation for different problems are also seen in applications for obtaining the best suitable structural parameter to match the measured responses best. The sensitivity adopted is often obtained approximately by neglecting the higher order of the Taylor series. In this thesis, the sensitivity-based methods are used to find the damage vector to minimize the objective function which can be defined as,

$$J(\alpha) = \sum_{j=1}^{l} \sum_{i=1}^{nt} \{\hat{R}_{ij} - R_{ij}\}^T \mathbf{W} \{\hat{R}_{ij} - R_{ij}\} \qquad (3.28)$$

where *l* is the number of measurement locations, *nt* is the number of time instances to provide the measured data. $\boldsymbol{\alpha}$ is the vector of unknown stiffness parameter $(\alpha_1, \alpha_2, \cdots, \alpha_{ne})^T$ to be identified, $\mathbf{R}$ is the vector of calculated time series of the structure from a known set of $\boldsymbol{\alpha}$, which can be displacement response, acceleration response, wavelet coefficient of response, impulse response function, etc, and $\hat{\mathbf{R}}$ is the corresponding vector from measurement. $\mathbf{W}$ is the weighting matrix which is taken as a unity matrix in this thesis.

3.5.2 Penalty Function Method

Penalty function method is generally used for modal sensitivity with a truncated Taylor series expansion in terms of the unknown parameters (Friswell and Mottershead, 1995). The truncated series of the dynamic responses in terms of the stiffness parameter α_i of an element is used to derive the sensitivity-based formulation from the general dynamic responses. The identification problem can be expressed as follows to find the vector $\boldsymbol{\alpha}$ such that the calculated response best matches the measured response, i.e.

$$\mathbf{Q} \cdot \mathbf{R} = \hat{\mathbf{R}} \tag{3.29}$$

where the selection matrix $\mathbf{Q}$ is a constant matrix with elements of zeros or ones, matching the degrees-of-freedom corresponding to the measured response components. Vector $\mathbf{R}$ can be obtained from Equation (3.1) for a given set of $\boldsymbol{\alpha}$.

Let $$\delta\mathbf{z} = \hat{\mathbf{R}} - \mathbf{Q} \cdot \mathbf{R} = \hat{\mathbf{R}} - \mathbf{R}_{cal} \tag{3.30}$$

In the penalty function method, we have,

$$\delta\mathbf{z} = \mathbf{S}\delta\boldsymbol{\alpha} \tag{3.31}$$

where $\delta\mathbf{z}$ is the error in the measured output and $\delta\boldsymbol{\alpha}$ is the perturbation in the parameters, $\mathbf{S}$ is the two-dimensional sensitivity matrix which is one of the matrices at time *t* in the three-dimensional sensitivity matrix. For a finite element model with *ne* elements, the number of unknown elemental elastic modulus is *ne*, and only *ne* equations are needed to solve the parameters. Matrix $\mathbf{S}$ is on the parameter-*t* plane, and we can select any row of the three-dimensional sensitivity matrix, say, the *i*th row corresponding to the *i*th measurement for the purpose. When writing in full, Equation (3.30) can be written as,

$$\delta \mathbf{z} = \begin{Bmatrix} \hat{R}(t_1) \\ \hat{R}(t_2) \\ \vdots \\ \hat{R}(t_l) \end{Bmatrix} - \begin{Bmatrix} R_{cal}(t_1) \\ R_{cal}(t_2) \\ \vdots \\ R_{cal}(t_l) \end{Bmatrix} \tag{3.32}$$

with $l \geq NE$ to make sure that the set of equation is over-determined and this requirement is easily satisfied using the series data. Equation (3.31) can be solved according to the minimization criteria by different techniques such as the standard simple least-squares methods as follows,

$$\delta \boldsymbol{\alpha} = [\mathbf{S}^T \mathbf{S}]^{-1} \mathbf{S}^T \delta \mathbf{z} \tag{3.33}$$

where the superscripts $(\bullet)^{-1}$ and $(\bullet)^T$ indicate the inverse and the transpose of the matrix in this thesis. The residuals or the objective function in Equation (3.28) corresponding to Equation (3.33) are used to obtain the cost function is,

$$J_{LS}(\boldsymbol{\alpha}) = \left\| \mathbf{S} \cdot \delta \mathbf{z} - \delta \boldsymbol{\alpha} \right\|^2 = (\mathbf{S} \cdot \delta \mathbf{z} - \delta \boldsymbol{\alpha})^T \mathbf{W} (\mathbf{S} \cdot \delta \mathbf{z} - \delta \boldsymbol{\alpha}) \tag{3.34}$$

3.5.3 Updating the Analytical Model and Identifying Local Damages

The damage identification includes two separate stages of updating the analytical model and identifying local damages.

Divergence of the solution in the updating procedure not only comes from the large difference between the mathematical and the real model, but also stems from the computational error in the solution of a large number of unknowns. We need to exercise some engineering judgments in the case of dealing with a large structure with a large number of unknowns. This helps a lot in reducing the size of the problem and of course enhancing the convergence property of the solution.

With the usual case of solving Equation (3.31) only once can only handle small deviations from the FEM. But with the present iterative approach to update the deviations by small increments at a time, large deviation from the initial model can be updated with the improved FEM closer to the real structure after every iteration of model improvement. Then iterative approach is used for updating the model.

The initial analytical model is adopted for model updating in the first stage of the study, and $\mathbf{R}$ and matrix $\mathbf{S}$ are obtained from this initial model with an initial guess $\boldsymbol{\alpha}_0$ for the unknown vector $\boldsymbol{\alpha}$, usually, $\boldsymbol{\alpha}_0$ is taken as the original stiffness parameter. $\hat{\mathbf{R}}$ can be directly obtained or computed from the measurement from the intact state of the structure. Through solving Equation (3.31), the initial model is then updated and the corresponding $\mathbf{R}$ and its sensitivity $\mathbf{S}$ are again computed from the updated model for the next iteration. The procedure of iteration can be described as,

- Step 1: Solve Equation (3.1) at the *(k+1)th iteration* with known $\boldsymbol{\alpha}_k$ for $\mathbf{R}$ and compute the value $\delta \mathbf{z}_k$.
- Step 2: Solve Equation (3.27) at the *(k+1)th iteration* with known $\boldsymbol{\alpha}_k$ for $\frac{\partial \mathbf{R}}{\partial \alpha_i}$ to get the sensitivity matrix $\mathbf{S}$.
- Step 3: Find $\{\Delta \boldsymbol{\alpha}_k\}$ from Equation (3.31) or Equation (3.33).
- Step 4: Update the stiffness parameter vector by the formula:

$$\boldsymbol{\alpha}_{k+1} = \boldsymbol{\alpha}_k + \Delta \boldsymbol{\alpha}_k . \tag{3.35}$$

- Step 5: Repeat Steps 1 to 4 until both of the following two criteria are met:

$$\frac{\left\| \mathbf{R}_{k+1} - \mathbf{R}_k \right\|}{\left\| \mathbf{R}_{k+1} \right\|} \le toler\ \ 1, \frac{\left\| \boldsymbol{\alpha}_{k+1} - \boldsymbol{\alpha}_k \right\|}{\left\| \boldsymbol{\alpha}_{k+1} \right\|} \le toler\ \ 2 \tag{3.36}$$

The tolerances equal to 1.0×10^{-6} in this thesis unless otherwise stated.

After the analytical model is updated to the converging state, then the updated analytical model is used to represent the first (intact) state of the structure. The same procedure in the updating analytical model can be followed for identifying the local damage. The updated intact model of the structure can be updated to the damaged model of the structure by best matching the measured dynamic responses with that from the damaged structure. The final set of identified parameter increments correspond to the changes occurred in between the intact and damaged model of the structure and the damage vector can be obtained.

3.6 Regularization Technique

Like many other inverse problems, the solution of Equation (3.31) is ill-conditioned. In order to provide bounds to the solution, regularization techniques are needed to be applied to the solution. The aim is to promote certain regions of parameter space where, we believe the model realization should be. Tikhonov achieved a controlled influence of the regularizing information by forming a weighted sum of the original cost function J_{LS} and a new cost function $J_{\mathrm{Re}g}$ based on the regularizing information, given by

$$\mathbf{d} = \mathbf{C}\delta\boldsymbol{\alpha} \tag{3.37}$$

From Equation (3.37) the residuals are used to give the second cost function,

$$J_{\mathrm{Re}g}(\boldsymbol{\alpha}) = \left\|\mathbf{C}\boldsymbol{\alpha} - \mathbf{d}\right\|^2 = (\mathbf{C}\boldsymbol{\alpha} - \mathbf{d})^T \mathbf{W}_\alpha (\mathbf{C}\boldsymbol{\alpha} - \mathbf{d}) \tag{3.38}$$

where W_α is a symmetric positive definite weighting matrix. Thus there are two cost functions, J_{LS} and $J_{\mathrm{Re}g}$, that need to be minimized concurrently. A composite cost function J_{LSR} is formulated as,

$$J_{LSR} = J_{LS} + \lambda J_{\mathrm{Re}g} = \left\|\mathbf{S}\cdot\delta\boldsymbol{\alpha} - \delta\mathbf{z}\right\|^2 + \lambda\left\|\mathbf{C}\boldsymbol{\alpha} - \mathbf{d}\right\|^2 \qquad (3.39)$$

Where, $\lambda \geq 0$ is the regularization parameter, and $J_{\mathrm{Re}g}$ is the stabilizing/regularization part. The parameter λ controls the extent to which regularization is applied to the nominal problem. If λ is too small then the problem will be too close to the original ill-posed problem, but if λ is too large then the problem solved will have little connection with the original problem.

The matrix $\mathbf{C}$ is typically either the identity matrix $\mathbf{I}_m$ or a discrete approximation to a derivative operator (Phillips, 1962). The correct choice of $\mathbf{C}$ is important to obtain meaningful parameters α. Varah (1983) showed that a wrong choice of $\mathbf{C}$ can lead to completely erroneous results. Additional information should be introduced by means of the side constraint in the model updating or damage assessment process. In this thesis, the damage vector is the vector with nonzeros in several elements and zeros in most elements and the obtained vector $\delta\boldsymbol{\alpha}$ in every updating procedure is small. Therefore it can be assumed that $\delta\boldsymbol{\alpha} \to 0$ and this can be used as the side constraint. When $\mathbf{C}$ is chosen as the identity matrix, Equation (39) becomes,

$$J(\delta\boldsymbol{\alpha}, \lambda) = \left\|\mathbf{S}\delta\boldsymbol{\alpha} - \delta\mathbf{z}\right\|^2 + \lambda\left\|\delta\boldsymbol{\alpha}\right\|^2 \qquad (3.40)$$

Then the regularization solution from minimizing the function in Equation (3.40) can be written in the following form as,

$$\delta\boldsymbol{\alpha}(\lambda) = (\mathbf{S}^T\mathbf{S} + \lambda\mathbf{I})^{-1}\mathbf{S}^T\delta\mathbf{z} \qquad (3.41)$$

The determination of the regularization parameter λ can be determined by different techniques such as L-Curve method and cross validation. In this thesis, L-Curve method was adopted and some improvements were performed.

3.7 Uncertainty Analysis

In practice, uncertainties always exist in the measured vibration data and the analytical model. In order to study the effect of uncertainties to the damage identification, the uncertainties in the analytical model are represented by variations in the structural parameters such as density, stiffness, damping and force data and so on. Artificial noise is added to the computed responses to simulate the measured responses containing the noise caused by environmental and other factors.

White noise is added to the calculated responses to simulate the polluted measurements as follows,

$$\mathbf{R}_{measured} = \mathbf{R}_{calculated} + Ep * \mathbf{N}_{oise} * \mathrm{var}(\mathbf{R}_{calculated}) \qquad (3.42)$$

where $\mathbf{R}_{measured}$ is the vector of polluted responses; Ep is the noise level ; N_{oise} is a standard normal distribution vector with zero mean and unit standard deviation; var(•) is the variance of the time history; $\mathbf{R}_{calculated}$ is the vector of calculated responses.

3.8 Summaries

In most existing technical literature, time series data are becoming more popular for damage detection. Time series data can be obtained directly from the experimental measurement without modal extraction procedure, and it can preserve more information of the structure. This thesis presents the damage detection algorithm based on time series

data using an output error estimator based on general measurement (displacement, acceleration, etc.). The proposed damage detection algorithm estimates structural parameters through the minimization of an error function defined by the weighted least-squared error between the measured and the calculated dynamic time series. Since the error function is defined only from the time history of acceleration (displacement) measured at a few locations, the algorithm does not require any other measured information other than acceleration (displacement).

In comparison with other damage detection methods, the proposed method has the following advantages: (1) the number of measurements can be very small; (2) the identification process is fast and the identified results are accurate; (3) the number of identification equation can be adjusted according to the duration of time, this indicates that the identification equation can always be over-determined; (4) several types of measurements can be used for the damage detection, i. e., displacement, acceleration, strain measurement etc, or any combination of these measurements can be used; (5) only a short duration of dynamic response measurement is needed in the identification; (6) the proposed method has the potential for identifying large number of structural parameters.

CHAPTER 4 DAMAGE DETECTION DIRECTLY FROM TIME RESPONSE VIA WAVELET AND WAVELET PACKET TRANSFORM

4.1 Introduction

Damage detection based on modal properties was firstly applied to engineering structures. However the limitations for modal damage diagnostics exist and restrict the practical and further application in engineering system. Many researchers tried to directly use the time series data without the modal extraction from measured responses for structural condition assessment.

Cattarius and Inman (1997) used the phase shift in the time history of structural vibration response to identify the presence of damage in smart structures. Majumder and Manohar (2003) proposed a time domain approach for damage detection in beam structures using vibration data with a moving oscillator as an excitation source. Choi and Stubbs (2004) formed the damage index directly from the time response to locate and size damage in a structure and the method tries to remove certain drawbacks associated with commonly used modal extraction parameter methods. Lu and Gao (2005) proposed a new method for damage diagnosis using time-series analysis of vibration signals which is formulated in a novel form of ARX model with acceleration response signals. Kang et al. (2005) presented a system identification scheme in time domain to estimate stiffness and damping parameters of a structure using measured accelerations and the method is demonstrated with a numerical simulation study on a two-span truss bridge and an

experimental laboratory study on a three-story shear building model. More recently the sensitivity matrix of response with respect to a system parameter is derived analytically (Lu and Law, 2007), and it is used directly in an inverse problem for structural damage identification. Though time responses can be used to detect damage directly and easily, and they can locate damages and quantify the severity very accurately using as few as a single sensor, the results are subject to the effect of measurement noise and model error.

Any signal can be decomposed into wavelets and some of them can be proved to be sensitive to local changes in the system parameters as shown later in this section. The Fourier analysis transforms the signal from a time-based or space-based domain to a frequency-based domain. The wavelet transform has many virtues that the Fourier transform lacks.

Wavelet analysis may be viewed as an extension of the traditional Fourier transform with adjustable window location and size. Over the past ten years, wavelet theory (Wong and Chen, 2001) has become one of the emerging and fast-evolving mathematical and signal processing tools because of its many distinct merits. The wavelet transform is different from the Gabor transform in that it can be used for multi-scale analysis of a signal through dilation and translation, such that the time-frequency features of a signal can be extracted effectively. The merits of wavelet analysis also lie in its ability to examine local data with a ‘‘zoom lens having an adjustable focus’’ to provide multiple levels of details and approximations of the original signal. Therefore the transient characteristics of the signal can be retained.

A possible drawback of the wavelet transform is that the frequency resolution is quite poor in the high frequency region. Hence there are difficulties when discriminating

signals containing high frequency components. The wavelet packet transform is an extension of the wavelet transform that provides complete level-by-level decomposition. The wavelet packets are alternative bases formed by linear combinations of the usual wavelet functions (Coifman and Wickerhauser, 1992). As a result, the wavelet packet transform enables the extraction of features from signals containing stationary and non-stationary components with arbitrary time-frequency resolution.

Sun and Chang (2002a) used a wavelet packet signature to detect damage. Law et al. (2005) developed the sensitivity-based damage detection method basing on the wavelet packet energy of the measured accelerations and the method can identify damage of a structure from a few measurement locations. To adopt the plenty time domain data and make the damage identification over-determined, the sensitivity of the wavelet coefficient from structural response is also derived to identify damage with much better results especially in structures with noise and model error (Law and Li, 2006).

All structures are subject to ambient excitations like wind, rain, ground micro-tremor and temperature effects as well as the operation loads. Most of these excitations are from the environment and they are usually small, while the force from operation loads is significant. Most existing methods on condition assessment of structure require an input which may be the ambient environmental forces or artificial forced excitation. The operation loads are usually treated as random forces or just ignored. This practice may be appropriate for a large structure such as a suspension bridge but not for the usual types of infrastructure such as a box-section bridge deck. Method including the moving operation load in the system identification is scarce. The provision of sufficiently large energy input for the identification of such a structure is formidable. It is necessary to find a way to get

around the above problem by including the ground micro-tremor excitation in the condition assessment. Acceleration responses at only the support and at limited number of locations of the structure are required.

In order to have methods mainly used the time responses for damage detection more practical and powerful, time responses combined with wavelet and wavelet packet transform techniques are adopted to identify damage in structures in the chapter. It consists of the three parts: (a) structural damage detection from wavelet packet energy of acceleration responses, (b) structural damage detection from wavelet coefficient of acceleration responses with model errors and noise, and (c) structural condition assessment from measured accelerations in the structure under support excitation.

4.2 Structural Damage Detection from Wavelet Packet Energy of Time Responses

In this section, the sensitivity of wavelet packet transform component energy with respect to local change in the system parameters is derived analytically. Measured response signals from a structure are first decomposed into wavelet packet components. The (WPT) component energy sensitivity is classified into two types and their inclusion in the identification equation is discussed. Components that contain much of the structural system information are identified, and their energy and first order sensitivity to local damage are calculated. The identification equations are solved using measured responses from two states of the structure with regularization in the solution. Both acceleration and strain responses have been used separately or in combination, and the sensitivity of acceleration with respect to local change of parameter is shown both

analytical and numerically much better than that from strains. The proposed method is also shown both numerically and analytically not sensitivity to measurement noise. The method can differentiate damages at close proximity with good resolution from using very short duration of measured data from only two sensors. Experimental results from a steel beam also confirm the effectiveness of the proposed method.

4.2.1 Dynamic Response Sensitivity

The equation of motion of a damped structural dynamic system is expressed as,

$$\mathbf{M}\ddot{\mathbf{z}} + \mathbf{C}\dot{\mathbf{z}} + \mathbf{K}\mathbf{z} = \mathbf{G}F(t) \qquad (4.1.a)$$

It can also be written in the state-space form as,

$$\dot{\mathbf{x}} = \mathbf{A}\mathbf{x} + \mathbf{B}F(t) \qquad (4.1.b)$$

$$s = \bar{\mathbf{C}}\mathbf{x} + \bar{\mathbf{D}}F(t) + v\,,\ \varepsilon = \bar{\mathbf{C}}_2\mathbf{x} + \bar{v} \qquad (4.2)$$

where $\mathbf{x} = \begin{Bmatrix} \mathbf{z} \\ \dot{\mathbf{z}} \end{Bmatrix}$, $\mathbf{A} = \begin{bmatrix} 0 & \mathbf{I} \\ -\mathbf{M}^{-1}\mathbf{K} & -\mathbf{M}^{-1}\mathbf{C} \end{bmatrix}$, $\mathbf{B} = \begin{bmatrix} 0 \\ \mathbf{M}^{-1}\mathbf{G} \end{bmatrix}$

$$\bar{\mathbf{C}} = \begin{bmatrix} -\mathbf{L}\mathbf{M}^{-1}\mathbf{K} & -\mathbf{L}\mathbf{M}^{-1}\mathbf{C} \end{bmatrix},\ \bar{\mathbf{D}} = \begin{bmatrix} \mathbf{L}\mathbf{M}^{-1}\mathbf{G} \end{bmatrix},\ \bar{\mathbf{C}}_2 = \begin{bmatrix} \bar{\mathbf{L}} & 0 \end{bmatrix}$$

$\mathbf{M}, \mathbf{C}, \mathbf{K}$ are the mass, damping, stiffness matrices respectively. $\mathbf{G}$ is the mapping matrix relating the force $F(t)$ to the corresponding DOFs of the system. $\mathbf{z}$, $\dot{\mathbf{z}}$, $\ddot{\mathbf{z}}$ are the displacement, velocity, acceleration vectors respectively. s is the measured acceleration output at the sensor location. ε is the strain vector. v and $\bar{v}$ are the noise vectors. $\mathbf{L}$ and $\bar{\mathbf{L}}$ are the mapping vectors on the measured locations.

Considering the finite difference approximation of x_{k+1},

$$\mathbf{x}_{k+1} = \mathbf{x}_k + \frac{1}{2}(\dot{\mathbf{x}}_{k+1} + \dot{\mathbf{x}}_k)\Delta t \qquad (4.3)$$

where k denotes the k th time instance. We note that Equation (4.1b) can also be written as,

$$\dot{\mathbf{x}}_{k+1} = \mathbf{A}\mathbf{x}_{k+1} + \mathbf{B}\mathbf{F}_{k+1} \qquad (4.1c)$$

Substituting Equation (4.3) into the above equation and rearranging, we have

$$(\mathbf{I} - \mathbf{A}\cdot\frac{\Delta t}{2})\mathbf{x}_{k+1} = (\mathbf{I} + \mathbf{A}\cdot\frac{\Delta t}{2})\mathbf{x}_k + \mathbf{B}\cdot\frac{\Delta t}{2}\cdot(F_k + F_{k+1}) \qquad (4.4)$$

If we have zero initial conditions, i.e. $x_0 = 0$, $F_0 = 0$, Equation (4.4) becomes

$$\mathbf{x}_k = \overline{\mathbf{A}}^{k-1}\overline{\mathbf{B}}F_1 + \overline{\mathbf{A}}^{k-2}\overline{\mathbf{B}}(F_1 + F_2) + \overline{\mathbf{A}}^{k-3}\overline{\mathbf{B}}(F_2 + F_3) + \cdots + \overline{\mathbf{A}}^{0}\overline{\mathbf{B}}(F_{k-1} + F_k)$$

$$= \sum_{i=0}^{k-1}\overline{\mathbf{A}}^{(k-1-i)}\overline{\mathbf{B}}(F_i + F_{i+1}) \qquad (4.5)$$

with $\overline{\mathbf{A}} = (\mathbf{I} - \mathbf{A}\cdot\frac{\Delta t}{2})^{-1}\cdot(\mathbf{I} + \mathbf{A}\cdot\frac{\Delta t}{2})$ and $\overline{\mathbf{B}} = (\mathbf{I} - \mathbf{A}\cdot\frac{\Delta t}{2})^{-1}\cdot\mathbf{B}\cdot\frac{\Delta t}{2}$, where $\overline{\mathbf{A}}^{(k-1-i)}$ denotes the $(k-1-i)$ times power of $\overline{\mathbf{A}}$.

The adopted damage model was described as in Section 3.3. Differentiate Equation (4.4) with respect to α_i which is the fractional stiffness of an element, we get

$$(\mathbf{I} - \mathbf{A}\cdot\frac{\Delta t}{2})\frac{\partial \mathbf{x}_{k+1}}{\partial \alpha_i} = (\mathbf{I} + \mathbf{A}\cdot\frac{\Delta t}{2})\frac{\partial \mathbf{x}_k}{\partial \alpha_i} + \frac{\partial \mathbf{A}}{\partial \alpha_i}\cdot\frac{\Delta t}{2}\cdot(\mathbf{x}_k + \mathbf{x}_{k+1}) \qquad (4.6)$$

put $\overline{\mathbf{E}} = (\mathbf{I} - \mathbf{A}\cdot\frac{\Delta t}{2})^{-1}\cdot\frac{\partial \mathbf{A}}{\partial \alpha_i}\cdot\frac{\Delta t}{2}$, $\frac{\partial \mathbf{A}}{\partial \alpha_i} = \begin{bmatrix} 0 & 0 \\ -\mathbf{M}^{-1}\frac{\partial \mathbf{K}}{\partial \alpha_i} & 0 \end{bmatrix}$.

we have $$\frac{\partial \mathbf{x}_k}{\partial \alpha_i} = \sum_{i=0}^{k-1}\overline{\mathbf{A}}^{(k-1-i)}\overline{\mathbf{E}}(\mathbf{x}_i + \mathbf{x}_{i+1}) \qquad (4.7)$$

After substituting Equation (4.5) into (4.7), we have

$$\frac{\partial \mathbf{x}_k}{\partial \alpha_i} = \sum_{i=0}^{k-1} \left\{ \overline{\mathbf{A}}^{(k-1-i)} \overline{\mathbf{E}} \left(\sum_{m=0}^{i-1} \overline{\mathbf{A}}^{(i-1-m)} \overline{\mathbf{B}} (F_m + F_{m+1}) + \sum_{m=0}^{i} \overline{\mathbf{A}}^{(i-m)} \overline{\mathbf{B}} (F_m + F_{m+1}) \right) \right\} \qquad (4.8)$$

We also note that Equation (4.2) gives the following responses for the *k*th time instance,

$$s_k = f_k + v_k, \varepsilon_k = r_k + \bar{v}_k \qquad (4.9)$$

where $$f_k = \overline{\mathbf{C}} x_k + \overline{\mathbf{D}} F_k, \quad r_k = \bar{\mathbf{C}}_2 \mathbf{x}_k \qquad (4.10)$$

Differentiating Equation (4.10) gives

$$\frac{\partial f_k}{\partial \alpha_i} = \frac{\partial \overline{\mathbf{C}}}{\partial \alpha_i} x_k + \overline{\mathbf{C}} \frac{\partial \mathbf{x}_k}{\partial \alpha_i}, \quad \frac{\partial r_k}{\partial \alpha_i} = \overline{\mathbf{C}_2} \frac{\partial \mathbf{x}_k}{\partial \alpha_i} \qquad (4.11)$$

where $$\frac{\partial \overline{\mathbf{C}}}{\partial \alpha_i} = \left[-\mathbf{L}\mathbf{M}^{-1} \frac{\partial \mathbf{K}}{\partial \alpha_i} \quad 0 \right]$$

Then $\frac{\partial f_k}{\partial \alpha_i}$ and $\frac{\partial r_k}{\partial \alpha_i}$ can be obtained by Equations (4.11) and (4.5) and (4.8). It is noted that the response sensitivities shown in Equation (4.11) indicate that the strain is less sensitive to a parameter change than the acceleration because the acceleration response sensitivity contains two terms relating to the parameter change, however the strain response sensitivity contains only one term.

4.2.2 Sensitivity of Wavelet Packet Transform Component Energy

The measured response is represented by Haar wavelet basis function through the dyadic wavelet transformation. The bandwidths of each level of the dyadic wavelet transform are octaves, and this enables a direct comparison of the energy content of the wavelet packets as shown below. The WPT component function of the measured acceleration $s(t)$ and strain $\varepsilon(t)$ can be reconstructed from the wavelet packet coefficients,

$$s_j^i(t) = \sum_{k=-\infty}^{+\infty} c_{j,k}^i \psi_{j,k}^i(t) = \mathbf{R}_j^i \mathbf{c}_j^i = \mathbf{R}_j^i \mathbf{D}_j^i s(t), \quad \varepsilon_j^i = \sum_{k=-\infty}^{+\infty} d_{j,k}^i \psi_{j,k}^i(t) = \mathbf{R}_j^i \mathbf{d}_j^i = \mathbf{R}_j^i \mathbf{D}_j^i \varepsilon(t)$$

where

$$\mathbf{R}_j^i = [\psi_{j,0}^i \quad \psi_{j,2}^i \quad \cdots \quad \psi_{j,l}^i], \quad l = 0,1,\cdots,N/2^j - 1$$

and $\mathbf{D}_{j+1}^{2i} = \mathbf{H}^{j+1}\mathbf{D}_j^i$, $\mathbf{D}_{j+1}^{2i+1} = \mathbf{G}^{j+1}\mathbf{D}_j^i$, $\mathbf{D}_1^0 = \mathbf{H}^1$, $\mathbf{D}_1^1 = \mathbf{G}^1$, $\mathbf{H}^{j+1}$ and $\mathbf{G}^{j+1}$ are matrices formed by the low-pass filter function and high-pass filter function respectively (Section 3.2.2.3 or Sun and Chang, 2002b), where $\mathbf{c}_j^i$ and $\mathbf{d}_j^i$ are the wavelet packet coefficients for the acceleration and strain respectively with $c_{j,k}^i = \mathbf{D}_j^i s(t)$ and $d_{j,k}^i = \mathbf{D}_j^i \varepsilon(t)$. The i th wavelet packet transform component energy of the acceleration $s(t)$ and strain $\varepsilon(t)$ at the j th level of decomposition, E_{sj}^i and $E_{\varepsilon j}^i$ respectively, are defined as,

$$\begin{aligned} E_{sj}^i &= (\mathbf{s}_j^i)^T(\mathbf{s}_j^i) \\ &= \mathbf{s}^T(\mathbf{R}_j^i\mathbf{D}_j^i)^T(\mathbf{R}_j^i\mathbf{D}_j^i)\mathbf{s} \\ &= \mathbf{s}^T\mathbf{T}_j^i\mathbf{s} \end{aligned} \qquad (4.12a)$$

$$\begin{aligned} E_{\varepsilon j}^i &= (\boldsymbol{\varepsilon}_j^i)^T(\boldsymbol{\varepsilon}_j^i) \\ &= \boldsymbol{\varepsilon}^T(\mathbf{R}_j^i\mathbf{D}_j^i)^T(\mathbf{R}_j^i\mathbf{D}_j^i)\boldsymbol{\varepsilon} \\ &= \boldsymbol{\varepsilon}^T\mathbf{T}_j^i\boldsymbol{\varepsilon} \end{aligned} \qquad (4.12b)$$

The sensitivity of E_{sj}^i and $E_{\varepsilon j}^i$ with respect to the elemental damage is then computed as

$$\frac{\partial E_{sj}^i}{\partial \alpha_i} = \frac{\partial \mathbf{s}^T}{\partial \alpha_i}\mathbf{T}_j^i\mathbf{s} + \mathbf{s}^T\mathbf{T}_j^i\frac{\partial \mathbf{s}}{\partial \alpha_i}, \qquad \frac{\partial E_{\varepsilon j}^i}{\partial \alpha_i} = \frac{\partial \boldsymbol{\varepsilon}^T}{\partial \alpha_i}\mathbf{T}_j^i\boldsymbol{\varepsilon} + \boldsymbol{\varepsilon}^T\mathbf{T}_j^i\frac{\partial \boldsymbol{\varepsilon}}{\partial \alpha_i} \qquad (4.13)$$

and $\mathbf{T}_j^i = (\mathbf{R}_j^i\mathbf{D}_j^i)^T(\mathbf{R}_j^i\mathbf{D}_j^i)$, which is not a function of the signal and is determined only by the wavelet type, and therefore $\partial\mathbf{T}_j^i/\partial\alpha_i = 0$. It is noted that the sensitivity given in Equation (4.13) is based on the dynamic response sensitivity in Equation (4.11) and is

different from the sensitivity given by Sun and Chang (2002b) which is based on the impulse response function.

4.2.3 Equation for Damage Assessment

Vectors E_a and E_e are the vectors of the wavelet packet transform component energies of the analytical model and the experimental model respectively. $\partial E / \partial \alpha$ is the sensitivity with respect to the fractional stiffness from the analytical model. We have the equation corresponding to Equation (3.31),

$$\mathbf{E}_a - \mathbf{E}_e = \frac{\partial \mathbf{E}}{\partial \alpha} \cdot \Delta \boldsymbol{\alpha} \qquad (4.14)$$

where $\Delta \boldsymbol{\alpha}$ is the vector of parameter changes of the system. The damage detection procedure can be performed as in Section 3.5.

When measurement from the first state of the structure is obtained, the wavelet packet component energy and its sensitivity are first computed basing on the analytical model of the structure and the input force obtained in experiment. The increment of parameter is then obtained from Equation (4.14) using the experimental obtained WPT component energy. The analytical model is then updated and the corresponding component energy and its sensitivity are again computed for the next iteration. The criteria corresponding to Equation (3.36) for convergence are,

$$\frac{\left\| \mathbf{E}_{k+1} - \mathbf{E}_k \right\|}{\left\| \mathbf{E}_{k+1} \right\|} \le toler\ 1, \qquad \frac{\left\| \boldsymbol{\alpha}_{k+1} - \boldsymbol{\alpha}_k \right\|}{\left\| \boldsymbol{\alpha}_{k+1} \right\|} \le toler\ 2 \qquad (4.15)$$

where k is the kth time instance. When measurement from the second state is obtained, the updated analytical model is used in the iteration in the same way as that using the measurement from the first state. The final set of identified parameter increments

correspond to the changes occurred in between the two states of the structure. Because ill-conditioning problems exist in Equation (4.14), in the damage identification procedure, the regularization technique described in Section 3.6 and L-Curve method for determining the regularization parameter are applied to obtain the solution.

4.2.4 Numerical Study

A 4-metre long simply supported concrete beam with 0.2 *m* breadth and 0.3 *m* height uniform rectangular cross-section subject to different types of excitations is considered. The Young's modulus and Poisson ratio are respectively 35.8 *GPa* and 0.197, and the density of material is $2376.21\,kg/m^3$. The beam is divided into twelve equal Euler-Bernoulli beam elements as shown in Figure 4.1. The vertical stiffness of the support are simulated with springs of 1.93×10^8 *kN/m* and 0.47×10^8 *kN/m*. The damping ratios for the first six modes are respectively 3.1, 14.3, 7.6, 10.4, 1.6 and 1.4 % which are obtained from other experiments and used here for simulating practical situation.

The intact beam is first excited with a triangular impulsive force applied at one-third point of the beam from the left support with 2197 *N* peak value and it lasts for 0.005 second. The sampling rate is 2000 *Hz*, and acceleration response in 1.0 second obtained from the quarter-span of the beam (shown in Figure 4.1) is used for the identification. The acceleration response collected is decomposed into four levels of wavelets and the associated wavelet packets. The first five seconds acceleration response is Fourier transformed with a FFT size of 8192 for an inspection on the frequency content, and the frequencies of the spectral peaks observed are shown in Table 4.1. It is noted that the frequencies obtained are all slightly higher than those from eigenvalue analysis because

of the forced excitation. Mode 4 cannot be detected from the spectrum because of the location of the sensor. The largest shift in the natural frequency is in the first mode which is only 1.61 %.

Damage is then created in the fourth element of the beam by reducing its bending rigidity by 20%, and the beam is subject again to the same excitation. The spectral frequencies obtained from the acceleration responses are also shown in Table 4.1. Shift in the natural frequency of the two different states occurs in all the modes. The frequency bandwidth of the decomposed wavelet packets are also shown in Table 4.1. All the packets have the same bandwidth of 62.5 *Hz* and it is noted that the 1^{st}, 2^{nd}, 3^{rd}, 7^{th} and 13^{th} wavelet packet encompass one natural frequency of the structure.

Study on the packet energy distribution

Figure 4.2 shows the energy distribution in the sixteen wavelet packets of the response, and they are plotted as percentage of the total energy of the response signal. The first few packets with their energy content ranked in descending order are number 1, 4, 2, 6, 3, 14, 8 and 7. It is noted that those packets contribute the larger percentage of energy also encompass a natural frequency of the beam, or with the frequency included in an adjacent packet. Since all information in the measured response has been decomposed into these sixteen wavelet packets, damage information in the structure will be carried in some or all of these wavelet packets in the form of a shift in the energy content of the wavelets. At the same time, those packets which have large vibration energy are associated with a larger signal to noise ratio, and hence they are best selected for the damage detection.

Variation of WPT component energy with damage extent

The flexural rigidity in element 4 is varied with 0 % to 50% reduction in 2% decrement, and the WPT component energy is computed from the response collected at node 5 of the beam under the same impulsive excitation as for last study as well as under the excitation of a sinusoidal excitation of $F = 20\sin(2\pi ft)$ at the fundamental natural frequency of the beam. The WPT component energy is plotted against the damage extent in Figures 4.3 and 4.4 for both types of excitations as percentage of the total energy in the response. The wavelet packet transform component energy can be categorized into two types: Type I energy varies monotonously with the damage extent and Type II energy exhibits a maximum or minimum in the variation. It is known that if Type II packet energy alone is used in the identification, it would give non-unique solution. Fortunately, the Type I energy packets contribute greatly to the total energy of the response (packets no. 1, 4, 2, 6, 3, 14, 8 and 7 for the case with impulsive excitation, and packet no. 1 for the case of sinusoidal excitation.) and they are much more sensitive to the local change in the physical parameter than the Type II energy packets. Then it can be concluded that the best wavelet packets are found mainly related with the frequency content of the structure, and they also depend on the characteristics of the damage because the variation curve of the WPE behaves from monotonously to non-monotonously with increasing damage extent especially when under the sinusoidal excitation. It is recommended to select those wavelet packets dominated by a structural vibration mode for the identification. However a detail study on the selection of the best wavelet packet is not a subject of this study.

All sixteen packet energy sensitivities will be used in the following simulation studies. The accuracy and uniqueness of the solution are still dominated by the Type I WPT component energy based on the above observations. There is also no need to select the wavelet packets to be taken into account and on their respective weighting in the analysis. Sun and Chang (2002b) have proposed two normalized packet energy change parameters for the identification which enhances the sensitivity of Type II packets, and this will degenerate the final identified results from the above discussions. Also a scheme on optimizing for the best packets is needed.

Damage scenario and their detection

Twelve damage scenarios are studied with different damage extent and from different types of response as listed in Table 4.2. In fact, three patterns of damage (single damage, two adjacent damages and three damages) are considered and each damage pattern is identified from acceleration response, strain response and both types of responses. The first nine scenarios are studied using the vertical response from node 7 when the beam is subject to the same impulsive excitation at one-third span as for last study. Results shown in Figure 4.5 show that either acceleration along or both acceleration and strain responses together can identify the damage accurately with a very small error. We also notice the bad results in Scenario 8. It confirms that the strain response is less sensitive to local damage as predicted in its formulation in Equation (4.11).

Damage Scenarios 10 to 12 are studied using the vertical measured responses from nodes 7 and 8 when the beam is subject to a sinusoidal excitation at one-third span

at the frequency of 30Hz close to the fundamental frequency of the beam**.** The magnitude of the force is 20 *N*. Results in Figure 4.5 show that this arrangement could identify the damage very accurately with virtually no false alarms in other elements with a large error. And we also notice that the acceleration and strain responses when used together can get more accurate results than using any of the two separately as shown in Scenario 12 in Figure 4.5.

Noise effect and model error

In order to study the noise effect, the polluted measured vibration data are simulated as in Equation (3.42). Two damage scenarios are analyzed for noise effect. Damage Scenarios 13 and 14 as listed in Table 4.2 are studied with 5% noise in the measured responses. Acceleration measurements from nodes 5 and 6 are used with impulsive excitation applied at node 4 as described previously, and the identified results are shown in Figure 4.6. The presence of noise seems not adversely affecting the identified result on the damaged elements. This maybe because the error is assigned to the different wavelet packets and the noise effect in each bandwidth is reduced. The other explanation maybe because the structure is simple and the damage can easily be identified. With the damage information distributed to a large number of time-scale wavelet packets, the solution of the respective system of equations implies an averaging of more samples, which is beneficial with respect to noise-contaminated data.

Scenarios 15(a) and (b) includes a model error of an under-estimation in the flexural rigidity of the whole beam structure in the finite element model plus two adjacent damages in the beam with and without 5% noise in the measured acceleration. The

excitation and measuring points are the same as for the last two Scenarios. The identified results for the no noise case show very accurate increase of approximately 3% in elements 3 to 5 and 9 to 11 and reduction of 2% and 7.3% for the damaged elements 6 and 7. The identified 2% and 7.3% reductions are relative to the original modeled flexural rigidity. However when 5% noise is included the identified results degenerate badly, but the damaged elements can still be localized with no false alarm in other elements.

The proposed wavelet packet transform component energy sensitivity has the following advantages when applied to the damage detection of structures: It needs only short duration of measured acceleration from as few as a single sensor. The identified result is noise insensitive and with few false alarms in the undamaged finite elements. It is also not sensitive to model errors. These properties arise from the fact that the time-scale representation of the dynamic response gives a more detailed description of the system characteristic properties than the information from either a time series or its Fourier transform.

4.2.5 Experimental Study

The damage detection method based on the sensitivity of wavelet packet transform component energy was further studied with results from a steel beam tested in the laboratory. The test set-up is shown in Figure 4.7. The dimensions of the beam are 1996, 50.75, 9.69mm which are the beam length, width and height of cross-section respectively. The Young's modulus is 191.1GPa, and density is $7790.6 kg/m^3$. Seven strain gauges are evenly distributed at the bottom of the beam. The local damage is simulated by removing 0.9mm thick of material on both the top and bottom of the beam

and over a length of 9mm across the full width of the beam. This corresponds to an equivalent damage in element *16* of 11.5% reduction in the flexural rigidity of the element after applying Guyan reduction to condense the middle degrees-of-freedom to the end nodes of the element. The first ten natural frequencies and the associated damping ratios obtained from modal test before and after the damage are shown in Table 4.3. The shift in the natural frequency is found very small, but there is significant change in the 1^{st}, 2^{nd}, 7^{th} and 8^{th} modal damping ratios. The damping ratio of each mode is calculated by using the half-power point method on the basis of the frequency response function. The variation of the damping ratios is complicated as it is caused by many factors.

The free vibration strain responses induced by the sudden release of a hanging steel block of 23.274 *kg* are collected. The sampling rate is 2000 Hz and the measured strain responses obtained from the 4^{th} and 5^{th} strain gauges from the left with B&K 4370 accelerometers are used in the identification. The choice of data from the 4^{th} and 5^{th} strain gauges is because they are closest to the middle span which has large deflection and also larger strain. A commercial data logging system INV303 with the associated data analysis system DASP2003 are used in the data acquisition. The first 2000 data are used. The measured strain responses and the corresponding calculated responses using the identified local damages are shown in Figures 4.8(a) and (b). The responses match each other very well. The identified result on the damage is shown in Figure 4.8(c) indicating a fairly accurate result in element *16* but with a 4% reduction false alarm in element *15*. This phenomenon is rather common with many existing identification techniques since element *15* is in immediate adjacent to the damaged element and its vibration energy will

be more highly affected than those in other elements (Shi et al, 2000b). It should be noted that the WPT component energy is a global measure of the vibrational response of the structure, and results identified from these energy changes would also be affected by the changes in the modal damping ratios.

4.2.6 Conclusions

The wavelet packet component energy can be applied for damage detection successfully from the measured vibration responses. The wavelet packet transforms containing a structural vibration mode are most suitable for the identification with a larger energy content and higher sensitivity to the parameter change. Both acceleration and strain responses have been used separately or in combination in the simulation study, and the sensitivity of acceleration with respect to local change of parameter is shown both analytical and numerically much better than that for strains. The proposed method is also shown both analytically and numerically not sensitive to measurement noise. The method can differentiate damages at close proximity with good resolution from using very short duration of measured data from only two sensors.

4.3 Structural Damage Detection from Wavelet Coefficient of Time Responses with Model Errors

In the above section, wavelet packet energy of time responses from several measurement locations can be applied for detection damage successfully. When the number of the structural degrees-of-freedom (DOFs) increases, the number of measurement sensors is also required to be increased. In order to fully make use of the

properties of time domain data in acceleration responses and reduce the number of measurement sensors, wavelet coefficients of acceleration responses are tried to identify damage.

This section presents the analytical formulation on the wavelet coefficient sensitivity of structural responses with respect to a system parameter for structural damage detection. The frequency content of the wavelets is analyzed and the selection on the best wavelets for the detection is discussed. The effect of model error in the mass density, stiffness of elements, support stiffness, damping, excitation frequency and amplitudes to the damage identification is also discussed. Simulations using a single storey plane frame structure and experimental studies with a reinforced concrete beam in the laboratory are performed to demonstrate the proposed method.

4.3.1 Wavelet Coefficient Sensitivity

The time signal $f(t)$ can be decomposed by wavelet transform into the following series

$$f(t) = \sum_{j,k} d_{j,k} \psi_{j,k}(t) \tag{4.16}$$

where $d_{j,k}$ is the wavelet coefficient. If the wavelet is orthogonal, $d_{j,k}$ can be obtained from,

$$d_{j,k} = \int_R f(t) \psi_{j,k}(t) dt \tag{4.17}$$

The response signal is transformed into Daubechies wavelet of order 4 (Db4) by 4 scales in this study. Daubechies wavelets are compactly supported wavelets with extremal phase and highest number of vanishing moments for a given support width.

The formulation on the wavelet coefficient sensitivity can be derived for any physical parameter of the structural system. In the following derivation, α_h represents a physical parameter of the hth finite element, e.g. the Young's modulus of material, a dimension, the second moment of inertia of a cross-section, etc. Both analytical and computational forms of the sensitivity of wavelet coefficient are given below.

Analytical approach

Express the responses $\mathbf{z}$, $\dot{\mathbf{z}}$ and $\ddot{\mathbf{z}}$ in terms of the wavelet transforms and substituting into the equation of motion of the structural system described as Equation (4.1a), we have

$$\mathbf{M}\begin{Bmatrix} \sum_{j,k} d_{j,k}^1 \ddot{\psi}_{j,k}(t) \\ \sum_{j,k} d_{j,k}^2 \ddot{\psi}_{j,k}(t) \\ \cdots \\ \sum_{j,k} d_{j,k}^N \ddot{\psi}_{j,k}(t) \end{Bmatrix} + \mathbf{C}\begin{Bmatrix} \sum_{j,k} d_{j,k}^1 \dot{\psi}_{j,k}(t) \\ \sum_{j,k} d_{j,k}^2 \dot{\psi}_{j,k}(t) \\ \cdots \\ \sum_{j,k} d_{j,k}^N \dot{\psi}_{j,k}(t) \end{Bmatrix} + \mathbf{K}\begin{Bmatrix} \sum_{j,k} d_{j,k}^1 \psi_{j,k}(t) \\ \sum_{j,k} d_{j,k}^2 \psi_{j,k}(t) \\ \cdots \\ \sum_{j,k} d_{j,k}^N \psi_{j,k}(t) \end{Bmatrix} = \mathbf{D}\sum_{j,k} d_{j,k}^F \psi_{j,k}(t) \quad (4.18)$$

where D instead of G in Equation (4.1a) is the mapping matrix relating the force vector $F(t)$ to the corresponding degrees-of-freedom of the system, and $d_{j,k}^F = \int_R F(t)\psi_{j,k}(t)dt$.

Performing inner product with $\psi_{j,k}(t)$ to both sides of Equation (4.18), and noting the orthogonal property of the wavelets, we have

$$(\mathbf{M}\int \ddot{\psi}_{j,k}(t)\psi_{j,k}(t)dt + \mathbf{C}\int \dot{\psi}_{j,k}(t)\psi_{j,k}(t)dt + \mathbf{K})\begin{Bmatrix} d_{j,k}^1 \\ d_{j,k}^2 \\ \cdots \\ d_{j,k}^N \end{Bmatrix} = \mathbf{D}d_{j,k}^F \quad (4.19)$$

Since $\int \ddot{\psi}_{j,k}(t)\psi_{j,k}(t)dt$ and $\int \dot{\psi}_{j,k}(t)\psi_{j,k}(t)dt$ are functions of the wavelets only, put

$$a_{j,k} = \int \ddot{\psi}_{j,k}(t)\psi_{j,k}(t)dt, \qquad b_{j,k} = \int \dot{\psi}_{j,k}(t)\psi_{j,k}(t)dt$$

and Equation (4.19) becomes

$$(\mathbf{M}\mathbf{a}_{j,k} + \mathbf{C}\mathbf{b}_{j,k} + \mathbf{K})\left\{d_{j,k}^1 \quad d_{j,k}^2 \quad \cdots \quad d_{j,k}^N\right\}^T = \mathbf{D}d_{j,k}^F \tag{4.20}$$

rewriting

$$\left\{d_{j,k}^1 \quad d_{j,k}^2 \quad \cdots \quad d_{j,k}^N\right\}^T = (\mathbf{M}a_{j,k} + \mathbf{C}b_{j,k} + \mathbf{K})^{-1}\mathbf{D}d_{j,k}^F \tag{4.21}$$

Differentiating both sides of Equation (4.20) with respect to α_h, we have

$$(\frac{\partial \mathbf{M}}{\partial \alpha_h}a_{j,k} + \frac{\partial \mathbf{C}}{\partial \alpha_h}b_{j,k} + \frac{\partial \mathbf{K}}{\partial \alpha_h})\begin{Bmatrix} d_{j,k}^1 \\ d_{j,k}^2 \\ \cdots \\ d_{j,k}^N \end{Bmatrix} + (\mathbf{M}a_{j,k} + \mathbf{C}b_{j,k} + \mathbf{K})\begin{Bmatrix} \frac{\partial d_{j,k}^1}{\partial \alpha_h} \\ \frac{\partial d_{j,k}^2}{\partial \alpha_h} \\ \cdots \\ \frac{\partial d_{j,k}^N}{\partial \alpha_h} \end{Bmatrix} = 0 \tag{4.22}$$

Substituting Equation (4.21) into (4.22), we finally obtain the wavelet coefficient sensitivity in terms of the system parameter as,

$$\begin{Bmatrix} \frac{\partial d_{j,k}^1}{\partial \alpha_h} & \frac{\partial d_{j,k}^2}{\partial \alpha_h} & \cdots & \frac{\partial d_{j,k}^N}{\partial \alpha_h} \end{Bmatrix}^T = -(\mathbf{M}\mathbf{a}_{j,k} + \mathbf{C}\mathbf{b}_{j,k} + \mathbf{K})^{-1} \cdot (\frac{\partial \mathbf{M}}{\partial \alpha_h}\mathbf{a}_{j,k} + \frac{\partial \mathbf{C}}{\partial \alpha_h}\mathbf{b}_{j,k} + \frac{\partial \mathbf{K}}{\partial \alpha_h}) \cdot (\mathbf{M}\mathbf{a}_{j,k} + \mathbf{C}\mathbf{b}_{j,k} + \mathbf{K})^{-1}\mathbf{D}d_{j,k}^F \tag{4.23}$$

Computational approach

Differentiate Equation (4.17) with respect to α_h, we get

$$\frac{\partial d_{j,k}}{\partial \alpha_h} = \frac{\partial}{\partial \alpha_h}\left(\int_R f(t)\psi_{j,k}(t)dt\right)$$

Since $\psi_{j,k}(t)$ is not related to α_h, we have

$$\frac{\partial d_{j,k}}{\partial \alpha_h} = \int_R \frac{\partial f(t)}{\partial \alpha_h}\psi_{j,k}(t)dt \tag{4.24}$$

where $\partial f(t)/\partial \alpha_h$ is the sensitivity of response to a local change in α_h. Equation (4.24) can also be obtained in an alternative formulation. Express the response sensitivity $\partial f(t)/\partial \alpha_h$ in terms of wavelets, the wavelet coefficient $c_{j,k}$ is obtained as

$$c_{j,k} = \int_R \frac{\partial f(t)}{\partial \alpha_h}\psi_{j,k}(t)dt \tag{4.25}$$

Comparing Equations (4.24) and (4.25), we have

$$\frac{\partial d_{j,k}}{\partial \alpha_h} = c_{j,k} \tag{4.26}$$

Therefore the wavelet coefficient sensitivity of function $f(t)$ can be computed from the wavelet transform of the sensitivity of response $f(t)$.

The response sensitivity can be easily computed from Equation (3.27). The response sensitivity can also be obtained through the analytical state space formulation shown in Equation (4.11) for a general structural system. In the measurement state, since

$$f = \mathbf{L}\ddot{\mathbf{z}} \tag{4.27}$$

where f is the response vector at an arbitrary set of measured locations, and L is the mapping vector relating the measured degrees-of-freedom to the total degrees-of-freedom of the system. We have

$$\frac{\partial f(t)}{\partial \alpha_h} = \mathbf{L}\frac{\partial \ddot{\mathbf{z}}}{\partial \alpha_h} \tag{4.28}$$

Substituting Equation (4.28) into (4.24), we have the wavelet coefficient sensitivity from measurement as

$$\frac{\partial d_{j,k}}{\partial \alpha_h} = \int_R \mathbf{L}\frac{\partial \ddot{\mathbf{z}}}{\partial \alpha_h}\psi_{j,k}(t)dt \tag{4.29}$$

4.3.2 Damage Identification

$\mathbf{D}_0$ and $\mathbf{D}_d$ are vectors of the wavelet coefficient of the two states of the structure, e.g. the intact and damaged states respectively. $\partial\mathbf{D}_0/\partial\alpha$ are the sensitivity matrices of the wavelet coefficient of the first state of the system. $\Delta\boldsymbol{\alpha}$ is the vector of parameter changes of the system. We have the identification equation as,

$$\begin{aligned}\mathbf{D}_d - \mathbf{D}_0 &= \frac{\partial \mathbf{D}_0}{\partial \alpha}\cdot\Delta\boldsymbol{\alpha} \\ &= \mathbf{S}\cdot\Delta\boldsymbol{\alpha}\end{aligned} \tag{4.30}$$

When measurement from the first state of the structure is obtained, the wavelet coefficient and its sensitivity are first computed basing on the analytical model of the structure and the input force obtained in experiment. The increment of parameter is then obtained from Equation (4.30) using the experimental obtained wavelet coefficient. The analytical model is then updated and the corresponding wavelet coefficient and its sensitivity are again computed for the next iteration. Convergence is considered achieved when both the following two criteria are met,

$$\frac{\left\|\{\mathbf{d}_{j,k}\}_{i+1} - \{\mathbf{d}_{j,k}\}_i\right\|}{\left\|\{\mathbf{d}_{j,k}\}_{i+1}\right\|} \le toler\ 1, \qquad \frac{\left\|\boldsymbol{\alpha}_{i+1} - \boldsymbol{\alpha}_i\right\|}{\left\|\boldsymbol{\alpha}_{i+1}\right\|} \le toler\ 2 \tag{4.31}$$

where i refers to the ith iteration. When measurement from the second state is obtained, the updated analytical model is used in the iteration in the same way as that using the measurement from the first state. The final set of identified parameter increments correspond to the changes occurred in between the two states of the structure. Both the response sensitivity and the wavelet coefficient sensitivity are obtained from the computational approach in this section. Regularization techniques described in Section 3.6 are used in the procedure of solving Equation (4.30) to provide bounds to the solution.

4.3.3 Simulation

The one-story plane frame structure as shown in Figure 4.9 serves for the numerical study. The structure is subject to a sinusoidal excitation $F(t) = 10\sin(12\pi t)$ N applied vertically at node 6. The columns are 1.2 m high and the cross-beam is 0.6 m long, and each member has 10mm depth and 20mm breadth uniform rectangular cross-section. The modulus of elasticity and mass density of material are respectively 69×10^9 N/m^2 and $2700\,kg/m^3$.

The finite element model of the structure consists of four and three equal beam-column elements in each vertical and horizontal member respectively. The translational and rotational restraints at the supports are represented by large stiffnesses of 1.5×10^{10} kN/m and 1.5×10^{9} $kN\text{-}m/rad$ respectively. Rayleigh damping is adopted for the system with ξ=0.01. The first 12 natural frequencies of the structure are 13.09, 57.31, 76.7, 152.4, 196.5, 227.3, 374.7, 382.5, 580.2, 699.3, 765.3 and 983.3 Hz. The sampling frequency is 2000 Hz. The tolerance limits for both convergence criteria have been set equal to 1.0×10^{-6}.

Frequency and energy content of wavelet coefficients

Horizontal acceleration response computed at node 9 for a duration of one second after application of excitation is decomposed into four levels of Daubechies Db4 wavelets. The wavelets are divided into Groups *A* and *D* with different bandwidth as shown in Table 4.4. Those in Group A are the low-frequency wavelet coefficients, and those in Group D are the high-frequency wavelet coefficients. Wavelets *A1* and *D1* are the largest scale wavelets and *A4* and *D4* are the smallest scale wavelets. The large scale wavelets, *D1* and *A1*, have better time resolution than the small scale wavelets, *D4* and *A4*, because of their wider bandwidths. The low frequency wavelet coefficients have been checked to be larger compared with those for the high frequency wavelet coefficients, indicating a larger vibration energy in the low frequency responses. This is because the low frequency wavelets include the first few vibration modes of the structure, but the high frequency wavelets include only some of the higher vibration modes of the structure.

Comparison with response sensitivity

The relative sensitivity of the wavelet coefficient to the parameter S_{wc} and the relative response sensitivity S_r are defined as the following for the comparison.

$$S_{wc} = \frac{\left\| \partial \mathbf{d}_{j,k} / \partial \alpha_h \right\|}{\left\| \mathbf{d}_{j,k} \right\|}, \quad S_r = \frac{\left\| \partial \mathbf{f}(t) / \partial \alpha_h \right\|}{\left\| \mathbf{f}(t) \right\|} \tag{4.32}$$

A comparison is performed on the sensitivity of each wavelet coefficients and the response and they are shown in Table 4.5 for a perturbation in the flexural rigidity of each of the finite element. The response sensitivity is comparative low compared with

those from the wavelets. Large scale wavelets are always more sensitive than small scale wavelets, and high frequency wavelet coefficients are more sensitive than low frequency coefficients. Wavelet coefficient *D1* has the highest sensitivity contributed by the damage information carried by vibration modes 9 to 12 as shown in Table 4.4. While wavelet coefficient *D2* is second to *D1* but contributed only by modes 7 and 8. This shows that modes 7 and 8 are the two more significant modes that carry much of the damage information.

Wavelet coefficient sensitivity is in general much higher than that of the response, except coefficients *A3* and *A4* which are contributed by the first few modes. This shows that the lower vibration modes do not carry significant damage information.

Damage identification

The same plane frame structure as for last study is used. The excitation force $F(t) = 10\sin(12\pi t)N$ is applied at node 6 in the vertical direction. Horizontal acceleration response computed at node 9 for a duration of quarter of a second after application of excitation is used for the wavelet decomposition. The sampling rate is 2000 Hz and the following damage Scenarios are with different percentage reduction in the flexural rigidity in an element.

- Scenario 1 – 5% reduction in element 2.
- Scenario 2 – 15% reduction in element 4.
- Scenario 3 – 5% and 10% reduction in elements 3 and 4 respectively.
- Scenario 4 – 10% reduction in element 1.

- Scenario 5 – 15%, 5% and 10% reduction in elements 3, 6 and 8 respectively.

The identified results obtained from the response sensitivity, each of the eight wavelet coefficients and a combination of wavelet coefficients *A4, D1, D2, D3* and *D4* which cover the whole frequency range of the response, are very close to the true value with a maximum error of identification in each Scenario highlighted in Table 4.6. The number of iteration required for convergence in the different damage Scenarios are also given in the table.

The performance of the combined group of wavelet coefficients is similar to the response sensitivity. Wavelet coefficients *D4* and *A4* perform badly in the cases of adjacent damages and with the damage adjacent to the support. More detail inspection shows that Component *A4* consists of only the first two vibration modes of the structure and *D4* consists of the 3rd vibration mode only. This again confirms previous observation that the first few vibration modes do not carry significant information on the changes in the stiffness properties of the structure. In general, small scale wavelet coefficients give less accurate results than the large scale wavelet coefficients, and this is consistent with observations from last study.

Figure 4.10 shows the identified stiffness change in all the elements for Scenarios 3 to 5 using wavelet coefficients *A1, A2, D1* and *D2* in the identification. Both the damage location and severity are identified very accurately without any false alarm in other elements.

Effect of model error

The finite element model would not fully represent the real life structures with assumptions on the linearity, damping models, dynamic behavior, joint flexibilities and constitutive laws of materials, etc. These assumptions are necessary to focus on the problem under study and to reduce the number of unknowns in the solution, or otherwise, including different models on the damping, damages, semi-rigid joints and different forms of finite element for the structure. The latter approach complicates the problem leading to computational errors in the identified results. On the other hand, the violation of the initial assumptions on the model would lead to bias errors which cannot be differentiated with those from computation and measurement noise. In the present and many existing damage assessment techniques, engineering judgments were made on the structural behavior and the standard finite element model on the structure is used. Parameters of the model are considered prone to model inaccuracy, and this effect is investigated in detail with the following list of model error introduced into the finite element model of the plane frame. The same excitation force and sampling rate of signal as for last study is used. The horizontal response from node 9 is used for the decomposition. All the following Scenarios are with 10% reduction in the flexural rigidity of element 3.

- Scenario 6– both the support rotational and translational stiffnesses have been over-estimated ten times
- Scenario 7 – 5% over-estimation in the flexural stiffness of all elements
- Scenario 8 – 2% under-estimation in the density of material
- Scenario 9 – the Rayleigh damping is over-estimated from 0.01 to 0.02
- Scenario 10 – 10% under-estimation in the amplitude of excitation force

- Scenario 11- 5% over-estimation in the excitation frequency
- Scenario 12- includes all the model errors listed from Scenarios 6 to 11

The identified results on the stiffness changes in all the elements are shown in Figure 4.11 for Scenarios 6 to 8 where sensitivity of the response, wavelet coefficients *D1, A4* and a combination of *A4, D1, D2, D3* and *D4* are used in the identification. The results from the response and the combination of wavelet coefficients are similar, while wavelet coefficient *A4* gives many false alarms indicating that model error of a mass density change cannot be detected using low frequency and low scale wavelet coefficients. Wavelet coefficient *D1* gives consistently very good results in these three damage Scenarios. Results not shown indicate that wavelet *D1* can also identify the damage element with similar accuracy with 3% under-estimation in the mass density, but there are also many false alarms in other elements with up to 7% stiffness reduction. All other wavelet coefficients fail in the identification of this damage scenario. In the case of Scenario 7, all the wavelets except *D3* and *D4* could identify the local damage in element 3 with similar results.

Figure 4.12 gives the results for Scenarios 9 to 12 using the response sensitivity and wavelet coefficient *D1* sensitivity. The latter gives consistently very good results even in Scenario 12 when all the different types of model errors exist. It is noted that all the wavelets except wavelet *D1* fail to give meaningful identified results for all the above Scenarios.

Noise effect

Noise effect to the identification is also studied. White noise is added to the calculated accelerations to simulate the polluted measurements as in Equation (3.42). The same excitation force and sampling rate of signal as for last study is used. The horizontal response from node 9 is used for the decomposition. Three damage Scenarios as listed below are studied:

- Scenario 13 – 10% reduction in the flexural rigidity of element 3 with 5% noise.
- Scenario 14 – ditto but with 10% noise.
- Scenario 15 – 10% reduction in element 3 with 1%, 2% and 3% noise respectively and with all the model errors as studied in Scenario 12.

The identified results from the response sensitivity, wavelet coefficient *A1* and coefficient *D1*, are shown in Figure 4.13 for the first two scenarios, and only results from wavelet *D1* are shown for Scenario 15. The 5% noise causes a smaller identified value in the damaged element and with false alarm in other elements. This effect becomes larger with noise, and high frequency wavelet coefficient *D1* is found less resistant to the effect of random measurement noise than the response and the low frequency wavelet coefficient *A1*.

The random noise is noted to give random errors in the elements while the model errors lead to bias error in the finite elements as shown in Scenario 15. Acceptable results can be obtained only with 1% noise level. A small percentage of noise level can reduce the quality of identification greatly when model errors are included.

4.3.4 Experimental Verification

The proposed method was verified with results from a reinforced concrete beam tested in the laboratory. The experimental set-up is shown in Figure 4.14. The beam is 4 metres long with 200.35*mm* width and 300.21*mm* depth uniform cross-section. The Young's modulus and mass density of material are $30.165\times10^{9}\,N/m^{2}$ and $2420.8\,kg/m^{3}$ respectively, and the flexural rigidity of the beam is calculated as 1.3574×10^{7} *kN-m*^{2}. The mass density is obtained by weighing the beam specimen. Seven model B&K 4370 accelerometers are evenly distributed at the bottom of the beam. The responses are low-pass filtered at 1000 Hz, and a commercial data logging system INV303 with the associated data analysis system DASP2003 are used in the data acquisition.

The finite element model consists of 19 beam-column elements with 17 of them between the supports as shown. The length of elements is not equal due to the presence of a rectangular steel hoop between nodes 7 and 9. This hoop is also modeled with a lump mass. The local damages are cracks produced by keeping 50 *kN* static load at the three-quarter point of the beam close to node 14 for half an hour. Cracks developed during the static test are between nodes 12 to 16, and the location and length of which are also shown in Figure 4.14. This corresponds to an equivalent damage in elements 12, 13, 14 and 15 of 9.3%, 22.5%, 20.6% and 5.1% reduction in the flexural rigidity of these elements respectively by integrating over the finite element without considering the concrete between the cracks.

Modal test is performed before and after the static loading test with impacts from a Dystran Instruments 12 lbs instrumented impulse hammer model 5803A in the vertical direction at *5/8L* of the beam as shown in Figure 4.14. The sampling frequency is 2000 Hz. Frequency response function (FRF) is calculated for each hammer test and the natural

frequency and modal damping ratios are calculated from the FRF averaged over twenty hammer tests. The first six natural frequencies and the associated damping ratios obtained from the two states of the beam are shown in Table 4.7. The shift in the natural frequency is found very small, but there is significant change in the second and third modal damping ratios. The experimental damping ratios of the intact beam have been included in the computation of the responses for subsequent damage detection of the damaged beam.

The updating of the beam always refers the experimental sample to the finite element model as described in the paragraph immediately after Equation (4.30). (a) It refers the undamaged experimental beam to the original FEM in the updating on the model errors. (b) After the FEM is improved, the improved FEM is used as the reference model to compare with the experimental damaged sample. Therefore there is no need to have equal hammer force for the undamaged and the damaged samples. In the case of (a), the experimental impact force on the undamaged beam is recorded and included in the FEM as excitation to generate the analytical response D_0. The experimental response D_d and the calculated D_0 are then used in Equation (4.30) to obtain vector $\Delta\alpha$. Similarly for the case of (b), the impact force acting on the damaged beam is recorded and input into the improved FEM as excitation force to calculate the responses D_0, and the record experimental response of the damaged beam D_d together with D_0 are then used in Equation (4.30).

Updating the analytical model errors

The beam is supported on steel blocks which in turn fixed to a large concrete block resting on the strong floor of the laboratory. These cannot be considered as rigid supports. Both the support stiffnesses and the flexural rigidity of the beam cross-section are prone to model error while the mass density is taken as correct from direct weighing of the sample. These three parameters are improved using the measured acceleration obtained from the intact state of the structure. The first second of acceleration responses obtained from the second to the sixth accelerometers after each hammer hit are decomposed into wavelets, and the wavelet coefficients *D1*, *D2*, *D3*, *D4* and *A4* are used together in the sensitivity approach as per Equation (4.30) to update the three unknowns giving $3.5225\times10^{9}\ N/m$ and $5.7679\times10^{9}\ N/m$ for the left and right vertical support stiffnesses and $1.8305\times10^{7}\ kN-m^{2}$ on the flexural rigidity of the beam section. This combination includes all possible measured information in the identification. The natural frequencies of the updated beam is calculated and shown in the first column of Table 4.7.

Damage identification

The vibration of the cracked beam is inherently nonlinear in nature. It is weakly nonlinear and can be approximated by the piecewise linear relation as shown in Equation (4.30) for a small change $\Delta\alpha$. Acceleration responses from the second to the sixth accelerometers in the damaged state of the beam are decomposed into wavelets, and again the wavelet coefficients *D1, D2, D3, D4* and *A4* are used to update the elemental flexural rigidities. Data from the first second after a hammer hit is used. The identified changes in elemental flexural rigidity are shown in Figure 4.15. The large reduction in elements 14 and 15 are accurately identified while false alarms of 7.2% reduction exists

in elements 10 and 17. However the pattern of damage is clearly identified with a clear damage zone spreading from elements 12 to 16.

The accuracy of the identified results is further checked by comparing the acceleration response from the second accelerometer obtained in the two states of the beam, and the first 0.2 seconds of these responses are plotted in Figure 4.16. The computed responses are from the updated beam model in the undamaged state, and including the identified changes in the flexural rigidity in the damaged state. They are found matching the measured responses very well except in the first 0.02 second due to the presence of many transient high frequency components immediately after the hammer hit. Despite the relatively large convergence errors of 0.342 and 0.257 in the two stages of updating in this example, it may be concluded that the reinforced concrete beam has been updated correctly.

4.3.5 Conclusions

The wavelet coefficient sensitivity of structural responses with respect to a system parameter is presented both analytically and computationally. This sensitivity is shown to be more sensitive to local structural changes than the response sensitivity. The frequency content of the wavelets is analyzed and the selection on the best wavelets for the detection is discussed. The new damage indicator is shown with the help of a single storey plane frame structure, to be not sensitive to model errors in the mass density, stiffness of elements, support stiffness, damping, excitation frequency and amplitudes. Simulation results show that the damage information is carried mostly in the higher vibration modes of the structure as diagnosed with the corresponding wavelet coefficients

from its dynamic responses. While a combination of wavelets encompasses all the available frequency bandwidth is adopted to include all possible measured information in the successful identification of a reinforced concrete beam in the laboratory.

4.4 Condition Assessment from Wavelet Coefficients of Acceleration Response in Structures under Support Excitation

Most existing methods on condition assessment of structure require an input which may be ambient or forced excitation. The ambient excitation is usually taken as random in nature. This section includes the ground micro-tremor as the forced excitation in the condition assessment. The capability of wavelet packet transform coefficient sensitivity is studied particularly with short duration of data sampled at a low frequency. The performance of this sensitivity and the response sensitivity is compared in the simulation and experimental studies with a three-dimensional steel frame structure under support excitation in three directions.

4.4.1 Response of Structures under Support

The equation of motion of a N degrees-of-freedom (DOFs) damped structural system under support excitation is given as

$$\mathbf{M}\ddot{\mathbf{x}}+\mathbf{C}\dot{\mathbf{x}}+\mathbf{K}\mathbf{x}=-\mathbf{M}\cdot\mathbf{L}\cdot\ddot{x}_s(t) \qquad (4.33)$$

where $\mathbf{M},\mathbf{C},\mathbf{K}$ are the $N\times N$ mass, damping and stiffness matrices respectively. $\mathbf{L}$ is the mapping vector relating the DOFs with the force input to the corresponding DOFs of the system. $\mathbf{x}$, $\dot{\mathbf{x}}$, $\ddot{\mathbf{x}}$ are the $N\times 1$ displacement, velocity, acceleration vectors

respectively. $\ddot{x}_s$ is the support acceleration. $\mathbf{x}$, $\dot{\mathbf{x}}$, $\ddot{\mathbf{x}}$ is computed from Equation (4.33) with a time-stepping integral method such as Newmark Method.

Differentiating Equation (4.33) with respect to α_i, we get

$$\mathbf{M}\frac{\partial \ddot{\mathbf{x}}}{\partial \alpha_i} + \mathbf{C}\frac{\partial \dot{\mathbf{x}}}{\partial \alpha_i} + \mathbf{K}\frac{\partial \mathbf{x}}{\partial \alpha_i} = -\frac{\partial \mathbf{K}}{\partial \alpha_i}\mathbf{x} - \frac{\partial \mathbf{C}}{\partial \alpha_i}\dot{\mathbf{x}} \qquad (4.34)$$

Equation (4.34) is same as Equation (3.27) and can be solved as described in Section 3.4.

4.4.2 Sensitivity of Wavelet Packet Transform Coefficients

The original signal can also be reconstructed from the WPT coefficients as,

$$f(t) = \sum_{i=0}^{2^j-1} f_j^i(t), \qquad \text{and} \qquad f_j^i(t) = \sum_{k=-\infty}^{+\infty} c_{j,k}^i \psi_{j,k}^i(t) \qquad (4.35)$$

where $f_j^i(t)$ denotes the signal component in the i th frequency band.

The WPT is applied to $\frac{\partial \ddot{x}_l}{\partial \alpha}$ and $\ddot{x}_l$ separately, where l denotes the l th DOF of the structure. The relation between $WPT(\frac{\partial \ddot{x}_l}{\partial \alpha_i})$ and $WPT(\ddot{x}_l)$ has been given by Law and Li (2006) as,

$$WPT(\frac{\partial \ddot{x}_l}{\partial \alpha_i}) = \frac{\partial}{\partial \alpha_i} WPT(\ddot{x}_l) \qquad (4.36)$$

where $WPT(\frac{\partial \ddot{x}_l}{\partial \alpha_i})$ and $WPT(\ddot{x}_l)$ are the WPT coefficients of $\frac{\partial \ddot{x}_l}{\partial \alpha_i}$ and $\ddot{x}_l$ respectively. Using Equations (4.34) and (4.36), we can form the sensitivity matrix of the WPT coefficients as

$$\mathbf{S} = \left[\frac{\partial}{\partial \alpha_1} WPT(\ddot{x}_l) \quad \frac{\partial}{\partial \alpha_2} WPT(\ddot{x}_l) \quad \cdots \quad \frac{\partial}{\partial \alpha_m} WPT(\ddot{x}_l) \right] \tag{4.37}$$

4.4.3 The Sensitivity-based Approach

We consider a general structure which behaves linearly before and after the occurrence of damage for the illustration of the proposed approach. The damage identification includes two separate stages of updating the analytical model and identifying local damages. $WPT(\ddot{x}_l)_0$ and $WPT(\ddot{x}_l)_d$ are vectors of the WPT coefficient of the acceleration response at the *l*th DOF of the intact and damaged structures respectively. *S* is the sensitivity matrix of the WPT coefficient calculated from the first state of the system using Equation (4.37). $\Delta\alpha$ is the vector of fractional change of the parameters of the system. We have the identification equation as

$$\mathbf{S} \cdot \Delta\boldsymbol{\alpha} = WPT(\ddot{x}_l)_d - WPT(\ddot{x}_l)_0 \tag{4.38}$$

The initial analytical model is adopted for model updating in the first stage of the study, and $WPT(\ddot{x}_l)_0$ and matrix **S** are obtained from this initial model. Acceleration measurement from the intact state of the structure is obtained and the corresponding WPT coefficient $WPT(\ddot{x}_l)_d$ is computed. The initial model is then updated in Equation (4.38) and the corresponding $WPT(\ddot{x}_l)_0$ and its sensitivity *S* are again computed from the updated model for the next iteration. The final updated analytical model is obtained when both of the following two criteria are met,

$$\frac{\left\| \{WPT(\ddot{x}_l)\}_{m+1} - \{WPT(\ddot{x}_l)\}_m \right\|}{\left\| \{WPT(\ddot{x}_l)\}_{m+1} \right\|} \le toler\ \ 1, \quad \frac{\left\| \boldsymbol{\alpha}_{m+1} - \boldsymbol{\alpha}_m \right\|}{\left\| \boldsymbol{\alpha}_{m+1} \right\|} \le toler\ \ 2 \quad (4.39)$$

where m refers to the m th iteration, and *toler1* and *toler2* are the two specified criteria of convergence.

Then the updated analytical model is used to represent the first (original) state of the structure and the damaged state of the real structure is regarded as the second state in the identification. Measurement from the damaged state is obtained, and the same iteration computations as in the first stage are carried out. The final set of identified parameter increments correspond to the changes occurred in between the intact and damaged states of the structure. Regularization techniques are applied to the solution of the inverse problem.

4.4.4 Simulation

A five-bay three-dimensional frame structure as shown in Figure 4.17 serves for the numerical study. The finite element model consists of thirty-seven three-dimensional Euler beam elements and seventeen nodes. The length of all the horizontal, vertical and diagonal tube members between the centers of two adjacent nodes is exactly 0.5m. The structure orientates horizontally and is fixed into a rigid support at three nodes at one end. Table 4.8 gives a summary of the main material and geometrical properties of the members of the frame structure. Each node has six DOFs, and altogether there are 102 DOFs for the whole structure. The elastic modulus of material of all the elements is taken as unknown in the identification.

The translational and rotational restraints at the supports are represented by large stiffnesses of 1.5×10^{11} *kN/m* and 1.5×10^{10} *kN-m/rad* respectively in six directions. Rayleigh damping is adopted for the system with ξ_1=0.01 and ξ_2=0.005. The first 12 natural frequencies of the structure are 9.21, 28.26, 33.71, 49.01, 49.72, 71.02, 89.80, 153.93, 194.33, 209.80, 256.51 and 274.82 *Hz* from the eigenvalue analysis of the structure. The sampling frequency is 200 *Hz* .

The structure is subject to the El-Centro ground motion in three directions decimated 100 times as plotted in Figure 4.18 to simulate a micro-tremor. The response of the structure is computed at all the DOFs from Equation (4.33) and is subsequently resampled in the ratio of 1 in 4 corresponding to a sampling rate of 50 Hz to form a subset of the response. The vertical acceleration response at node 5 of the structure is recorded for a duration of ten seconds after the excitation begins. The response is decomposed into four levels of Daubechies Db4 wavelet packets, which are 16 signal components represented by their WPT coefficients, and each has the same frequency bandwidth of 1.5625Hz.

The Sensitivities

The sensitivities of the calculated response with respect to the elastic modulus of material are also computed from Equation (4.34) and resampled again in the ratio of 1 in 4, and the corresponding WPT coefficients with respect to the elastic modulus of material of the 4^{th} and 20^{th} elements of the structure are shown in Figure 4.19. The WPT coefficient sensitivities are arranged in a vector in their order of frequency band. The number of WPT coefficient is seen to be more than the number of original data because

in the extraction of the wavelets, zero padding is performed at the end of the data series in case the number of original data cannot be equally divided. It can be seen from Figure 4.19 that some of the WPT coefficients are more sensitive than the response (Lu and Law, 2007). Hence, the WPT coefficients from the 6^{th} to 16^{th} sets of wavelets are used to detect damage in the following simulation study for a better performance (Law and Li, 2006). These coefficients have been checked to correspond to a higher frequency range and are more sensitive to a stiffness change.

Local damage identification from WPT coefficient sensitivity and response sensitivity

Five damage scenarios as listed in Table 4.9 are studied encompassing the cases with single and multiple damages, with and without noise and initial model error. Ten seconds of the response are used except in Scenario 5 where the first 50 seconds of response is used with the low sampling frequency of 10 Hz. The tolerance limits for both convergence criteria have been set equal to 1.0×10^{-8} except for Scenario 1 where 1.0×10^{-6} is adopted. The "measured" acceleration responses are obtained through computation using the Newmark method with a time step of 0.005s between two consecutive time instances.

The identified results from WPT coefficients for Scenario 1 without noise and model errors are shown in Figure 4.20 and they are very close to the true values. The results obtained from the response sensitivity are also close to the true values at the damage locations, but there are a number of false alarms in other elements, such as element 28. The response sensitivities are obtained from Equation (4.34) using Newmark

method. It is noted that the convergence criteria is 1.0×10^{-6} for this Scenario. If the iteration for the identification is allowed to continue with a convergence criteria of 1.0×10^{-8}, the false alarms will disappear and the results obtained would be very similar to those from the WPT coefficients. This indicates that the response sensitivity can also be used to identify damage accurately but converge more slowly than the WPT coefficients sensitivity. This can be explained by the fact that the selected WPT coefficients obtained from the higher frequency response components are more sensitive to damage than response sensitivity (Law and Li, 2006). This also demonstrates that by a proper selection of the WPT coefficients, the non-sensitive components can be removed resulting in a higher accuracy and faster convergence of the results.

Effect of model error and noise

Many existing techniques on condition assessment cannot handle the problem when the original model carries initial model errors which may be errors with the boundary conditions, element connectivity and element stiffness. In this study, only an error in the elastic modulus of material of an element is considered. An error in the element connectivity will be considered in the experimental study. Scenario 2 has 1% over-estimation in the elastic modulus of material of each member of the structure. The same excitation force, sampling rate of signal, convergence criteria, measured location and WPT coefficients as for Scenario 1 are used. The identified results shown in Figure 4.20 show that the method can tolerate some model error with good accuracy.

White noise is added to the calculated accelerations to simulate the polluted measurements as in Equation (3.42). The same excitation, response, sampling rate and

WPT coefficients as for the last study are used. Damage Scenario 3 has 5% noise in the "measured" acceleration. The location and extent of damage can be identified with some accuracy as shown in Figure 4.20, but there are also alarms in several adjacent elements. The random noise is noted to give error in the identified damage of the damaged element, though good indication on the damage location is still achieved. This shows that the identified results are easily corrupted by measurement noise, and noise reduction prior to identification is needed.

Scenario 4 is studied with damage in two adjacent elements to test the resolution capability of the proposed approach with close proximity of two damages. Results in Figure 4.20 indicate that WPT coefficients can identify the damage elements quite accurately but with some error in the damage magnitude. It is believed that more spatial information of the structure can be captured from using responses from more locations of the structure to mitigate the noise effect.

Performance from a subset of the measured response

In practice, most of the on-line health monitoring systems is operating with a high sampling frequency sufficient to cover a wide range of the structural response. Scenario 5 is on the use of a subset of the original response resampled in the ratio of 1 in 20. All the sixteen sets of WPT coefficients are used in the identification. The identified results in Figure 4.20 show that this subset of the "measured" response yields very accurate results.

It should be noted that for all the Scenarios in Table 4.9, the response obtained from Equation (4.33) contains components from all the structural vibration modes with frequencies below 100 Hz, and the resampling of the response only results in a subset of

the response measurement. The time series approach does not mainly depend on the frequency information of the measured response as the frequency domain method, and it also makes use of the vibration amplitude in the solution process as from the following discussions.

The amplitude of the structural response, when expressed in the form of Duhamel integral of $\sum_{i=1}^{n}\int \frac{e^{-\xi_i \omega_i \tau}}{\omega_{id}} \sin(\omega_{id}\tau)\cdot F(t-\tau)d\tau$, includes the structural information in the two terms of $\sin(\omega_{id}\tau)$ and $e^{-\xi_i\omega_i\tau}/\omega_{id}$. The Nyquist frequency has to be satisfied if the structural vibration information (both the amplitude and frequency) is sought from the term $\sin(\omega_{id}\tau)$. However the term $e^{-\xi_n\omega_n\tau}$ is an exponential function and is independent of the sampling frequency. The time series method is therefore less dependent on the Nyquist frequency and the damage detection can be performed successfully with a low sampling rate.

Another comparison is made in Scenario 6 with two set of responses. The first set is computed from Equation (4.33) with a sampling rate of 200 Hz, and the other set is obtained from resampling the first set of response in the ratio of 1 in 2. The first eight sets of WPT coefficients from the first set and all the sixteen sets of WPT coefficients from the second set of response are used for the identification covering the same bandwidth of 0 ~ 50.0 Hz. Accurate identified results shown in Figure 4.20 provide further evidences to the above discussions.

Though the simulation studies shown above are discussed with reference to ground micro-tremor excitation, yet the proposed approach can be used for the case with

ground-borne blast excitation or traffic excitations which can be easily achieved in practice.

4.4.5 Experimental Verification

A nine-bay three-dimensional frame structure shown in Figure 4.21(a) serves for the experimental study. It is fabricated in the laboratory using Meroform M12 construction system. It consists of sixty-nine 22mm diameter alloy steel tubes jointed together by twenty-nine standard Meroform ball nodes. Each tube is fitted with a screwed end connector which, when tightened into the node, also clamps the tube by means of an internal compression fitting. All the connection bolts are tightened with the same torsional moment to avoid asymmetry or nonlinear effects caused by man-made assembly errors. The whole experimental setup is shown in Figure 4.21(a) and the support is plotted in Figure 4.21(b). The finite element model of the structure is shown in Figure 4.22. The structure has the same material and geometric properties as shown in Table 4.8.

Modeling of the structure

The Meroform ball joints have been installed as semi-rigid joints, and a finite element model of a hybrid beam with semi-rigid end connections has been proposed (Law et al, 2001). This section adopts this hybrid beam model for the model improvement of the structure. The initial model assumes a large fixity factor p for the rotational stiffness of the joints which is taken equal to 0.999 with 1.0 equal to that for a rigid joint.

Dynamic Test for damage detection

The structure is excited with impact from a Dystran Instruments 12 lbs instrumented impulse hammer model 5803A hitting approximately at the centroid of the support in the *y*-direction. The support is very rigid and heavy compared with the frame and it is hold down to the strong floor with four steel bolts. The acceleration responses of the support along the three principal directions are measured. Only the response in the *y*-direction is significant and those in the other two directions are very small to be neglected. Nine accelerometers are placed at nodes 2 to 10 in the *y*-direction for recording the acceleration response time histories. The sampling frequency is 2000 Hz.The acceleration time history at the support in the *y*-direction is shown in Figure 4.23(a).

Damage scenarios

After performing the dynamic test on the intact frame structure, local faults are introduced by replacing three intact members with damaged ones. The artificial damage is of two types. Type I is a perforated slot cut in the central length of the member. The length of slot is 13.7 cm, and the remaining depth of the tube in the cut-cross-section is 14.375 mm. Type II is the removal of a layer of material from the surface of the member. The external diameter of the tube is reduced from 22.02mm to 21.47mm, and the length of the weakened section is 202 mm, located in the middle of the beam leaving 99mm and 75mm length of original tube cross-section on both sides. Figure 4.21(c) gives a close up view of the damaged frame members. Type I damage is located in element 10 and Type II damage is located in elements 27 and 68. The equivalent damages computed by Guyon

method are 5% and 9.5% reduction in the modulus of elasticity of element 10 and elements 27 and 68 respectively.

Model improvement for damage detection

The two-stage approach is adopted for the damage detection. The first stage updates the rotational stiffness at the joints and obtains an improved analytical model for the intact structure. Two y-direction acceleration responses obtained from nodes 6 and 7 are used in Equation (4.38) for the identification. There are 69×6=414 unknowns in the identification. The first 500 data points of each acceleration response are used and the responses are decomposed into four levels of Daubechies Db4 wavelet packets, which are 16 signal components represented by their WPT coefficients, and each has the same frequency bandwidth of 62.5Hz. All the sixteen sets of WPT coefficients are used in the experimental identification procedure with $16 \times 2 \times 37 = 1184$ identification equations. The measured modal damping ratios from the intact structure have been used in Equations (4.33) and (4.34) for the computation of the analytical responses. The first 12 measured natural frequencies of the intact structure are 5.202, 11.197, 15.183, 19.222, 27.716, 39.841, 52.197, 61.052, 65.784, 78.523, 85.550, 90.484Hz. The updated rotational stiffness do not differ too much from the original value with the largest change in member 20 at node 22 with the updated $p=0.86$ for the x-axis rotational stiffness. After this updating, this model is considered accurate for the next stage of damage assessment.

The second stage updates the local faults in all the members of the structure in terms of their modulus of elasticity. Again the y-direction responses from nodes 6 and 7 are used in Equation (4.38) for the identification. There are 69 unknowns in the

identification. The first 500 data points of each response are used and all WPT coefficients are used in Equation (4.38). The identified damage extent for all the elements are shown in Figure 4.24. The identified reduction in the modulus of elasticity in the damaged members are 5.18%, 9.65% and 9.08% for elements 10, 27 and 68 respectively which are quite close to the values of 5%, 9.5% and 9.5% respectively. There are indications of local damage in element 5 with a reduction of 1.6% and in element 69 with a reduction of 1.89% even though they are in real case undamaged. The measured responses from nodes 6 and 7 and the computed responses from the final updated analytical model are shown in Figure 4.23(b) and (c) and they are very close to each other.

4.4.6 Conclusions

In this section, acceleration responses at only the support and at limited number of locations of the structure are required for damage detection. The performance from the response sensitivity approach and the WPT coefficient sensitivity approach under support excitation is compared. The latter is concluded to converge faster with a proper selection of the wavelet packets for a three-dimensional steel frame structure. The use of subsets of the measured response at different resampling rates is discussed and a subset would yield similar identified results as from the full set of measured response since similar structural information is included in the subset of data. Simulation results show that the location and the extent of damage of the structure can be identified accurately under the support excitation without any special artificial excitation. The multiple damage scenario with an experimental nine-bay three dimensional frame structure also confirms the effectiveness of the proposed method.

4.5 Summaries

In this chapter, acceleration responses are adopted to detect damage via sensitivity analysis and model updating techniques. Wavelet packet component energy and wavelet coefficients are computed from acceleration responses and applied in the identification equation. The former concentrates the energy of the acceleration responses to different component energy according to different frequency bandwidth with good tolerance to noise but requires more measurement locations especially in the structures with large number of DOF than the latter. The wavelet coefficient methods are studied in the structures under general excitation and support excitation which can be measured by accelerometers and increase the accuracy of the measurement of excitation force. Both of them can tolerate certain extent of model error and noise. Numerical studies and experimental verifications are performed for every method and satisfactory results obtained.

Table 4.1 - Natural frequencies of the response from the two states of structure

Natural Frequency (Hz)			Wavelet packet number	Frequency Bandwidth (Hz)
FEM	Experiment			
	Intact	Damaged		
30.94	31.01	30.52	1st	0~62.5
100.78	104.25	103.03	2nd	62.5~ 125
184.14	185.06	184.57	3rd	125~187.5
-	-	-	4th	187.5~250
305.29	-	-	5th	250~312.5
-	-	-	6th	312.5~375
-	404.30	400.39	7th	375~437.5
468.48	-	-	8th	437.5~500
-	-	-	9th	500~562.5
-	-	-	10th	562.5~625
-	-	-	11th	625~687.5
706.31	-	-	12th	687.5~750
-	767.09	766.11	13th	750~812.5
-	-	-	14th	812.5~875
-	-	-	15th	875~937.5
-	-	-	16th	937.5~1000

Table 4.2 - Damage Scenarios

Damage Scenario	Damage extent	Damage locations	Response type	Excitation type
1	10%	11^{th} element	acceleration	Impulsive excitation at node 5
2	10%	11^{th} element	strain	
3	10%	11^{th} element	acceleration and strain	
4	5%,10%	6^{th} ,7^{th} element	acceleration	
5	5%,10%	6^{th} ,7^{th} element	strain	
6	5%,10%	6^{th} ,7^{th} element	acceleration and strain	
7	5%,10%,15%	3^{rd}, 4^{th} ,8^{th} element	acceleration	
8	5%,10%,15%	3^{rd}, 4^{th} ,8^{th} element	strain	
9	5%,10%,15%	3^{rd}, 4^{th} ,8^{th} element	acceleration and strain	
10	5%,10%	6^{th} ,7^{th} element	acceleration	Sinusoidal excitation at node 5
11	5%,10%	6^{th} ,7^{th} element	strain	
12	5%,10%	6^{th} ,7^{th} element	acceleration and strain	
13	10%	2^{nd} element	acceleration with 5% noise	Impulsive excitation at node 4
14	5%, 10%	6^{th} ,7^{th} element		
15(a)	5%, 10%	6^{th} ,7^{th} element		Impulsive excitation at node 4 with -3% model error in all elements
15(b)	5%, 10%	6^{th} ,7^{th} element	No noise	

Table 4.3 - The experimental natural frequencies (Hz) and damping ratio of the steel beam

intact		damaged	
Frequency (Hz)	Damping ratio	Frequency (Hz)	Damping ratio
5.867	0.667	5.900	0.516
23.647	0.458	23.565	0.187
53.582	0.228	53.422	0.251
94.453	0.380	94.010	0.359
146.960	0.226	146.439	0.223
213.058	0.283	212.298	0.299
288.975	0.270	288.003	0.220
374.510	0.253	373.979	0.207
476.309	0.121	476.520	0.116
587.257	0.091	587.259	0.077

Table 4.4- The frequency content of the wavelet coefficients (Hz)

	response	Wavelet							
		A4	A3	A2	A1	D4	D3	D2	D1
Bandwidth	0~1000	0~62.5	0~125	0~250	0~500	62.5~125	125~250	250~500	500~1000
Modes	f_0 ~ f_{12}	f_0 ~ f_2	f_0 ~ f_3	f_0 ~ f_6	f_0 ~ f_8	f_3	f_4 ~ f_6	f_7 , f_8	f_9 ~ f_{12}

Note: f_0 denotes the excitation frequency, f_1 ~ f_{12} denotes the first 12 natural frequencies of the frame structure.

Table 4.5 - Comparison of response sensitivity to wavelet sensitivity

		Perturbation in the following finite element										
		1	2	3	4	5	6	7	8	9	10	11
S_r	response	18.28	16.62	17.28	15.64	9.39	13.27	9.39	15.65	17.28	16.62	18.27
S_{wc}	A1	17.92	16.31	17.01	15.35	9.18	13.24	9.18	15.35	17.01	16.31	17.92
	A2	13.16	12.94	13.51	11.25	7.24	12.5	7.24	11.25	13.5	12.94	13.15
	A3	8.38	5.23	7.33	4.67	3.56	5.93	3.56	4.67	7.33	5.23	8.36
	A4	7.08	3.29	5.92	2.76	2.70	3.53	2.70	2.76	5.92	3.29	7.06
	D1	52.02	46.9	45.1	44.7	28.5	18.6	28.5	44.7	45.1	46.9	52.0
	D2	49.14	40.7	42.48	42.18	23.24	21.27	23.24	42.18	42.48	40.70	49.14
	D3	26.49	29.74	29.06	25.69	16.0	27.76	16.0	25.68	29.06	29.74	26.49
	D4	14.28	11.75	13.22	11.04	6.91	13.84	6.91	11.04	13.22	11.75	14.26

Table 4.6 - Error of Identification in percentage

	Scenario 1	Scenario 2	Scenario 3	Scenario 4	Scenario 5
Response	-2.03/7	0.00/20	0.00,0.00/20	-0.54/11	0.00,0.00,0.00/24
D1	0.00/17	-0.35/12	-0.44,-0.68/12	-0.31/9	0.04,-0.09,-0.52/12
D2	-0.41/9	-1.00/14	0.01,-2.88/14	-1.79/11	-0.09,0.08,0.10/13
D3	-0.57/9	0.02/16	-0.61,-0.24/16	-0.36/16	-0.25,-0.03,0.16/11
D4	-0.01/20	0.00/28	-0.03,-0.01/28	-21.51/8	fail
A1	-1.82/8	-0.31/13	-1.20,-0.09/13	-0.60/12	-0.85,-0.05,0.12/16
A2	-0.57/7	0.00/10	-1.29,0.08/10	-3.53/10	-0.49,-0.11,0.18/14
A3	-1.07/8	-0.11/11	-0.53,0.44/11	-3.33/12	1.08,0.19,0.11/66
A4	-0.47/9	-0.10/14	-2.60,1.24/14	-1.84/18	fail
A4 + D1 + D2 + D3 + D4	-2.12/7	-0.22/20	0.00,0.00/20	-0.66/11	-0.65,0.00,0.03/16

Note: •/• denotes the error of identification (%)/required iteration number.

Table 4.7 - The natural frequencies (Hz) and experimental damping ratio of the reinforced concrete beam

computed		Measured			
intact	damaged	intact state		damaged state	
Frequency (Hz)	Frequency (Hz)	Frequency (Hz)	Damping ratio (%)	Frequency (Hz)	Damping ratio (%)
32.73	32.69	32.75	3.1	32.30	3.1
130.37	129.97	133.82	4.0	134.34	5.5
290.73	289.10	281.87	6.3	278.83	7.5
504.97	501.34	565.88	1.1	555.57	1.8
768.32	763.73	792.75	1.0	790.67	1.2
976.35	974.91	983.63	0.9	981.03	1.1

Table 4.8 - Material and geometrical properties

Properties	Member
Young modulus [N/m^2]	2.10E11
Area [m^2]	6.597E-5
Density [kg/m^3]	1.2126E4
Mass [kg]	0.32
Poisson ratio	0.3
Moment of area I_y [m^4]	3.645E-9
Moment of area I_z [m^4]	3.645E-9
Torsional rigidity J [m^4]	7.290E-9

Table 4.9 - Damage scenario

Scenario	Damage	Noise	Model error	Sampling rate (Hz)
1	5% in element 16 10% in element 26 10% in element 27	-	-	50
2	5% in element 16 10% in element 26 10% in element 27	-	1% increase in the elastic modulus of all elements	50
3	10% in element 7	5%	-	50
4	5% in element 26 5% in element 27	5%	1% increase in the elastic modulus of all elements	50
5	5% in element 16 10% in element 26 10% in element 27	-	-	10
6	5% in element 16 10% in element 26 10% in element 27	-	-	100, 200

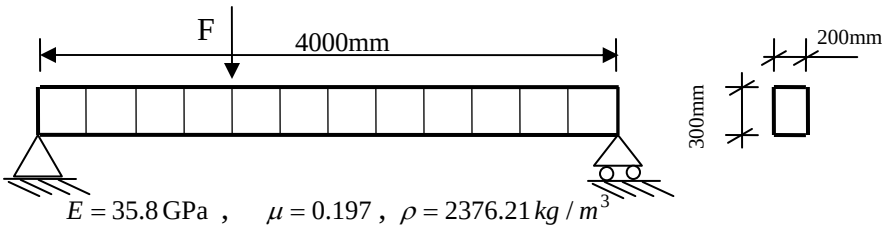

Figure 4.1 - Simply supported concrete beam

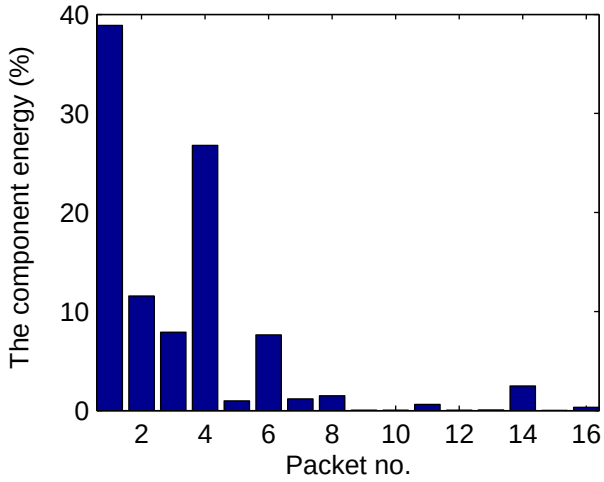

Figure 4.2 - The Wavelet Packet Transform Component Energy

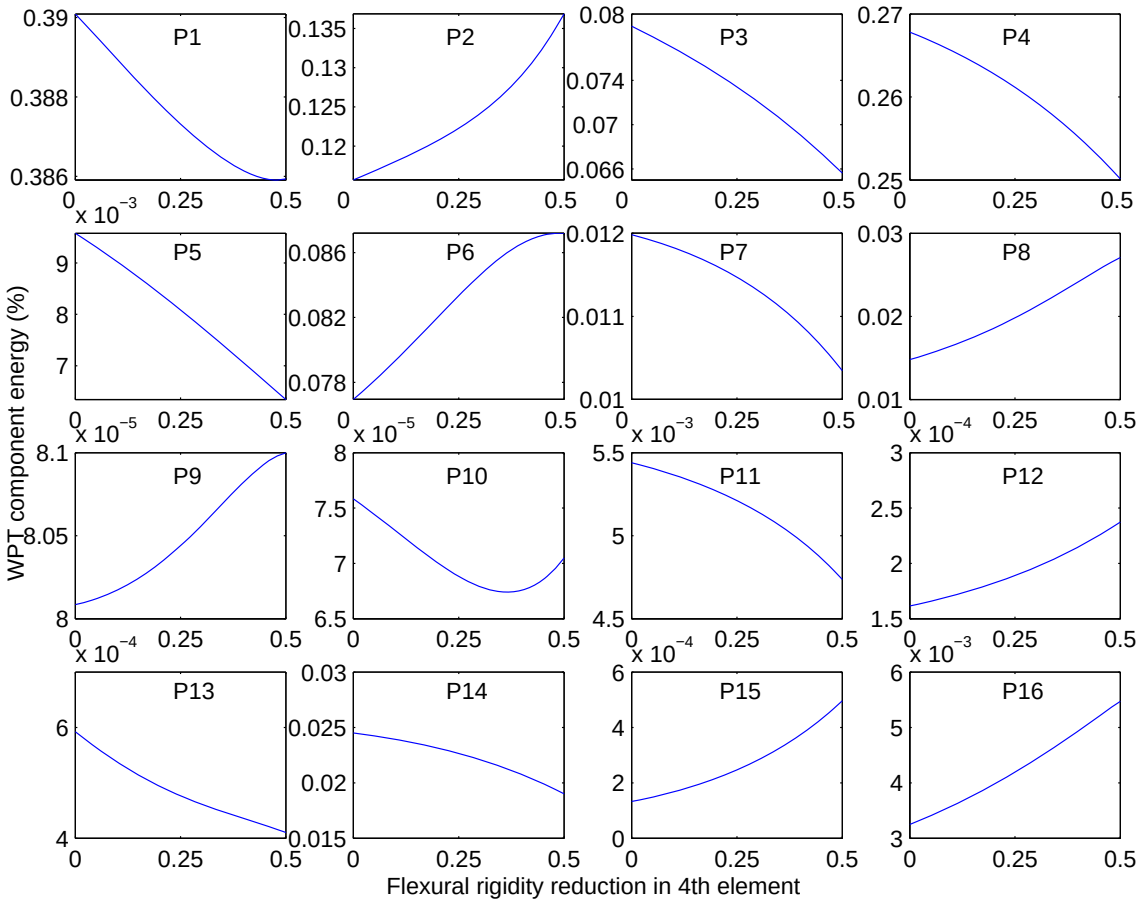

Figure 4.3 - Variation of Wavelet Packet Transform Component Energy under impulsive excitation

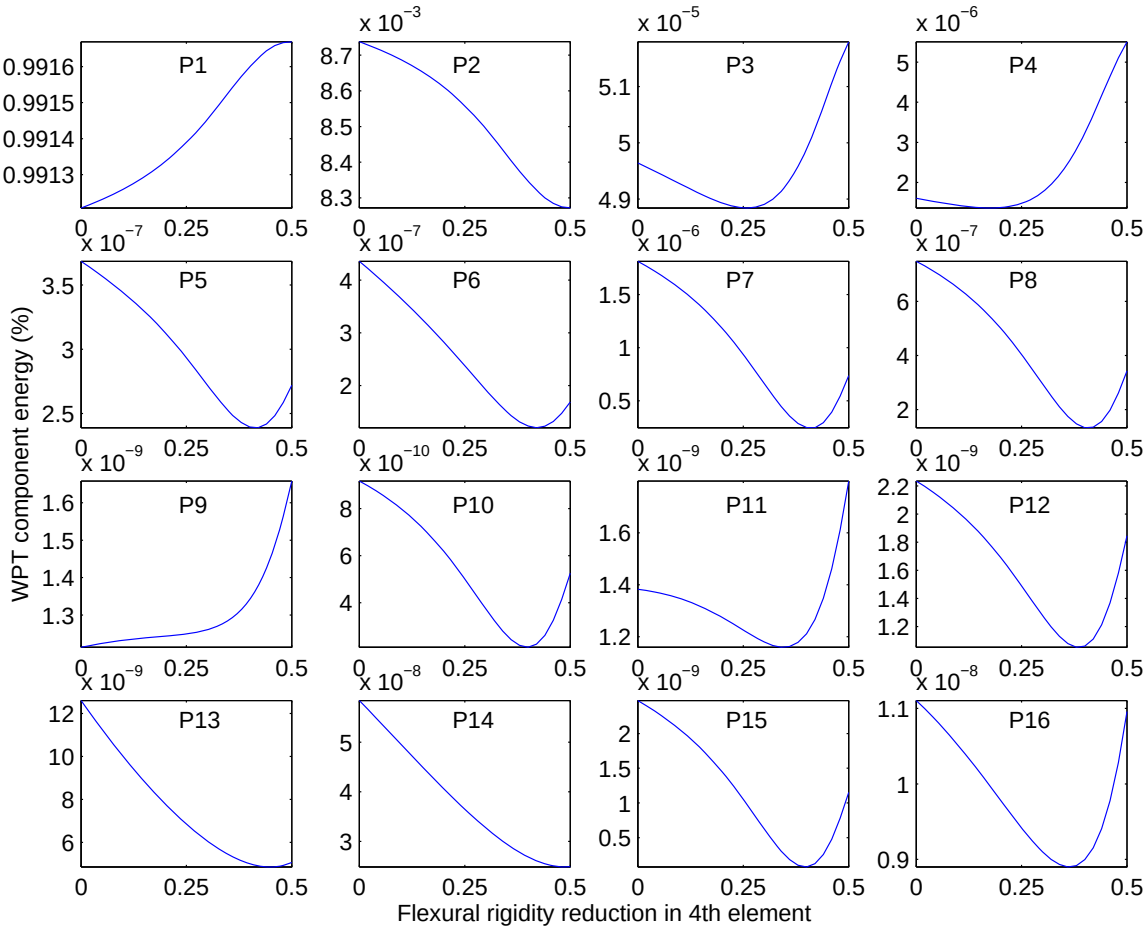

Figure 4.4 - Variation of Wavelet Packet Transform Component Energy under sinusoidal excitation

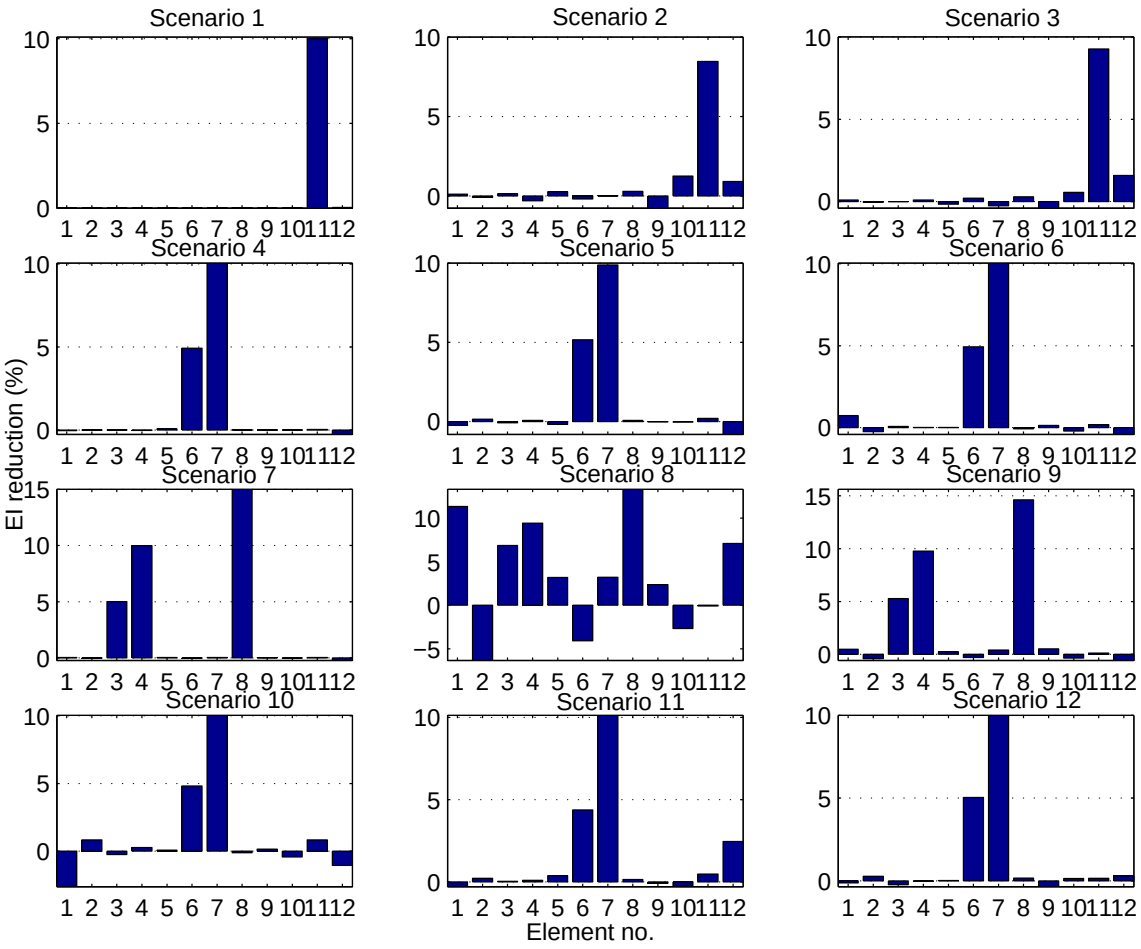

Figure 4.5 - Identified results for Scenarios 1 to 12

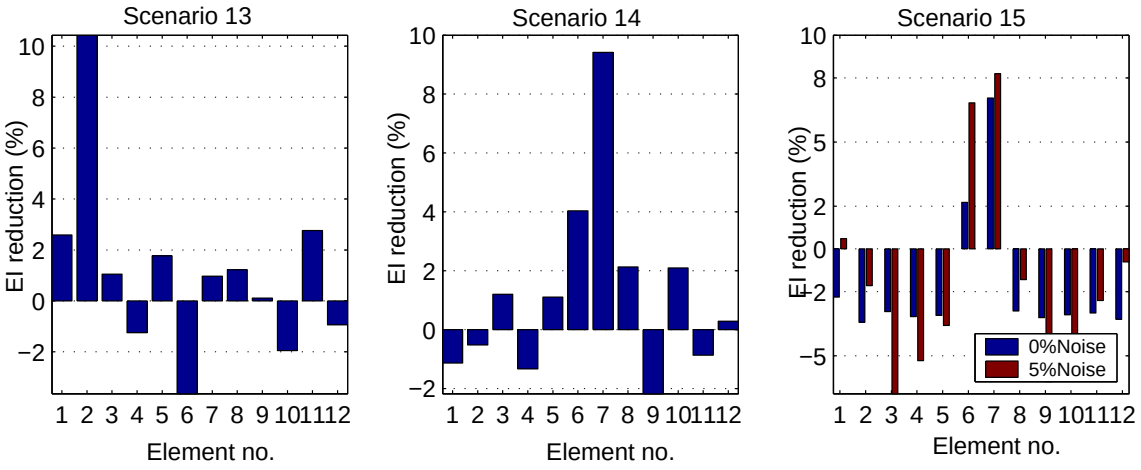

Figure 4.6 - Identified results for Scenarios 13 to 15

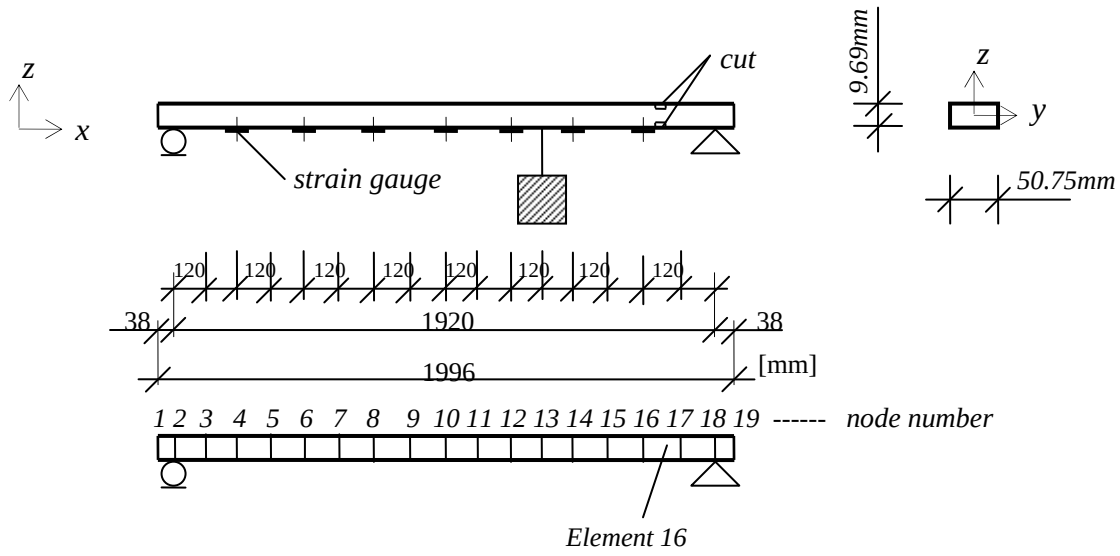

Figure 4.7 - Dynamic test set-up of a steel beam and its finite element model

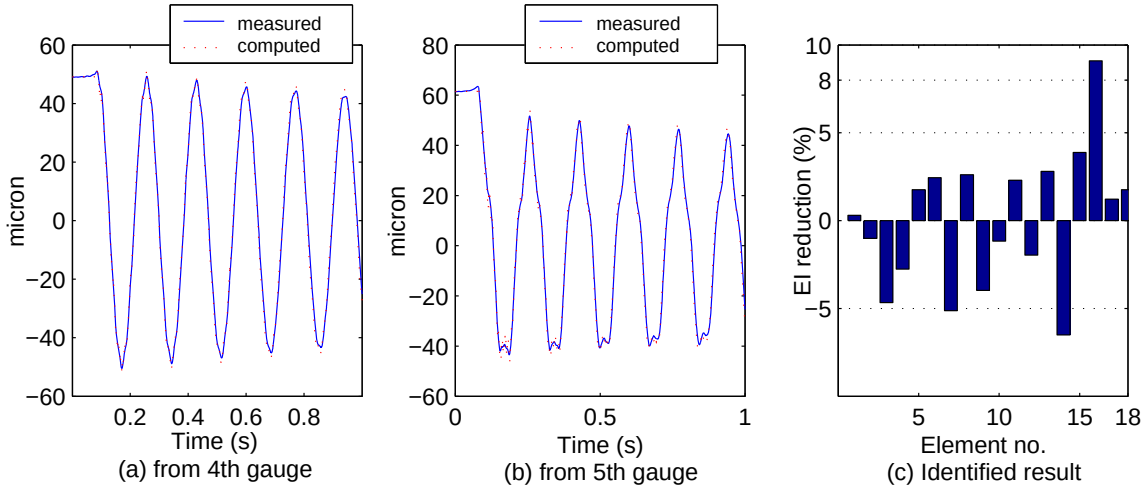

Figure 4.8 - The measured and computed strain responses and the identified result

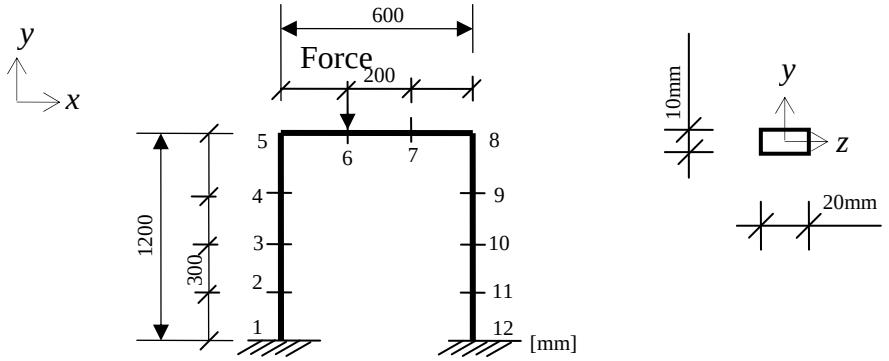

Figure 4.9 - The one-story plane frame structure

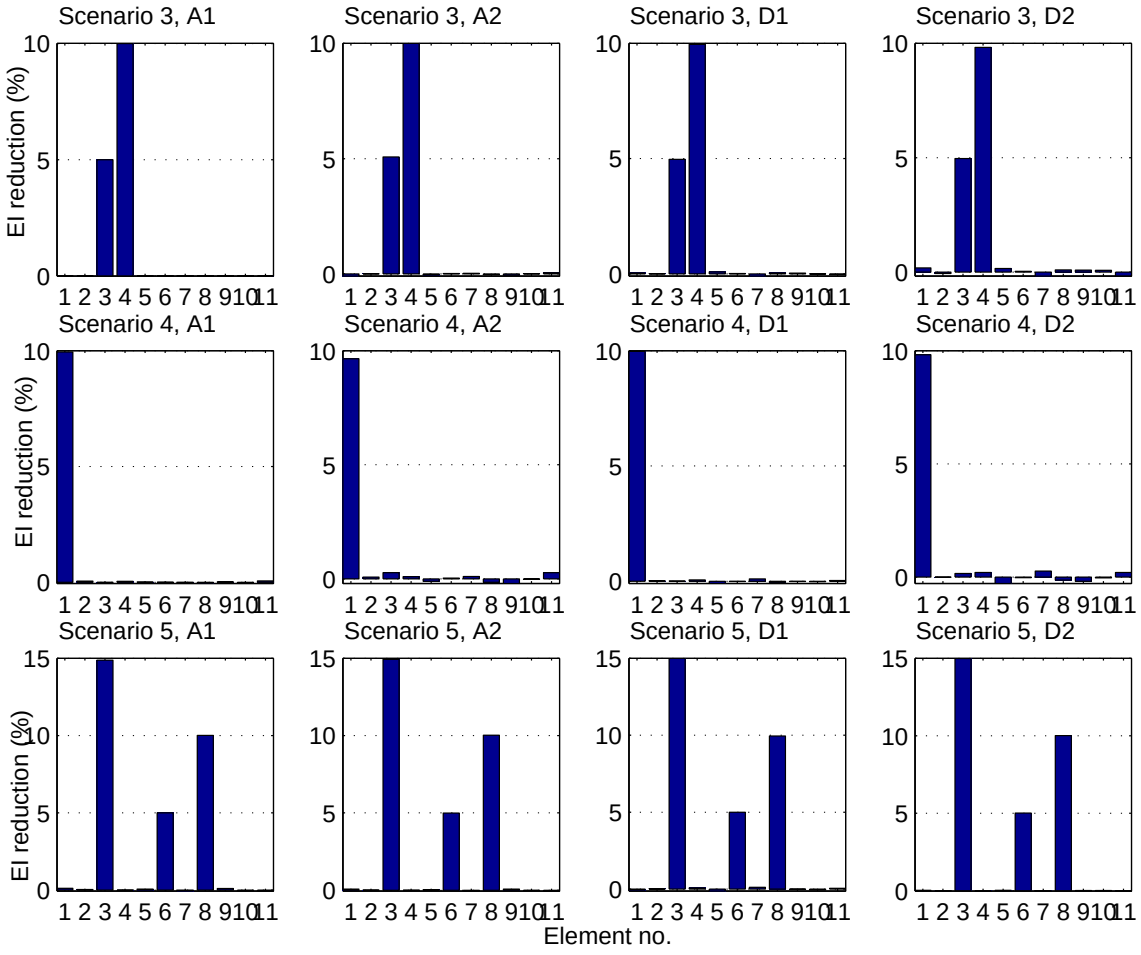

Figure 4.10 - Identified results for Scenarios 3 to 5

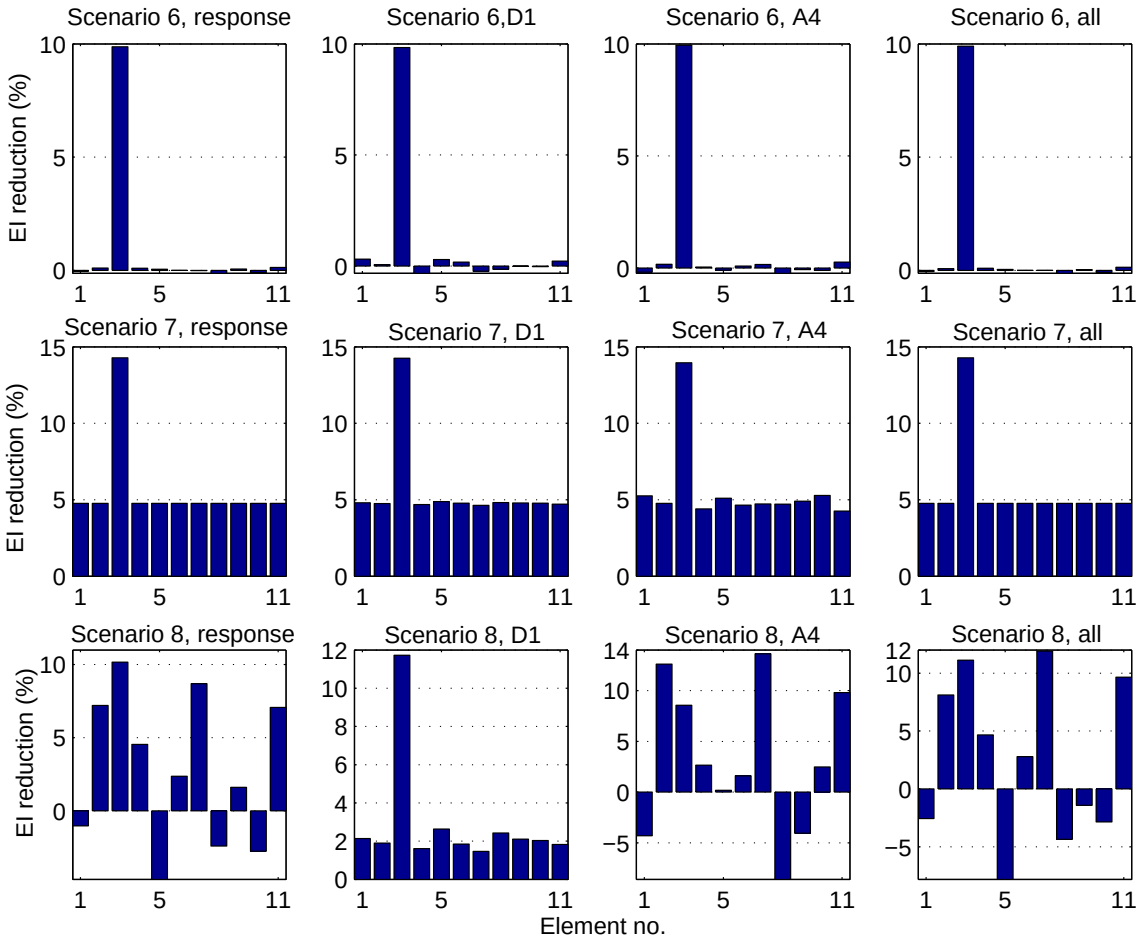

Figure 4.11 - Identified results for Scenarios 6 to 8

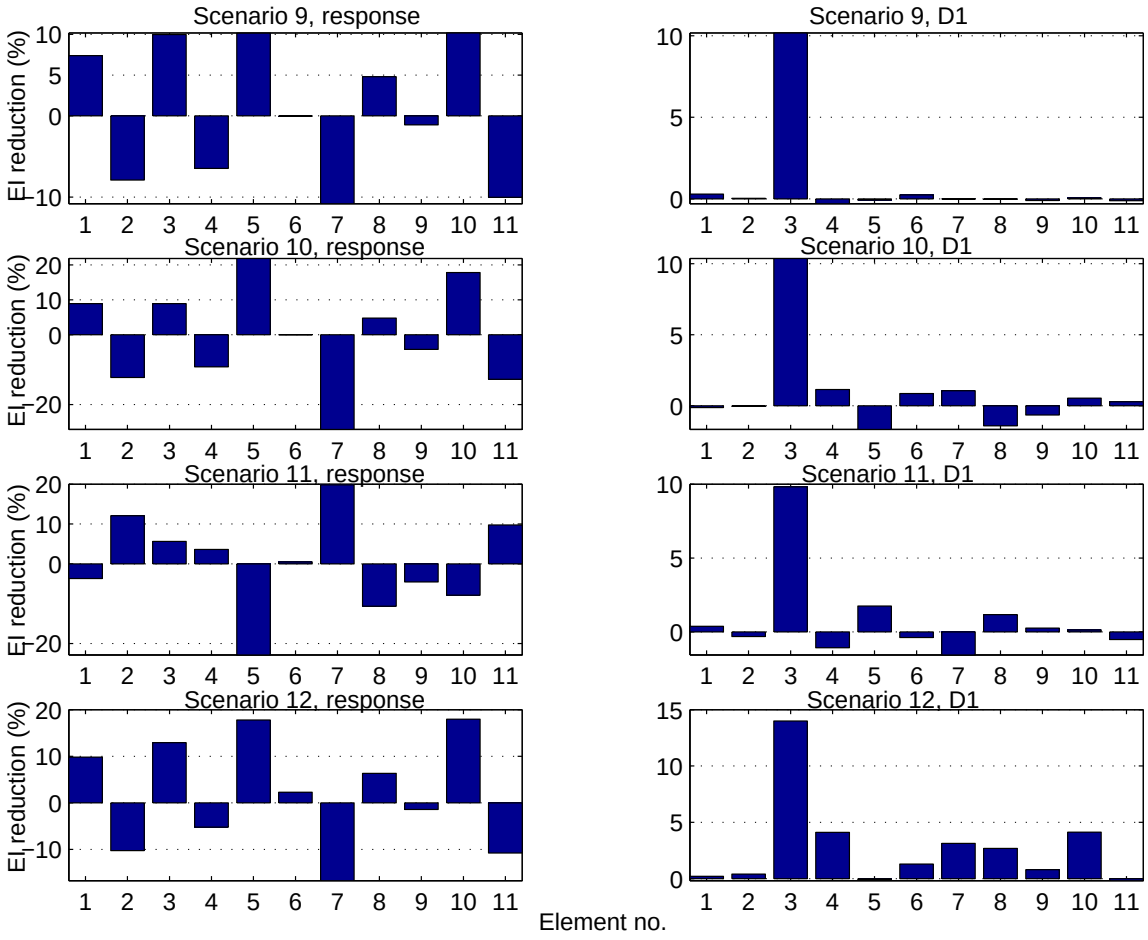

Figure 4.12 - Identified results for Scenarios 9 to 12

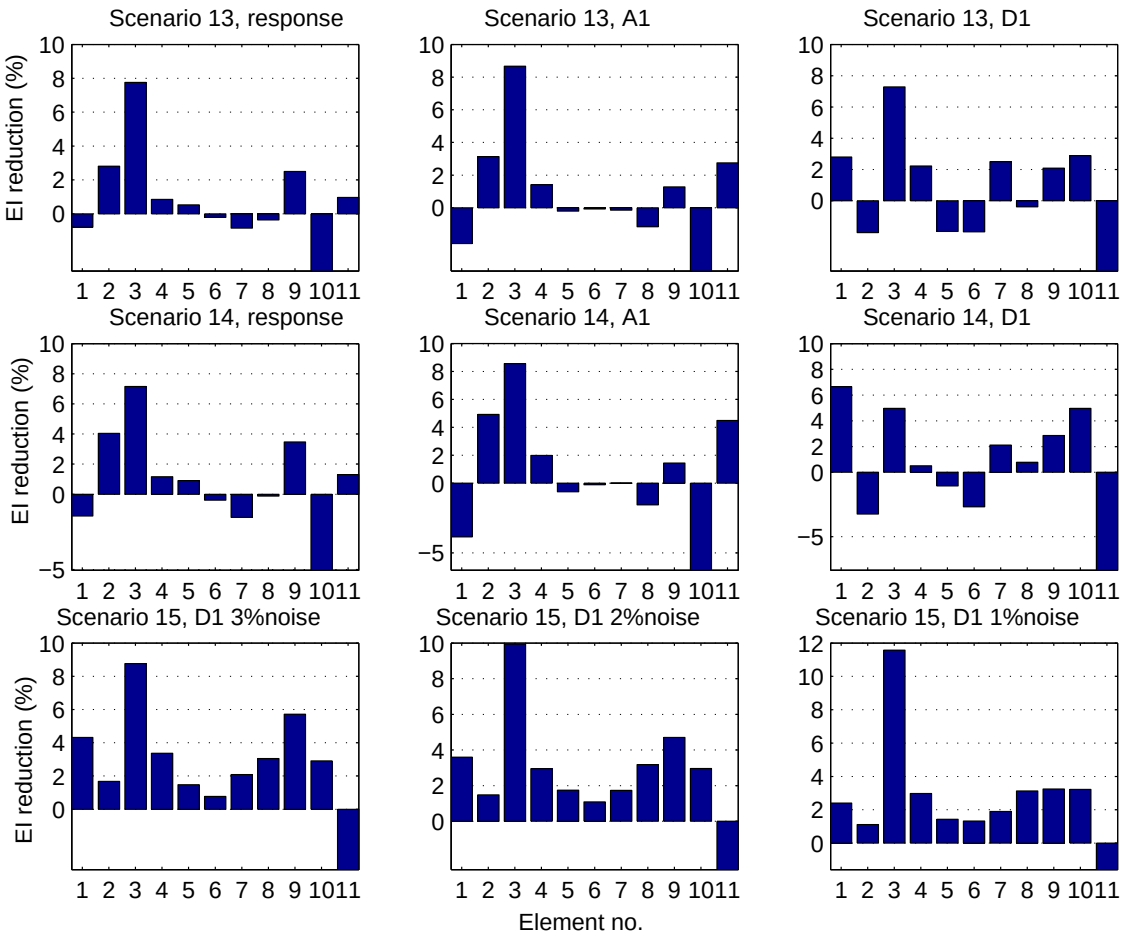

Figure 4.13 - Identified results for Scenarios 13 to 15

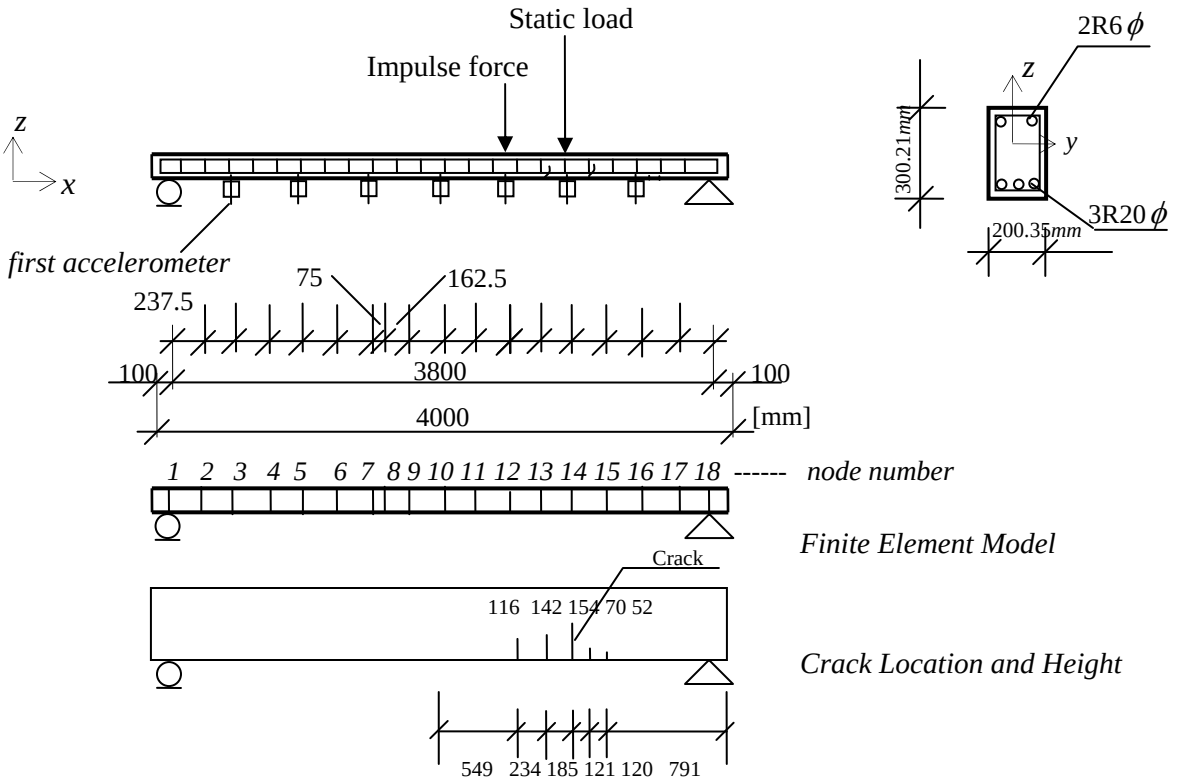

Figure 4.14 - Dynamic test set-up of a RC beam and its finite element model

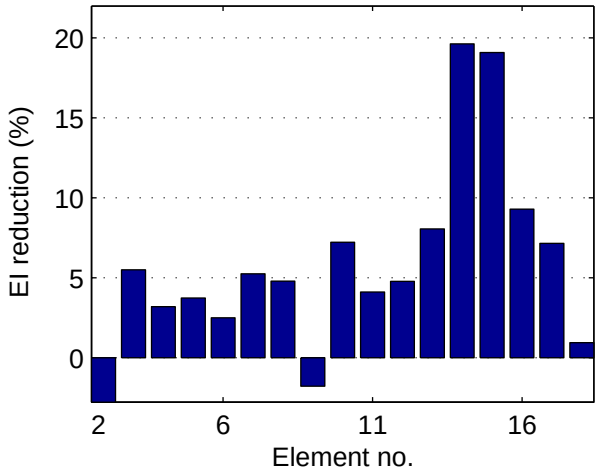

Figure 4.15 - Experimental Identified results

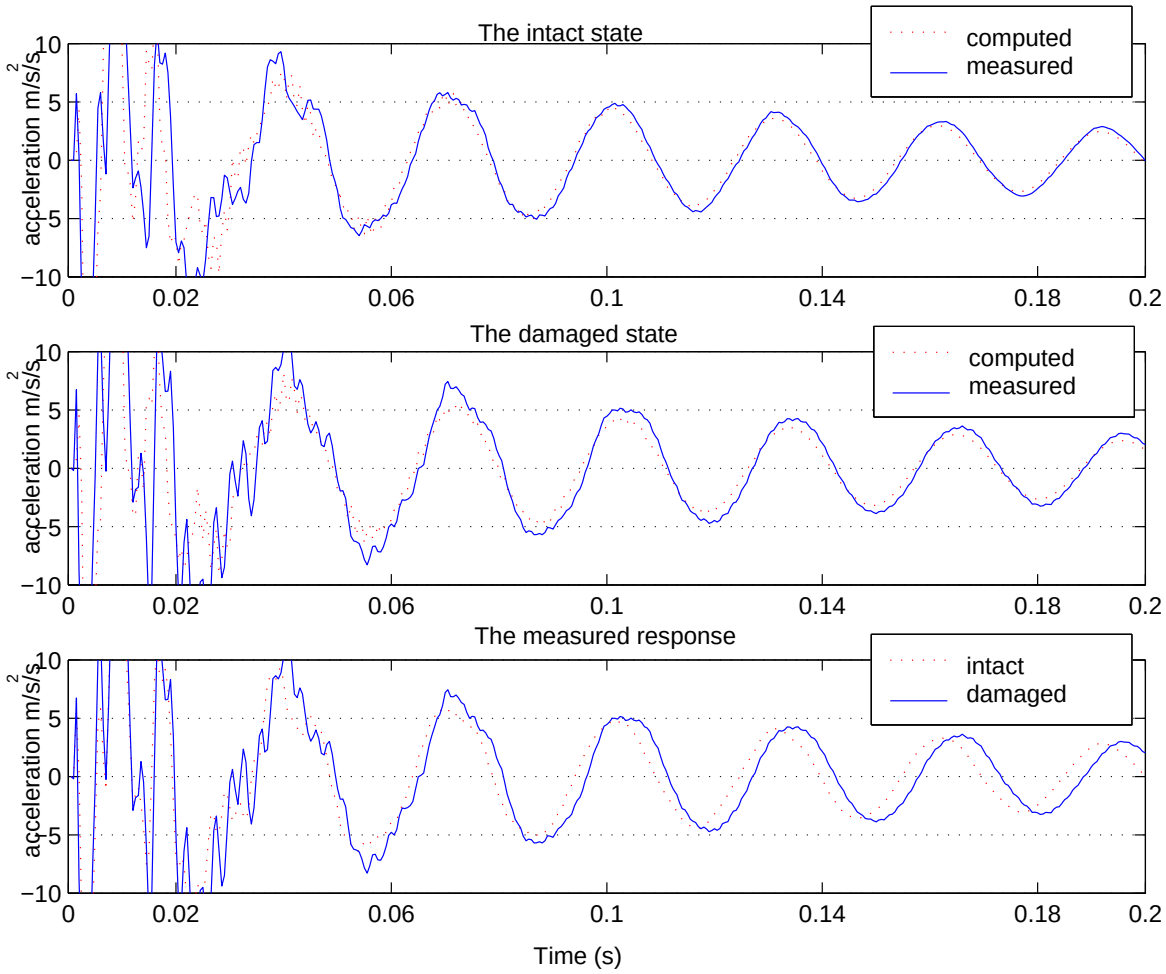

Figure 4.16 - Acceleration responses from the second accelerometer

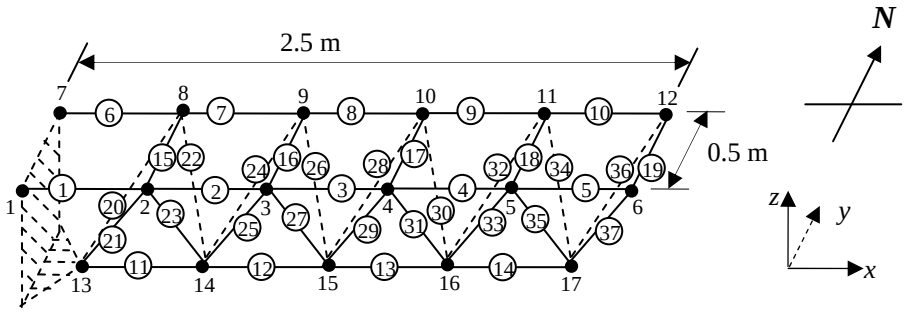

Figure 4.17 - A five-bay three-dimensional frame structure

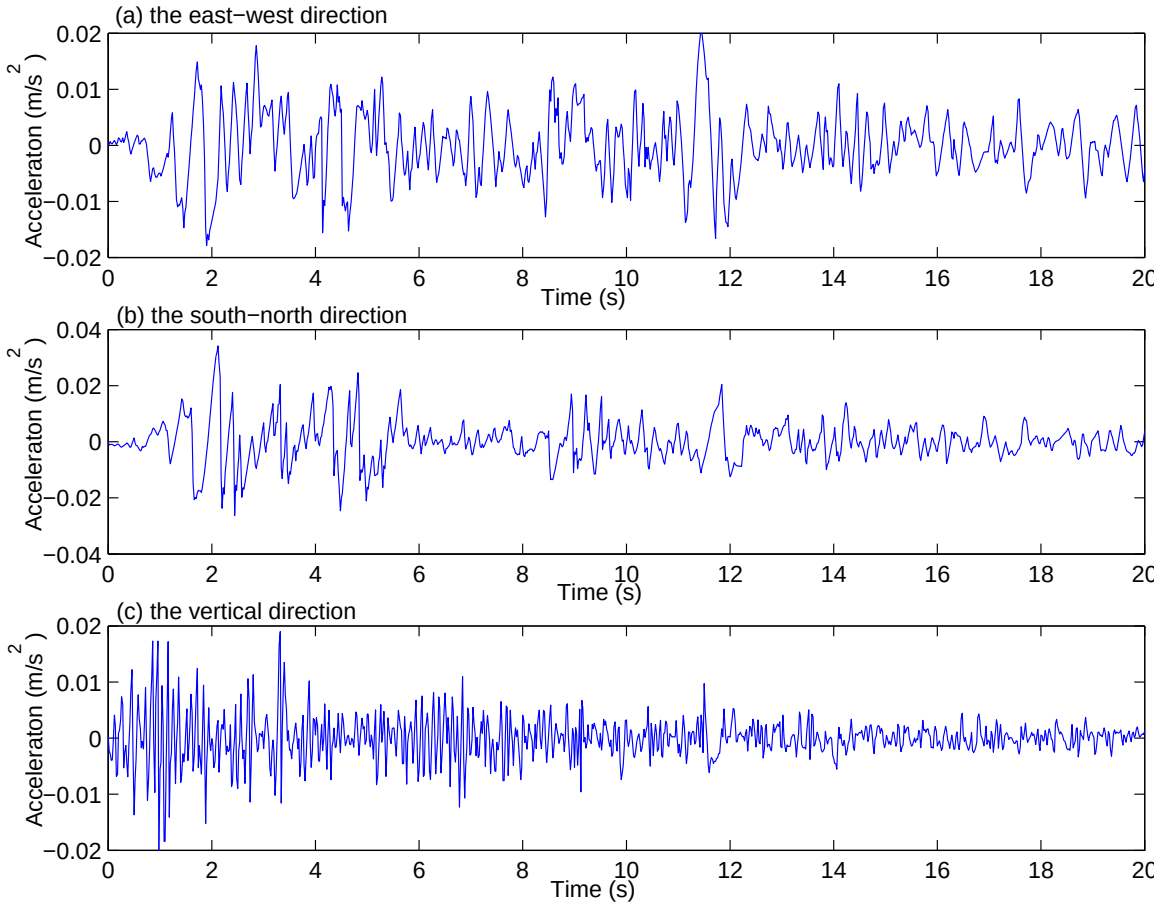

Figure 4.18 - The excitation at the support of the structure

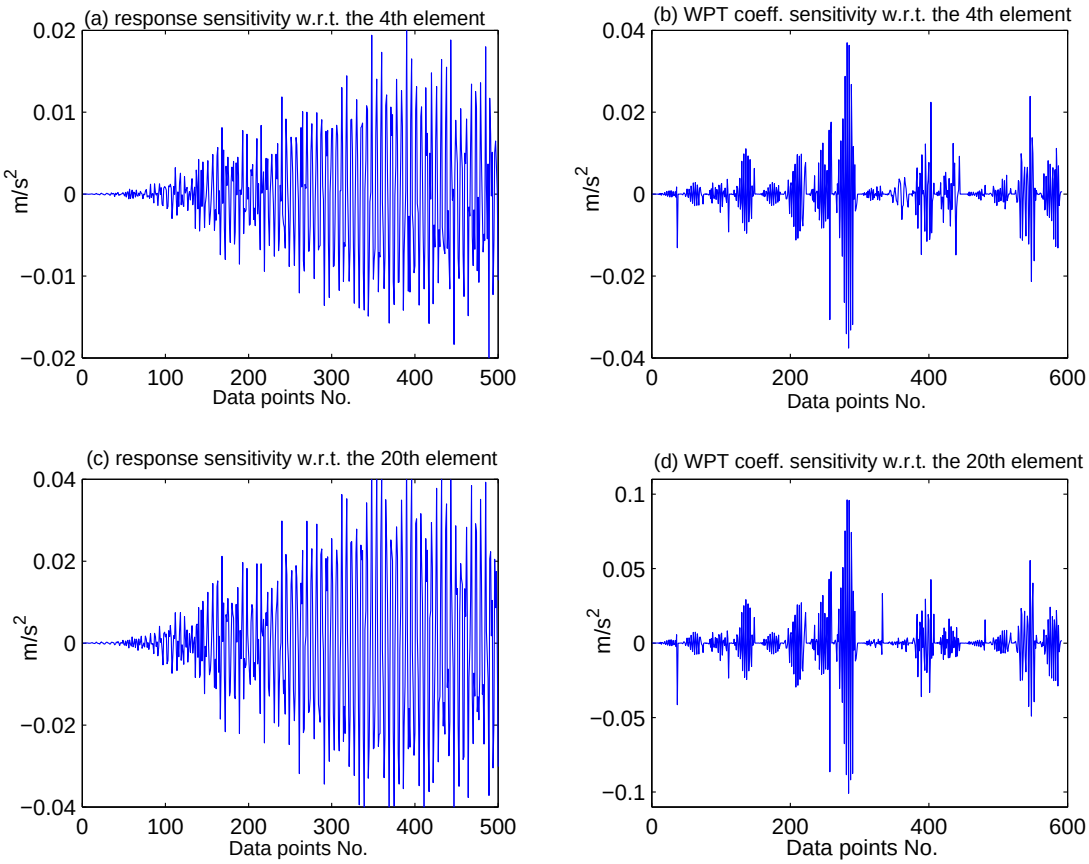

Figure 4.19 - Sensitivities of the response and the WPT coefficients with respect to the elemental stiffness

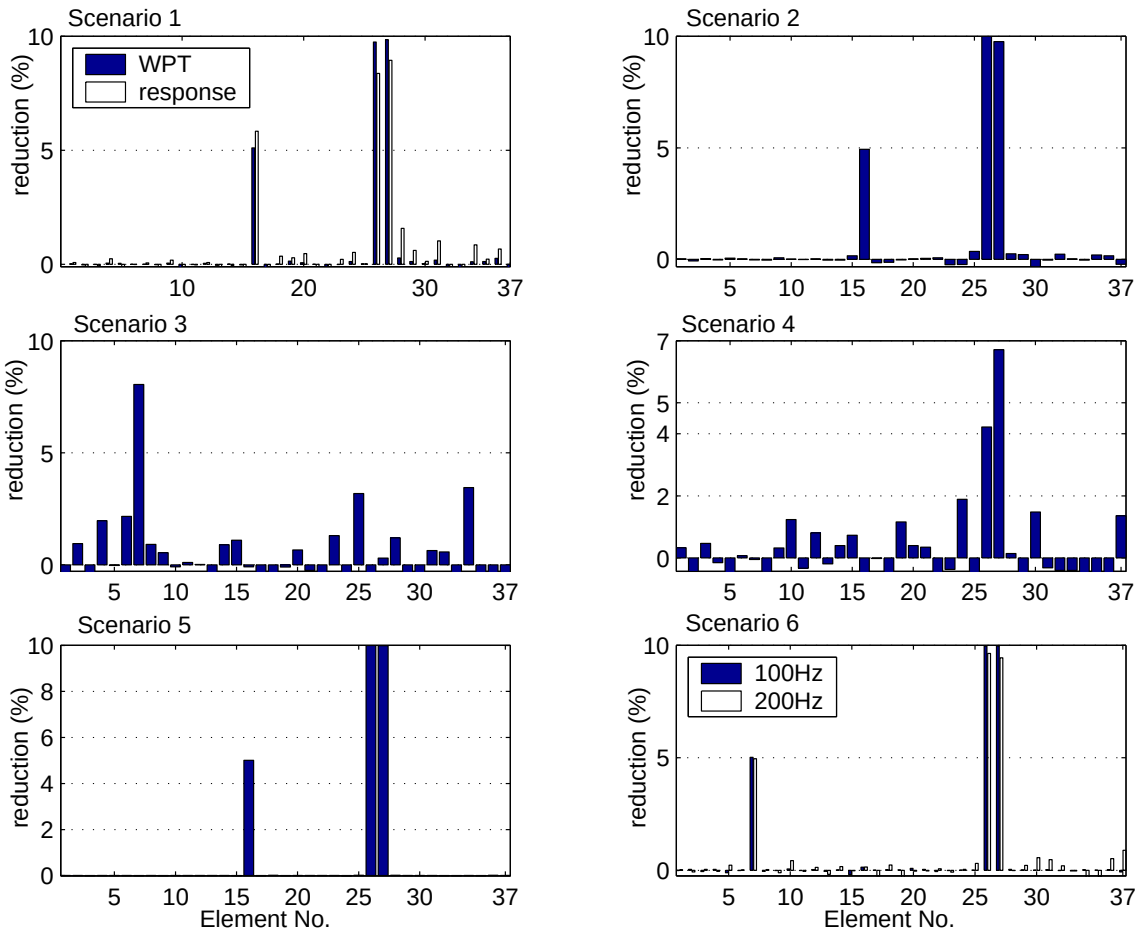

Figure 4.20 - Identified results for Scenarios 1 to 6

(a) The cantilevered 3D steel tube frame structure

(b) The rigid concrete support

(c) The damaged elements

Figure 4.21 - The experimental set up and the damaged elements of the nine-bay frame structure

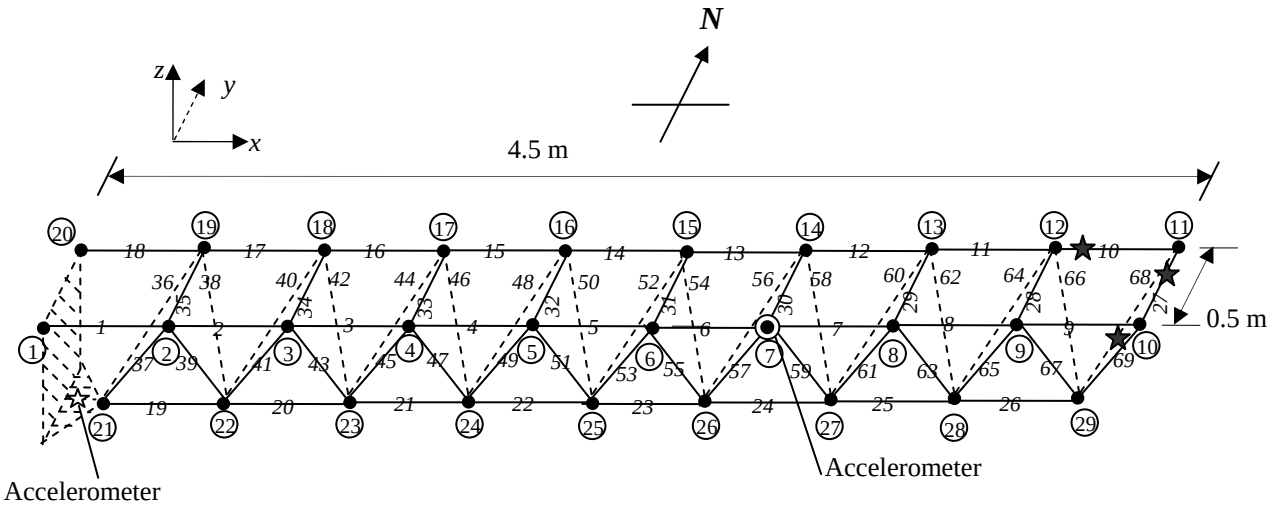

Figure 4.22 – A nine-bay three-dimensional frame structure
(★- a damaged element)

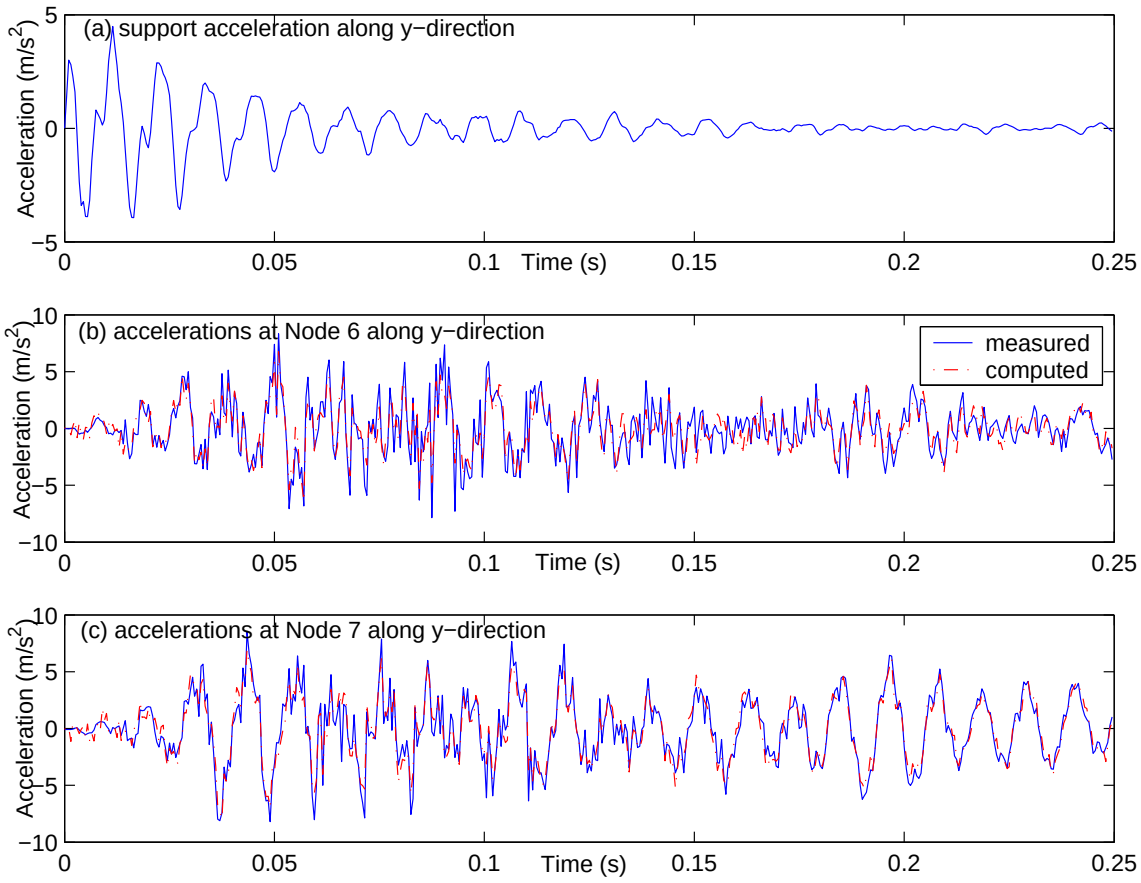

Figure 4.23 - Support acceleration and comparison of the measured and the computed accelerations

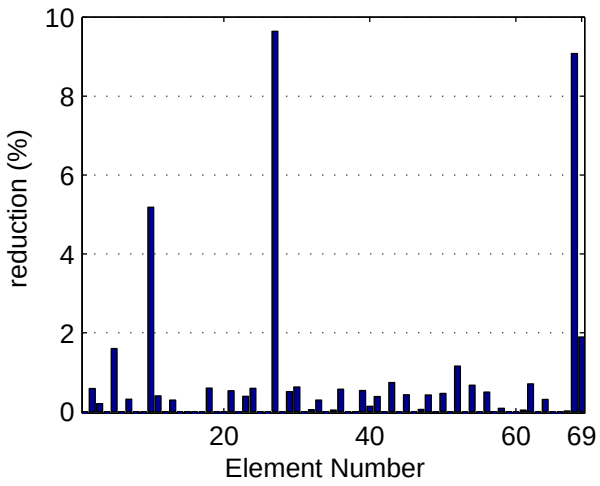

Figure 4.24- Identified results from experiment

CHAPTER 5 STRUCTURAL DAMAGE DETECTION VIA WAVELET-BASED IMPULSE RESPONSE FUNCTION

Though acceleration responses can be applied for damage detection directly, damage detection still relied on the input excitation which will be measured and used in the analytical model. In order to reduce the dependence of the excitation force, wavelet-based impulse response function is used to identify damage in this chapter.

5.1 Introduction

To reduce the dependence of the excitation force, impulse response functions (IRFs) are considered instead of the acceleration responses in the damage detection process. Impulse response functions are intrinsic functions of the system given the excitation location, and they can be extracted from the measured response. Ziaei-Rad (1997) developed a FRF-based model updating by expanding the inverse matrix of FRF as a Taylor series function with respect to structural parameters. Numerical examples and experimental examples are applied to update the analytical model so that the FRFs match those obtained in testing. Ziaei-Rad and Imregun (1996) further discussed the experimental error bounds for convergence of this updating algorithm. Fritzen et al (1998) examines the problem of detecting the location and extent of structural damage using frequency response functions in the time domain based upon a mathematical model representing the undamaged vibrating structure and a local description of the damage, e.g. a finite element for a cracked beam.

Existing impulse response extraction techniques include Laplace transform-based extraction, conventional time-domain extraction and FFT-based extraction and so on (Robertson et al., 1998a; 1998b). FFT-based extraction is most commonly used to obtain the impulse response function. However, it has long been recognized that FFT-based vibration signal analysis exhibits several weakness. In contrast to the FFT-based extraction procedure which must process the data both in the time and frequency domains, the discrete wavelet transform (DWT)-based extraction procedure (Robertson et al., 1998a) handles the experimental data only in the time domain. This involves the forward and inverse DWT plus an inversion operation, and is indeed preferable. Impulse response function can be obtained from the measured response via the discrete wavelet transform to avoid errors with the Fourier Transformation of the vibration signal.

Amongst the many methods developed, sensitivity approach is commonly accepted and applied extensively in the engineering industry because of its clear mathematical background and quantitative indications. The inverse problem based on sensitivity approach is often associated with the solution of a set of linear equation, $\mathbf{Ax} - \mathbf{b} = 0$. But ill-conditioning problems often exist especially in the case with noise and model errors in practice. Many regularization methods have been proposed for obtaining the stationary solution of the above linear equation. In the regularization theory, it is recognized that the conventional output error can be made unrealistically small if the underlying process to be identified, which is the damage, is allowed to behave "badly", to have arbitrary large values and arbitrary large variation, or there may be infinite sets of solutions (ill-posed). By imposing certain constraints in the form of added penalty terms with adjustable weighting parameters, a stable solution scheme can be achieved. The

weighting parameters are adjusted based on *posterior* knowledge such as minimal norm of the damage vector.

One of the well-known methods is Tikhonov regularization (Tikhonov, 1963; Busby and Trujillo, 1997; Trujillo and Busby, 1989; Hansen, 1994). It includes a regularization parameter λ which controls the degree of smoothing or regularization applied to the problem. The regularized solution x_λ varies with the regularization parameter λ . The L-curve method is usually used for determining the optimal regularization parameter λ . When the problem includes no noise or very little noise in the measurement, Tikhonov regularization method gives the optimal solution with a small norm. But when the damage signal to noise ratio is small, e.g. with the inclusion of noise and model error (Law et al. 2006), the solution obtained from a poor regularization parameter is bad.

In this chapter, wavelet coefficients of unit impulse response function of the structures under general excitation and support excitation are obtained from the measured acceleration responses via wavelet transform and are applied to identify damage via sensitivity analysis and model updating techniques. For solving the identification equation, regularization techniques and L-curve method are adopted with some improvements.

5.2 Wavelet-based Sensitivity of Impulse Response Function for Damage Detection

In this section, the sensitivity of the discrete wavelet transform coefficient of the impulse response function was used for damage detection. Firstly, the analytical

formulation on the sensitivity of the DWT coefficient of the impulse response function with respect to a system parameter is deduced from an analytical model based on vibration theory and Newmark method. Then the method obtaining the IRFs from measured responses in damaged and intact states for damage detection is presented using DWT. Finally the damage detection equation is given and the damped least squares method for solving the equation is introduced, and a numerical example with a 31-bar truss structure is used to verify the proposed method.

5.2.1 Wavelet-based Unit Impulse Response

The equation of motion of a N degrees-of-freedom (DOFs) damped structural system under the unit impulse excitation is

$$\mathbf{M}\ddot{\mathbf{x}}+\mathbf{C}\dot{\mathbf{x}}+\mathbf{K}\mathbf{x}=\mathbf{D}\delta(t) \tag{5.1}$$

where $\mathbf{M},\mathbf{C},\mathbf{K}$ are the $N\times N$ mass, damping and stiffness matrices respectively. N is the number of degrees-of-freedom of the system. $\mathbf{D}$ is the mapping matrix relating the force excitation location to the corresponding DOFs of the system. $\mathbf{x}$, $\dot{\mathbf{x}}$, $\ddot{\mathbf{x}}$ are the $N\times 1$ displacement, velocity, acceleration vectors respectively. $\delta(t)$ is the Dirac delta function. Assuming the system is in static equilibrium before the unit impulse excitation occurs, based on the vibration theory, then the forced vibration with the unit impulse excitation can be converted to the free vibration with the initial condition as follows,

$$x(0)=0,\ \dot{x}(0)=\mathbf{M}^{-1}\mathbf{D} \tag{5.2}$$

Rewrite Equations (5.1) and (5.2), the unit impulse response function can be computed from the following,

$$\begin{cases} \mathbf{M}\ddot{h}+\mathbf{C}\dot{h}+\mathbf{K}h=0 \\ h(0)=0,\ \dot{h}(0)=\mathbf{M}^{-1}\mathbf{D} \end{cases} \tag{5.3}$$

where $\mathbf{h}$, $\dot{\mathbf{h}}$, $\ddot{\mathbf{h}}$ are the unit impulse displacement, velocity and acceleration vectors respectively. Using the Newmark method, the unit impulse response can easily be computed.

Differentiate Equation (5.3) with respect to α_i, we get

$$\begin{cases} \mathbf{M}\dfrac{\partial\ddot{\mathbf{h}}}{\partial\alpha_i}+\mathbf{C}\dfrac{\partial\dot{\mathbf{h}}}{\partial\alpha_i}+\mathbf{K}\dfrac{\partial\mathbf{h}}{\partial\alpha_i}=-\dfrac{\partial\mathbf{K}}{\partial\alpha_i}\mathbf{h}-\dfrac{\partial\mathbf{C}}{\partial\alpha_i}\dot{\mathbf{h}} \\ \dfrac{\partial\mathbf{h}(0)}{\partial\alpha_i}=0,\ \dfrac{\partial\dot{\mathbf{h}}(0)}{\partial\alpha_i}=\dfrac{\partial\mathbf{M}^{-1}\mathbf{D}}{\partial\alpha_i} \end{cases} \tag{5.4}$$

The sensitivities $\dfrac{\partial\mathbf{h}}{\partial\alpha_i}$, $\dfrac{\partial\dot{\mathbf{h}}}{\partial\alpha_i}$ and $\dfrac{\partial\ddot{\mathbf{h}}}{\partial\alpha_i}$ can then be obtained from Equation (5.4) with Newmark method.

It has been proved by Law and Li (2006) that wavelet coefficient sensitivity has advantage over the corresponding response sensitivity for the systems with noise and model error. Here the wavelet coefficient is used for damage detection. In this section, we employ Daubechies wavelets as they satisfy the two crucial requirements: the orthogonality of local basis functions and second-order accuracy or higher, depending on the dilation expression adopted.

A function $f(t)$ can therefore be approximated in terms of its DWT as

$$f(t)=f_0^{DWT}\varphi(t)+f_1^{DWT}\psi(t)+f_2^{DWT}\psi(2t)+\cdots+f_{2^j+k}^{DWT}\psi(2^jt-k) \tag{5.5}$$

where $\varphi(t)$ and $\psi(t)$ are the scaling function and the mother wavelet function respectively. $f_{2^j+k}^{DWT}$ is the wavelet transform coefficients. Because of the orthogonality of both the translation and scale of the Daubechies wavelets described by Equation (3.12), we have,

$$f_0^{DWT} = \int f(t)\varphi(t)dt\,;\; f_{2^j+k}^{DWT} = \int f(t)\psi_{j,k}(t)dt \tag{5.6}$$

Substitute Equation (5.6) to the vector of sensitivity $\frac{\partial \ddot{h}}{\partial \alpha_i}$,

$$(\frac{\partial \ddot{h}}{\partial \alpha_i})_{2^j+k}^{DWT} = \int \frac{\partial \ddot{h}}{\partial \alpha_i}\psi_{j,k}(t)dt \tag{5.7}$$

The wavelet coefficient of the impulse response function sensitivity has been shown (Law and Li, 2006) equal to the first derivative of the wavelet coefficients of the impulse response function with respect to the system parameter α_i, i.e.

$$DWT(\frac{\partial \ddot{h}}{\partial \alpha_i}) = \frac{\partial \ddot{h}^{DWT}}{\partial \alpha_i} \tag{5.8}$$

where $DWT(\frac{\partial \ddot{h}}{\partial \alpha_i})$ is the discrete wavelet coefficient of $\frac{\partial \ddot{h}}{\partial \alpha_i}$. We can form the sensitivity matrix from Equation (5.8) as

$$\mathbf{S} = \begin{bmatrix} \frac{\partial \ddot{h}_l^{DWT}}{\partial \alpha_1} & \frac{\partial \ddot{h}_l^{DWT}}{\partial \alpha_2} & \cdots & \frac{\partial \ddot{h}_l^{DWT}}{\partial \alpha_m} \end{bmatrix} \tag{5.9}$$

where $\ddot{h}_l^{DWT}$ is the DWT coefficient of $\ddot{h}_l$, and $\ddot{h}_l$ denotes the acceleration impulse response function at location l, and m is the number of structural parameters.

5.2.2 Impulse Response Function via Discrete Wavelet Transform

The unit impulse response (UIR) (or the Markov parameters) is the response function of the system under the input of a unit pulse (Robertson et al., 1998a; 1998b). It is an intrinsic function of the structural system. Since the unit impulse is ideal and it cannot be directly applied onto the structure, unit impulse response function cannot be obtained directly from measurement. Traditionally, Fast Fourier Transform (FFT) is used to extract the Markov parameters from measured input and output (Juang, 1985). However the unit impulse response function is obtained via the Discrete Wavelet Transform (DWT) in this study to alleviate the Gibb's phenomenon with the FFT-based methods.

The equation of motion of a N DOFs damped structural system under general excitation is

$$\mathbf{M}\ddot{\mathbf{x}}+\mathbf{C}\dot{\mathbf{x}}+\mathbf{K}\mathbf{x}=\mathbf{D}F(t) \tag{5.10}$$

where $F(t)$ is the vector of excitation force. If the system has zero initial condition, the solution of Equation (5.10) can be expressed as,

$$\mathbf{x}(t)=\int_0^t \mathbf{h}(t-\tau)F(\tau)d\tau \tag{5.11}$$

The acceleration response $\ddot{x}_l(t_n)$ from location l at time t_n is,

$$\ddot{x}_l(t_n)=\int_0^{t_n} \ddot{h}_l(\tau)\cdot F(t_n-\tau)d\tau \tag{5.12}$$

Applying DWT to $\ddot{h}_l(\tau)$ and $F(t_n-\tau)$ respectively, we can get,

$$\ddot{h}_l(\tau)=\ddot{h}_{l,0}^{DWT}\ \varphi(\tau)+\ddot{h}_{l,1}^{DWT}\ \psi(\tau)+\cdots+\ddot{h}_{l,2^j+k}^{DWT}\psi(2^j\tau-k) \tag{5.13}$$

$$F(t_n-\tau)=F_0^{DWT}(t_n)\cdot\varphi(\tau)+F_1^{DWT}(t_n)\cdot\psi(\tau)+\cdots+F_{2^j+k}^{DWT}(t_n)\cdot\psi(2^j\tau-k) \tag{5.14}$$

Substituting Equations (5.13) and (5.14) into Equation (5.12), then

$$\ddot{x}_l(t_n) = \int_0^{t_n} (\ddot{h}_{l,0}^{DWT}\varphi(\tau) + \ddot{h}_{l,1}^{DWT}\psi(\tau) + \cdots + \ddot{h}_{l,2^j+k}^{DWT}\psi(2^j\tau - k)) \cdot (F_0^{DWT}(t_n)\cdot\varphi(\tau) + F_1^{DWT}(t_n)\cdot\psi(\tau) + \cdots + F_{2^j+k}^{DWT}(t_n)\cdot\psi(2^j\tau - k))d\tau \quad (5.15)$$

Because of the orthogonal condition shown in Equation (3.12), we get

$$\begin{cases} \int_0^{t_n} \varphi(t)\varphi(t)dt = 1 \\ \int_0^{t_n} \varphi(t)\psi(2^j t - k)dt = 0 \\ \int_0^{t_n} \psi(2^j t - k)\psi(2^m t - n)dt = \delta_{j,m}\delta_{k,n}/2^j \end{cases} \quad (5.16)$$

Substituting Equation (5.16) into (5.15), we have

$$\ddot{x}_l(t_n) = \ddot{h}_{l,0}^{DWT} F_0^{DWT}(t_n) + \ddot{h}_{l,1}^{DWT} F_1^{DWT}(t_n) + \cdots + \ddot{h}_{l,2^j+k}^{DWT} F_{2^j+k}^{DWT}(t_n)/2^j \quad (5.17)$$

Rewriting Equation (5.17) in the matrix form,

$$\ddot{x}_l(t_n) = F^{DWT}(t_n)\cdot\ddot{h}_l^{DWT} \quad (5.18)$$

where $F^{DWT}(t_n) = \left[F_0^{DWT}(t_n) \quad F_1^{DWT}(t_n) \quad \cdots \quad F_{2^j+k}^{DWT}(t_n)/2^j\right]$,

$$\ddot{h}_l^{DWT} = \left[\ddot{h}_{l,0}^{DWT} \quad \ddot{h}_{l,1}^{DWT} \quad \cdots \quad \ddot{h}_{l,2^j+k}^{DWT}\right]^T$$

Equation (5.18) can be re-written for a time series as follows,

$$\ddot{\mathbf{x}}_l = \mathbf{F}^{DWT}\cdot\ddot{\mathbf{h}}_l^{DWT} \quad (5.19)$$

where $\ddot{\mathbf{x}}_l = \left[\ddot{x}_l(t_1) \quad \ddot{x}_l(t_2) \quad \cdots \quad \ddot{x}_l(t_n)\right]^T$, $\mathbf{F}^{DWT} = \begin{bmatrix} F^{DWT}(t_1) \\ F^{DWT}(t_2) \\ \cdots \\ F^{DWT}(t_n) \end{bmatrix}$

Finally, $\ddot{\mathbf{h}}_l^{DWT}$ can be computed in the form of a pseudo-inverse as

$$\ddot{\mathbf{h}}_l^{DWT} = (\mathbf{F}^{DWT^T}\cdot\mathbf{F}^{DWT})^{-1}\cdot\mathbf{F}^{DWT^T}\cdot\ddot{\mathbf{x}}_l \quad (5.20)$$

5.2.3 Damage Identification Equation

$\ddot{\mathbf{h}}_{l0}^{DWT}$ and $\ddot{\mathbf{h}}_{ld}^{DWT}$ are vectors of the DWT coefficient of the impulse response function from the two states of the structure, i.e. the intact and damaged states respectively. $\frac{\partial \ddot{\mathbf{h}}_{l0}^{DWT}}{\partial \alpha}$ is the sensitivity matrix of the DWT coefficient with respect to the local damage with reference to the intact state. $\Delta\alpha$ is the vector of parameter changes of the system. We have the identification equation as,

$$\begin{aligned} \ddot{\mathbf{h}}_{ld}^{DWT} - \ddot{\mathbf{h}}_{l0}^{DWT} &= \frac{\partial \ddot{\mathbf{h}}_{l0}^{DWT}}{\partial \alpha} \cdot \Delta\boldsymbol{\alpha} \\ &= \mathbf{S} \cdot \Delta\boldsymbol{\alpha} \end{aligned} \qquad (5.21)$$

When measurements from the intact state of the structure are obtained, $\ddot{\mathbf{h}}_{l0}^{DWT}$ is taken as the DWT coefficients computed from the analytical model. $\ddot{\mathbf{h}}_{ld}^{DWT}$ is computed with the measured responses and the input forces obtained in experiments from the intact state. The left-hand-side of Equation (5.21) is the difference between the analytical and experimentally obtained DWT coefficients of the IRF. The sensitivity matrix $\frac{\partial \ddot{\mathbf{h}}_{l0}^{DWT}}{\partial \alpha}$ is computed from the analytical model of the structure at the initially assuming state. The analytical model is then updated and the corresponding wavelet coefficient and its sensitivity are again computed for the next iteration. Convergence is considered achieved when both the following two criteria are met,

$$\frac{\left\| \{\ddot{h}_l^{DWT}\}_{i+1} - \{\ddot{h}_l^{DWT}\}_i \right\|}{\left\| \{\ddot{h}_l^{DWT}\}_{i+1} \right\|} \le toler\ 1, \qquad \frac{\left\| \boldsymbol{\alpha}_{i+1} - \boldsymbol{\alpha}_i \right\|}{\left\| \boldsymbol{\alpha}_{i+1} \right\|} \le toler\ 2 \qquad (5.22)$$

where i refers to the ith iteration.

When measurement from the damaged state is obtained, the updated analytical model is used in the iteration in the same way as that using the measurement from the intact state. The final set of identified parameter increments correspond to the changes occurred in between the two states of the structure. Like many other inverse problems, the solution of Equation (5.21) is often ill-conditioned. In order to provide bounds to the solution, the damped least-squares method (DLS) (Tikhonov, 1963) is used and singular-value decomposition is used in the pseudo-inverse calculation.

5.2.4 Simulation

The 31-bar truss, shown in Figure 5.1, was modeled using 31 finite elements without internal nodes in the bars giving 28 degrees of freedom. The cross-sectional area of the bar is $0.0025\,m^2$. Damage in the structure was introduced as a reduction in the stiffness of individual bars, but the inertial properties were unchanged. The translational restraints at the supports are both represented by large stiffnesses of 1.0×10^{10} *kN/m*. Rayleigh damping is adopted for the system with $\xi_1 = 0.01$ and $\xi_2 = 0.01$. The first 12 natural frequencies of the structure are 36.415, 75.839, 133.608, 222.904, 249.323, 358.011, 372.509, 441.722, 477.834, 507.943, 538.1246 and 547.393 *Hz*. The sampling frequency is 2000 *Hz*. The tolerance limits for both convergence criteria have been set

equal to 1.0×10^{-6}. The excitation is applied in the downward direction at node 5 while the vertical acceleration measurement at node 4 is recorded as shown in Figure 5.1.

Dependence on input excitation

The excitations adopted in this study are shown in Figure 5.2. The first excitation is a triangular impulsive force with 320.4*N* peak value and it lasts for 0.005 second. The second excitation is the sinusoidal excitation of $F = 20\sin(2\pi \cdot 20 \cdot t)$ *N*. Figure 5.2(c) shows the impulse response at node 4, *htt0*, computed from Equation (5.3) as well as the impulse response functions, *hw0* and *hw2*, computed from the proposed wavelet formulation in Equation (5.20) for the first and second excitation forces respectively. Figure 5.2(d) gives details of part of the impulse response functions in Figure 5.3(c) within the time interval of 0.1s to 0.125s. Both Figure 5.2(c) and (d) show that the three impulse response functions computed from the response and the wavelet approaches and with different excitations are overlapping. It may be concluded that the impulse response function obtained using DWT extraction matches the solution from existing theoretical analysis very well. The impulse response function obtained is independent of the input excitation, which in the present case, are the impulsive excitation and the sinusoidal excitation.

Damage identification

The same truss structure as for last study is used for numerical verification of the proposed wavelet approach. The excitation and measurement locations are the same as in previous study. Two different excitations are used in the different states of the structure.

Excitation for the intact state is the impulsive force. The impulsive response function wavelet coefficient sensitivity matrix is computed from the analytical model using Equations (5.4) and (5.9) without the need of the input excitation. Excitation for the damaged state is the sinusoidal force. The sampling rate is 2000 Hz and the first 0.25 second of the response is used for the damage identification.

Four damage scenarios are studied with different damage extent listed as Scenario 1 to 4 in Table 5.1. Local damage is modeled as a reduction in the flexural rigidity of an element. In fact, three patterns of damage (single damage, two adjacent damages and three damages) are considered and each damage pattern is identified from the IRFs extracted from measured acceleration response. Results in Figure 5.3 show that both the location and the severity can be identified accurately without any alarms in other elements.

Noise effect

The same excitation force and sampling rate of signal as for last study is used. The vertical acceleration response from node 4 is extracted to obtain the unit impulse response. Damage Scenarios 5 and 6 as listed in Table 5.1 are studied with 1% and 5% random noise respectively. In order to reduce noise effect, some techniques are applied in the damage identification process. Since IRF is an intrinsic function of the structure that is independent of the input excitation, we repeatedly measure the acceleration response and excitation time histories and a set of IRFs using Equation (5.20) can be obtained. The final IRF obtained is from averaging the set of IRFs. When the damped least square method with Tikhonov regularization is used to solve the set of inverse equation, small

singular values contributed by noise and model error can cause perturbation in the solution. So during the solution process, small singular values which are smaller than a given threshold are truncated (Tikhonov, 1963). The identified results are shown in Figure 5.4. The random noise causes error in the identified value in the damaged element and with alarm in several other elements. The random noise is noted leading to random errors in the elements. Comparing the results in Figure 5.4 with those for scenarios without noise shown in Figure 5.3, it can be concluded that the proposed method is affected by noise to some extent. This can be explained that unit impulse response function is obtained from the measured acceleration responses and the measure input excitation by wavelet transform. When noise exists in the measured acceleration or excitation, the noise effect in the unit impulse response function will be amplified via Equation (5.20).

Model error

This effect of model error is investigated with different types of model errors introduced into the finite element model of the truss structure as listed under Scenarios 7 to 10 in Table 5.1. The same excitation force and sampling rate of signal as for last study is used. Response from the same location as for last study is extracted for obtaining the impulse response functions. The identified results are shown in Figure 5.4. Acceptable results are obtained in the damage element while there is alarm in other elements. The presence of random noise in the measured data is noted to amplify the erroneous effect due to the model errors.

Discussions

From the above numerical example analysis, it can be concluded that the proposed method can perform damage detection successfully in structures. Especially in the scenarios without noise and model error, the results are perfect. But when the system includes noise or model error, the results obtained by this method is affected to some extent though acceptable results can still be obtained. When the proposed method applying to the real structures, it is natural that noise level and model error will influence its application largely. It is required that the analytical model must be updated to reduce the model error. In real application, noise can not be neglected. When the noise component is larger than the signal change due to damage, the method will fail in the detection. Though the method has advantages including time domain analysis, needing as few as one sensor measurement, not needing the same input excitation in two states, efforts should be paid to reducing the rely on analytical model and offering a more effective regularization method for separating damage and noise signal in order that the proposed method detects damage in real structures more easily.

5.3 Impulse Response Function from Structures under Support Excitation for Damage Identification

In the above section, impulse response functions are obtained from the measured acceleration responses. The excitation force needs to be measured but it is not used in the analytical model. In order to increase the robust application of the wavelet-based IRF method, support excitation is introduced in the structure and both the support acceleration responses and structural responses are needed.

In this section, Unit Impulse Responses obtained from the structure under support excitation are used to identify local damages. The method on the extraction of UIRs from accelerations of the structure and the support is briefly introduced. The sensitivity matrix of UIRs of the structure is obtained based on the finite element model and the time-stepping integral method. A two-step updating method is adopted for identifying the local damage based on the computed sensitivity matrix of UIRs from several accelerometers. Statistical analysis is included in the damage identification procedure and measurement noise is taken as an independent random variable in the UIRs from measurement.

5.3.1 Unit Impulse Response from Measurement

Support excitation is universal for all structures, and its effect is represented in terms of $x_s, \dot{x}_s, \ddot{x}_s$, which are the displacement, velocity and acceleration respectively at the degrees-of-freedoms *s* of the support of the structure. This study assumes that acceleration input at the support DOFs exist with zero initial conditions. The acceleration response function of the structure can be expressed as,

$$\ddot{x}_l(t_n) = \int_0^{t_n} \ddot{h}_l(\tau) \cdot \ddot{x}_s(t_n - \tau) d\tau \qquad (5.23)$$

where $\ddot{x}_l(t_n)$ is the acceleration response from location *l* at time instance t_n, $\ddot{h}_l(\tau)$ is the unit impulse function from location l when the support is subject only to unit impulse acceleration, $\ddot{x}_s(\tau)$ is the support acceleration.

Applying DWT to $\ddot{x}_s(t_n - \tau)$ in Equation (5.5), we get,

$$\ddot{x}_s(t_n - \tau) = \ddot{x}_{s0}^{DWT}(t_n) \cdot \varphi(\tau) + \ddot{x}_{s1}^{DWT}(t_n) \cdot \psi(\tau) + \cdots + \ddot{x}_{s_{2^j+k}}^{DWT}(t_n) \cdot \psi(2^j \tau - k) \quad (5.24)$$

Substituting Equations (5.13) and (5.24) into Equation (5.23), we have

$$\ddot{x}_l(t_n) = \int_0^{t_n} (\ddot{h}_{l,0}^{DWT}\ \varphi(\tau) + \ddot{h}_{l,1}^{DWT}\ \psi(\tau) + \cdots + \ddot{h}_{l,2^j+k}^{DWT}\ \psi(2^j\tau - k)) \cdot (\ddot{x}_{s0}^{DWT}(t_n) \cdot \varphi(\tau) + \ddot{x}_{s1}^{DWT}(t_n) \cdot \psi(\tau) + \cdots + \ddot{x}_{s_{2^j+k}}^{DWT}(t_n) \cdot \psi(2^j\tau - k))d\tau \quad (5.25)$$

Because of the orthogonal condition in Equation (5.16), we get,

$$\ddot{x}_l(t_n) = \ddot{h}_{l,0}^{DWT}\ \ddot{x}_{s0}^{DWT}(t_n) + \ddot{h}_{l,1}^{DWT}\ \ddot{x}_{s1}^{DWT}(t_n) + \cdots + \ddot{h}_{l,2^j+k}^{DWT}\ \ddot{x}_{s_{2^j+k}}^{DWT}(t_n)/2^j \quad (5.26)$$

Rewriting Equation (5.26) in the matrix form,

$$\ddot{x}_l(t_n) = \ddot{x}_s^{DWT}(t_n) \cdot \ddot{h}_l^{DWT} \quad (5.27)$$

where

$$\ddot{\mathbf{x}}_s^{DWT}(t_n) = \left[\ddot{x}_{s0}^{DWT}(t_n) \quad \ddot{x}_{s1}^{DWT}(t_n) \quad \cdots \quad \ddot{x}_{s2^j+k}^{DWT}(t_n)/2^j \right],$$

$$\ddot{\mathbf{h}}_l^{DWT} = \left[\ddot{h}_{l,0}^{DWT} \quad \ddot{h}_{l,1}^{DWT} \quad \cdots \quad \ddot{h}_{l,2^j+k}^{DWT} \right]^T$$

Equation (5.27) can be re-written for a time series with *n* data,

$$\ddot{\mathbf{x}}_l = \ddot{\mathbf{x}}_s^{DWT} \cdot \ddot{\mathbf{h}}_l^{DWT} \quad (5.28)$$

where $\ddot{\mathbf{x}}_l = \left[\ddot{x}_l(t_1) \quad \ddot{x}_l(t_2) \quad \cdots \quad \ddot{x}_l(t_n) \right]^T$, $\ddot{\mathbf{x}}_s^{DWT} = \begin{bmatrix} \ddot{x}_s^{DWT}(t_1) \\ \ddot{x}_s^{DWT}(t_2) \\ \cdots \\ \ddot{x}_s^{DWT}(t_n) \end{bmatrix}$

Finally, $\ddot{\mathbf{h}}_l^{DWT}$ can be computed in the form of a pseudo-inverse as

$$\ddot{\mathbf{h}}_l^{DWT} = (\ddot{\mathbf{x}}_s^{DWT^T} \cdot \ddot{\mathbf{x}}_s^{DWT})^{-1} \cdot \ddot{\mathbf{x}}_s^{DWT^T} \cdot \ddot{\mathbf{x}}_l \quad (5.29)$$

The UIR, $\ddot{\mathbf{h}}_l$, can be reconstructed from $\ddot{\mathbf{h}}_l^{DWT}$ using Equation (5.5). The authors found in this study that the wavelet-based unit impulse responses are accurate when the system is subject to continuous input signals which at least have the first-order derivative, such as the harmonic input signals. Non-smooth varying input signal, such as random input signals, contains large discretization errors leading to a poor unit impulse response. High sampling rate is therefore required to have a good accuracy when the system is subject to random input excitation.

5.3.2 Sensitivity Matrix from Analytical Finite Element Model

The equation of motion of a N degrees-of-freedom (DOFs) damped structural system under support excitation is given as

$$\mathbf{M}\ddot{\mathbf{x}}+\mathbf{C}\dot{\mathbf{x}}+\mathbf{K}\mathbf{x}=-\mathbf{M}\cdot\mathbf{L}\cdot\ddot{\mathbf{x}}_s(t) \qquad (5.30)$$

where $\mathbf{M},\mathbf{C},\mathbf{K}$ are the $N\times N$ mass, damping and stiffness matrices respectively. $\mathbf{L}$ is the mapping vector relating the DOFs with support input to the corresponding DOFs of the system. $\mathbf{x},\dot{\mathbf{x}},\ddot{\mathbf{x}}$ are the $N\times 1$ displacement, velocity, acceleration vectors respectively.

When $\ddot{x}_s$ is a unit impulse acceleration, Equation (5.30) can be written as,

$$\mathbf{M}\ddot{\mathbf{x}}+\mathbf{C}\dot{\mathbf{x}}+\mathbf{K}\mathbf{x}=-\mathbf{M}\cdot\mathbf{L}\cdot\delta(t) \qquad (5.31)$$

where $\delta(t)$ is the Dirac delta function. Assuming the system has zero initial conditions before the occurrence of the unit impulse acceleration excitation, the forced vibration state under the unit impulse support excitation can be represented by a free vibration state with the following initial conditions,

$$x(0) = 0\,,\ \dot{x}(0) = -\mathbf{M}^{-1}\cdot\mathbf{M}\cdot\mathbf{L} \tag{5.32}$$

Rewrite Equations (5.31) and (5.32), the unit impulse response function can be computed as

$$\begin{cases} \mathbf{M}\ddot{\mathbf{h}} + \mathbf{C}\dot{\mathbf{h}} + \mathbf{K}\mathbf{h} = 0 \\ \mathbf{h}(0) = 0,\ \dot{\mathbf{h}}(0) = -\mathbf{M}^{-1}\cdot\mathbf{M}\cdot\mathbf{L} \end{cases} \tag{5.33}$$

where $\mathbf{h}$, $\dot{\mathbf{h}}$, $\ddot{\mathbf{h}}$ are the unit impulse displacement, velocity and acceleration vectors respectively. Using the time-stepping integral method such as Newmark method, the unit impulse response can easily be computed from the analytical finite element model.

Differentiate Equation (5.33) with respect to α_i where α_i is the fractional stiffness of i th element, we get

$$\begin{cases} \mathbf{M}\dfrac{\partial\ddot{\mathbf{h}}}{\partial\alpha_i} + \mathbf{C}\dfrac{\partial\dot{\mathbf{h}}}{\partial\alpha_i} + \mathbf{K}\dfrac{\partial\mathbf{h}}{\partial\alpha_i} = -\dfrac{\partial\mathbf{C}}{\partial\alpha_i}\mathbf{h} - \dfrac{\partial\mathbf{K}}{\partial\alpha_i}\mathbf{h} \\ \dfrac{\partial\mathbf{h}(0)}{\partial\alpha_i} = 0,\ \dfrac{\partial\dot{\mathbf{h}}(0)}{\partial\alpha_i} = -\dfrac{\partial\mathbf{M}^{-1}\cdot\mathbf{M}\cdot\mathbf{L}}{\partial\alpha_i} \end{cases} \tag{5.34}$$

The sensitivities $\dfrac{\partial\mathbf{h}}{\partial\alpha_i}$, $\dfrac{\partial\dot{\mathbf{h}}}{\partial\alpha_i}$ and $\dfrac{\partial\ddot{\mathbf{h}}}{\partial\alpha_i}$ can then be obtained from Equations (5.33) and (5.34) with time-stepping integral method such as Newmark Method treating the right-hand-side of Equation (5.33) as the equivalent force input. The significance of sampling rate in the computation of the time response and its sensitivities has been discussed in reference (Low and Hao, 2001).

The sensitivity matrix **S** can be obtained for all the suspected elements of the structure as

$$\mathbf{S} = \left[\frac{\partial \ddot{h}_l}{\partial \alpha_1} \quad \frac{\partial \ddot{h}_l}{\partial \alpha_2} \quad \cdots \quad \frac{\partial \ddot{h}_l}{\partial \alpha_m} \right] \tag{5.35}$$

where $\ddot{h}_l$ denotes the unit impulse acceleration response of the l th DOF of the system under support excitation. m is the number of the structural parameters.

5.3.3 Damage Identification

In order to identify damage from the measured vibration characteristics, a two-step model updating method is used. Firstly, accelerations from the intact structure, including those obtained from the structure and at the support, are measured. The unit impulse acceleration response $(\ddot{\mathbf{h}})_2$ can be obtained from Equation (5.29). Then based on the prior knowledge of the structure, we can establish an analytical finite element model from which the sensitivity matrix S can be computed using Equation (5.35), and the unit impulse acceleration response $(\ddot{\mathbf{h}})_1$ can be obtained from Equation (5.33). From the following identification equation,

$$\mathbf{S} \cdot \Delta\boldsymbol{\alpha} = \Delta\ddot{\mathbf{h}} = (\ddot{\mathbf{h}})_2 - (\ddot{\mathbf{h}})_1 \tag{5.36}$$

The updating fractional stiffness $\Delta\alpha$ can be obtained as,

$$\Delta\boldsymbol{\alpha} = (\mathbf{S}^T\mathbf{S})^{-1} \cdot \mathbf{S}^T \cdot ((\ddot{\mathbf{h}})_2 - (\ddot{\mathbf{h}})_1) \tag{5.37}$$

where the superscripts $(\bullet)^T$ and $(\bullet)^{-1}$ denotes the transpose and the inverse of the matrix. The intact structure is updated with Equation (5.37) to a more accurate analytical model.

Secondly, accelerations from the damaged structure are measured, including also measurements from the structure and at the support. The updated analytical model from

the first stage is used as the reference model. Corresponding sensitivity matrix and unit impulse acceleration response can be computed. The damaged structure can be updated in a similar way using Equation (5.37) to a more accurate analytical model. The differences between the two updated analytical models for the intact structure and the damaged structure is the set of local damages incurred in the structure.

5.3.4 Statistical Analysis

The above algorithm is developed based on the assumption that both the finite element model and the measured accelerations are accurate. But in real applications, errors in the damage detection procedure generally include the discretization error, configuration error, mechanical parameter errors and measurement errors. The errors that occur in the measured vibration characteristics may be divided into two classes: biased (systematic) error and random error. Biased error is from the malfunction of equipment or/and environment sources. It may not have zero mean and have different types of distributions. Random error, on the other hand, has zero mean and is usually modeled as normally distributed (Robert and Casella, 1999).

Existing techniques of model updating can improve the finite element model whenever the errors are related to the stiffness of the structure, and the problem of incorrect initial model can be partially eliminated using the above two-stage approach. But errors other than those associated with stiffness related parameters and the random errors in measurement have to be handled carefully not to erode the identification accuracy of the algorithm. In the present study, only the random error in the UIR obtained from measured accelerations is considered.

The uncertainties in the measurement data are assumed as normally distributed random variables with zero mean and given covariance. The UIR obtained from measurement is equal to the true UIR plus the random noise as

$$(\ddot{h}_i)_2 = (\ddot{h}_i)_2^0 + (\ddot{h}_i)_2^0 X_i = (\ddot{h}_i)_2^0 (1 + X_i),\ (i = 1, 2, \cdots, nt) \qquad (5.38)$$

where nt is the number of the data point of the UIR. Superscript "0" represents the corresponding true value and subscript "2" represents the data obtained from measurement. $\ddot{h}_i$ denotes the i th data point of the UIR, X_i is the random noise in the measured UIR. For simplicity, X_i is written as a vector $\mathbf{X} = \begin{bmatrix} X_1 & X_2 & \cdots & X_{nt} \end{bmatrix}^T$.

The expectation value of the identified stiffness fractional changes $\Delta\alpha$ can be obtained from Equation (5.37) as

$$\begin{aligned} E(\Delta\boldsymbol{\alpha}) &= E((\mathbf{S}^T\mathbf{S})^{-1} \cdot \mathbf{S}^T \cdot (\ddot{\mathbf{h}})_2 - (\ddot{\mathbf{h}})_1) \\ &= (\mathbf{S}^T\mathbf{S})^{-1} \cdot \mathbf{S}^T \cdot ((\ddot{\mathbf{h}})_2^0 - (\ddot{\mathbf{h}})_1) \end{aligned} \qquad (5.39)$$

The derivative of $\Delta\boldsymbol{\alpha}$ with respect to the random variable X basing on Equations (5.37) and (5.38) is

$$\begin{aligned} \frac{\partial \Delta\boldsymbol{\alpha}}{\partial X_i} &= \frac{\partial}{\partial X_i}\{(\mathbf{S}^T\mathbf{S})^{-1} \cdot \mathbf{S}^T \cdot ((\ddot{\mathbf{h}})_2 - (\ddot{\mathbf{h}})_1)\} \\ &= (\mathbf{S}^T\mathbf{S})^{-1} \cdot \mathbf{S}^T \cdot \frac{\partial (\ddot{\mathbf{h}})_2}{\partial X_i} = (\mathbf{S}^T\mathbf{S})^{-1} \cdot \mathbf{S}^T \cdot \mathbf{H}_i \end{aligned} \qquad (5.40)$$

where $\mathbf{H}_i = \begin{bmatrix} 0 & \cdots & (\ddot{h}_i)_2^0 & \cdots & 0 \end{bmatrix}^T$ in which the i th element is $(\ddot{h}_i)_2^0$ with all other elements equal to zeros. On the other hand, $\Delta\boldsymbol{\alpha}$ can also be expressed as the Taylor series of the random variable X with the second and higher terms neglected as

$$\Delta\boldsymbol{\alpha}(\varepsilon) = \Delta\boldsymbol{\alpha}(0) + \sum_{i=1}^{nt} \frac{\partial \Delta\boldsymbol{\alpha}(0)}{\partial X_i} X_i + \frac{1}{2} \sum_{i=1}^{nt} \sum_{j=1}^{nt} \frac{\partial^2 \Delta\boldsymbol{\alpha}(0)}{\partial X_i \partial X_j} X_i X_j \qquad (5.41)$$

The covariance matrix of $\Delta\boldsymbol{\alpha}$ (Xia, et al. 2002) is,

$$[\mathrm{cov}(\Delta\boldsymbol{\alpha}, \Delta\boldsymbol{\alpha})]_{m\times m} = [\frac{\partial \Delta\boldsymbol{\alpha}}{\partial X}]_{m\times nt} [\mathrm{cov}(\mathbf{X}, \mathbf{X})]_{nt\times nt} [\frac{\partial \Delta\boldsymbol{\alpha}}{\partial X}]^T_{m\times nt} \qquad (5.42)$$

Since random variables X_i and X_j $(i \neq j)$ are independent, we have

$$[\mathrm{cov}(\mathbf{X}, \mathbf{X})]_{nt\times nt} = \begin{bmatrix} \mathrm{cov}(X_1, X_1) & 0 & \cdots & 0 \\ 0 & \mathrm{cov}(X_2, X_2) & \cdots & 0 \\ \cdots & \cdots & \cdots & \cdots \\ 0 & 0 & \cdots & \mathrm{cov}(X_{nt}, X_{nt}) \end{bmatrix} \qquad (5.43)$$

from Equations (5.40) and (5.42).

In the damage identification procedure, the vector of stiffness changes of the intact structure obtained in the first step is $\boldsymbol{\alpha}_u = \boldsymbol{\alpha}_0 + \Delta\boldsymbol{\alpha}_0$, where $\boldsymbol{\alpha}_0$ and $\boldsymbol{\alpha}_u$ correspond to the original analytical model and the updated model respectively, and $\Delta\boldsymbol{\alpha}_0$ is obtained by Equation (5.39). The corresponding vector of stiffness changes in the damaged structure is $\boldsymbol{\alpha}_d = \boldsymbol{\alpha}_2 + \Delta\boldsymbol{\alpha}_2$. Finally, the stiffness fractional changes between the intact and the damaged structure is,

$$\Delta\boldsymbol{\alpha} = \boldsymbol{\alpha}_d - \boldsymbol{\alpha}_u = \boldsymbol{\alpha}_2 + \Delta\boldsymbol{\alpha}_2 - (\boldsymbol{\alpha}_0 + \Delta\boldsymbol{\alpha}_0) \qquad (5.44)$$

and the expectation value of $\Delta\boldsymbol{\alpha}$ is ,

$$\begin{aligned} E(\Delta\boldsymbol{\alpha}) &= E(\boldsymbol{\alpha}_2 - \boldsymbol{\alpha}_0 + (\Delta\boldsymbol{\alpha}_2 - \Delta\boldsymbol{\alpha}_0)) \\ &= \boldsymbol{\alpha}_2 - \boldsymbol{\alpha}_0 + E(\Delta\boldsymbol{\alpha}_2) - E(\Delta\boldsymbol{\alpha}_0) \end{aligned} \qquad (5.45)$$

where $E(\Delta\boldsymbol{\alpha}_2)$ and $E(\Delta\boldsymbol{\alpha}_0)$ are determined from Equation (5.41). The covariance of $\Delta\boldsymbol{\alpha}$ can be computed as,

$$
\begin{aligned}
&[\mathrm{cov}(\Delta\boldsymbol{\alpha},\Delta\boldsymbol{\alpha})]_{m\times m} = \mathrm{cov}(\boldsymbol{\alpha}_2+\Delta\boldsymbol{\alpha}_2-(\boldsymbol{\alpha}_0+\Delta\boldsymbol{\alpha}_0),\boldsymbol{\alpha}_2+\Delta\boldsymbol{\alpha}_2-(\boldsymbol{\alpha}_0+\Delta\boldsymbol{\alpha}_0))\\
&=\mathrm{cov}(\boldsymbol{\alpha}_2+\Delta\boldsymbol{\alpha}_2,\boldsymbol{\alpha}_2+\Delta\boldsymbol{\alpha}_2)-2\,\mathrm{cov}(\boldsymbol{\alpha}_2+\Delta\boldsymbol{\alpha}_2,\boldsymbol{\alpha}_0+\Delta\boldsymbol{\alpha}_0)+\mathrm{cov}(\boldsymbol{\alpha}_0+\Delta\boldsymbol{\alpha}_0,\boldsymbol{\alpha}_0+\Delta\boldsymbol{\alpha}_0) \quad (5.46)\\
&=\mathrm{cov}(\Delta\boldsymbol{\alpha}_2,\Delta\boldsymbol{\alpha}_2)+\mathrm{cov}(\Delta\boldsymbol{\alpha}_0,\Delta\boldsymbol{\alpha}_0)
\end{aligned}
$$

which is the sum of the covariance of the stiffness changes from both the original structure and the damaged structure. $\mathrm{cov}(\Delta\boldsymbol{\alpha}_2,\Delta\boldsymbol{\alpha}_2)$ and $\mathrm{cov}(\Delta\boldsymbol{\alpha}_0,\Delta\boldsymbol{\alpha}_0)$ can be obtained from Equation (5.42).

After the mean value and the covariance of the stiffness fractional change $\Delta\alpha$ are determined, the structural condition can be assessed. Firstly, damage localization is performed with a new damage localization index $\frac{\mu(\Delta\alpha_i)}{\sigma(\Delta\alpha_i)}\left|\frac{\mu(\Delta\alpha_i)}{\sigma(\Delta\alpha_i)}\right|$ where $\mu(\Delta\alpha)$ and $\sigma(\Delta\alpha)$ are the mean and the standard deviation respectively. It is obvious that a large value of the damage index corresponds to a bigger chance of damage occurrence. Also a threshold value z_η can be chosen with $\frac{\mu(\Delta\alpha_i)}{\sigma(\Delta\alpha_i)}\left|\frac{\mu(\Delta\alpha_i)}{\sigma(\Delta\alpha_i)}\right| \geq z_\eta$ indicating that the i th element is damaged. The threshold value z_η is related to the noise level and the system errors and it varies with the type of problem. After the damage locations are determined, the damage severity is given by the mean value $\mu(\Delta\alpha_i)$.

5.3.5 Numerical Verification

A nine-bay three-dimensional frame structural system shown in Figure 4.22 serves for the numerical study. The finite element model consists of sixty-nine three-dimensional Euler beam elements with twenty-nine nodes. The length of all the horizontal, vertical and diagonal members between the centers of two adjacent nodes is exactly 0.5m. The structure orientates horizontally and is fixed into a rigid concrete

support at three nodes at one end. Table 4.8 gives a summary of the main material and geometrical properties of the frame structure. Each node has six DOFs, and altogether there are 174 DOFs for the whole structure.

The translational and rotational restraints at the supports are represented by large stiffnesses of 1.5×10^{11} *kN/m* and 1.5×10^{10} *kN-m/rad* respectively in six directions. Rayleigh damping is adopted for the system with ξ_1=0.01 and ξ_2=0.005 for the first two modes. The first twelve natural frequencies of the structure are 5.11, 10.95, 15.06, 19.27, 27.37, 39.44, 52.19, 60.89, 65.64, 79.07, 87.45 and 91.33 *Hz* . The sampling frequency is 2000 *Hz* . The structure is subject to El-Centro seismic acceleration reduced to one-tenth of its original value along the *y*-axis at the support as shown in Figure 5.5(a). The same acceleration is assumed acting at all the three supporting nodes. The vertical (*z*-direction) and horizontal (*y*-direction) acceleration responses at node 7 of the structure are recorded for a duration of 0.5 seconds after the support excitation begins. The UIRs obtained from Equation (5.29) are shown in Figures 5.5(b) and 5.5(c). It is noted that the support excitation is not perfectly smooth and there will be some discretization errors in the UIRs extracted.

The scenario with damage occurrences in the 4th, 15th, 21st, 34th, 40th and 41st element with 5%, 5%, 10%, 5%, 5%, 10% reduction in the modulus of elasticity of material respectively is considered. The intact structural model is assumed known as an accurate model without the need of updating. The statistical characteristics of the vector of stiffness changes of the intact state $\mu(\Delta\boldsymbol{\alpha}_0)$ and $\sigma(\Delta\boldsymbol{\alpha}_0)$ are therefore equal to zeros. The intact structural model is then chosen as the reference analytical model of the damaged structure. Vector $\Delta\boldsymbol{\alpha}$ is equal to $\Delta\boldsymbol{\alpha}_2$, and it only needs to identify the mean

value and the standard derivation of $\Delta\boldsymbol{\alpha}_2$. Assuming the UIRs computed from the "measured" accelerations contain 5%, 10% and 15% noise in turn, $\mu(\Delta\alpha)$ and $\sigma(\Delta\alpha)$ are identified for each case, and the results for the case with 15% random noise level are compared with those obtained by Monte Carlo Technique (MCT) (Robert and Casella, 1999) in Figure 5.6.

Table 5.2 gives the identified percentage reduction in the modulus of elasticity of the damaged elements with noise and without noise. The noise level has been shown not having any effects on the identified result in Equation (5.39) and therefore only one set of results is shown in column 3 of the Table. Columns 4 to 6 are results obtained from the MCT with different level of noise. A conclusion can be made that the mean values obtained from UIRs with different level of noise and without noise from the proposed method and those from MCT are all very close to each other and have slight difference with the true value. This slight difference is due to the dicretization error and the error caused by the linear Taylor series expansion in Equation (5.41). Figure 5.6(a) also indicates that the results from both the proposed and MCT techniques are close together and both methods do not give false alarm in the undamaged elements.

The standard deviations for each element obtained from the two methods are close to each other as shown in Figure 5.6(b) indicating the correctness of the proposed method. The standard deviation increases with an increase in the noise level which is as expected. Further inspection on the results (not shown) obtained from using 5% and 10% random noise show that the pattern of the standard deviation in the different elements is maintained no matter what the noise level is. The magnitudes change by a scalar which is equal to the fractional change in the noise level included in the analysis. This can be

explained by an inspection of Equations (5.42) and (5.43). The derivatives on the right-hand-side of Equation (5.42) are independent of the noise level, while the covariance term in Equation (4.3) includes the noise level which can be extracted as a scalar when the random variables are of the same types of distribution.

The damage localization indices of all the elements are shown in Figure 5.6(c). The indices for the damaged elements are much larger than those for the undamaged element and there is no false warning in all the undamaged elements. The formulation of the damage index includes the two statistical moments giving strong indications on those elements with damages. The variation of the magnitude of the indices for each element with the noise level also has a fixed pattern but with different magnitude with the same reason as explained for the standard deviation. In spite of 15% noise in UIRs, the index for the damaged 15^{th} element is less than 0.1, but it is still far larger than those for the undamaged elements. This shows that this new damage index is robust in the damage localization. A threshold value z_η can be selected from the distribution but there is no need to do so with the present tidy set of damage indices.

5.3.6 Experimental Verification

The nine-bay three-dimensional frame structure described in the numerical study is fabricated in the laboratory using Meroform M12 construction system. It consists of sixty-nine 22mm diameter alloy steel tubes jointed together by twenty-nine standard Meroform ball nodes. Each tube is fitted with a screwed end connector which, when tightened into the node, also clamps the tube by means of an internal compression fitting. All the connection bolts are tightened with the same torsional moment to avoid

asymmetry or nonlinear effects caused by man-made assembly errors. The whole experimental setup is shown in Figure 4.21(a) and the support is shown in Figure 4.21(b). The structure has the material and geometric properties as listed in Table 4.8.

The Modal analysis

The modal test is performed with a dynamic hammer model B&K 8202 hitting horizontally along the *y*-direction near node 11 of the frame. Only the horizontal (*y*-direction) and vertical (*z*-direction) accelerations at all the nodes, excluding those at the supports, are recorded with a total of 52 DOFs. They are measured with nine B&K 4371 piezoelectric accelerometers in six sets of measurements with all nine sensors in a set for the DOFs in the upper members and seven sensors in a set for the DOFs in the lower member. All sensors are orientated in either the vertical or horizontal direction in each set of measurement. An additional mass of 72 g weight is added to each joint to balance the effect of the moving accelerometers. The sampling frequency is 2000 Hz. The responses are low-pass filtered at 1000 Hz, and a commercial data logging system INV303 with the associated data analysis system DASP2003 are used in the data acquisition. Frequency response function (FRF) is calculated for all the measured responses, and the first twelve natural frequencies and modal damping ratios averaged over twenty FRFs are listed in the fifth column of Table 5.3. The corresponding measured mode shapes are given in Figure 5.7. Only a few pure bending modes are identified while most of them have coupled bending and torsional vibrations.

Modelling of the structure

The Meroform ball joints have been treated as semi-rigid joints, and a finite element model of a hybrid beam with semi-rigid end connections has been proposed (Law et al, 2001). This section adopts this hybrid beam model for the model improvement of the structure. The initial model assumes a large fixity factor *p* for the rotational stiffness of the joints which is taken equal to 0.999 with 1.0 equal to that for a rigid joint. The total weight of the ball and half of the weight of the bolt connecting the ball with the frame element are placed at each node as lump mass. The other half of the weight of the bolt is considered as part of the finite element. In additional, another lump mass of 72 g weight is added to each node to represent the weight of the moving accelerometers. The first twelve analytical natural frequencies are listed in the second column of Table 5.3. It is noted that the finite element model is in general more stiffer than the real structure with larger difference in the higher modes.

Dynamic test for damage detection

The structure is excited with impact from a Dystran Instruments 12 lbs instrumented impulse hammer model 5803A hitting approximately at the centroid of the support in the *y*-direction. The support is very rigid and heavy compared with the frame and it is hold down to the strong floor of the laboratory with four steel bolts. The acceleration responses of the support along the three principal directions are measured. Only the response in the *y*-direction is significant and those in the other two directions are very small. Nine accelerometers are placed at nodes 2 to 10 in the *y*-direction for recording the acceleration response time histories. The sampling frequency is 2000 Hz. The typical acceleration time history at the support in the *y*-direction is shown in Figure

5.8(a) and the UIR obtained from the acceleration in the *y*-direction at node 6 is shown in Figure 5.8(b). This test is repeated for many times for the statistical mean.

Damage scenario

After performing the dynamic test on the intact frame structure, local faults are introduced by replacing three intact members with damaged ones. The artificial damage is of two types. Type I is a perforated slot cut in the central length of the member. The length of slot is 13.7 cm, and the remaining depth of the tube in the cross-section is 14.375 mm. Type II is the removal of a layer of material from the surface of the member. The external diameter of the tube is reduced from 22.02mm to 21.47mm, and the length of the weakened section is 202 mm, located in the middle of the beam leaving 99mm and 75mm length of original tube cross-section on both sides. Figure 4.21(c) gives a close up view of the damaged frame members. Type I damage is located in element 10 and Type II damage is located in elements 27 and 68. They are illustrated with a solid star on the member in Figure 4.22. The equivalent damages computed by Guyon method are 5% and 9.5% reduction in the modulus of elasticity of element 10 and elements 27 and 68 respectively. The three members cluster together at the end of the structure with small strain energy under deformation. The damage in each member is difficult to resolve with most existing damage detection algorithms.

Modal analysis on the damaged structure

Modal analysis is performed on the damaged structure in a similar way as for the original structure. The first twelve natural frequencies and the damping ratios averaged

over twenty FRFs are listed in the last two columns of Table 5.3. There are cases of increase and decrease in the natural frequencies compared to those of the intact structure. The damping ratios are in general smaller than those of the intact structure. This may be due to the release of hidden frictional elements during the process of testing.

Model improvement for damage detection

The two-stage approach is adopted for the damage detection. The first stage updates the rotational stiffness at the member ends for an updated analytical model of the intact structure. Three UIRs obtained from nodes 5, 6 and 7 are used for the identification. There are 69×6=414 unknown rotational stiffness in the identification. The first 500 data points of each UIR are used and there are 1500 equations in Equation (5.36). The measured modal damping ratios from the intact structure have been used in Equations (5.30) and (5.34) for the computation of the analytical UIRs. For simplicity, the updated analytical model in section 4.4.5 is directly used here which have the updated rotational stiffnesses not differing too much from the original value with the largest change in member 20 at node 22 with the updated $p=0.86$ for the x-axis rotational stiffness (see section 4.4.5). The natural frequencies of the updated structure are shown in the third column of Table 5.3. They are close to the measured values with a maximum error of approximately 1% in modes 6 and 12. This model is therefore considered accurate for the next stage of damage assessment.

The second stage updates the local faults in all the members of the structure in terms of their modulus of elasticity with the updated finite element model from the first stage as the reference model. Again the UIRs from nodes 5, 6 and 7 are used for the

identification. There are 69 unknowns in the identification. The first 500 data points of each UIR are used and there are 1500 equations in Equation (5.36). The identification is conducted with results from 60 sets of measurement, and the mean and standard deviation of the identified $\Delta\alpha$ are computed. The damage location indices are obtained and shown in Figure 5.9(a) and the identified damage extent for all the elements are also shown in Figure 5.9(b). The identified reduction in the modulus of elasticity in the damaged members are 5.14%, 8.62% and 10.14% for elements 10, 27 and 68 respectively which are quite close to the calculated values of 5%, 9.5% and 9.5% respectively. There is an indication of local damage in element 47 with a reduction of 3.23% even though it is in real case undamaged. Its existence cannot be explained with the two sets of results from the two stages of model improvement. The natural frequencies calculated from the updated model of the damaged structure are list in the fourth column of Table 5.3. The errors between the measured frequencies are in general larger than those found for the updated model for Stage I with an error larger than 1% in the 10^{th} mode and upwards.

5.3.7 Discussions

The proposed technique theoretically should give satisfactory results from using different types of support excitation. However further study with natural ground excitation with similar order of vibration magnitude in the laboratory fails. This raises an important requirement on the type of excitation for the use of this technique. Both the simulation study and the laboratory example make use of excitations with plenty of low-frequency components. The natural random excitation consisting of plenty of high frequency components and it could not generate sufficient responses from the structure.

Also the non-smooth random input signal, as discussed previously, would lead to large discretization error causing further deterioration in the identified results.

The unit impulse response functions extracted via discrete wavelet transform from measured accelerations of a structure and at its support are used to assess the structural health condition. Discrete wavelet transform is employed in the extraction procedure to avoid the end effects with Fourier transform. Support excitation is commonly encountered and man-made ground excitation and low-level seismic tremor are very suitable for this approach. Random environmental excitation is not preferred as it contains mainly of high frequency components which have little effect in exciting the structure. The UIRs are obtained in the time domain and therefore the damage detection can be conducted with measurement from a few sensors. A statistical analysis on the UIRs with measurement noise is conducted and the results compared favorably with those from MCT. A new damage localization index is proposed based on the statistical moments of the identified results.

A nine-bay three-dimensional frame structure is studied numerically and experimentally with damage scenarios of multiple damages and different level of noise. Measured accelerations from only three sensors are used in the experimental study with satisfactory results indicating the effectiveness of the proposed approach.

5.4 Improved Regularization Techniques for IRF-based Damage Detection

This section used unit impulse response function for damage detection with improved regularization techniques. The improvements include additional constraints on the regularization solution x_λ to determine the regularization parameter. Constraints

added to the regularization solution include a small norm $\|x_\lambda\|$ and a limited range for x_λ. Similarity between successive sets of computed x_λ is ensured by checking on their correlation using a Multiple Parameter Correlation Coefficient (MPCC). A one-story plane frame and a thirty-one bar plane truss structure are used to demonstrate the proposed techniques.

5.4.1 Regularization Method for Identification Equation

The identification equation based on the sensitivity approach for damage detection described in the thesis can be written as,

$$\mathbf{Ax} - \mathbf{b} = 0 \qquad (5.47a)$$

where $\mathbf{A} \in R^{N_A \times N_x}$ is the sensitivity matrix with respect to the structural parameters, $\mathbf{b} \in R^{N_A}$ is the vector of measured structural characteristic changes, $\mathbf{x} \in R^{N_x}$ is the solution vector representing the damages which are the changes in the structural parameters. Equation (5.47a) is linear and usually over-determined when the time series data are used directly in the Equation. It is often solved with the least-squares method based on the minimization of the weighted norm $\|\mathbf{Ax} - \mathbf{b}\|_W^2$ or the Euclidian norm $\|\mathbf{Ax} - \mathbf{b}\|_2^2$. For simplicity, the Euclidian norm is adopted in this section, that is,

$$J_{LS}(\mathbf{x}) = \|\mathbf{Ax} - \mathbf{b}\|_2^2 = (\mathbf{Ax} - \mathbf{b})^T \cdot (\mathbf{Ax} - \mathbf{b}) \qquad (5.48)$$

From the minimization of Equation (5.48), i.e $\frac{\partial J_{LS}(\mathbf{x})}{\partial \mathbf{x}} = 0$, the least squares solution of Equation (5.47a) can be obtained as,

$$\mathbf{x}_{LS} = (\mathbf{A}^T\mathbf{A})^{-1}\mathbf{A}^T\mathbf{b} \qquad (5.49a)$$

However, in many cases, the least squares solution is not satisfactory due to ill-conditioning problems. In order to obtain the steady unique solution of Equation (5.47a) which is often ill-conditioning, the regularization condition is needed as,

$$C(x) = 0 \tag{5.50}$$

Where $C(\bullet)$ contains N_c equations. In this section we assume $C(\bullet)$ takes the form $C(x) = \mathbf{C}\mathbf{x} - \mathbf{d}$, with $\mathbf{C} \in R^{N_C \times N_x}$ and $\mathbf{d} \in R^{N_C}$, which represents the general linear problem $Cx = d$. For implementation in iterative model updating, the incremental form of this equation is $\mathbf{C}\delta\mathbf{x} = \mathbf{d}_k$, where $\mathbf{d}_k = \mathbf{d} - \mathbf{C}\mathbf{x}_k$. The residuals corresponding to this equation are used to give the second cost function,

$$J_{\mathrm{Re}g}(x) = \left\|\mathbf{C}\mathbf{x} - \mathbf{d}\right\|_2^2 = (\mathbf{C}\mathbf{x} - \mathbf{d})^T \cdot (\mathbf{C}\mathbf{x} - \mathbf{d}) \tag{5.51}$$

Thus there are two cost functions, J_{LS} and $J_{\mathrm{Re}g}$, that need to be minimized concurrently. A composite cost function J_{LSR} is formulated as,

$$J_{LSR} = J_{LS} + \lambda J_{\mathrm{Re}g} = \left\|\mathbf{A}\mathbf{x} - \mathbf{b}\right\|_2^2 + \lambda \left\|\mathbf{C}\mathbf{x} - \mathbf{d}\right\|_2^2 \tag{5.52}$$

where, $\lambda \geq 0$ is the regularization parameter, and $J_{\mathrm{Re}g}$ is stabilizing/regularization part. The parameter λ controls the extent to which regularization is applied to the nominal problem. Usually used $J_{\mathrm{Re}g}$ in the damage identification based on model updating are based on engineering assumptions concerning the parameter variations during iterations. The most frequently used conditions include: 1) $\mathbf{x} \to 0$, i.e. that the parameter values will be small; 2) $\mathbf{x} \to \mathbf{x}_0$, i.e. that the parameter changes with respect to the reference model will be small; and 3) $\delta\mathbf{x} \to 0$, i.e. that the parameter step between iterations will be small.

In this section, condition (3) is adopted according to the engineering assumptions. Equation (5.50) can be written as,

$$\mathbf{I} \cdot \delta \mathbf{x} = 0 \tag{5.53}$$

This regularization conditions based on Equation (5.53) aim to reduce the magnitude of the parameter change at the iteration step towards zero. This condition results in a smooth transition between the non-Regularized least squares solution and $\delta \mathbf{x}(\lambda) \to 0$ in the direction $-\nabla J_{LS}$ as $\lambda \to \infty$. From Equation (5.53), the cost function J_{LSR} in Equation (5.52) can be written as,

$$J_{LSR} = J_{LS} + \lambda J_{\mathrm{Re}g} = \left\| \mathbf{A}\mathbf{x} - \mathbf{b} \right\|_2^2 + \lambda \left\| \mathbf{x} \right\|_2^2 \tag{5.54}$$

From the minimization of Equation (5.54) $\dfrac{\partial J_{LSR}(\mathbf{x})}{\partial \mathbf{x}} = 0$, the regularization solution of Equation (5.47a) can be obtained as,

$$x_{\mathrm{Re}g} = (\mathbf{A}^T \mathbf{A} + \lambda \mathbf{I})^{-1} \mathbf{A}^T \mathbf{b} \tag{5.55a}$$

To display the influence of the regularization parameter in the solution, then the singular value decomposition of the matrix A is firstly performed as,

$$[\mathbf{U}, \Sigma, \mathbf{V}] = \mathrm{csvd}(\mathbf{A}) \text{ or } \mathbf{A} = \mathbf{U} \cdot \mathrm{diag}(\Sigma) \cdot \mathbf{V}^{\mathrm{T}} \tag{5.56}$$

where "csvd" denotes the compact singular value decomposition. "diag(Σ)" denotes the diagonal matrix formed from the vector of singular values Σ. The vector of singular values Σ can be expressed as,

$$\Sigma = \begin{bmatrix} \sigma_1 & \sigma_2 & \cdots & \sigma_n \end{bmatrix}, \qquad \sigma_1 \geq \sigma_2 \geq \cdots \geq \sigma_n \tag{5.57}$$

where σ_i is the ith singular value.

Substituting Equation (5.56) into Equation (5.49a), the least squares solution can also be written as,

$$\mathbf{x}_{LS} = \mathbf{V} \cdot diag(\vartheta) \cdot \mathbf{U}^T \cdot \mathbf{b} \qquad (5.49b)$$

Where $\vartheta = \left[\frac{1}{\sigma_1} \quad \frac{1}{\sigma_2} \quad \cdots \quad \frac{1}{\sigma_n} \right]$ (5.58)

Similarly, substituting Equation (5.56) into Equation (5.55a), having

$$\mathbf{x}_{\mathrm{Re}g} = \mathbf{V} \cdot diag(\mathbf{f}) \cdot \mathbf{U}^T \mathbf{b} \qquad (5.55b)$$

with $\mathbf{f} = \left[\frac{1}{\sigma_1(1+\frac{\lambda}{\sigma_1^2})} \quad \frac{1}{\sigma_2(1+\frac{\lambda}{\sigma_2^2})} \quad \cdots \quad \frac{1}{\sigma_n(1+\frac{\lambda}{\sigma_n^2})} \right]$ (5.59)

Comparing Equation (5.49b) and Equation (5.55b), the influence of the regularization parameter λ can be seen. The following cases can be derived from Equation (5.55b),

Case (1): When $\lambda = 0$, $\mathbf{f} = \vartheta == \left[\frac{1}{\sigma_1} \quad \frac{1}{\sigma_2} \quad \cdots \quad \frac{1}{\sigma_n} \right]$, and $\mathbf{x}_{Reg} = \mathbf{x}_{LS}$

Case (2): When $\lambda = \sigma_n^2$, $\mathbf{f} = \left[\frac{1}{\sigma_1(1+\frac{\sigma_n^2}{\sigma_1^2})} \quad \frac{1}{\sigma_2(1+\frac{\sigma_n^2}{\sigma_2^2})} \quad \cdots \quad \frac{1}{\sigma_n(1+\frac{\sigma_n^2}{\sigma_n^2})} \right]$, and $\left\| \mathbf{A}\mathbf{x}_{reg} - \mathbf{b} \right\|$

is very small and close to $\left\| \mathbf{A}\mathbf{x} - \mathbf{b} \right\|$

Case (3): When $\lambda = \sigma_1^2$, $\mathbf{f} = \left[\frac{1}{\sigma_1(1+\frac{\sigma_1^2}{\sigma_1^2})} \quad \frac{1}{\sigma_2(1+\frac{\sigma_1^2}{\sigma_2^2})} \quad \cdots \quad \frac{1}{\sigma_n(1+\frac{\sigma_1^2}{\sigma_n^2})} \right]$ which is close

to $\left[\frac{1}{2\sigma_1} \quad 0 \quad \cdots \quad 0 \right]$, and $\left\| \mathbf{x}_{reg} \right\|$ is very small but $\left\| \mathbf{A}\mathbf{x}_{reg} - \mathbf{b} \right\|$ is comparative large.

Case (4): When $\lambda = \infty$, $\mathbf{f} = \left[0 \quad 0 \quad \cdots \quad 0 \right]$, then $\left\| \mathbf{x}_{reg} \right\|$ and $\mathbf{x}_{reg}$ are zeros.

The vector **f** is the filter vector that affects the value of the solution with the regularization parameter λ. This shows that how to determine the value of λ is important.

5.4.2 Determination of regularization parameters

From the above analysis, there exists an optimal value of λ which ensures both $\left\|\mathbf{x}_{reg}\right\|$ and $\left\|\mathbf{A}\mathbf{x}_{reg}-\mathbf{b}\right\|$ are small. The optimal λ can be determined with the cross validation method and L-curve method. In this section, L-curve method is adopted. In L-curve method, the optimal λ corresponds to a point on the L-curve as shown in Figure 5.10 with $\eta=\left\|\mathbf{x}_{reg}\right\|_2$ and $\rho=\left\|\mathbf{A}\mathbf{x}_{reg}-\mathbf{b}\right\|_2$, and both are functions of λ. The inflexional point on the curve corresponds to a balance between $\left\|\mathbf{x}_{reg}\right\|$ and $\left\|\mathbf{A}\mathbf{x}_{reg}-\mathbf{b}\right\|$. The optimal λ corresponds to the physical inflexional point where the curvature is smallest. The subsequent computational process for determining the optimal λ is based on the fact that the curvature of the curve is smallest at this point.

The curvature $1/\rho_c$ of the L-curve is defined as,

$$\frac{1}{\rho_c}=\frac{d\theta}{ds}=\frac{\dfrac{d^2\eta}{d\rho^2}}{(1+(\dfrac{d\eta}{d\rho})^2)^{1.5}} \tag{5.60a}$$

In order to determine the optimal λ, the term $\dfrac{d^2\eta}{d\rho^2}/(1+(\dfrac{d\eta}{d\rho})^2)^{1.5}$ has to be minimized. From the above definition, we have $\eta=\left\|\mathbf{x}_{reg}\right\|_2=\sqrt{\mathbf{x}_{reg}^T\cdot\mathbf{x}_{reg}}$, $\rho=\left\|\mathbf{A}\mathbf{x}_{reg}-\mathbf{b}\right\|_2$, and

$$\left\|\mathbf{x}_{reg}\right\|_2^2=\mathbf{x}_{reg}^T\cdot\mathbf{x}_{reg}=(\mathbf{V}\cdot diag(\mathbf{f})\cdot\mathbf{U}^T\cdot\mathbf{b})^T\cdot(\mathbf{V}\cdot diag(\mathbf{f})\cdot\mathbf{U}^T\cdot\mathbf{b})$$

$$= (\mathbf{U}^T\mathbf{b})^T \cdot (diag(\mathbf{f}))^2 \cdot (\mathbf{U}^T\mathbf{b}) \tag{5.61}$$

$$\left\|\mathbf{A}\mathbf{x}_{reg} - \mathbf{b}\right\|_2^2 = (\mathbf{A}\mathbf{x}_{reg} - \mathbf{b})^T (\mathbf{A}\mathbf{x}_{reg} - \mathbf{b}) \tag{5.62a}$$

Since $\mathbf{b} = \mathbf{A}\mathbf{x}$, Equation (5.62a) can be expressed as,

$$\begin{aligned} &\left\|\mathbf{A}\mathbf{x}_{reg} - \mathbf{b}\right\|_2^2 = (\mathbf{A}(\mathbf{x}_{reg} - \mathbf{x}))^T (\mathbf{A}(\mathbf{x}_{reg} - \mathbf{x})) = (\mathbf{x}_{reg} - \mathbf{x})^T \cdot \mathbf{A}^T\mathbf{A} \cdot (\mathbf{x}_{reg} - \mathbf{x}) \\ &= (\mathbf{U}^T\mathbf{b})^T (diag(\mathbf{f} - \vartheta) \cdot diag(\boldsymbol{\Sigma}))^2 (\mathbf{U}^T\mathbf{b}) \end{aligned} \tag{5.62b}$$

The first derivatives of η and ρ with respect to parameter λ are defined as, $\eta' = d\eta / d\lambda$, $\rho' = d\rho / d\lambda$. Substituting, the curvature in Equation (5.60a) we get,

$$\begin{aligned} \frac{d\theta}{ds} &= \frac{\frac{d^2\eta}{d\rho^2}}{(1+(\frac{d\eta}{d\rho})^2)^{1.5}} = \frac{\frac{d^2\eta}{d\rho^2}}{(1+(\frac{d\eta / d\lambda}{d\rho / d\lambda})^2)^{1.5}} \\ &= \frac{(\rho')^3 \frac{d^2\eta}{d\rho^2}}{(\rho')^3(1+(\frac{d\eta / d\lambda}{d\rho / d\lambda})^2)^{1.5}} = \frac{(\rho')^3 \frac{d^2\eta}{d\rho^2}}{((\rho')^2 + (\eta')^2)^{1.5}} \end{aligned} \tag{5.63}$$

Also we have the second differential as

$$\frac{d^2\eta}{d\rho^2} = \frac{d(d\eta / d\rho)}{d\rho} = \frac{d(\eta' / \rho')}{d\lambda}\frac{d\lambda}{d\rho} = \frac{d(\eta' / \rho') / d\lambda}{\rho'} = (\frac{1}{(\rho')^2}\eta'' - \frac{\eta'}{(\rho')^3}\rho'')$$

Finally the curvature in Equation (5.60a) becomes

$$\frac{d\theta}{ds} = \frac{(\rho')^3(\frac{1}{(\rho')^2}\eta'' - \frac{\eta'}{(\rho')^3}\rho'')}{((\rho')^2 + (\eta')^2)^{1.5}} = \frac{\rho'\eta'' - \eta'\rho''}{((\rho')^2 + (\eta')^2)^{1.5}} \tag{5.60b}$$

The optimal λ can be obtained by maximizing Equation (5.60b), and the optimal regularized solution x_{reg} is determined from Equation (5.55b).

In damage detection, the system carries no noise and no model errors, $\mathbf{x}_{Reg}$ would be very close to $\mathbf{x}_{LS}$, because it corresponds to a small $\|\mathbf{Ax}-\mathbf{b}\|$. But when the system carries noise or model error, the regularization solution $\mathbf{x}_{Reg}$ deviates from the least-squares solution due to the presence of noise and model errors in the iteration process, and $\|\mathbf{Ax}-\mathbf{b}\|$ is not small. In this case, Equation (5.47a) can be rewritten as

$$\mathbf{A}_r\mathbf{x}-\mathbf{b}_r=0 \tag{5.64}$$

where $\mathbf{A}_r$, $\mathbf{b}_r$ are for the system with noise or model errors. It is noted that even if the system has noise or model errors (it is noted that model errors are limited to the small ranges), $\mathbf{A}_r$ is close to $\mathbf{A}$. i.e. $\mathbf{A}_r \approx \mathbf{A}$. But $\mathbf{b}_r$ will comprise of three parts,

$$\mathbf{b}_r=\mathbf{b}_d+\mathbf{b}_n+\mathbf{b}_m, \tag{5.65}$$

where $\mathbf{b}_d$ is due to damage, $\mathbf{b}_n$ is due to noise, and $\mathbf{b}_m$ is due to model error.

Equation (5.64) is then rewritten approximately as

$$\mathbf{Ax}-\mathbf{b}_r=0 \text{ or } \mathbf{Ax}=\mathbf{b}_d+\mathbf{b}_n+\mathbf{b}_m \tag{5.66}$$

The engineering solution $\mathbf{x}_e$ (which denotes the correct parameter change vector) will have two objectives: a small $\|\mathbf{x}_e\|$ and minimized $\|\mathbf{Ax}_e-\mathbf{b}\|$. But there is a contradiction with the least-squares solution as it only minimizes $\|\mathbf{Ax}-\mathbf{b}_r\|$ but not $\|\mathbf{Ax}_e-\mathbf{b}_d\|$.

Then the regularization solution in Equation (5.55b) becomes,

$$\begin{aligned}\mathbf{x}_{Reg} &= \mathbf{V}\cdot diag(\mathbf{f})\cdot\mathbf{U}^T\cdot(\mathbf{b}_d+\mathbf{b}_n+\mathbf{b}_m)\\ &= \mathbf{V}\cdot diag(\mathbf{f})\cdot\mathbf{U}^T\cdot\mathbf{b}_d+\mathbf{V}\cdot diag(\mathbf{f})\cdot\mathbf{U}^T\cdot\mathbf{b}_n+\mathbf{V}\cdot diag(\mathbf{f})\cdot\mathbf{U}^T\cdot\mathbf{b}_m\end{aligned} \tag{5.67}$$

Here $\mathbf{x}_{Reg}$ composes of three terms. The first term is $\mathbf{x}_e$ which corresponds to the system with no noise and model errors. The second and third terms are perturbed terms corresponding respectively to the noise and model errors. In the iterative sensitivity approach of damage detection, the signal to noise ratio will decrease dramatically after a few iterations, and the noise or model error dominates in the vector $\mathbf{b}_r$ causing $\mathbf{x}_{Reg}(\lambda)$ deviates from $\mathbf{x}_e$. The aim of this section is to find a value λ' that can make $\mathbf{x}_{Reg}(\lambda') \approx \mathbf{x}_e$.

The above discussions show that the Tikhonov method with L-curve technique cannot be used effectively in all iterations and an improved method for determining the regularization parameter must be provided. In order to find the appropriate λ', we add some constraints to the regularization process. Since in the inverse damage detection problem, damage is often represented by a percentage change in the system parameters, and each component of the damage vector is always less than unity, i.e.

$$\left| x_{reg}(\lambda)_i \right| < 1 \tag{5.68a}$$

It is also well known that satisfactory results, which may be exact, can be obtained when the solution is convergent. In other words there is great similarity in the solutions obtained in successive iterations. Therefore we can make use of this property to improve the performance of the Tikhonov method. The similarity is computed according to the Multiple Parameter Correlation Criteria (*MPCC*),

$$MPCC_{i+1} = 1 - \frac{(\Delta x_{reg(i+1)}^T x_{regi})^2}{(\Delta x_{reg(i+1)}^T \Delta x_{reg(i+1)})(x_{regi}^T x_{regi})} \tag{5.68b}$$

which has been referred to as Multiple Damage Location Assurance Criterion (MDLAC) (Shi and Law, 2000a) for damage location correlation. Such a rename is to justify its use as a correlation criterion for measuring the resemblance of two patterns of parameters in

the iterative process. The resemblance is assured with proportional changes in $\mathbf{x}_{Reg}$ in successive iterations as noted in Equation (5.68b). λ_{opt} is obtained in the improved regularization by minimizing the *MPCC*. The improved regularization process is shown below as

Step 1: Parameter λ_{opt} is obtained by Tikhonov method with Equation (5.68a) as the constraint. Then calculate $x_{reg(i)}$ with $i=1$. Repeat for $i=2$. Then calculate $MPCC_i$.

Step 2: Compare the value *of* $MPCC_i$ with a prescribed threshold value $MPCC_{th}$ which is taken to be 0.5. Discussion on this threshold value can be found towards the end of this paper.

If $MPCC_i < MPCC_{th}$, the solution is stable and go to Step 3.

If $MPCC_i \geq MPCC_{th}$, the solution is considered diverged and the optimal λ_{opt} is recalculated from minimizing *MPCC* . The new $x_{reg(i)}$ and the new $MPCC_i$ are computed, and go to Step 3.

Step 3: Compare with the termination criteria such as those in Equation (5.22). If they are not satisfied, go to Step 2 for the next iteration. If they are satisfied, stop the iteration.

The optimal identification results $\mathbf{x}_{reg}$ can be obtained from the above process with the corresponding λ_{opt} .

5.4.3 Noise Reduction prior to Regularization

If the system carries noise, Equation (5.47a) can be expressed as,

$$\mathbf{A}\mathbf{x} = \mathbf{b}_d + \mathbf{b}_n \qquad (5.47b)$$

Equation (5.47b) can also be expressed as,

$$\mathbf{A}(\mathbf{x}_d + \mathbf{x}_n) = \mathbf{b}_d + \mathbf{b}_n \qquad (5.47c)$$

where $\mathbf{A}\mathbf{x}_d = \mathbf{b}_d$, $\mathbf{A}\mathbf{x}_n = \mathbf{b}_n$. To find the expected value of Equation (5.47c), we have

$$E(\mathbf{A}(\mathbf{x}_d + \mathbf{x}_n)) = E(\mathbf{b}_d + \mathbf{b}_n) \qquad (5.69a)$$

If white noise with zero mean is assumed, both $\mathbf{x}_n$ and $\mathbf{b}_n$ are random variables, and Equation (5.69a) becomes

$$\mathbf{A}(\mathbf{x}_d + \mathbf{E}(\mathbf{x}_n)) = \mathbf{b}_d + \mathbf{E}(\mathbf{b}_n) \qquad (5.69b)$$

Since $E(\mathbf{x}_n) = E(\mathbf{b}_n) = 0$, Equation (5.69b) can be rewritten as

$$\mathbf{A}\mathbf{x}_d = \mathbf{b}_d \qquad (5.69c)$$

Equation (5.69c) shows that when the structural characteristics can be measured repeatedly, using expected value of the measurement can reduce noise effect.

5.4.4 Simulation

The method described in section 5.2 using the wavelet-based sensitivity of impulse response function for damage detection is adopted here to demonstrate the improved regularization method in the model updating procedure. The expected value of unit impulse response function is used to take advantage of the fact that it can be measured repeatedly to find the mean and thus reducing the noise effect.

Two structural systems serve for the numerical study. The first system is a one-story plane frame as shown in Figure 4.9. The structure is subject to a sinusoidal excitation $F(t) = 10\sin(12\pi t)$ N applied vertically at node 6. The horizontal acceleration at node 9 is collected for the study. The columns are 1.2 m high and the cross-beam is 0.6

m long, and each member has 10*mm* depth and 20*mm* breadth uniform rectangular cross-section. The modulus of elasticity and the mass density of materials are respectively $69\times10^9\ N/m^2$ and $2700\,kg/m^3$.

The finite element model of the structure consists of four and three equal beam-column elements in each vertical and horizontal member respectively. The translational and rotational restraints at the supports are represented by large stiffnesses of 1.5×10^{10} *kN/m* and 1.5×10^{9} *kN-m/rad* respectively. Rayleigh damping is adopted for the system with $\xi_1 = 0.01$ and $\xi_2 = 0.01$ for the first two modes. The first 12 natural frequencies of the structure are 13.09, 57.31, 76.7, 152.4, 196.5, 227.3, 374.7, 382.5, 580.2, 699.3, 765.3 and 983.3 *Hz*. The sampling frequency is 2000 *Hz* and 0.25 s of measured data is used. The limits for both convergence criteria have been set equal to 1.0×10^{-6}. The measurement errors are simulated by adding white noise to the calculated accelerations to simulate the polluted measurements as described in Equation (3.42).

Four damage scenarios listed in Table 5.4 are studied. These scenarios include the cases without noise and model errors, with 5% noise, with 10% noise and with noise and model errors. The results are shown in Figure 5.11. In the first case without noise and model errors, the proposed techniques do not have advantage over the Tikhonov method. But when the system includes noise and model errors (Scenarios 2 to 4), the inclusion of the proposed techniques has significant improvements in the identification results. It is noted that the existence of noise in the measurement greatly increases the identification errors due to the model errors when the original Tikhonov method is used.

The second structural system is the thirty-one bar plane truss structure as shown in Figure 5.1, which is modeled using 31 finite elements without internal nodes giving 28

degrees of freedom. The cross-sectional area of the bar is $0.0025\,m^2$. Damage in the structure is introduced as a reduction in the axial stiffness of individual bars, but the inertial properties are unchanged.

Both the vertical and horizontal translational restraints at the supports are modeled by large springs of 1.0×10^{10} *kN/m*. Rayleigh damping is adopted for the system with $\xi_1 = 0.01$ and $\xi_2 = 0.02$ for the first two modes. The first 12 natural frequencies of the structure are 36.415, 75.839, 133.608, 222.904, 249.323, 358.011, 372.509, 441.722, 477.834, 507.943, 538.125 and 547.393 *Hz*. The sampling frequency is 2000 *Hz*. The limits for both convergence criteria have been set equal to 1.0×10^{-6}. The excitation force is applied vertically at node 5 and vertical acceleration measurement is recorded at node 4 as shown in Figure 5.1. The excitation adopted in the structure is a triangular impulsive force with 320.4*N* peak value and it lasts for 0.005 second and 0.25 s of measured data is used. Damage Scenarios 5 to 10 as listed in Table 5.4 are studied to demonstrate the efficiency of the proposed techniques, and results are shown in Figure 5.12. Scenario 5 involves no noise and model errors in the system. There is very small difference in the identification results obtained using the proposed techniques or not. Scenarios 6 and 7 carry 5% and 10% noise in the system respectively, and the damage locations and extent can be determined by using a combination of Tikhonov regularization and the proposed techniques. If the Tikhonov regularization method is used only, the identified result begins to diverge from the 7th iteration onwards for both Scenarios 6 and 7. Scenario 8 has 1% model error in the material density. The results begin to diverge from the 6th iteration and fail to detect damage when only the Tikhonov regularization is used. Scenarios 9 and 10 are the case with both noise and model errors and they have the same

problem as Scenarios 6 and 7 in that the results will diverge after several iterations when only Tikhonov method is used. But the damages can be identified fairly accurately with the proposed techniques.

The above numerical studies show that the combined use of Equation (5.68a) and the similarity requirement in the successively sets of identified results from the conventional Tikhonov method can give satisfactory results in damage detection problem when the system carries model and noise errors and with no divergence in the iteration process.

Discussions

To further illustrate the effectiveness of the proposed improved regularization techniques, Figure 5.13 is plotted to show the variation of the convergence norm $\frac{\left\|\Delta\boldsymbol{\alpha}_{i+1}-\Delta\boldsymbol{\alpha}_{i}\right\|}{\left\|\Delta\boldsymbol{\alpha}_{i+1}\right\|}$ and the *MPCC* with iterations for the second example. The norm decreases with iteration with peaks each corresponds to a slight deviation of resemblance of two successively identified solution as noted in the curve of *MPCC*. The deviation of parameter vector in iterations 3 and 7 is small and Tikhonov regularization can give an appropriate x_{reg} but with a relatively large norm. The deviation of parameter vector obtained from Tikhonov regularization in iteration 10 is very large according to the *MPCC* curve and a new λ_{opt} is obtained from minimizing *MPCC* leading to a small norm of 1.73×10^{-5}. If nothing is done to avoid divergence of solution, Tikhonov regularization fails here. Subsequent iterations 11, 14 and 15 also need the recalculation of λ_{opt} to put the solution back on the path of convergence. The solution obtain after iteration 16 is stable

and with a norm equals 6.4×10^{-6}. The threshold value for *MPCC* is arbitrary selected to be 0.5 to signify the degree of parameter change deviation from Tikhonov regularization which needs the proposed stabilization process. A larger threshold value would allow more variations with the parameter change such that the solution would not fall in the local minimum. However a small threshold value can be selected as it is known that the pattern of parameter change x has been approximately determined in the first few cycles of iteration.

It should also be noted that only small model error is studied in this work. The proposed technique and all existing model-based approach of model updating for damage detection have the limitation of dealing with small local damages and small model errors. This leads to the need of another stage of initial model improvement prior to the second stage of damage detection as adopted in this study. The initial finite element model has to be sufficiently accurate for the second stage of local damage detection. Furthermore, large perturbation of the system parameters would lead to non-linear responses which cannot be handled appropriately using the proposed approach which is a linear approach.

5.5 Summaries

In this chapter, unit impulse response functions via wavelet-based sensitivity and model updating are used to detect damage in the structures under general excitations and support excitations. The unit impulse response functions obtained via discrete wavelet transform of the measured accelerations of a structure and the measured excitation force or measured accelerations at its support are used to assess the structural health condition. Discrete wavelet transform is employed in the extraction procedure to avoid the end

effects with Fourier transform. The UIRs are obtained in the time domain and therefore the damage detection can be conducted with measurement from a few sensors. In order to study the noise effect in the UIR-based method, a statistical analysis on the UIRs with measurement noise is conducted and the results compared favorably with those from Monte Carlo Technique (MCT). A new damage localization index is proposed based on the statistical moments of the identified results. Since the damage detection is also based on model updating, the ill-conditioning problem is solved with an improved regularization techniques in the inverse problem with noise and model errors for damage detection. The range of percentage damage is limited in the determination of the regularization parameter λ in the regularization method. Also there will be large similarity between the sets of results from two successive iterations. The convergence of results is further ensured by checking on such similarity using a Multiple Parameter Correlation Criteria. Numerical studies and experimental verifications are performed with the proposed methods and improved techniques. Satisfactory results are obtained indicating the effectiveness of the proposed approach.

Table 5.1 – Damage scenarios

Damage Scenario	Damage extent	Damage locations	Noise	Model error
1	10%	28th element	no	no
2	10%	31st element	no	no
3	5%,10%	22nd, 26th element	no	no
4	5%,10%,10%	28th, 30th, 31st element	no	no
5	10%	28th element	1%	no
6	10%	28th element	5%	no
7	5%,10%	22nd, 26th element	no	2% reduction in the stiffness in all elements
8	5%,10%	22nd, 26th element	no	50% increase in the support stiffness at two supports
9	5%,10%	22nd, 26th element	no	2% decrease in the Rayleigh damping coefficients
10	5%,10%	22nd, 26th element	5%	Include all the above model errors

Table 5.2 – Identified percentage reduction in the modulus of elasticity

Damaged Element No.	True value	no noise	Noise level *		
			5%	10%	15%
4	5	4.56	4.10	4.56	4.68
15	5	4.90	5.00	4.93	4.42
21	10	11.96	11.85	11.97	12.94
34	5	4.74	4.84	4.62	4.40
40	5	4.81	4.71	5.35	5.19
41	10	11.35	11.24	11.04	10.82

Note: Superscript * denotes results obtained from MCT.

Table 5.3 – The natural frequencies (Hz) and damping ratio of the frame structure

Mode type	FEM			Measured			
	Frequency (Hz)/error (%)			intact		damaged	
	intact	Stage I	Stage II	frequency (Hz)	damping ratio	frequency (Hz)	damping ratio
1H	5.207	5.165/-0.58%	5.184/-0.61%	5.196	0.443	5.216	0.196
1V	11.076	10.951/0.09%	10.870/0.70%	10.942	0.928	10.794	0.418
2H	15.305	15.063/-0.72%	15.108/-0.38%	15.172	0.282	15.166	0.251
V+T	19.493	19.276/-0.59%	19.352/-0.18%	19.390	0.155	19.387	0.155
3H	27.888	27.646/-0.20%	27.253/-0.76%	27.702	0.307	27.462	0.299
H	40.211	39.445/-0.93%	39.052/-0.19%	39.815	0.335	39.127	0.346
H	53.234	52.203/0.11%	51.426/0.80%	52.146	0.423	51.018	0.403
2V	61.565	61.517/-0.68%	61.371/-0.15%	61.938	0.155	61.463	0.432
H+T	66.979	65.655/-0.23%	64.514/0.58%	65.806	0.258	64.142	0.253
H+T	80.706	79.088/0.76%	77.788/1.53%	78.491	0.356	76.616	0.333
T	88.239	87.462/0.20%	87.706/-1.76%	87.287	0.908	89.277	0.333
H+T	93.269	91.334/0.98%	96.918/-1.23%	90.448	0.340	98.125	0.312

Note: (2H) – second horizontal mode; (1V) –first vertical mode; (V+T)- coupled vertical and torsional mode.

Table 5.4 – Damage scenarios

	Damage Scenario	Damage extent	Damage locations	Noise	Model error
plane frame	1	10%	2nd element	No	No
	2	10%	2nd element	5%	No
	3	10%	2nd element	10%	No
	4	10%	2nd element	5%	1% reduction in the flexural stiffness in all elements. 1% increase in the density. 10% increase in the Rayleigh damping coefficients
plane truss	5	5%,5%	8th, 15th element	No	No
	6	5%,5%	8th, 15th element	5%	No
	7	5%,5%	8th, 15th element	10%	No
	8	5%,5%	8th, 15th element	No	1% increase in the material density
	9	5%,5%	8th, 15th element	5%	1% reduction in the stiffness in all elements, 5% reduction in the Rayleigh damping coefficients, 0.1% increase in the density
	10	5%,5%	8th, 15th element	10%	1% reduction in the stiffness in all elements, 5% reduction in the Rayleigh damping coefficients, 0.1% increase in the density, 1% reduction in the stiffness support

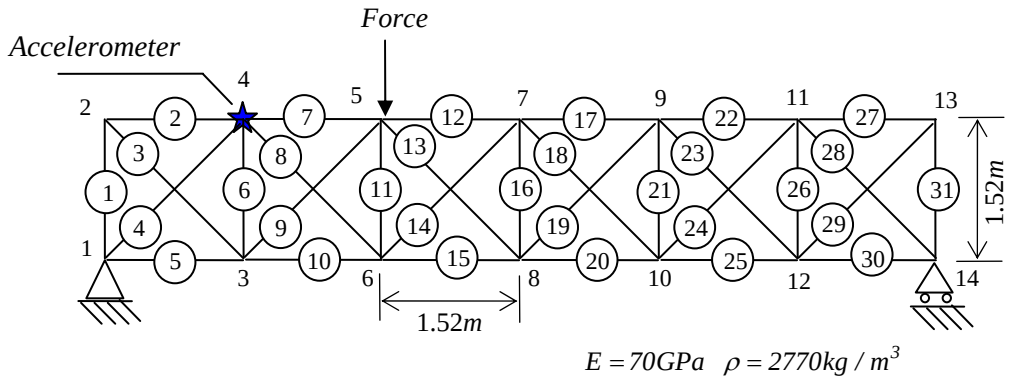

Figure 5.1 - Thirty-one bar plane truss structure

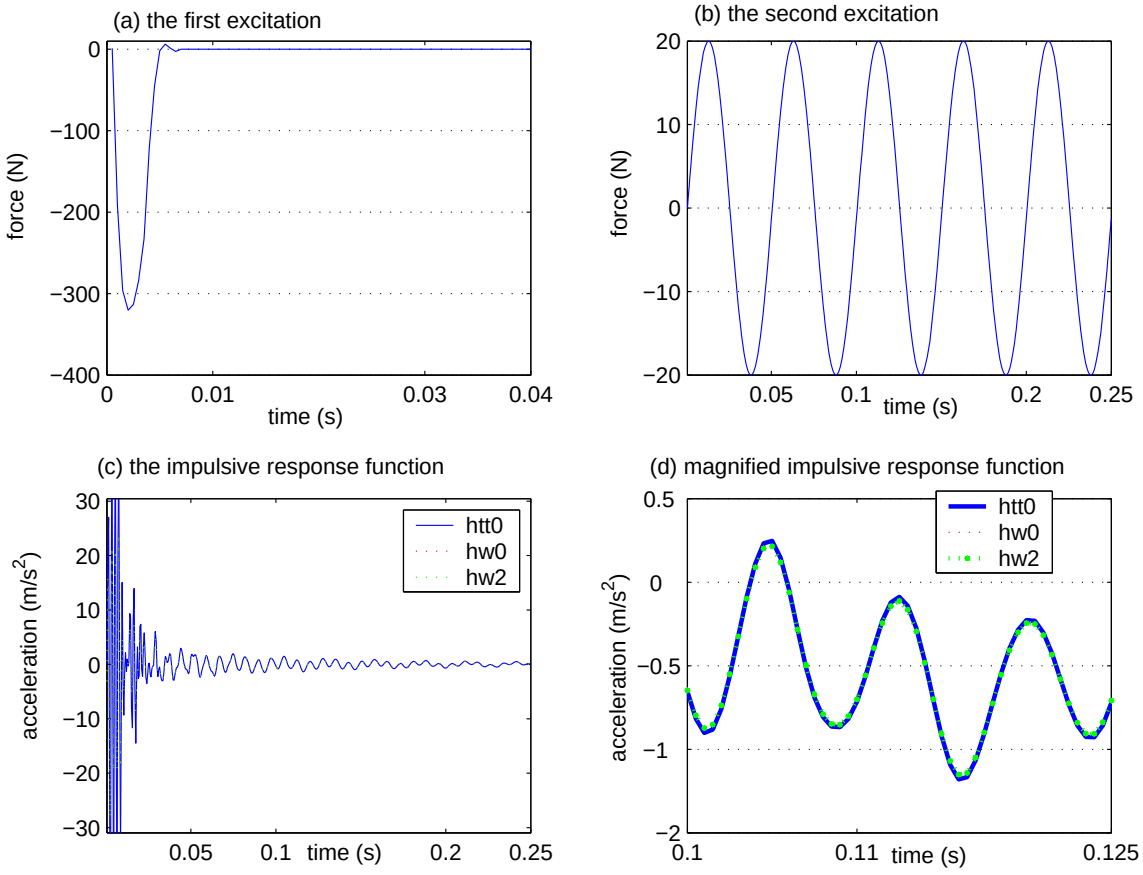

Figure 5.2 - The Impulsive response functions from different excitations

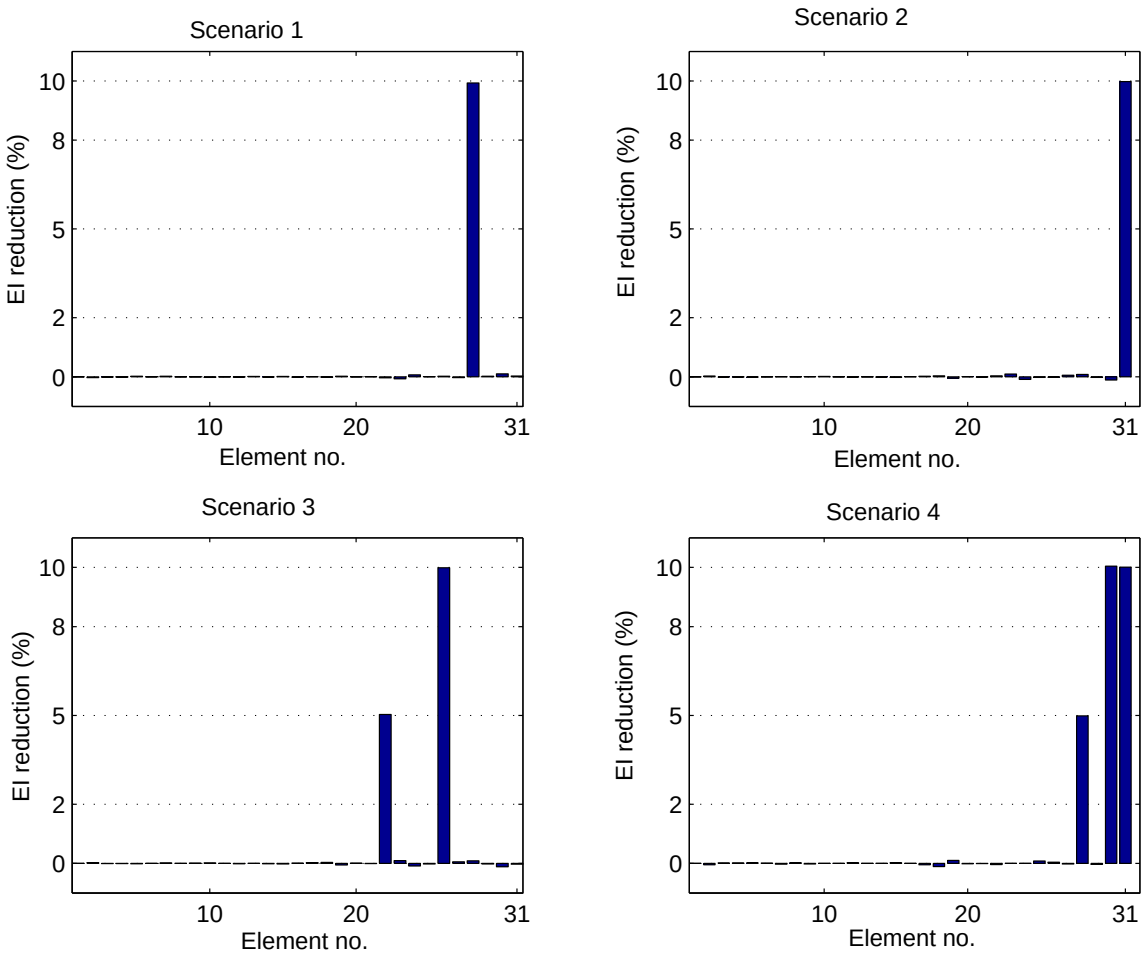

Figure 5.3 - Identified results for Scenarios 1 to 4

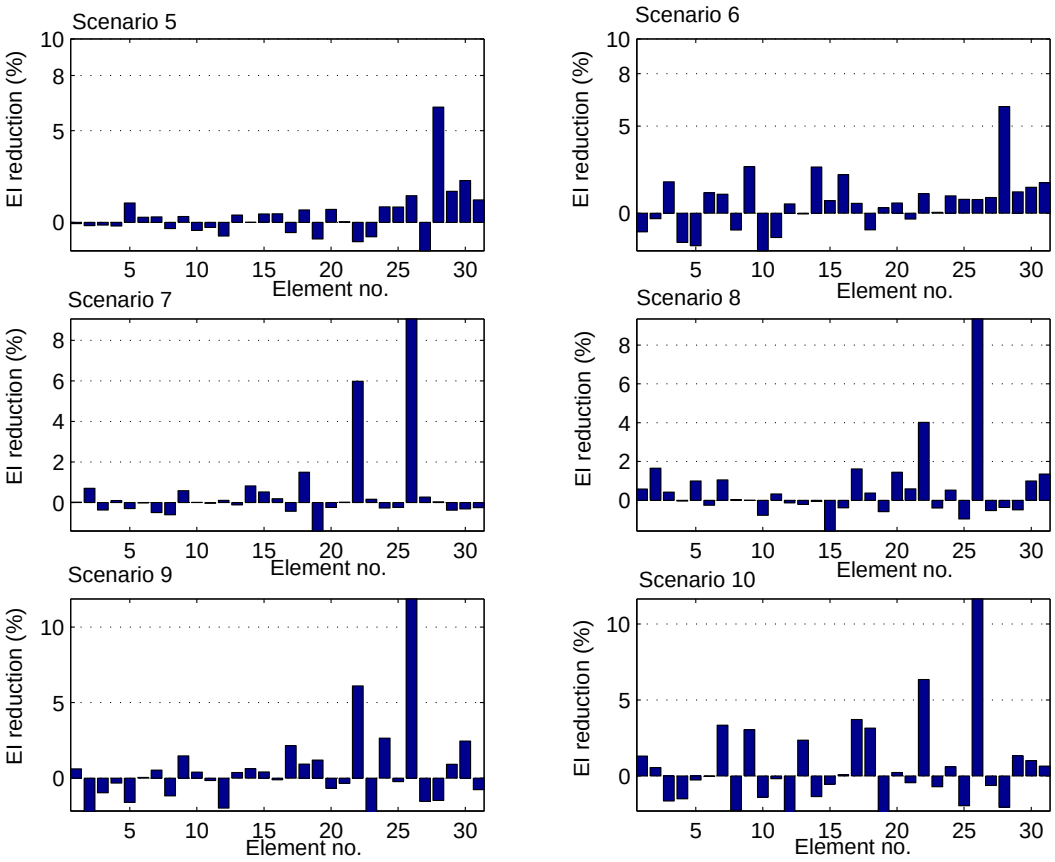

Figure 5.4 -Identified results for Scenarios 5 to 10

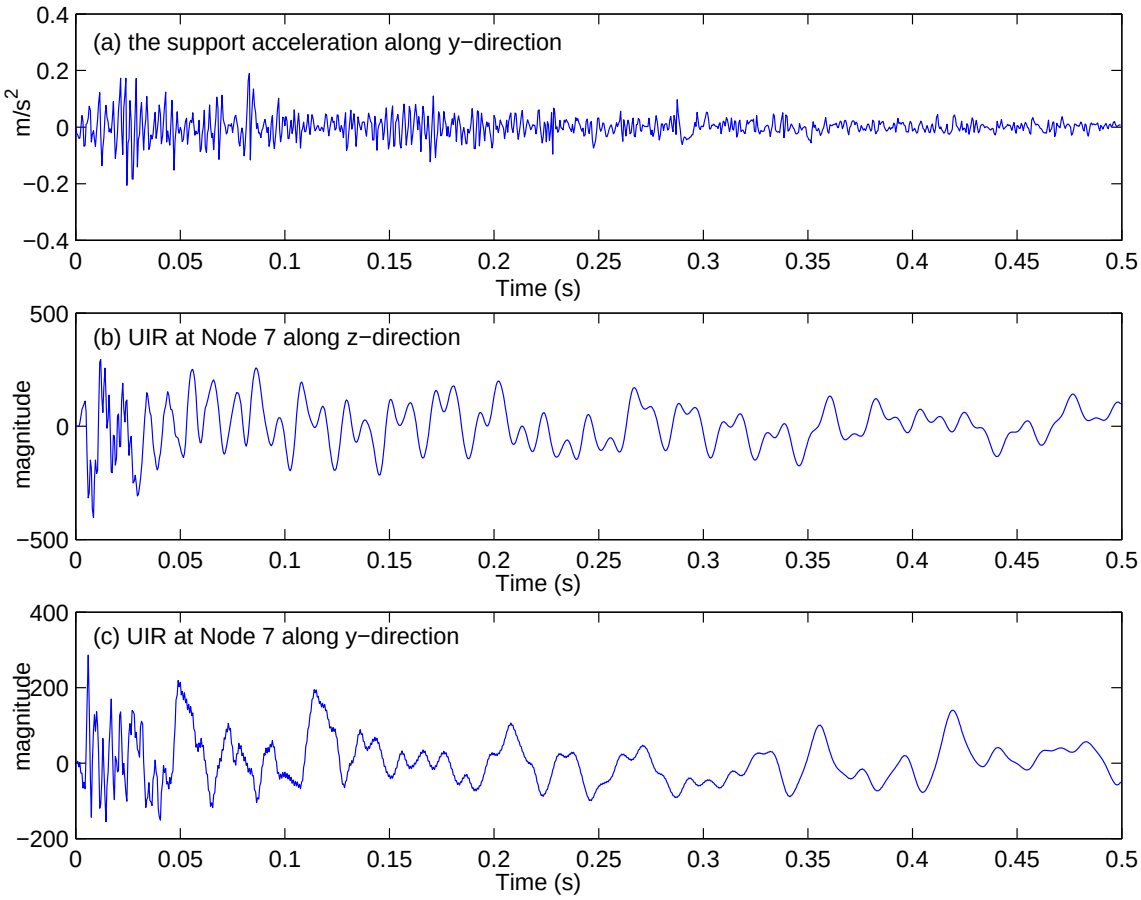

Figure 5.5 - The support acceleration and UIRs obtained at Node 7

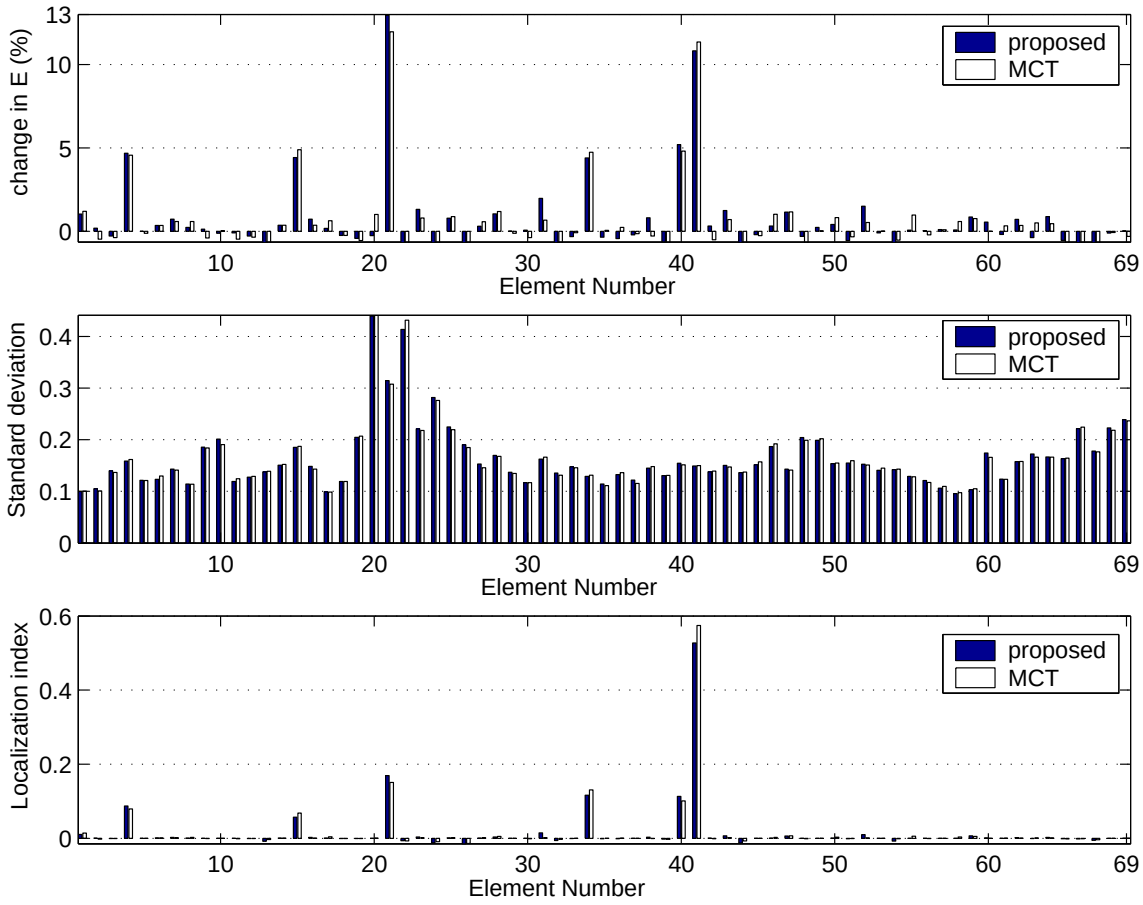

Figure 5.6 - Identified results from response with 15% noise level

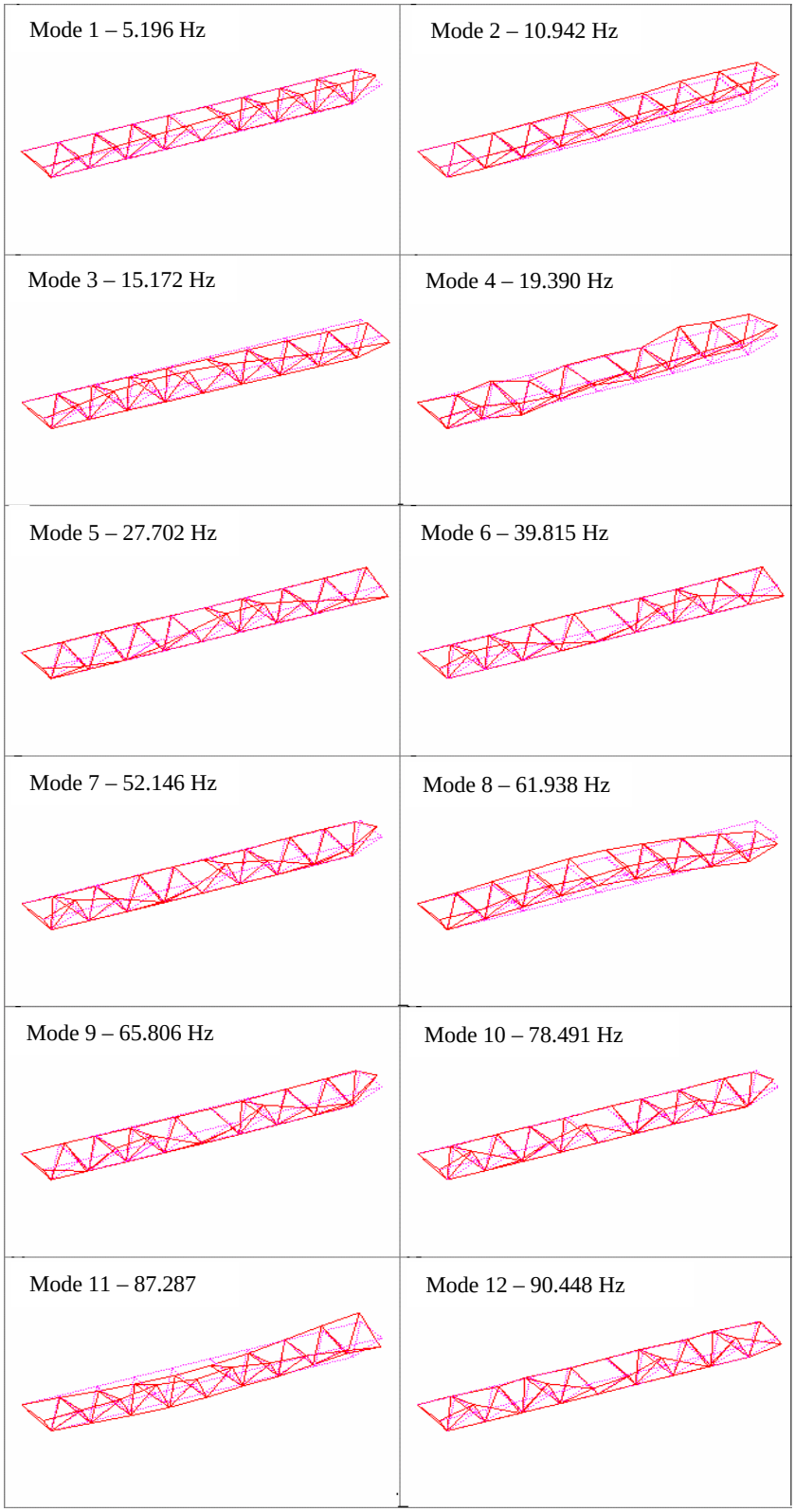

Figure 5.7 - The measured mode shapes of the intact steel frame structure

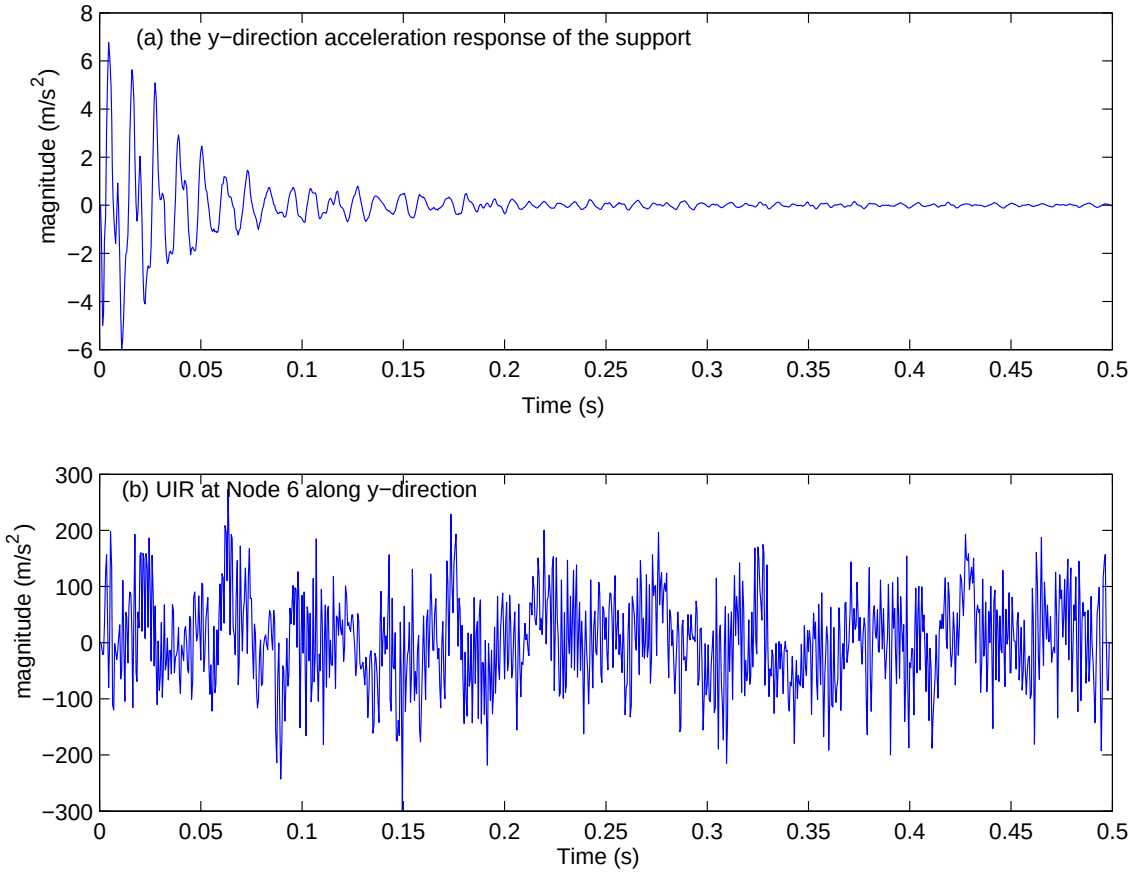

Figure 5.8 - Measured support acceleration and UIR at Node 6

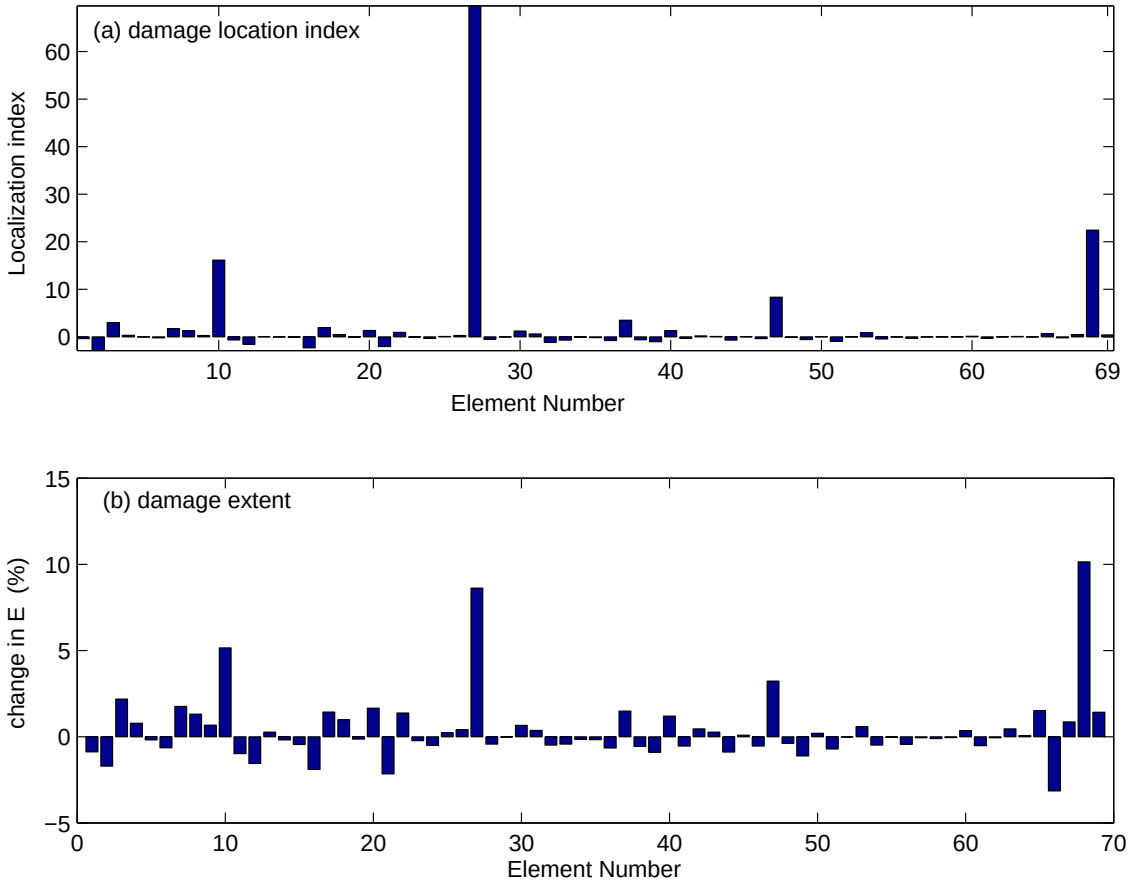

Figure 5.9 - Identified experimental results

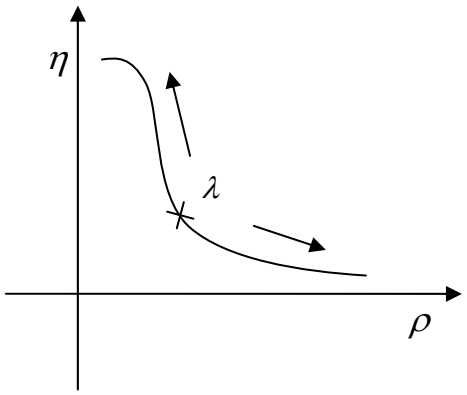

Figure 5.10 - The L-Curve

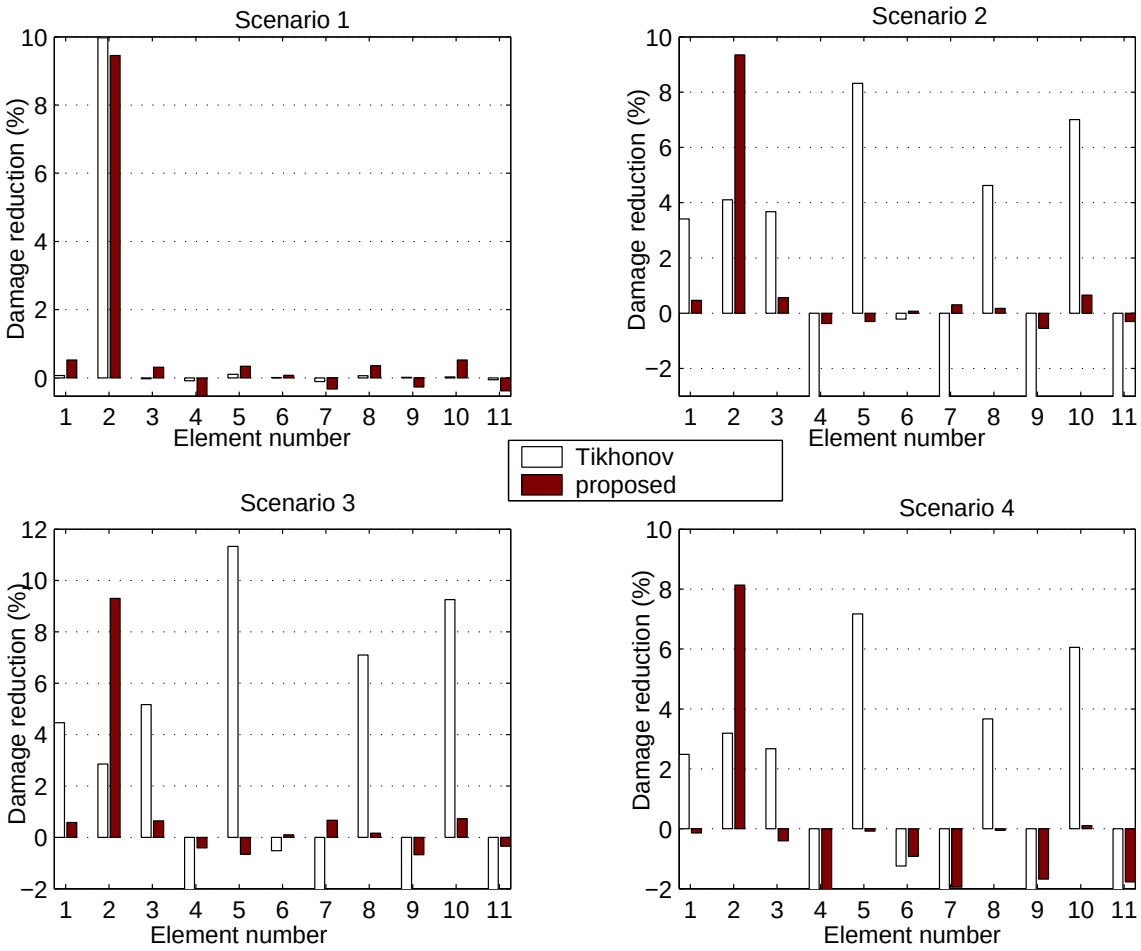

Figure 5.11 - Identified results for Scenarios 1 to 4

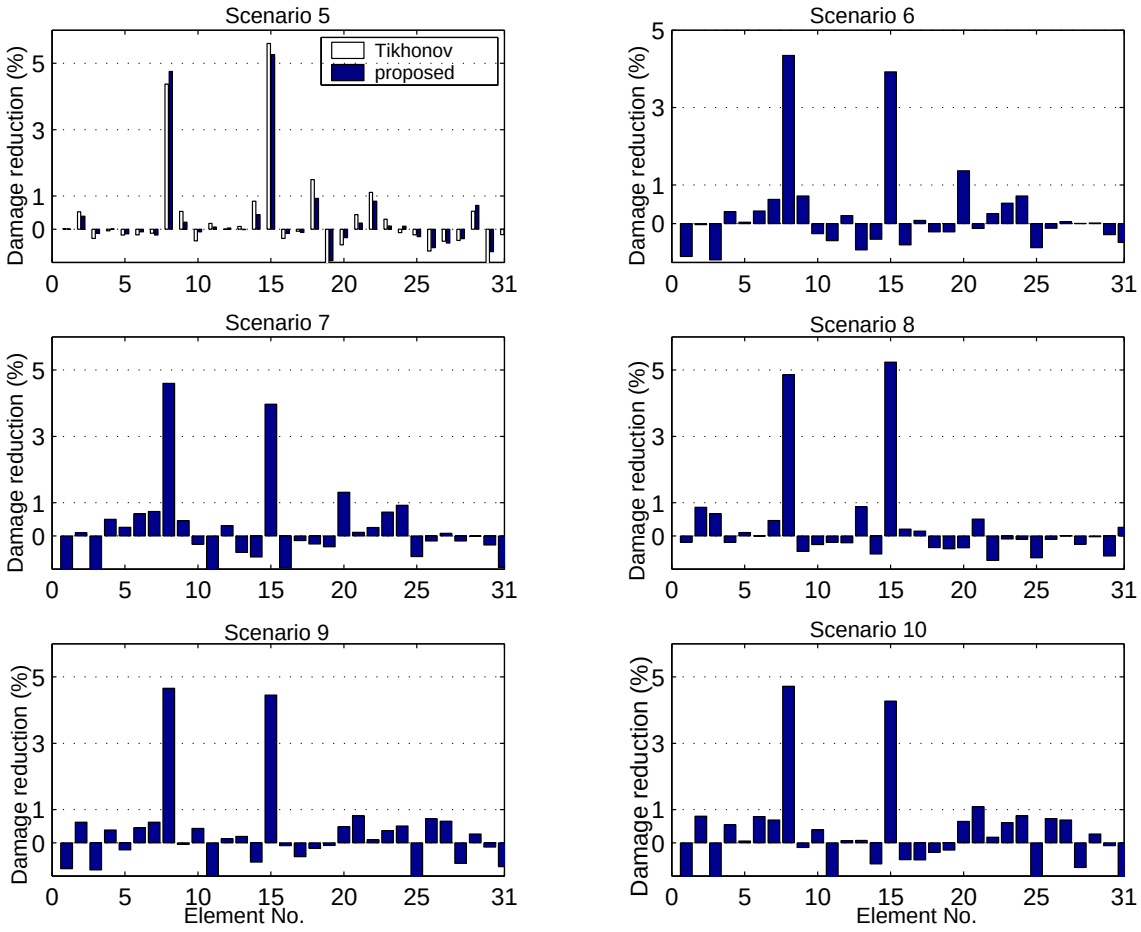

Figure 5.12 - Identified results for Scenarios 5 to 10

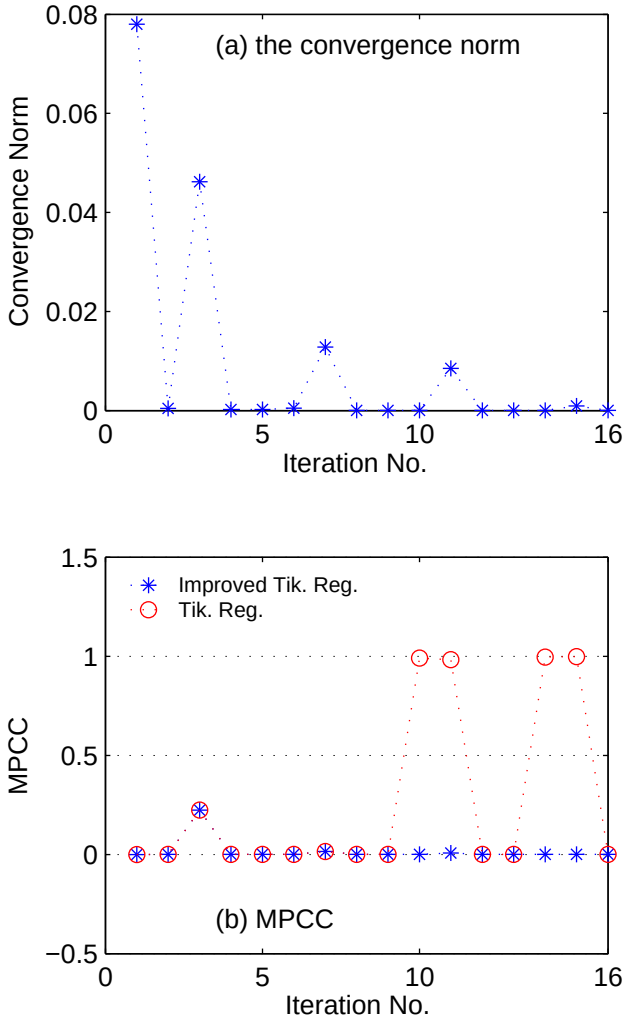

Figure 5.13 - The convergence norm and MPCC

CHAPTER 6 STRUCTURAL DAMAGE DETECTION UNDER AMBIENT EXCITATION

6.1 Introduction

The information required for system identification or damage detection of a dynamic system generally consists of both the input force and the resulting responses. However, it would be very difficult and expensive to measure the actual excitation (such as wind, vehicular and wave excitation) (Shen et al 2003) for a large structure (such as bridges, offshore platforms, and wind turbines). The huge amount of energy necessary to create structural vibrations may cause local damage in the structure if it can be generated artificially. Therefore, system identification or damage detection is preferably to be done with the response-only measurement. For large engineering structures, such as bridges, offshore platform and high-rise buildings, structural health monitoring based on ambient excitation (environmental excitation or traffic vibration) seems to be the most desirable approach with the advantages of low cost and easy operation. For practical monitoring of operating structures, the ideal system should include non-contact and embedded measurements taken from a structure from excitation under the operation environment together with automated or semi-automated signal processing (Farrar and Doebling, 1997). It is noted that most of the existing health monitoring of civil structures are operating continuously, and only ambient excitation can be used for the damage detection of these structures (Peters, 2000).

There are methods on system identification from output-only data. The method of system identification from ambient response measurements has been summarized by Bendat and Piersol (1980). The covariance of responses obtained from ambient excitation has been used to estimate modal parameter and further assess the structural health condition. Methods on the estimate of the modal parameter from the covariance of responses include peak-picking from power spectral density (PSD) functions (Luz and Wallaschek, 1992), least-squares curve fitting techniques (Chalko and Haritos, 1997), autoregressive moving average (ARMA) models (Larbi and Lardies 2000), the subspace techniques (Hermans and Auweraer, 1999, Lardies, 1998), and the natural excitation technique coupled with some time-domain modal identification schemes such as the random decrement processing with the Ibrahim time-domain (ITD) technique (Chiang and Cheng, 1999), the maximum entropy method (MEM) (Desforges et al., 1995), and the polyreference least-squares complex exponential (PRLSCE) method (Hermans and Auweraer, 1999). The natural excitation technique using cross-correlation functions in time domain has been a very powerful tool for the modal analysis of structures under ambient excitation. The peak-picking method has been a typical frequency-domain method on response-only, but it suffers from some disadvantages. For example, the modes of the structure should be sufficiently far apart and requires a lot of engineering skills to select the peaks that correspond to system resonances. Although the curve-fitting technique can eliminate these disadvantages, it often meets the minimization problem that is strongly non-linear and methods of linear algebra are not directly applicable to get the solution.

In Chapter 5, the author has developed an approach for damage assessment making use of the unit impulse response function of a structure in the wavelet domain. This Chapter attempts to extent this method with the structure under ambient excitation as experienced by most of the large-scale structures. Firstly, covariance of acceleration responses is computed based on the unit impulse response function. Then, the wavelet packet energy of covariance of measured acceleration responses of structures under ambient excitation was adopted for damage detection assuming that the ambient excitation is of white noise distribution.

6.2 Covariance of Responses under Ambient Excitation

The covariance of responses from ambient excitation is expressed explicitly as a function of the impulse response function of the system under single or multiple ambient excitations. The sensitivity of the covariance of responses with respect to the physical parameters of the structure is derived analytically. Two numerical examples are studied to illustrate the accuracy of the proposed formulation on the correlation functions with accurate results.

6.2.1 Covariance of Measured Responses

The equation of motion of a N DOFs damped structural system under general excitation from the k th DOF is

$$\mathbf{M}\ddot{\mathbf{x}}+\mathbf{C}\dot{\mathbf{x}}+\mathbf{K}\mathbf{x}=\mathbf{D}_k F_k(t) \qquad (6.1)$$

where $F_k(t)$ is the excitation force at k th DOF. If the system has zero initial conditions, the solution of Equation (6.1) can be expressed as,

$$x_k(t) = \int_{-\infty}^{t} h_k(t-\tau) F_k(\tau) d\tau \qquad (6.2)$$

where $h_k(t)$ is the vector of impulse response of the system under a unit impulse excitation at the k th DOF. The measured acceleration responses $\ddot{x}_{pk}(t)$ from location p at time t and $\ddot{x}_{qk}(t+\tau)$ from location q at time $t+\tau$ are respectively,

$$\ddot{x}_{pk}(t) = \int_{-\infty}^{t} \ddot{h}_{pk}(t-\sigma) \cdot F_k(\sigma) d\sigma, \qquad \ddot{x}_{qk}(t+\tau) = \int_{-\infty}^{t+\tau} \ddot{h}_{qk}(t+\tau-\sigma) \cdot F_k(\sigma) d\sigma \quad (6.3)$$

The cross-correlation function $R_{pqk}(\tau)$ relating the two measured responses is given by Bendat and Piersol (1980) as

$$R_{pqk}(\tau) = E\left\{ \ddot{x}_{pk}(t) \ddot{x}_{qk}(t+\tau) \right\} \qquad (6.4)$$

where $E\{\ \}$ indicates the expectation operator. Equation (6.4) can further be written as,

$$\begin{aligned} R_{pqk}(\tau) &= \lim_{T\to\infty} \frac{1}{T} \int_0^T \ddot{x}_{pk}(t) \ddot{x}_{qk}(t+\tau) dt \\ &= \lim_{NN\to\infty} \frac{1}{NN} \sum_{n=0}^{NN} \ddot{x}_{pk}(n \cdot \Delta t) \ddot{x}_{qk}(n \cdot \Delta t + \tau) \end{aligned} \qquad (6.5)$$

where NN is the number of data point within the duration T under studied. The cross-correlation function $R_{pqk}(\tau)$ is then obtained from two measured responses of a structure.

6.2.2 Covariance of Responses based on the Structural System

Under single random excitation

Alternatively, $R_{pqk}(\tau)$ can be formulated in terms of the physical structural parameters of the system. The accelerations $\ddot{x}_{pk}(t)$ and $\ddot{x}_{qk}(t+\tau)$ are calculated for the

N DOFs damped structural system defined by Equation (6.1) using Equation (6.2). Substituting the calculated accelerations into Equation (6.4), we have,

$$R_{pqk}(\tau) = E\left\{\int_{-\infty}^{t} \ddot{h}_{pk}(t-\sigma_1)\cdot F_k(\sigma_1)d\sigma_1 \int_{-\infty}^{t+\tau} \ddot{h}_{qk}(t+\tau-\sigma_2)\cdot F_k(\sigma_2)d\sigma_2\right\} \qquad (6.6)$$

With random excitation, $F_k(\bullet)$ is random in Equation (6.6), and the equation can be re-written as,

$$R_{pqk}(\tau) = \int_{-\infty}^{t}\int_{-\infty}^{t+\tau} \ddot{h}_{pk}(t-\sigma_1)\ddot{h}_{qk}(t+\tau-\sigma_2)\cdot E(F_k(\sigma_1)F_k(\sigma_2))d\sigma_1 d\sigma_2 \quad (6.7)$$

F_k is assumed to be of white noise distribution, the autocorrelation function of F_k becomes,

$$E(F_k(\sigma_1)F_k(\sigma_2)) = S_k\delta(\sigma_1-\sigma_2) \qquad (6.8)$$

where S_k is a constant and $\delta(t)$ is the Dirac delta function. Substituting Equation (6.8) into (6.7) with $\int_{-\infty}^{+\infty} f(t)\delta(t)dt = f(0)$, we have

$$\begin{aligned} R_{pqk}(\tau) &= S_k\int_{-\infty}^{t} \ddot{h}_{pk}(t-\sigma_1)d\sigma_1 \int_{-\infty}^{t+\tau} \ddot{h}_{qk}(t+\tau-\sigma_2)\cdot\delta(\sigma_1-\sigma_2)d\sigma_2 \\ &= S_k\int_{-\infty}^{t} \ddot{h}_{pk}(t-\sigma_1)\ddot{h}_{qk}(t+\tau-\sigma_1)d\sigma_1 \end{aligned} \qquad (6.9a)$$

or,
$$R_{pqk}(\tau) = S_k\int_{0}^{+\infty} \ddot{h}_{pk}(t)\ddot{h}_{qk}(\tau+t)dt \qquad (6.9b)$$

It should be noted that $\ddot{h}_{pk}(t)$ is an intrinsic function of the structure and is dependent only on the excitation location. Equation (6.9b) also shows that $R_{pqk}(\tau)$ has the same property as $\ddot{h}_{pk}(t)$. The auto-correlation function can also be derived in the same way by putting *q=p* in Equation (6.9). Equation (6.9b) can then be computed directly by integration.

$R_{pqk}(\tau)$ can also be obtained by discrete wavelet transform. Applying DWT to $\ddot{h}_{pk}(t)$ and $\ddot{h}_{qk}(\tau+t)$ respectively, we can get,

$$\ddot{h}_{pk}(t) = \ddot{h}^{DWT}_{pk,0}\ \varphi(t) + \ddot{h}^{DWT}_{pk,1}\ \psi(t) + \cdots + \ddot{h}^{DWT}_{pk,2^j+l}\ \psi(2^j t - l) \qquad (6.10)$$

$$\ddot{h}_{qk}(\tau+t) = \ddot{h}^{DWT}_{qk,0}\ (\tau)\varphi(t) + \ddot{h}^{DWT}_{qk,1}\ (\tau)\psi(t) + \cdots + \ddot{h}^{DWT}_{qk,2^j+l}(\tau)\psi(2^j t - l) \qquad (6.11)$$

Substituting Equations (6.10) and (6.11) into Equation (6.9b), we have

$$R_{pqk}(\tau) = S_k \int_0^{+\infty} \begin{array}{l} (\ddot{h}^{DWT}_{pk,0} \cdot \varphi(t) + \ddot{h}^{DWT}_{pk,1} \cdot \psi(t) + \cdots + \ddot{h}^{DWT}_{pk,2^j+l} \cdot \psi(2^j t - l)) \\ (\ddot{h}^{DWT}_{qk,0}\ (\tau) \cdot \varphi(t) + \ddot{h}^{DWT}_{qk,1}\ (\tau) \cdot \psi(t) + \cdots + \ddot{h}^{DWT}_{qk,2^j+l}(\tau) \cdot \psi(2^j t - l))dt \end{array} \qquad (6.12)$$

Because of the orthogonal condition of the wavelets described in Equation (3.12), Equation (6.12) can be expressed as,

$$R_{pqk}(\tau) = S_k(\ddot{h}^{DWT}_{pk,0}\ \ddot{h}^{DWT}_{qk,0}\ (\tau) + \ddot{h}^{DWT}_{pk,1}\ \ddot{h}^{DWT}_{qk,1}\ (\tau) + \cdots + \ddot{h}^{DWT}_{pk,2^j+l}\ \ddot{h}^{DWT}_{qk,2^j+l}(\tau)/2^j) \qquad (6.13)$$

Rewriting in matrix form, we have the cross-correlation function expressed in terms of the discrete wavelet coefficient as

$$\mathbf{R}_{pqk} = S_k\, \ddot{\mathbf{h}}^{DWT}_{qk}\ \ddot{\mathbf{h}}^{DWT}_{pk} \qquad (6.14)$$

where

$$\mathbf{R}_{pqk} = \begin{bmatrix} R_{pqk}(\tau_0) \\ R_{pqk}(\tau_1) \\ \cdots \\ R_{pqk}(\tau_n) \end{bmatrix}, \ddot{\mathbf{h}}^{DWT}_{pk} = \begin{bmatrix} \ddot{h}^{DWT}_{pk,0} \\ \ddot{h}^{DWT}_{pk,1} \\ \cdots \\ \ddot{h}^{DWT}_{pk,2^j+l} \end{bmatrix}, \quad \ddot{\mathbf{h}}^{DWT}_{qk} = \begin{bmatrix} \ddot{h}^{DWT}_{qk}\ (\tau_0) \\ \ddot{h}^{DWT}_{qk}\ (\tau_1) \\ \cdots \\ \ddot{h}^{DWT}_{qk}\ (\tau_n) \end{bmatrix}, \ddot{\mathbf{h}}^{DWT}_{qk}\ (\tau_i) = \begin{bmatrix} \ddot{h}^{DWT}_{qk,0}\ (\tau_i) \\ \ddot{h}^{DWT}_{qk,1}\ (\tau_i) \\ \cdots \\ \ddot{h}^{DWT}_{qk,2^j+l}(\tau_i)/2^j \end{bmatrix}^T$$

This formulation relates the cross-correlation function with the physical structural system via the impulse response function.

Under multiple random excitations

When the N DOFs damped structural system is under multiple excitations, Equation (6.1) can be written as,

$$\mathbf{M}\ddot{\mathbf{x}}+\mathbf{C}\dot{\mathbf{x}}+\mathbf{K}\mathbf{x}=\mathbf{D}_1F_1(t)+\mathbf{D}_2F_2(t)+\cdots\mathbf{D}_NF_N(t) \qquad (6.15)$$

where $\mathbf{D}_i=[0,0,\cdots,1,\cdots,0]^T$, with the i th element in $\mathbf{D}_i$ equals one and others equal zero. If there is no excitation at the i th DOF of the structure $F_i(t)=0$. Based on linear superposition theory and from zero initial conditions, Equation (6.3) gives,

$$\ddot{x}_p(t)=\int_{-\infty}^{t}\ddot{h}_{p1}(t-\sigma)\cdot F_1(\sigma)d\sigma+\int_{-\infty}^{t}\ddot{h}_{p2}(t-\sigma)\cdot F_2(\sigma)d\sigma+\cdots+\int_{-\infty}^{t}\ddot{h}_{pN}(t-\sigma)\cdot F_N(\sigma)d\sigma$$
$$\ddot{x}_q(t)=\int_{-\infty}^{t}\ddot{h}_{q1}(t-\sigma)\cdot F_1(\sigma)d\sigma+\int_{-\infty}^{t}\ddot{h}_{q2}(t-\sigma)\cdot F_2(\sigma)d\sigma+\cdots+\int_{-\infty}^{t}\ddot{h}_{qN}(t-\sigma)\cdot F_N(\sigma)d\sigma \qquad (6.16)$$

where $\ddot{x}_p(t)$ and $\ddot{x}_q(t)$ are the acceleration responses from locations p and q respectively, $\ddot{h}_{pi}(t)$ and $\ddot{h}_{qi}(t)$ are unit impulse acceleration responses at time t from locations p and q respectively. Then the cross-correlation functions of $\ddot{x}_p(t)$ and $\ddot{x}_q(t+\tau)$ can be obtained similar to Equation (6.6) as,

$$R_{pqk}(\tau)=E\left\{\sum_{i=1}^{N}\int_{-\infty}^{t}\ddot{h}_{pi}(t-\sigma_1)\cdot F_i(\sigma_1)d\sigma_1\cdot\sum_{j=1}^{N}\int_{-\infty}^{t+\tau}\ddot{h}_{qj}(t+\tau-\sigma_2)\cdot F_j(\sigma_2)d\sigma_2\right\} \qquad (6.17a)$$

Equation (6.17a) can be rewritten similar to Equation (6.7) as,

$$R_{pqk}(\tau)=\sum_{i=1}^{N}\sum_{j=1}^{N}\int_{-\infty}^{t+\tau}\int_{-\infty}^{t}\ddot{h}_{pi}(t+\tau-\sigma_1)\ddot{h}_{qj}(t-\sigma_2)E(F_i(\sigma_1)F_j(\sigma_2))d\sigma_1d\sigma_2 \qquad (6.17b)$$

With random excitation, $F_i(\sigma_1)$ and $F_j(\sigma_2)$ are white noise functions, and we have,

$$E(F_i(\sigma_1)F_j(\sigma_2)) = S_i\delta(i-j)\delta(\sigma_1-\sigma_2) \qquad (6.18)$$

where S_i is a constant determined from the amplitude level of the random excitation. Substituting Equation (6.18) into Equation (6.17b), we have,

$$R_{pq}(\tau) = \sum_{i=1}^{N}\sum_{j=1}^{N}\int_{-\infty}^{t+\tau}\int_{-\infty}^{t} \ddot{h}_{pi}(t+\tau-\sigma_1)\ddot{h}_{qj}(t-\sigma_2)S_i\delta(i-j)\delta(\sigma_1-\sigma_2)d\sigma_1 d\sigma_2 \quad (6.17c)$$

Considering the property of the Dirac delta function, Equation (6.17c) can be written as,

$$R_{pq}(\tau) = \sum_{k=1}^{N} S_k \int_0^{+\infty} \ddot{h}_{pk}(t)\ddot{h}_{qk}(t+\tau)dt \qquad (6.17d)$$

Comparing Equation (6.17d) with (6.9b), Equation (6.9b) is a special case in Equation (6.17d) with ($S_k = 0, (i \neq k)$) indicating single excitation. Equation (6.17d) can further be simplified similar to Equation (6.14) as,

$$\mathbf{R}_{pq} = \sum_{k=1}^{N} S_k \ddot{\mathbf{h}}_{qk}^{DWT} \ddot{\mathbf{h}}_{pk}^{DWT} \qquad (6.19)$$

where

$$\mathbf{R}_{pq} = \begin{bmatrix} R_{pq}(\tau_0) \\ R_{pq}(\tau_1) \\ \cdots \\ R_{pq}(\tau_n) \end{bmatrix}, \ddot{\mathbf{h}}_{pk}^{DWT} = \begin{bmatrix} \ddot{h}_{pk,0}^{DWT} \\ \ddot{h}_{pk,1}^{DWT} \\ \cdots \\ \ddot{h}_{pk,2^j+l}^{DWT} \end{bmatrix}, \ddot{\mathbf{h}}_{qk}^{DWT} = \begin{bmatrix} \ddot{h}_{qk}^{DWT}(\tau_0) \\ \ddot{h}_{qk}^{DWT}(\tau_1) \\ \cdots \\ \ddot{h}_{qk}^{DWT}(\tau_n) \end{bmatrix}, \ddot{\mathbf{h}}_{qk}^{DWT}(\tau_i) = \begin{bmatrix} \ddot{h}_{qk,0}^{DWT}(\tau_i) \\ \ddot{h}_{qk,1}^{DWT}(\tau_i) \\ \cdots \\ \ddot{h}_{qk,2^j+l}^{DWT}(\tau_i)/2^j \end{bmatrix}^T$$

6.2.3 Sensitivity of the Cross-Correlation Function

The sensitivity of the cross-correlation function $R_{pq}(\tau)$ can be obtained from Equation (6.17d) as,

$$\frac{\partial R_{pq}(\tau)}{\partial \alpha_i} = \sum_{k=1}^{N} S_k \left(\int_0^{+\infty} \frac{\partial \ddot{h}_{pk}(t)}{\partial \alpha_i} \ddot{h}_{qk}(t+\tau) dt + \int_0^{+\infty} \ddot{h}_{pk}(t) \frac{\partial \ddot{h}_{qk}(t+\tau)}{\partial \alpha_i} dt \right) \quad (6.20)$$

where $\frac{\partial \ddot{h}_{pk}(t)}{\partial \alpha_i}$ and $\frac{\partial \ddot{h}_{qk}(t+\tau)}{\partial \alpha_i}$ are obtained numerically from Equation (6.4).

Alternatively the sensitivity can be obtained from Equation (6.19) with the aid of DWT as,

$$\frac{\partial R_{pq}}{\partial \alpha_i} = \sum_{k=1}^{N} S_k \left(\frac{\partial \ddot{h}_{qk}^{DWT}}{\partial \alpha_i} \ddot{h}_{pk}^{DWT} + \ddot{h}_{qk}^{DWT} \frac{\partial \ddot{h}_{pk}^{DWT}}{\partial \alpha_i} \right) \quad (6.21)$$

where $\frac{\partial \ddot{h}_{qk}^{DWT}}{\partial \alpha_i} = DWT\left(\frac{\partial \ddot{h}_{qk}}{\partial \alpha_i}\right)$ and $\frac{\partial \ddot{h}_{pk}^{DWT}}{\partial \alpha_i} = DWT\left(\frac{\partial \ddot{h}_{pk}}{\partial \alpha_i}\right)$ indicating that the wavelet coefficient of the sensitivity $\frac{\partial \ddot{h}_{qk}}{\partial \alpha_i}$ is equal to the first derivative of the wavelet coefficients of $\ddot{h}_{qk}$ with respect to the system parameter α_i (Law and Li, 2006).

6.2.4 Numerical Experiments

The accuracy of the covariance in terms of the structural parameters is checked in the following examples. The first structure is a one-story plane frame, and the second one is a 31-bar plane truss. The two structures are all subjected to ambient excitations. The "measured" acceleration responses are obtained by Newmark method instead of from experiment. The covariance obtained from signal processing is compared with the covariance computed from the unit impulse response function.

The one-story plane frame structure is shown in Figure 6.1. The columns are 1.2 m high and the cross beam is 0.6 m long, and each member has 10*mm* depth and 20*mm*

breadth uniform rectangular cross-section. The modulus of elasticity and the mass density of materials are respectively 69×10^9 N/m^2 and $2700\,kg/m^3$. Random excitation is applied vertically at node 6 with a magnitude of 10N. The horizontal accelerations at nodes 9 and 10 are collected for the study.

The finite element model of the structure consists of four and three equal beam-column elements in each vertical and horizontal member respectively. The translational and rotational restraints at the supports are represented by large stiffness of 1.5×10^{10} *kN/m* and 1.5×10^{9} *kN-m/rad* respectively. Rayleigh damping is adopted for the system with $\xi_1 = 0.01$ and $\xi_2 = 0.02$ for the first two modes. The first 12 natural frequencies of the structure are 13.09, 57.31, 76.7, 152.4, 196.5, 227.3, 374.7, 382.5, 580.2, 699.3, 765.3 and 983.3 *Hz* . The sampling frequency is 2000 *Hz* . In order to obtain stationary statistical data, the first 70 seconds responses after load application are collected to compute the covariance. The acceleration responses are also random in nature. The auto- and cross-correlations of the two acceleration responses for the first 0.25 s at nodes 9 and 10 are shown in Figure 6.2. The solid line denotes the results from the proposed formulation in Equation (6.14), while the dashed line denotes the results obtained from signal processing of the measured responses (Equation (6.5)). The auto- and cross-correlations obtained from the measured responses are very close to those obtained from the proposed formulation with the norm of the percentage difference equal to 2.36%, 1.8%, 2.14% for the auto-correlations at nodes 9 and 10 and their cross-correlation function as shown in Fig. 6.2. This confirms that the accuracy of the proposed formulation of the correlation functions in terms of the unit impulse response function of the system.

The second structure of a 31-bar plane truss is shown in Figure 6.3. It is modeled with 31 truss elements without internal nodes in the bars giving 28 degrees-of-freedom. The cross-sectional area of the bar is $0.0025\,m^2$. The translational restraints at the supports are both represented by large stiffnesses of $1.0\times10^9\,kN/m$. Rayleigh damping is adopted for the system with $\xi_1 = 0.01$ and $\xi_2 = 0.01$ for the first two modes. The first 12 natural frequencies of the structure are 36.415, 75.839, 133.608, 222.904, 249.323, 358.011, 372.509, 441.722, 477.834, 507.943, 538.1246 and 547.393 Hz. Three random excitations are applied in the horizontal and vertical direction at node 1 and in the vertical direction at node 14 as shown in Figure 6.3 to simulate ambient excitation at the supports. The vector of amplitude level S of the excitation inputs is $S = [100 \quad 100 \quad 0 \quad ... \quad 0 \quad 100]^T$ with non-zero values at the three DOFs under excitation. Vertical accelerations at nodes 7 and 11 are measured for the analysis. The sampling frequency is 2000 Hz. The first 70 seconds responses after load application are recorded to compute the covariance. The auto- and cross-correlations of the two acceleration responses at nodes 7 and 11 are shown in Figure 6.4. The solid line denotes that the values calculated from the proposed formulation with multiple inputs from Equation (6.19), while the dashed line denotes the results obtained from signal processing of the measured responses. The auto- and cross- correlations obtained from the measured responses are compared with those obtained from the proposed formulation for multiple inputs with the norm of the percentage difference of 1.78%, 1.63% and 2.37% for the auto-correlations at nodes 7 and 11 and the cross-correlation as shown in Figure 6.4. It can be seen that large differences exist between the calculated and measured auto-correlation from Node 11 especially for the long duration response from Figure 6.4(b).

This can be explained that the covariances are computed from Equation (6.5) which denotes that a longer period T will give the better results. The results shown in Figure 6.4(b) are still not stationary, and the time-history responses of period T much longer than 70 seconds are required to compute the accurate covariance. On the whole, this case of study still demonstrates the accuracy of the correlation function in terms of the unit impulse response function when under multiple ambient excitation.

6.2.5 Conclusions

The covariance of responses of a dynamic system under ambient excitation has been shown to be a function of the physical structural parameters of the system in terms of its unit impulse response functions. The accuracy of the proposed formulation with good results was checked by two numerical examples. Since most of the large-scale structures are experiencing ambient excitation under service, the proposed formulation on the auto- and cross- correlation functions provides a possibility of in-service system identification or damage detection of the structure. It is noted that the covariance inherently contains measurement noise contaminating the identified results. The abundant random response provides unlimited data for repeated measurement to minimize the noise effect.

6.3 Condition Assessment of Structures under Ambient Excitation

In this section, a damage index is proposed for damage localization based on the elemental modal strain energy changes of the structure under ambient excitation which is assumed to be white noise. The damage severity quantification relies on the measured

acceleration responses of the structure before and after damage occurrence. The covariance of "measured" acceleration responses is simulated from finite element analysis. Wavelet packet transform (WPT) is applied to the covariance functions to find the wavelet packet energy. The sensitivity of this packet energy with respect to local damages is used in a linear identification equation for solving the unknowns. A five-bay cantilever truss structure is used to demonstrate the efficiency of the method with three damage scenarios. A nine-bay experimental structure is also tested with the proposed method using incomplete and noisy measurements and with initial model error.

6.3.1 The Wavelet Packet Energy of Cross-covariance of Acceleration Responses

The equation of motion can be rewritten for a N DOFs damped structural system under ground ambient excitation as

$$\mathbf{M}\ddot{\mathbf{x}}+\mathbf{C}\dot{\mathbf{x}}+\mathbf{K}\mathbf{x}=-\mathbf{M}\mathbf{L}\ddot{x}_s(t) \tag{6.22}$$

where $\ddot{x}_s$ is the ground acceleration. If the system has zero initial conditions, the solution of Equation (6.22) can be expressed as,

$$\ddot{x}_p(t)=\int_{-\infty}^{t}\ddot{h}_p(t-\tau)\ddot{x}_s(\tau)d\tau \tag{6.23}$$

where $\ddot{h}_p(\tau)$ is the impulse response of the p th DOF of the system under the unit impulse excitation. $\ddot{x}_p(t)$ is the acceleration responses from p th DOF at time t. Assuming the system is under ambient excitation, $\ddot{x}_s$ is assumed to be of white noise distribution, and the autocorrelation function of $\ddot{x}_s$ is similar to Equation (6.8) as,

$$E(\ddot{x}_s(\sigma_1)\ddot{x}_s(\sigma_2))=S\delta(\sigma_1-\sigma_2) \tag{6.24}$$

where S is a constant defining the magnitude of excitation of $\ddot{x}_s$ when $\sigma_1=\sigma_2$, and $\delta(t)$ is the Dirac delta function. Then the cross-covariance of the accelerations from p th and q th DOFs of the system, $R_{pq}(\tau)$, is as,

$$R_{pq}(\tau) = S\int_0^{+\infty} \ddot{h}_p(t)\,\ddot{h}_q(t+\tau)dt \qquad (6.25)$$

The corresponding sensitivity of the cross-correlation function $R_{pq}(\tau)$ with respect to the structural parameter α_i can be obtained in the same way as Equation (6.20) as,

$$\frac{\partial R_{pq}(\tau)}{\partial \alpha_i} = S\left(\int_0^{+\infty} \frac{\partial \ddot{h}_p(t)}{\partial \alpha_i}\ddot{h}_q(t+\tau)dt + \int_0^{+\infty} \ddot{h}_p(t)\frac{\partial \ddot{h}_q(t+\tau)}{\partial \alpha_i}dt\right) \quad (6.26)$$

where $\frac{\partial \ddot{h}_p(t)}{\partial \alpha_i}$ and $\frac{\partial \ddot{h}_q(t+\tau)}{\partial \alpha_i}$ are obtained numerically by the method described in Section 5.2.1.

The covariance of acceleration response obtained above can be represented by Daubechies (db4) wavelet basis function through the dyadic wavelet transformation. The bandwidths of each level of the dyadic wavelet transform are octaves. The wavelet packet transform (WPT) component function of the covariance $R_{pq}(t)$ can be reconstructed from the wavelet packet coefficients as

$$R_{pq,j}{}^{i}(t) = \sum_{k=-\infty}^{+\infty} c_{j,k}^{i}\psi_{j,k}^{i}(t) = \mathbf{Q}_j^i\mathbf{c}_j^i = \mathbf{Q}_j^i\mathbf{D}_j^i R_{pq}(t) \qquad (6.27)$$

where $\mathbf{Q}_j^i = [\psi_{j,0}^i \quad \psi_{j,2}^i \quad \cdots \quad \psi_{j,l}^i]$, $\qquad (l = 0,1,\cdots,N/2^j - 1)$

and $\mathbf{D}_{j+1}^{2i} = \mathbf{H}^{j+1}\mathbf{D}_j^i$, $\mathbf{D}_{j+1}^{2i+1} = \mathbf{G}^{j+1}\mathbf{D}_j^i$, $\mathbf{D}_1^0 = \mathbf{H}^1$, $\mathbf{D}_1^1 = \mathbf{G}^1$, $\mathbf{H}^{j+1}$ and $\mathbf{G}^{j+1}$ are matrices formed from the low-pass and high-pass filter functions. $\mathbf{c}_j^i$ are the wavelet packet

coefficients for the covariance response with $\mathbf{c}_j^i = \mathbf{D}_j^i R_{pq}(t)$. The i th WPT component energy of the covariance $R_{pq}(t)$ at the j th level of decomposition, E_j^i, is defined as,

$$\begin{aligned} E_j^i &= (\mathbf{R}_{pq,j}^{\ i})^T (\mathbf{R}_{pq,j}^{\ i}) \\ &= \mathbf{R}_{pq}^{\ T} (\mathbf{Q}_j^i \mathbf{D}_j^i)^T (\mathbf{Q}_j^i \mathbf{D}_j^i) \mathbf{R}_{pq} \\ &= \mathbf{R}_{pq}^{\ T} \mathbf{T}_j^i \mathbf{R}_{pq} \end{aligned} \tag{6.28}$$

where $\mathbf{T}_j^i = (\mathbf{Q}_j^i \mathbf{D}_j^i)^T (\mathbf{Q}_j^i \mathbf{D}_j^i)$ is not a function of the signal and is determined only by the wavelet type.

The sensitivity of E_j^i with respect to the structural parameters α_i is computed as,

$$\frac{\partial E_j^i}{\partial \alpha_i} = \frac{\partial \mathbf{R}_{pq}^T}{\partial \alpha_i} \mathbf{T}_j^i \mathbf{R}_{pq} + \mathbf{R}_{pq}^T \mathbf{T}_j^i \frac{\partial \mathbf{R}_{pq}}{\partial \alpha_i} = 2 \frac{\partial \mathbf{R}_{pq}^T}{\partial \alpha_i} \mathbf{T}_j^i \mathbf{R}_{pq} \tag{6.29}$$

where $\mathbf{R}_{pq}^T$ and $\frac{\partial \mathbf{R}_{pq}^T}{\partial \alpha_i}$ can be obtained from Equations (6.25) and (6.26). The sensitivity matrix $\mathbf{S}_p$ can then be obtained as,

$$\mathbf{S}_p = \left[\frac{\partial E_j^0}{\partial \alpha_i} \quad \frac{\partial E_j^1}{\partial \alpha_i} \quad \cdots \quad \frac{\partial E_j^{2^j-1}}{\partial \alpha_i} \right] \tag{6.30}$$

and the damage detection can then be performed as follows.

6.3.2 Damage Identification

Damage localization based on mode shape

The structural modal parameters (mode shape and natural frequencies) can be identified from the ambient vibration responses using the Natural Excitation Technique (Next) (James et al, 1995) in conjunction with the Eigensystem Realization Algorithm (ERA) (Juang and Pappa, 1985), or using the conventional peak-picking technique. The

obtained mode shapes Φ are then used for the damage localization as shown below. Since mode shapes of higher order are usually obtained with difficulties in real measurement, only the first mode shape is employed for the damage localization.

The modal strain energy of the i th element corresponding to the first mode shape from the healthy structure is defined as

$$s_{1i} = \mathbf{\Phi}_1^T \mathbf{K}_i \mathbf{\Phi}_1 \tag{6.31}$$

where K_i is the i th elemental stiffness matrix and Φ_1 is the first mode shape of the system. Then the total modal strain energy of the structure corresponding to the first mode is obtained as,

$$s_1 = \mathbf{\Phi}_1^T \mathbf{K} \mathbf{\Phi}_1 \tag{6.32}$$

The fractional contribution to the modal strain energy from the i th member is denoted as,

$$F_{1i} = \frac{s_{1i}}{s_1} \tag{6.33}$$

Similarly, for a damaged structure, the corresponding F_{1i}^d is defined as,

$$F_{1i}^d = \frac{s_{1i}^d}{s_1^d} \tag{6.34}$$

where $$s_{1i}^d = \left(\mathbf{\Phi}_1^d\right)^T \mathbf{K}_i^d \mathbf{\Phi}_1^d \tag{6.35a}$$

and $$s_1^d = \left(\mathbf{\Phi}_1^d\right)^T \mathbf{K}^d \mathbf{\Phi}_1^d \tag{6.36}$$

where $\mathbf{K}_i^d$ and $\mathbf{K}^d$ are the i th elemental stiffness matrix and the global stiffness matrix of the damaged structure respectively. $\mathbf{\Phi}_1^d$ is the first mode shape of the damaged structure.

Equation (6.35a) can be expressed as,

$$s_{1i}^{d} = \alpha_i \left(\boldsymbol{\Phi}_1^{d}\right)^T \mathbf{K}_i \boldsymbol{\Phi}_1^{d} \tag{6.35b}$$

For the case with relatively small damage in the structure, it can be assumed that

$$F_{1i} \approx F_{1i}^{d} \tag{6.37}$$

We further assume that $K^d \approx K$ for the cases with small local damages with

$$s_1^{d} = \left(\boldsymbol{\Phi}_1^{d}\right)^T \mathbf{K}^d \boldsymbol{\Phi}_1^{d} \approx \left(\boldsymbol{\Phi}_1^{d}\right)^T \mathbf{K} \boldsymbol{\Phi}_1^{d} \tag{6.38}$$

Substituting Equations (6.31) to (6.36) into Equation (6.37) yields a damage index as,

$$\Delta\alpha_i = 1 - \frac{(\boldsymbol{\Phi}_1^T \mathbf{K}_i \boldsymbol{\Phi}_1)\left(\left(\boldsymbol{\Phi}_1^{d}\right)^T \mathbf{K} \boldsymbol{\Phi}_1^{d}\right)}{\left(\left(\boldsymbol{\Phi}_1^{d}\right)^T \mathbf{K}_i \boldsymbol{\Phi}_1^{d}\right)(\boldsymbol{\Phi}_1^T \mathbf{K} \boldsymbol{\Phi}_1)} \tag{6.39}$$

It is noted that the above formulation on the damage index needs full measurement to obtain the mode shape. In the case of incomplete measurement, the measured information can be expanded to the full mode shape, or, only the measured information is taken into account in Equation (6.39). Both of these practices would lead to errors of different extent which is a feature with mode shape-based approach. It should be stated here that the localization stage serves to reduce the candidate set of possible damage elements for the next stage of damage quantification. Other frequency-domain or time-domain methods can also be used for this purpose.

Damage severity identification based on the sensitivity of the covariance

Because two assumptions have been made in Equations (6.37) and (6.38), the damage severity obtained from Equation (6.39) is not accurate. A refined damage severity quantification based on the sensitivity of the covariance with the reduced set of possible damaged elements is pursued here. We consider a general structure which

behaves linearly before and after the occurrence of damage for the illustration of the proposed approach.

The damage quantification includes two separate phases of updating the analytical model and identifying local damages. Each phase consists of the two stages of damage localization and quantification. $(E_j)_0$ and $(E_j)_d$ are vectors of the WPT component energy of the covariance of the acceleration responses at the p th and q th DOFs of the intact and damaged structures respectively. S_p is the sensitivity matrix of the WPT component energy calculated from the intact state of the system using Equation (6.30). $\Delta\alpha$ is the vector of fractional change of the parameters of the system. We have the identification equation as

$$\mathbf{S}_p \cdot \Delta\boldsymbol{\alpha} = (\mathbf{E}_j)_d - (\mathbf{E}_j)_0 \qquad (6.40)$$

Since the solution of Equation (6.40) is ill-conditioned, regularization is used with the L-curve method for determining the optimal regularization parameter.

The initial analytical model is adopted for model updating in the first stage of the study. Vector $(\mathbf{E}_j)_0$ and matrix $\mathbf{S}_p$ are obtained from this initial model. Acceleration measurement from the intact state of the structure is obtained, and the covariance as well as its WPT component energy vector $(\mathbf{E}_j)_d$ is computed. The initial model is then updated in Equation (6.40) and the corresponding $(\mathbf{E}_j)_0$ and its sensitivity $\mathbf{S}_p$ are again computed from the updated model for the next iteration. The final updated analytical model is obtained when both of the following two criteria are met,

$$\frac{\left\|\{\mathbf{E}_j\}_{m+1} - \{\mathbf{E}_j\}_m\right\|}{\left\|\{\mathbf{E}_j\}_{m+1}\right\|} \le toler\ 1, \qquad \frac{\left\|\Delta\boldsymbol{\alpha}_{m+1} - \Delta\boldsymbol{\alpha}_m\right\|}{\left\|\Delta\boldsymbol{\alpha}_{m+1}\right\|} \le toler\ 2$$

where m refers to the m th iteration, and *toler1* and *toler2* are the two specified criteria of convergence.

Then the updated analytical model is used to represent the first (intact) state of the structure and the damaged state of the real structure is regarded as the second state in the identification. Measurement from the damaged state is obtained, and the same iteration computations as in the first stage are carried out. The final set of identified parameter increments correspond to the changes occurred in between the intact and damaged states of the structure.

6.3.3 Numerical Study

A five-bay three-dimensional frame structure as shown in Figure 4.17 serves for the numerical study. The finite element model consists of thirty-seven three-dimensional Euler beam elements and seventeen nodes. The length of all the horizontal, vertical and diagonal tube members between the centers of two adjacent nodes is exactly 0.5m. The structure orientates horizontally and is fixed into a rigid support at three nodes at one end. Table 4.8 gives a summary of the main material and geometrical properties of the members of the frame structure. Each node has six DOFs, and altogether there are 102 DOFs for the whole structure.

The translational and rotational restraints at the supports are represented by large stiffnesses of 1.5×10^{11} *kN/m* and 1.5×10^{10} *kN-m/rad* respectively in six directions. Rayleigh damping is adopted for the system with ξ_1=0.01 and ξ_2=0.005 for the first two modes. The first 12 natural frequencies of the intact structure are 9.21, 28.26, 33.71,

49.01, 49.72, 71.02, 89.80, 153.93, 194.33, 209.80, 256.51 and 274.82 Hz from the eigenvalue analysis of the structure. The sampling frequency is 500 Hz.

The finite element model of the structure is used directly for the identification without updating. The structure is subject to an ideal white noise support motion in the *y*-direction with zero mean and a magnitude of 0.01 m^2/s^4. The first mode shape is obtained before and after damage occurrence for localizing the damages. The acceleration responses from nodes 5 and 6 in the *y*-direction are calculated for a duration of 300 seconds for both the healthy and the damaged structure to simulate the "measured" acceleration responses for the calculation of the cross-covariance. Three damage cases shown in Table 6.1 are studied to illustrate the proposed approach.

The flexural stiffness of element 2 is reduced by 10% in damage Scenario 1. In order to analyze the error introduced by the assumption in Equation (6.37), the fractional contributions of the modal strain energy F_{1i}, F_{1i}^d for both the intact and the damage states respectively are computed and compared in $\left\| \left(F_{1i}^d - F_{1i} \right) / F_{1i} \right\|$ and the result is shown in Figure 6.5(a). It shows that the relative error caused by the assumption is less than 4% in this case. The damage localization vector is obtained by using all the translational and rotational DOFs of the first mode shape. The vector shown in Figure 6.5(b) is not accurate although it still can identify the range of the damage location. However there exist false alarms in elements 7, 22, 23, 24 and 25. These elements are noted to be adjacent to and in the same bay as the damaged element. The cross-covariance is calculated from the "measured" acceleration responses and is decomposed by Daubechies (db4) wavelet in four levels with 16 wavelet packets. All the 16 WPT component energy constitute the measurement vector and sixteen equations are used in the identification.

Elements 2, 7, 22, 23, 24 and 25 are chosen to be the possible candidates for the next stage of quantification. The identified results from using the covariance sensitivity approach in Equation (6.40) are shown in Figure 6.5(c) with 9.82%, 0.14%, -0.38%, 0.52%, -0.36% and 0.34% of stiffness reduction in Elements 2, 7, 22, 23, 24 and 25 respectively, indicating the damage severity of element 2 can be obtained accurately without false alarming in other elements.

To study the case of multiple damages in different types of elements, damage Scenario 2 is studied where the flexural stiffness of elements 12, 16, 25 are reduced by 5% and that in element 27 is reduced by 10%. The fractional contribution F_{1i}^{d} is computed and compared with F_{1i} as for damage Scenario 1. The error introduced by the assumption in Equation (6.37) has a maximum of 4.96% as shown in Figure 6.6(a). The damage localization vector is computed similarly and shown in Figure 6.6(b) from which it can be seen that the assumption is valid but it affects the accuracy of the identified results. The identified damage localization vector contains both the real damage locations and false alarms in adjacent elements. These results are still useful for the damage quantification because the group of possible candidate has been reduced. Elements 12, 16, 24, 25, 26 and 27 are chosen as the possible damage elements for the quantification identification. The identified damage magnitudes are shown in Figure 6.6(c) with 4.95%, 5.02%, 0.05%, 4.96%, -0.01% and 9.99% of the flexural stiffness reduction in elements 12, 16, 24, 25, 26 and 27 respectively, indicating that the identified value are very accurate.

Despite the capability of the cross-covariance computation in reducing the noise effect, 10% noise is added to the “measured” acceleration responses while the damage

elements and severity are the same as in Scenario 2. White noise is added to the calculated accelerations to simulate the polluted measurements as described in Equation (3.42). This forms Scenario 3 in Table 6.1. The identified damage magnitudes are also shown in Figure 6.6(c) for comparison with those from without noise. The identified stiffness reduction in elements 12, 16, 24, 25, 26 and 27 are 4.12%, 5.29%, 0.72%, 4.25%, -0.07% and 9.90% respectively. The identified results are noted to be only slightly affected with noise in the "measured" acceleration.

It is always noted that the effect of model error would smear the identified damages throughout the structure with many of the existing damage quantification methods giving false alarms in other undamaged elements. This is a matter of accuracy with the identification method. Experiences with the author when using the wavelet approach for the damage identification (Law and Li, 2006) show that model errors related to the stiffness terms of the structure can also be identified as local damages while those related to the mass or damping terms would not show up clearly because of the lack of a clear relationship between the measured responses and these parameters with existing methods.

The results shown in Figures 6.5 and 6.6 indicate that the covariance approach can quantify local damage accurately provided that the number of unknowns in the identification is small. This can be improved by using more sets of covariance responses from different pairs of measured acceleration time histories. However the inclusion of the localization stage could eliminate some intact elements leaving a smaller candidate set of unknowns for a more accurate damage quantification in the next stage.

In the case of a structure where a few critical components are needed to be monitored continuously, the proposed covariance approach would be most suitable provided that a satisfactory finite element model of the intact structure has been updated prior to the implementation of the structural health monitoring.

6.3.4 Experimental Verification

The Structure

A nine-bay three-dimensional frame structure shown in Figure 4.21(a) serves for the experimental study. It is fabricated in the laboratory using Meroform M12 construction system. It consists of sixty-nine 22mm diameter alloy steel tubes jointed together by twenty-nine standard Meroform ball nodes. Each tube is fitted with a screwed end connector which, when tightened into the node, also clamps the tube by means of an internal compression fitting. All the connection bolts are tightened with the same torsional moment to avoid asymmetry or nonlinear effects caused by man-made assembly errors. The experimental setup is also shown in Figure 4.21(a) and the support is shown in Figure 4.21(b). The finite element model of the structure is shown in Figure 4.22. The structure has the same material and geometric properties as shown in Table 4.8.

The Modal test

The modal test on the both the intact and damaged structure is performed using SIMO method with a dynamic hammer model B&K 8202 hitting on element 10 along the *y*-direction and close to node 11 of the frame. A total of 52 translation DOFs at the unconstrained nodes are measured. An additional mass of 72 g weight is added to each

joint to balance the effect of the moving accelerometers. The sampling frequency is 2000 Hz. The responses are low-pass filtered at 1000 Hz, and a commercial data logging system INV303 with the associated data analysis system DASP2003 are used in the data acquisition. Frequency response function (FRF) is calculated for all the measured responses, and the first twelve natural frequencies and modal damping ratios averaged over twenty FRFs are listed in the second and third columns of Table 6.2. The corresponding measured mode shapes are given in Figure 5.7. Only a few pure bending modes are identified while most of them have coupled bending and torsional vibrations.

Modelling of the structure

The Meroform ball joints have been modeled as semi-rigid joints, and a finite element model of a hybrid beam with semi-rigid end connections has been proposed (Law et al, 2001). This section adopts this hybrid beam model for the model improvement of the structure. The initial model assumes a large fixity factor p for the rotational stiffness of the joints which is taken equal to 0.999 with 1.0 equal to that for a rigid joint.

The total weight of the ball and half of the weight of the bolt connecting the ball with the frame element are placed at each node as lump mass. The other half of the weight of the bolt is considered as part of the finite element. In additional, another lump mass of 72 g weight is added to each node to represent the weight of the moving accelerometers.

Ambient vibration test for damage detection

The structure is excited with a random white noise signal through a LING PO 300 exciter approximately at the centroid of the support in the *y*-direction. The support is very rigid and heavy compared with the frame and it is hold down to the strong floor with four steel bolts. The acceleration responses of the support along the three principal directions are measured. Only the response in the *y*-direction is significant and those in the other two directions are very small to be neglected. Nine accelerometers are placed at nodes 2 to 10 in the *y*-direction for recording the acceleration response time histories. The sampling frequency is 2000 Hz and the responses for a duration of 800s are used to calculate the auto-covariance. The auto-covariance of acceleration time history at the support in the *y*-direction has a magnitude of $0.0031\, m^2 / s^4$ at $t=0$ and small values for other time instances as shown in Figure 6.7(a) indicating a close to white noise excitation at the support (Equation (6.24)). The auto-covariance of acceleration time history from Node 8 before and after the damage occurrence is shown in Figures 6.7(b) and 6.7(c) respectively. The covariances are noted to be relatively smooth with a low noise level.

Damage scenarios

After performing the dynamic test on the intact frame structure, local faults are introduced by replacing three intact members with damaged ones. The artificial damage is of two types. Type I is a perforated slot cut in the central length of the member. The length of slot is 13.7 cm, and the remaining depth of the tube in the damaged cross-section is 14.375 mm. Type II is the removal of a layer of material from the surface of the member. The external diameter of the tube is reduced from 22.02mm to 21.47mm, and the length of the weakened section is 202 mm, located in the middle of the beam leaving

99mm and 75mm length of original tube cross-section on both sides. Figure 4.21(c) gives a close up view of the damaged frame members. Type I damage is located in element 10 and Type II damage is located in elements 27 and 68. The equivalent damages computed by Guyon method are 5% and 9.5% reduction in the modulus of elasticity of element 10 and elements 27 and 68 respectively.

Model improvement for damage detection

The two-stage approach is adopted for the damage detection. The first stage updates the rotational stiffness at the joints to obtain an improved analytical model for the intact structure. Nine *y*-direction acceleration responses obtained from nodes 2 to 10 are measured and the corresponding auto-covariance WPT energy components are computed for use in Equation (6.40). There are 69×6=414 unknown rotational stiffnesses in the identification. The first 2000 data points of auto-covariance of each acceleration response are decomposed into six levels of Daubechies Db4 wavelet packets to have 64 covariance WPT energy components, and each packet has the same frequency bandwidth of 15.625Hz. All the 64 WPT energy components are used in the experimental identification procedure and there are 9×64=576 equations in Equation (6.40). The measured modal damping ratios from the intact structure have been used in Equation (6.22) for the computation of the analytical auto-covariance. The updated rotational stiffness do not differ too much from the original value with the largest change in member 15 at node 17 with the updated $p=0.9$ for the *x*-axis rotational stiffness. This updated model is then considered accurate for the next stage of damage assessment.

The second stage updates the local faults in all the members of the structure in terms of their modulus of elasticity. The damage localization is performed firstly. The measured first mode shape with 52 translational DOFs from the intact and the damaged states of the structure are expanded to the full degrees-of-freedom by the dynamic condensation method with Gauss-Jordan elimination (Mario, 1997) and the obtained damage localization vector is shown in Figure 6.8(a) indicating that the real damaged members can be identified but with false alarming in other undamaged members because of the error due to measurement noise and the mode shape expansion.

The auto-covariance calculated from the *y*-direction response from nodes 2 and 10 are used in Equation (6.40) for the identification. There are 26 unknowns shown in Table 6.3 which are the suspected damaged elements shown in Figure 6.8(a) in the identification. The first 2000 data points of auto-covariance of each response are used and all 64×9=576 WPT energy components are used in Equation (6.40). The identified damage extent for all the elements are shown in Figure 6.8(b). The identified reduction in the modulus of elasticity in the damaged members are 4.76%, 7.09% and 6.73% for elements 10, 27 and 68 respectively which are fairly close to the values of 5%, 9.5% and 9.5% respectively. There are false alarms in elements 9, 50, 67 shown in Table 6.3 with a reduction of more than 2% even though they are in fact undamaged.

Further attempt has been made in using accelerations from 3, 5 and 7 sensors in the same group of sensors in the identification. The accuracy of the identified results is poorer than the above one. The combination of accelerations in both the vertical and lateral directions may be a better one but it has not been studied due to limitations with the test results. It may be concluded from the limited study that the measurement noise

and model errors have a significant effect on the identification with the proposed identification method using random input excitation.

6.4 Summaries

In this chapter, the covariance of responses of a dynamic system under ambient excitation has been shown to be a function of the physical structural parameters of the system in terms of its unit impulse response functions. A damage detection method is proposed based on the wavelet packet energy of the covariance calculated from the measured acceleration responses of structures under ambient excitation which is assumed to be white noise. Wavelet packet transform is applied to the covariance functions to find the wavelet packet energy. To reduce the number of the unknowns involved in the inverse problem, damage localization is carried out firstly using the elemental modal strain energy. The much reduced set of potential damage element then undergoes the next state of damage quantification. The proposed damage quantification method based on the sensitivity of the WPT energy of covariance has good capability in dealing with model error and measurement noise. A five-bay three-dimensional cantilever truss structure is used to demonstrate the efficiency of the method with three simulated damage cases, and a nine-bay three-dimensional frame structure is test in the laboratory with the proposed method. The identified results show that the method is applicable to locate and quantify local damages with incomplete and noisy measurement and with initial model error.

Table 6.1 - Damage scenarios

Scenario	Damaged member	Damage severity	Noise in acceleration responses
1	2^{th} element	10%	No
2	12^{th} ,16^{th} , 25^{th} and 27^{th} element	5%, 5%, 5%, 10%	No
3	12^{th}, 16^{th}, 25^{th} and 27^{th} element	5%, 5%, 5%, 10%	10%

Table 6.2 - The experimental natural frequencies (Hz) and damping ratio of the frame structure

Mode type	Measured			
	intact		damaged	
	frequency (Hz)	damping ratio	frequency (Hz)	damping ratio
1H	5.196	0.443	5.216	0.196
1V	10.942	0.928	10.794	0.418
2H	15.172	0.282	15.166	0.251
V+T	19.390	0.155	19.387	0.155
3H	27.702	0.307	27.462	0.299
H	39.815	0.335	39.127	0.346
H	52.146	0.423	51.018	0.403
2V	61.938	0.155	61.463	0.432
H+T	65.806	0.258	64.142	0.253
H+T	78.491	0.356	76.616	0.333
T	87.287	0.908	89.277	0.333
H+T	90.448	0.340	98.125	0.312

Note: (2H) – second horizontal mode; (1V) –first vertical mode; (V+T)- coupled vertical and torsional mode.

Table 6.3 - The identified results on the suspected damaged elements

Element No.	9	10	11	25	26	27	28	29	40	41
Identified value (%)	2.23	4.76	-0.34	1.66	0.84	7.09	-1.02	1.12	-2.02	0.49
Element No.	44	45	48	49	50	52	55	57	60	61
Identified value (%)	-0.02	-0.15	0.04	-0.76	0.23	0.28	-0.34	0.06	-1.32	1.1
Element No.	62	63	66	67	68	69				
Identified value (%)	-0.04	1.48	-2.61	2.19	6.73	1.5				

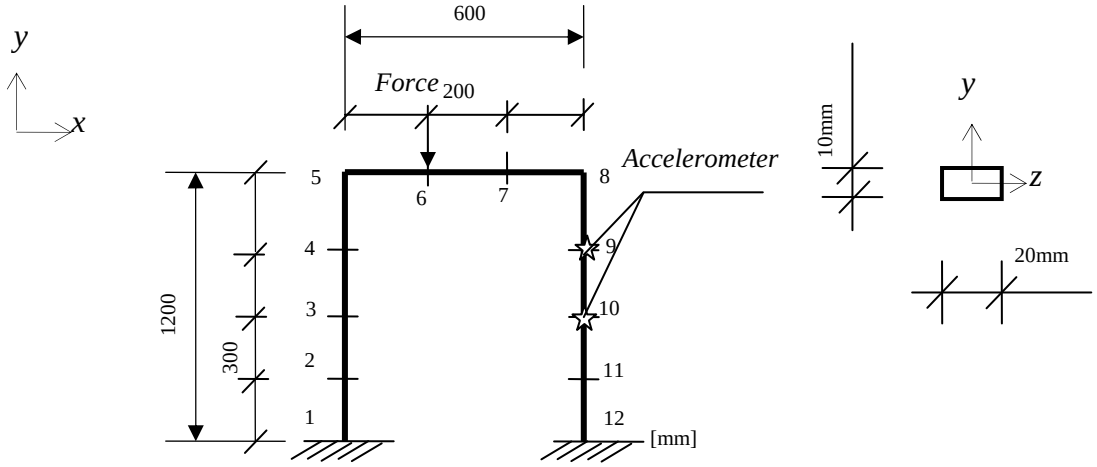

Figure 6.1 - The one-story frame structure

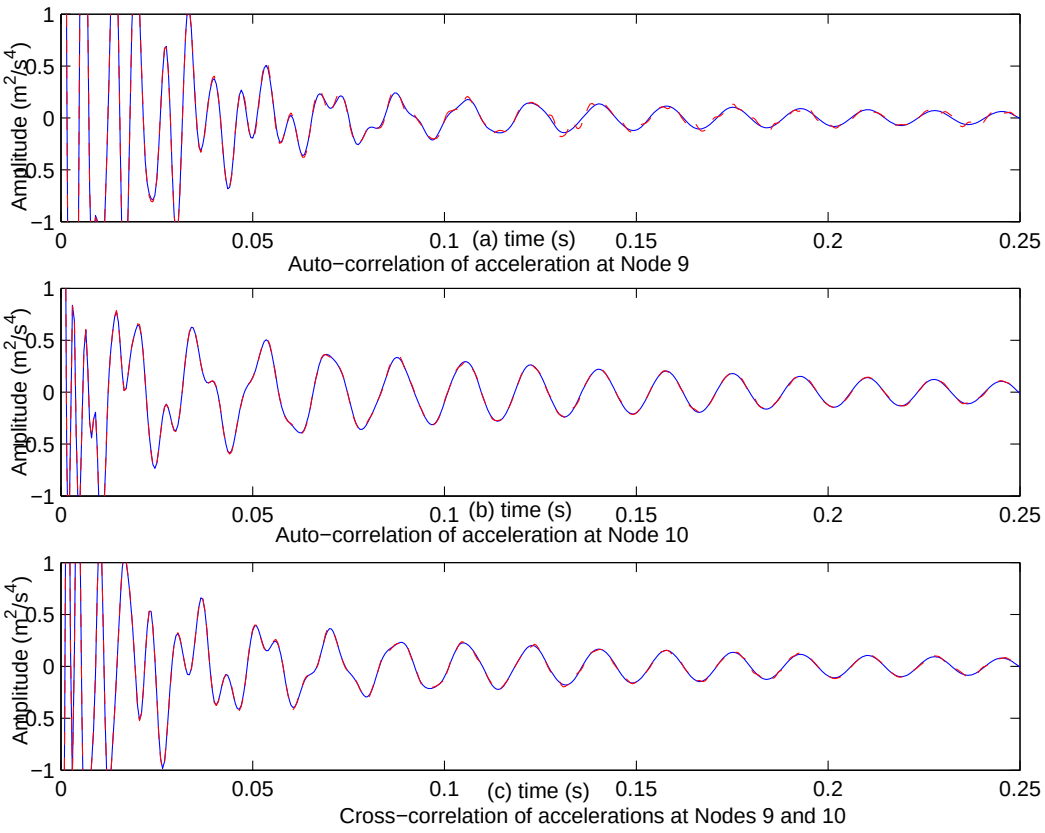

Figure 6.2 - Comparison of auto- and cross- correlation of accelerations from analytical and experimental

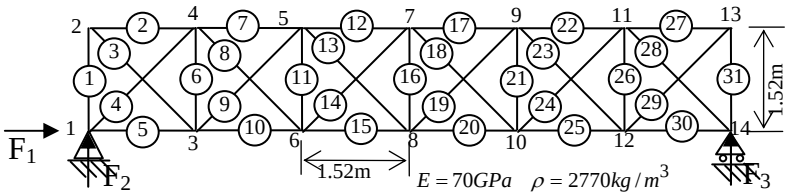

Figure 6.3 - Thirty-one-bar truss structure

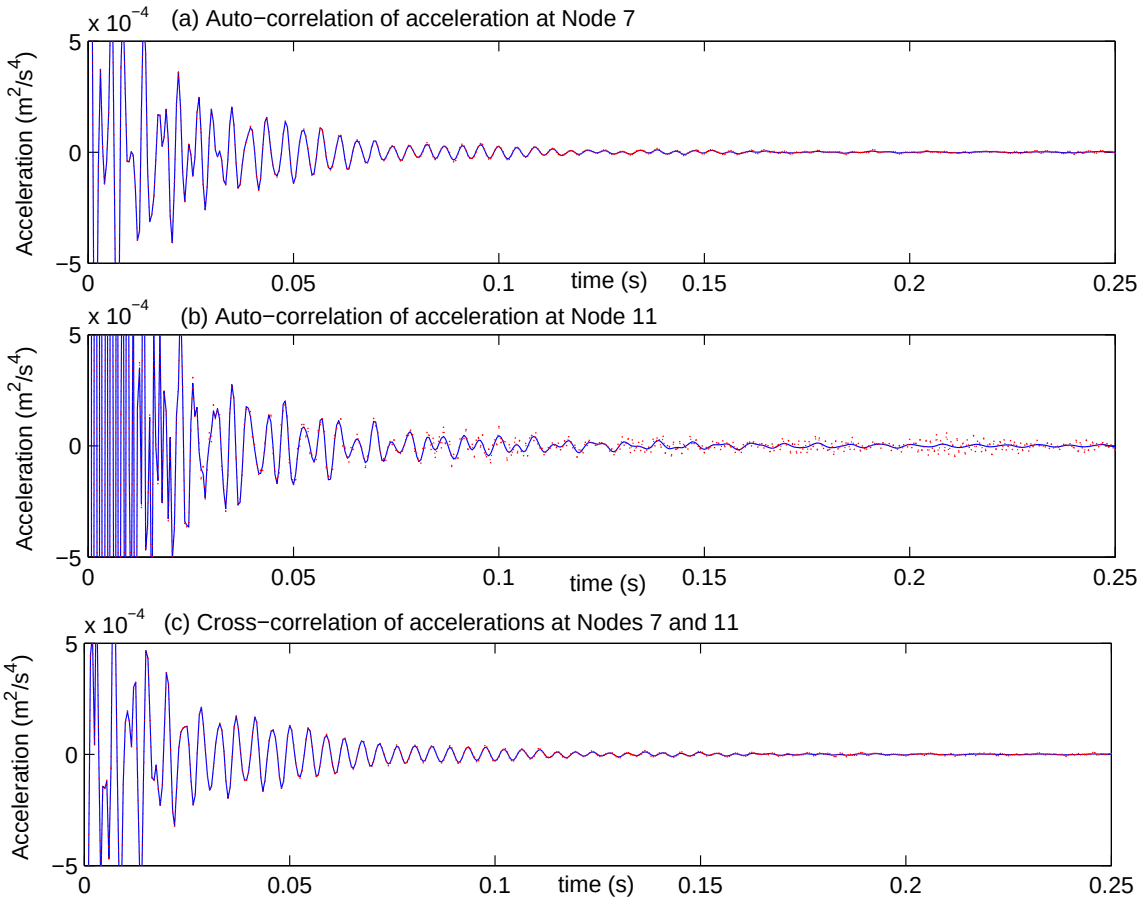

Figure 6.4 - Comparison of auto- and cross- correlation of acceleration from analytical and experimental

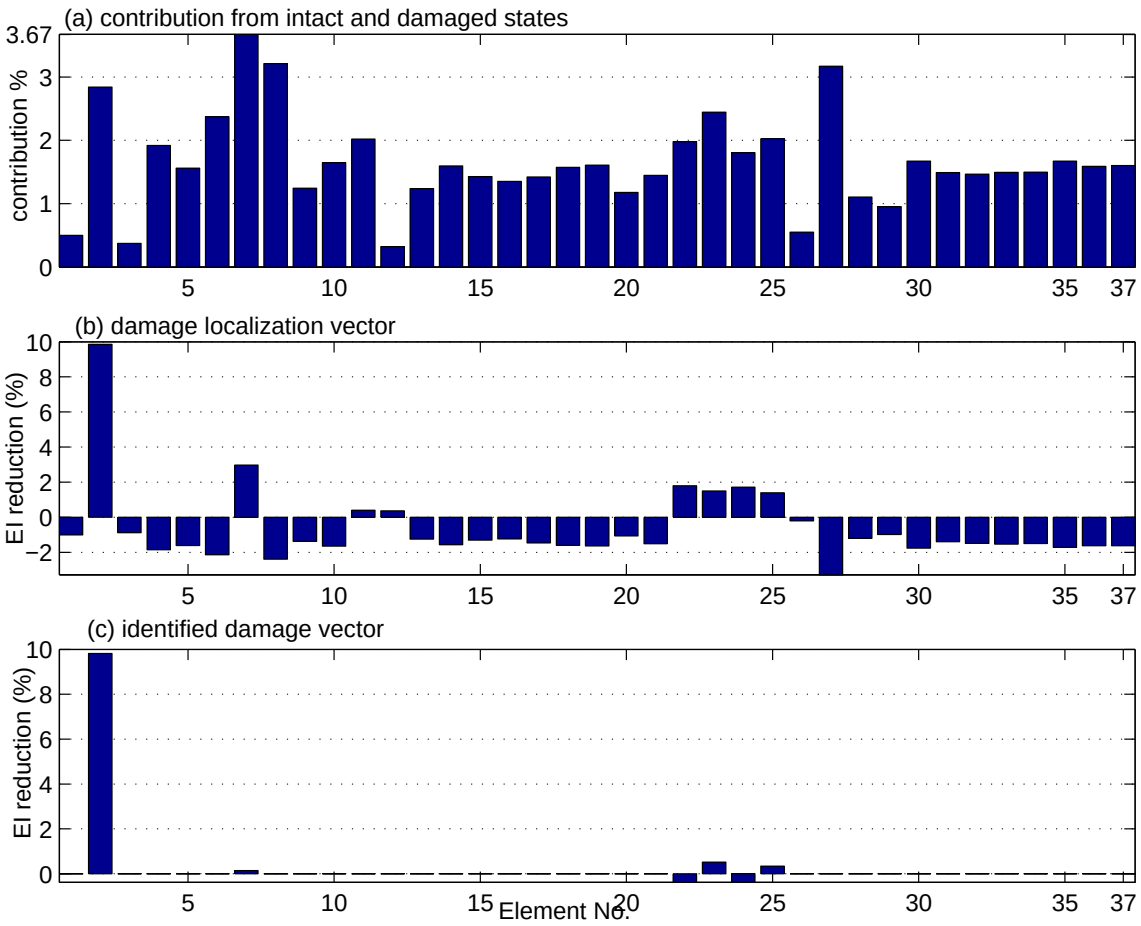

Figure 6.5 - Identified results for Damage Scenario 1

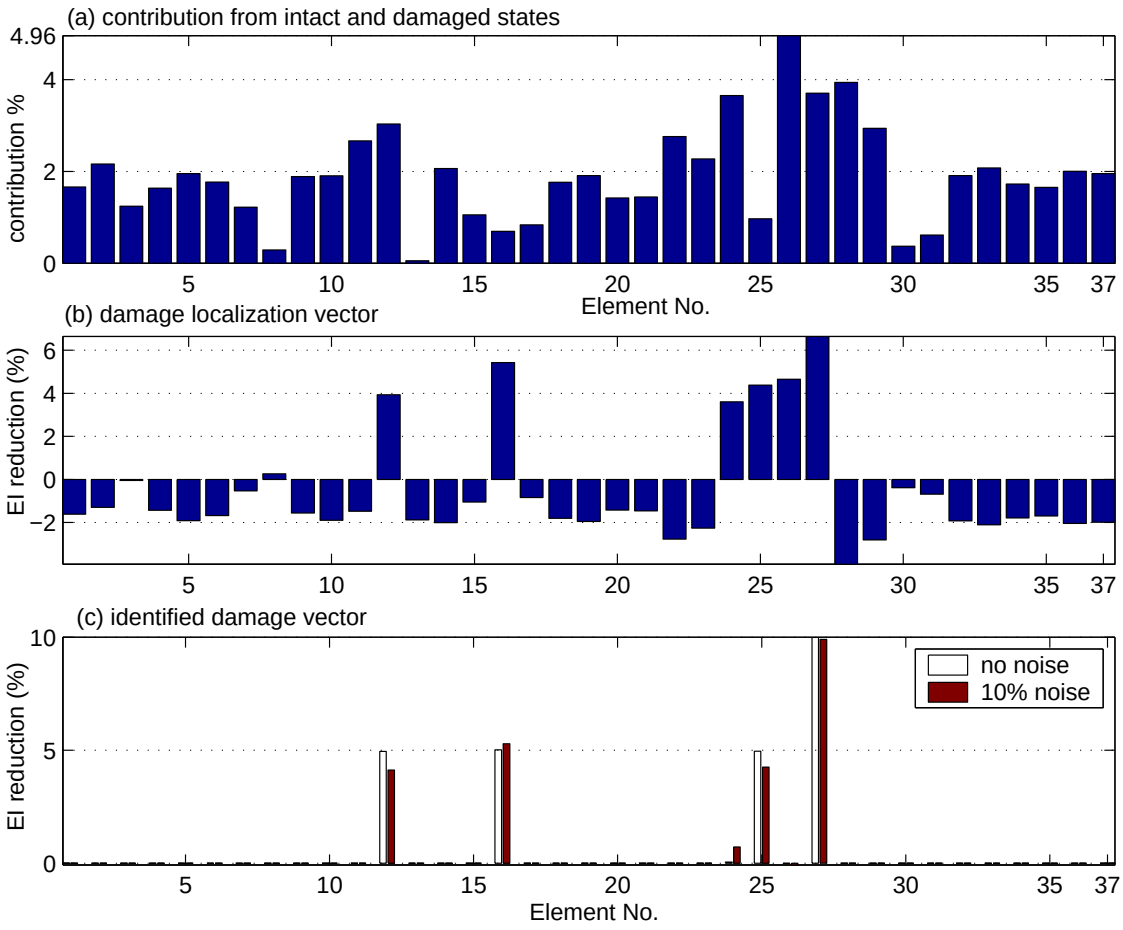

Figure 6.6 - Identified results for Damage Scenarios 2 and 3

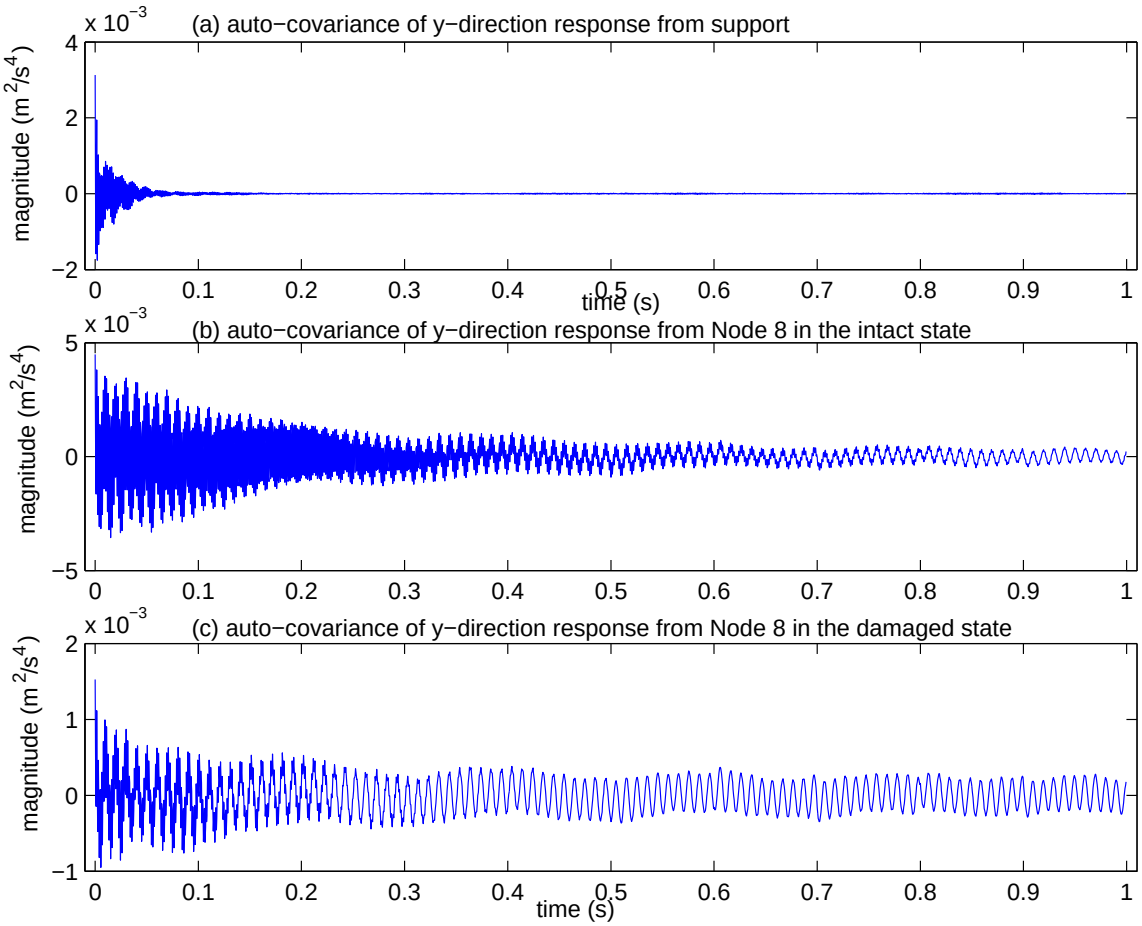

Figure 6.7 - Auto-covariance of accelerations at support and structure

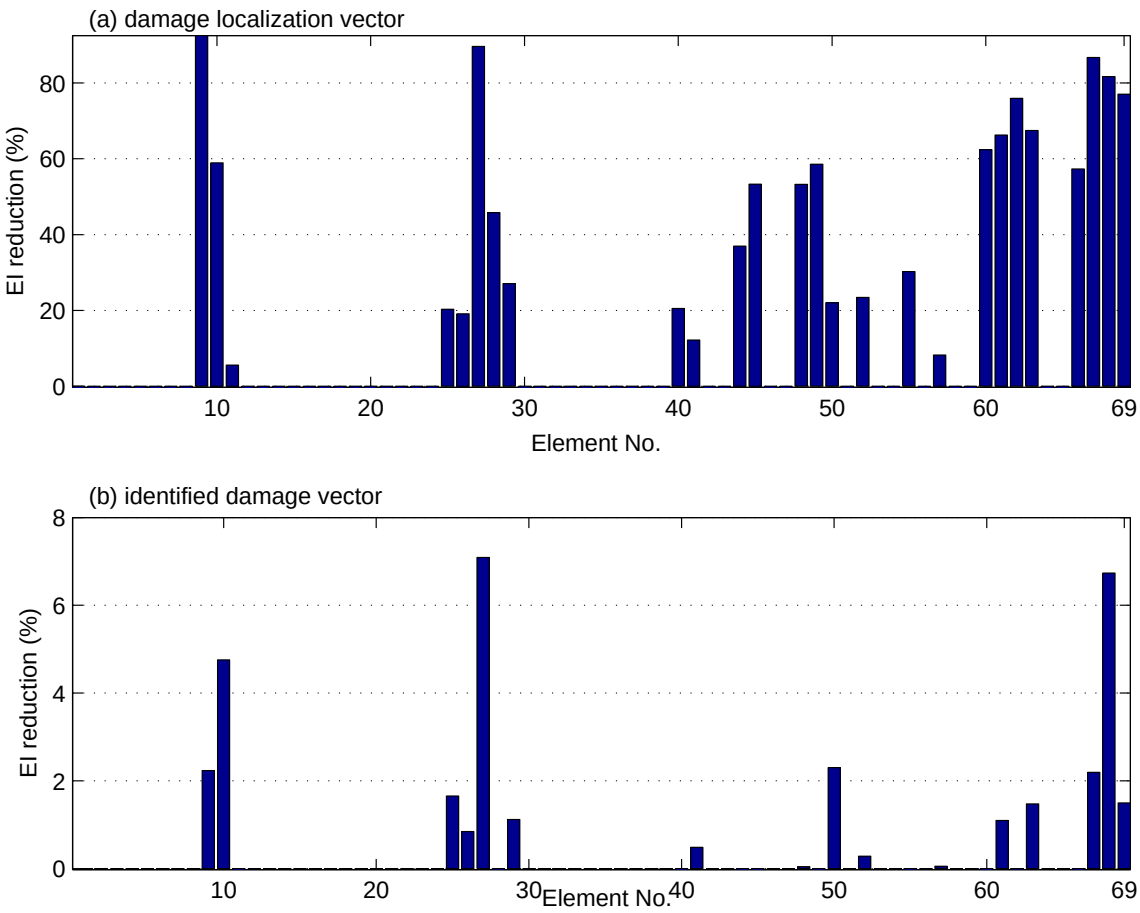

Figure 6.8 - Identified results for the experimental structure

CHAPTER 7 STRUCTURAL DAMAGE DETECTION USING STATISTICAL ANALYSIS WITH TIME SERIES DATA

In the previous chapters, deterministic damage detection methods based on time series data are presented. However, uncertainties always exist in the measured vibration data and in the analytical model, and the study of their effects to the damage detection methods is necessary. In this chapter, structural damage detection based on time series data and statistical analysis will be introduced.

7.1. Introduction

In practice, noise always exists in the measured vibration data and there are also uncertainties with the initial analytical model (which will be used in the damage detection methods based on model updating) leading to incorrect damage identification. Many current research efforts are paid to the study of influence of uncertainty on the results of vibration based damage detection (Collins et al, 1974; Papadopoulas and Garcia, 1998; Beck and Au, 2002; Xia et al, 2002; Xia and Hao, 2003; Zhou et al, 2003). Some of them have considered the effect of uncertainty on the model updating (Papadopoulas and Garcia, 1998; Beck and Au, 2002) where measured statistical changes in the natural frequencies and mode shapes along with a correlated analytical stochastic finite element model are used to assess the integrity of a structure. Later, Xia et al (2002, 2003) developed a statistical damage identification algorithm based on changes of frequency

and mode shape to account for the effects of random noise on both the vibration data and finite element model. The statistics of the parameters are estimated by the perturbation method and verified with Monte Carlo technique. However all existing works are on the uncertainty with the system parameter and natural frequencies and mode shapes, and the effects of uncertainties from other practical influencing parameters of the system in a time domain damage identification algorithm are not considered yet.

A statistical method for the structural damage detection based on measured acceleration response with a reference model is proposed in this section. Uncertainties in the system parameters, such as the structural parameters of the finite element model, the excitation force acting on the structure and the measured acceleration response from the perturbed state of the structure are analyzed and the analytical formula are given. They are included in the study for the damage detection. Each of these uncertainties is assumed to have a zero mean and normally distributed statistical characteristics. The effect of each of these uncertainties on the assessment results is studied incrementally in an updating damage detection algorithm based on the response sensitivity approach. The probability density function of the stiffness parameters in both the intact and perturbed states are compared in a subsequent reliability assessment. A three-dimensional five-bay steel frame structure is studied for illustration. The damaged state is simulated with the loss of stiffness in two members. The mean value and standard deviation of the stiffness parameters are computed with the proposed method and they are compared with those from Monte Carlo technique. The probability of the identified local damage is then computed giving a probability prediction on the identified results.

7.2. Theoretical Formulation

7.2.1 Damage Detection Procedure

The procedure of damage detection is described briefly as follows and it can be found in detail in reference (Lu and Law, 2007). The equation of motion of a N degrees-of-freedom (DOFs) damped structural system under general excitation is given as,

$$\mathbf{M}\ddot{\mathbf{x}}+\mathbf{C}\dot{\mathbf{x}}+\mathbf{K}\mathbf{x}=\mathbf{D}F(t) \tag{7.1}$$

where $\mathbf{M},\mathbf{C},\mathbf{K}$ are the $N\times N$ mass, damping and stiffness matrices respectively. $\mathbf{D}$ is the mapping vector relating the DOFs with the force input to the corresponding DOFs of the system. $\mathbf{x}$, $\dot{\mathbf{x}}$, $\ddot{\mathbf{x}}$ are the $N\times 1$ displacement, velocity, acceleration vectors respectively. $F(t)$ is the force excitation. $\mathbf{x},\dot{\mathbf{x}},\ddot{\mathbf{x}}$ can be computed from Equation (7.1) using a time-stepping integral method such as Newmark Method.

The damage identification equation from the damage identification method based on the acceleration response sensitivity (Lu and Law, 2007) is,

$$\mathbf{S}\cdot\Delta\boldsymbol{\alpha}=\Delta\ddot{\mathbf{x}}=\ddot{\mathbf{x}}_d-\ddot{\mathbf{x}}_u \tag{7.2}$$

where $\mathbf{S}=\left[\frac{\partial \ddot{x}_l}{\partial\alpha_1}\quad\frac{\partial \ddot{x}_l}{\partial\alpha_2}\quad\cdots\quad\frac{\partial \ddot{x}_l}{\partial\alpha_m}\right]$, which is the sensitivity matrix of the acceleration response $\ddot{x}_l$ with respect to the structural parameters. m is the number of the structural parameters to be identified and l denotes the location of the measured acceleration responses. $\Delta\boldsymbol{\alpha}$ is the vector of fractional change in the stiffness of the system. $\ddot{\mathbf{x}}_d$ and $\ddot{\mathbf{x}}_u$ are vectors of the acceleration response at the lth DOF of the damaged and intact structures respectively. In general, the acceleration response $\ddot{\mathbf{x}}_u$ from the intact structure

is computed from an analytical model by dynamic analysis. $\ddot{\mathbf{x}}_d$ is measured directly from the damaged structure. The damage vector $\Delta\alpha$ can be obtained from Equation (7.2) using least-squares method as,

$$\Delta\boldsymbol{\alpha} = (\mathbf{S}^T\mathbf{S})^{-1}\mathbf{S}^T(\ddot{\mathbf{x}}_d - \ddot{\mathbf{x}}_u) \tag{7.3}$$

Here $\mathbf{S}$ and $\ddot{\mathbf{x}}_u$ are computed from the analytical model. After $\Delta\boldsymbol{\alpha}$ is obtained, the analytical model is updated and the computation of Equations (7.1-7.3) is updated until convergence.

7.2.2 Uncertainties of the System

The above sensitivity algorithm has been developed basing on the assumption that both the finite element model and the measured dynamic characteristics are accurate. But in practice, errors in the damage detection procedure always exist which generally include the discretization error, configuration error, mechanical parameter errors and measurement errors. The errors that occur in the measured structural physical parameters and the measured vibration characteristics may be divided into two categories: biased (systematic) error and random error. Biased error is from the malfunction of equipment and/or environment sources. It may not have zero mean and have different types of distributions. Random error, on the other hand, has zero mean and is usually modeled as normally distributed (Ang and Tang, 1975).

In the above sensitivity method, there exist several types of random errors which arise from different sources. Since an initial analytical model is used, random errors will be introduced into the structural parameters which form the stiffness matrix, mass matrix and even the damping matrix leading to errors in the damage detection results. On the

other hand, the acceleration response from the reference analytical model of the structure is computed with the same force excitation as in the damaged state, the force excitation needs to be measured from the damaged structure and noise will be incurred during the measurement. The errors associated with the measured force data will unavoidably bring in some errors to the identified results. The acceleration response $\ddot{\mathbf{x}}_d$ in Equation (7.2) is directly measured from the damaged state. The measured acceleration response will contain noise and it needs to be considered in the statistical analysis. Since model updating technique is utilized in the proposed damage detection procedure, all the above random errors will be involved in the computation and they need to be analyzed further in the iteration process to check on how these errors would erode the identification results.

The above discussions show that the different uncertainties or random variables may originate from the structural parameters, the exciting forces and from the measurement. Assuming X_p denotes the random variables associated with the structural parameters of the initial analytical model. Broadly speaking, many parameters such as mass density, geometric parameters and the material elastic modulus, etc. can be regarded as an uncertain parameter of the initial analytical model. However only the parameters associated with the mass (the material density) and stiffness (the elastic modulus of material) are studied for illustration of the statistical analysis and they are denoted by X_ρ and X_E respectively as,

$$\tilde{\rho}_i = \rho_i(1+X_{\rho_i}), \quad \tilde{E}_i = E_i(1+X_{E_i}) \tag{7.4}$$

where $\tilde{\bullet}$ denotes the measured or assumed value, ρ_i and E_i denote the real value of the mass and stiffness parameters, i denotes the ith element. Every element is assigned these

random variables representing the uncertainties in the mass and stiffness properties of the element. The uncertainties with other structural parameters can be similarly defined.

The second type of uncertainty arising from the measured exciting forces is denoted with the random variable X_F, and the measured force excitation is related to the random variables as,

$$\tilde{F}_i = F_i + X_{F_i} \tag{7.5}$$

where i denotes the ith data of the excitation.

Similarly, the third type of uncertainty arising from the measured acceleration response is denoted with the random variable $X_{\ddot{x}}$ and it is related to the measured acceleration response as

$$\tilde{\ddot{x}}_{di} = \ddot{x}_{di} + X_{\ddot{x}_{di}} \tag{7.6}$$

where i denotes the ith data of the measured response.

7.2.3 Derivatives of local damage with respect to the uncertainties

The first derivative of Equation (7.2) with respect to the random variables X is give as

$$\frac{\partial \mathbf{S}}{\partial X} \cdot \Delta\boldsymbol{\alpha} + \mathbf{S} \cdot \frac{\partial \Delta\boldsymbol{\alpha}}{\partial X} = \frac{\partial \tilde{\ddot{\mathbf{x}}}_d}{\partial X} - \frac{\partial \ddot{\mathbf{x}}_u}{\partial X} \tag{7.7}$$

Substituting Equation (7.3) into Equation (7.7), $\frac{\partial \Delta\alpha}{\partial X}$ can be obtained as,

$$\frac{\partial \Delta\boldsymbol{\alpha}}{\partial X} = (\mathbf{S}^T\mathbf{S})^{-1}\mathbf{S}^T\left(\frac{\partial \tilde{\ddot{\mathbf{x}}}_d}{\partial X} - \frac{\partial \ddot{\mathbf{x}}_u}{\partial X} - \frac{\partial \mathbf{S}}{\partial X} \cdot (\mathbf{S}^T\mathbf{S})^{-1}\mathbf{S}^T(\tilde{\ddot{\mathbf{x}}}_d - \ddot{\mathbf{x}}_u)\right) \tag{7.8}$$

It is noted that all the random variables are assumed independent and no coupling effect is involved in the analysis.

Uncertainties in the system parameter

The sensitivity of local damage with respect to the system parameter uncertainty is obtained when only the random variable X_p is considered in Equation (7.8). The measured response is independent of the system parameter giving $\frac{\partial \tilde{\ddot{\mathbf{x}}}_d}{\partial X_p} = 0$. The sensitivity of the analytical response with respect to X_p, $\frac{\partial \ddot{\mathbf{x}}_u}{\partial X_p}$, can be obtained by taking the first derivation on Equation (7.1) with respect to X_p as,

$$\mathbf{M}\frac{\partial \ddot{\mathbf{x}}}{\partial X_p} + \mathbf{C}\frac{\partial \dot{\mathbf{x}}}{\partial X_p} + \mathbf{K}\frac{\partial \mathbf{x}}{\partial X_p} = -\frac{\partial \mathbf{M}}{\partial X_p}\ddot{\mathbf{x}} - \frac{\partial \mathbf{C}}{\partial X_p}\dot{\mathbf{x}} - \frac{\partial \mathbf{K}}{\partial X_p}\mathbf{x} \qquad (7.9)$$

The sensitivity $\frac{\partial \ddot{\mathbf{x}}_u}{\partial X_p}$ can be computed (Lu and Law, 2007) from Equations (7.1) and (7.9) using a time-stepping integral method, such as Newmark method.

The derivation of Equation (7.1) with respect to the stiffness fractional change α is

$$\mathbf{M}\frac{\partial \ddot{\mathbf{x}}}{\partial \alpha} + \mathbf{C}\frac{\partial \dot{\mathbf{x}}}{\partial \alpha} + \mathbf{K}\frac{\partial \mathbf{x}}{\partial \alpha} = -\frac{\partial \mathbf{K}}{\partial \alpha}\mathbf{x} \qquad (7.10)$$

from which the sensitivity matrix S can be obtained. Further differentiation of Equation (7.10) with respect to the random variable X_p gives

$$\mathbf{M}\frac{\partial^2 \ddot{\mathbf{x}}}{\partial\alpha\partial X_p}+\mathbf{C}\frac{\partial^2 \dot{\mathbf{x}}}{\partial\alpha\partial X_p}+\mathbf{K}\frac{\partial^2 \mathbf{x}}{\partial\alpha\partial X_p}=-\frac{\partial\mathbf{M}}{\partial X_p}\frac{\partial \ddot{\mathbf{x}}}{\partial\alpha}-\frac{\partial\mathbf{C}}{\partial X_p}\frac{\partial \dot{\mathbf{x}}}{\partial\alpha} -\frac{\partial\mathbf{K}}{\partial X_p}\frac{\partial\mathbf{x}}{\partial\alpha}-\frac{\partial\mathbf{K}}{\partial\alpha}\frac{\partial\mathbf{x}}{\partial X_p}-\frac{\partial^2\mathbf{K}}{\partial\alpha\partial X_p}\mathbf{x} \qquad (7.11)$$

Since $\frac{\partial\mathbf{x}}{\partial X_p}$ and $\frac{\partial \dot{\mathbf{x}}}{\partial X_p}$ have been obtained from Equation (7.9), $\frac{\partial\mathbf{x}}{\partial\alpha}$, $\frac{\partial \dot{\mathbf{x}}}{\partial\alpha}$ and $\frac{\partial \ddot{\mathbf{x}}}{\partial\alpha}$ are obtained from Equation (7.10) and x from Equation (7.1), $\frac{\partial^2 \ddot{\mathbf{x}}}{\partial\alpha\partial X_p}$ can be finally computed from Equation (7.11). And the sensitivity $\frac{\partial\mathbf{S}}{\partial X_p}$ can be determined as,

$$\frac{\partial\mathbf{S}}{\partial X_p}=\left[\frac{\partial^2 \ddot{x}_l}{\partial\alpha_1\partial X_p}\quad\frac{\partial^2 \ddot{x}_l}{\partial\alpha_2\partial X_p}\quad\cdots\quad\frac{\partial^2 \ddot{x}_l}{\partial\alpha_m\partial X_p}\right] \qquad (7.12)$$

and $\frac{\partial\Delta\boldsymbol{\alpha}}{\partial X_p}$ can be finally computed from Equation (7.8).

Uncertainty in the exciting force

When we consider the uncertainty in the exciting force X_F, we also have $\frac{\partial \tilde{\ddot{\mathbf{x}}}_d}{\partial X_F}=0$, and Equation (7.8) can be rewritten as,

$$\frac{\partial\Delta\boldsymbol{\alpha}}{\partial X_F}=-(\mathbf{S}^T\mathbf{S})^{-1}\mathbf{S}^T\left(\frac{\partial \ddot{\mathbf{x}}_u}{\partial X_F}+\frac{\partial\mathbf{S}}{\partial X_F}\cdot(\mathbf{S}^T\mathbf{S})^{-1}\mathbf{S}^T(\tilde{\ddot{\mathbf{x}}}_d-\ddot{\mathbf{x}}_u)\right) \qquad (7.13)$$

$\frac{\partial \ddot{\mathbf{x}}_u}{\partial X_F}$ can be computed from the derivation of Equation (7.1) with respect to X_F as,

$$\mathbf{M}\frac{\partial \ddot{\mathbf{x}}}{\partial X_F}+\mathbf{C}\frac{\partial \dot{\mathbf{x}}}{\partial X_F}+\mathbf{K}\frac{\partial \mathbf{x}}{\partial X_F}=\mathbf{D}\frac{\partial \tilde{F}}{\partial X_F}-\frac{\partial \mathbf{K}}{\partial X_F}\mathbf{x} \qquad (7.14)$$

We have from Equation (7.5)

$$\frac{\partial \tilde{F}(t)}{\partial X_{F_i}}=[0 \quad \cdots \quad 0 \quad 1 \quad 0 \quad \cdots \quad 0]^T \qquad (7.15)$$

where i denotes the i th time instance, and only the i th component of the vector is one with zeros in all the other components. For the initial analytical model, $\frac{\partial \mathbf{K}}{\partial X_F}=0$. But in the updated analytical model, the effect of force uncertainty has been accounted for in the updated value with $\frac{\partial \Delta\boldsymbol{\alpha}}{\partial X_F}\neq 0$, then $\frac{\partial \mathbf{K}}{\partial X_F}\neq 0$. The sensitivity $\frac{\partial \ddot{\mathbf{x}}_u}{\partial X_F}$ can be computed from Equations (7.14) and (7.15) by Newmark method.

Differentiating Equation (7.10) with respect to the random variable X_F we get

$$\mathbf{M}\frac{\partial^2 \ddot{\mathbf{x}}}{\partial\alpha\partial X_F}+\mathbf{C}\frac{\partial^2 \dot{\mathbf{x}}}{\partial\alpha\partial X_F}+\mathbf{K}\frac{\partial^2 \mathbf{x}}{\partial\alpha\partial X_F}=-\frac{\partial \mathbf{K}}{\partial\alpha}\frac{\partial \mathbf{x}}{\partial X_F}-\frac{\partial \mathbf{K}}{\partial X_F}\frac{\partial \mathbf{x}}{\partial\alpha}-\frac{\partial^2 \mathbf{K}}{\partial X_F\partial\alpha}\mathbf{x} \qquad (7.16)$$

which is similar to Equation (7.11). $\frac{\partial \mathbf{S}}{\partial X_F}$ can then be computed from Equations (7.15) and (7.16) using Newmark method and the sensitivity $\frac{\partial \Delta\boldsymbol{\alpha}}{\partial X_F}$ can be obtained from Equation (7.13).

Uncertainty in the structural response

The sensitivity of $\Delta\boldsymbol{\alpha}$ with respect to the random variable $X_{\ddot{x}}$ can also be obtained similar to that for the structural parameters. Since $\ddot{\mathbf{x}}_u$ and $\mathbf{S}$ are not related with $X_{\ddot{x}}$ in the initial analytical model, $\frac{\partial \ddot{\mathbf{x}}_u}{\partial X_{\ddot{x}}} = 0$ and $\frac{\partial \mathbf{S}}{\partial X_{\ddot{x}}} = 0$. Equation (7.8) then gives

$$\frac{\partial \Delta\boldsymbol{\alpha}}{\partial X_{\ddot{x}}} = (\mathbf{S}^T\mathbf{S})^{-1}\mathbf{S}^T \frac{\partial \tilde{\ddot{\mathbf{x}}}_d}{\partial X_{\ddot{x}}} \tag{7.17a}$$

However, for the updated analytical model, both $\ddot{\mathbf{x}}_u$ and $\mathbf{S}$ are related to $X_{\ddot{x}}$ with the uncertainties propagate in the system. Derivation of Equation (7.1) with respect to $X_{\ddot{x}}$ gives

$$\mathbf{M}\frac{\partial \ddot{\mathbf{x}}}{\partial X_{\ddot{x}}} + \mathbf{C}\frac{\partial \dot{\mathbf{x}}}{\partial X_{\ddot{x}}} + \mathbf{K}\frac{\partial \mathbf{x}}{\partial X_{\ddot{x}}} = -\frac{\partial \mathbf{K}}{\partial X_{\ddot{x}}}\mathbf{x} \tag{7.18}$$

The sensitivities $\frac{\partial \mathbf{x}}{\partial X_{\ddot{x}}}$ and $\frac{\partial \ddot{\mathbf{x}}}{\partial X_{\ddot{x}}}$ can be obtained from Equation (7.18) by Newmark method. Derivation of Equation (7.10) with respect to $X_{\ddot{x}}$ gives

$$\mathbf{M}\frac{\partial^2 \ddot{\mathbf{x}}}{\partial\alpha\partial X_{\ddot{x}}} + \mathbf{C}\frac{\partial^2 \dot{\mathbf{x}}}{\partial\alpha\partial X_{\ddot{x}}} + \mathbf{K}\frac{\partial^2 \mathbf{x}}{\partial\alpha\partial X_{\ddot{x}}} = -\frac{\partial \mathbf{K}}{\partial\alpha}\frac{\partial \mathbf{x}}{\partial X_{\ddot{x}}} - \frac{\partial^2 \mathbf{K}}{\partial\alpha\partial X_{\ddot{x}}}\mathbf{x} - \frac{\partial \mathbf{K}}{\partial X_{\ddot{x}}}\frac{\partial \mathbf{x}}{\partial\alpha} \tag{7.19}$$

and $\frac{\partial \Delta\boldsymbol{\alpha}}{\partial X_{\ddot{x}}}$ can be written as following incorporating Equations (7.18) and (7.19)

$$\frac{\partial \Delta\boldsymbol{\alpha}}{\partial X_{\ddot{x}}} = (\mathbf{S}^T\mathbf{S})^{-1}\mathbf{S}^T\left(\frac{\partial \tilde{\ddot{\mathbf{x}}}_d}{\partial X_{\ddot{x}}} - \frac{\partial \ddot{\mathbf{x}}_u}{\partial X_{\ddot{x}}} - \frac{\partial \mathbf{S}}{\partial X_{\ddot{x}}}\cdot(\mathbf{S}^T\mathbf{S})^{-1}\mathbf{S}^T(\tilde{\ddot{\mathbf{x}}}_d - \ddot{\mathbf{x}}_u)\right) \tag{7.17b}$$

Equation (7.20) is obtained from Equation (7.6) as

$$\frac{\partial \ddot{\tilde{x}}_d(t)}{\partial \ddot{X}_x} = [0 \quad \cdots \quad 0 \quad 1 \quad 0 \quad \cdots \quad 0]^T \tag{7.20}$$

and the sensitivity $\frac{\partial \Delta\boldsymbol{\alpha}}{\partial \ddot{X}_x}$ is obtained from Equations (7.17) and (7.20).

In summary, the vector of sensitivity $\frac{\partial \Delta\boldsymbol{\alpha}}{\partial X}$ can be obtained from Equations (7.8), (7.13) and (7.17) as,

$$\frac{\partial \Delta\boldsymbol{\alpha}}{\partial X} = [\frac{\partial \Delta\boldsymbol{\alpha}}{\partial X_p} \quad \frac{\partial \Delta\boldsymbol{\alpha}}{\partial X_F} \quad \frac{\partial \Delta\boldsymbol{\alpha}}{\partial \ddot{X}_x}] \tag{7.21}$$

7.2.4 The Statistical Characteristics of the Damage Vector

The mean value of the damage vector $\Delta\alpha$ can be obtained directly from Equation (7.3) as

$$E(\Delta\boldsymbol{\alpha}) = (\mathbf{S}^T\mathbf{S})^{-1}\mathbf{S}^T(\ddot{\mathbf{x}}_d - \ddot{\mathbf{x}}_u) \tag{7.22}$$

The damage vector $\Delta\alpha$ can be regarded as a function of the random variables, and it can be expressed as a truncated second order Taylor series as,

$$\Delta\boldsymbol{\alpha}(\varepsilon) = \Delta\boldsymbol{\alpha}(0) + \sum_{i=1}^{nt} \frac{\partial \Delta\boldsymbol{\alpha}(0)}{\partial X_i} X_i + \frac{1}{2}\sum_{i=1}^{nt}\sum_{j=1}^{nt} \frac{\partial^2 \Delta\boldsymbol{\alpha}(0)}{\partial X_i \partial X_j} X_i X_j \tag{7.23}$$

The covariance matrix of $\Delta\boldsymbol{\alpha}$ may be obtained as (Papadopoulas and Garcia, 1998)

$$[\mathrm{cov}(\Delta\boldsymbol{\alpha}, \Delta\boldsymbol{\alpha})]_{m\times m} \approx [\frac{\partial \Delta\boldsymbol{\alpha}}{\partial X}]_{m\times nt} [\mathrm{cov}(\mathbf{X}, \mathbf{X})]_{nt\times nt} [\frac{\partial \Delta\boldsymbol{\alpha}}{\partial X}]^T_{m\times nt} \tag{7.24}$$

Since the random variables X_i and X_j $(i \neq j)$ are independent, we have

$$[\mathrm{cov}(\mathbf{X},\mathbf{X})]_{mt\times mt}=\begin{bmatrix}\mathrm{cov}(X_1,X_1) & 0 & \cdots & 0\\ 0 & \mathrm{cov}(X_2,X_2) & \cdots & 0\\ \cdots & \cdots & \cdots & \cdots\\ 0 & 0 & \cdots & \mathrm{cov}(X_{mt},X_{mt})\end{bmatrix} \quad (7.25)$$

where mt is the number of the random variables in the statistical analysis. It is noted that the covariance of each random variable $\mathrm{cov}(\mathbf{X},\mathbf{X})$ needs to be computed separately.

Random variables X_p is usually assumed to take up the following form in the computation as

$$\mathbf{X}_p = Ep * \mathbf{N}_{oise} \quad (7.26)$$

where Ep is the noise level ; $\mathbf{N}_{oise}$ is a standard normal distribution vector with zero mean and unit standard deviation. We have

$$\mathrm{cov}(\mathbf{X}_p,\mathbf{X}_p)=\begin{bmatrix}(Ep)^2 & 0 & \cdots & 0\\ 0 & (Ep)^2 & \cdots & 0\\ \cdots & \cdots & \cdots & \cdots\\ 0 & 0 & \cdots & (Ep)^2\end{bmatrix} \quad (7.27)$$

For the random variable $\mathbf{X}_F$ with the excitation force in simulation, it is modeled as

$$\mathbf{X}_F = Ep * \mathbf{N}_{oise} * \mathrm{var}(\tilde{F}) \quad (7.28)$$

where $\tilde{F}$ is the vector of the polluted force excitation; var(•) is the variance of the time history. We have

$$\mathrm{cov}(\mathbf{X}_F,\mathbf{X}_F)=\begin{bmatrix}(Ep*\mathrm{var}(\tilde{F}))^2 & 0 & \cdots & 0\\ 0 & (Ep*\mathrm{var}(\tilde{F}))^2 & \cdots & 0\\ \cdots & \cdots & \cdots & \cdots\\ 0 & 0 & \cdots & (Ep*\mathrm{var}(\tilde{F}))^2\end{bmatrix} \quad (7.29)$$

For the random variables $\underset{x}{\ddot{\mathbf{X}}}$, which is the measurement noise in the acceleration response, we have

$$\underset{x}{\ddot{\mathbf{X}}} = Ep * \mathbf{N}_{oise} * \mathrm{var}(\tilde{\ddot{\mathbf{x}}}_d) \tag{7.30}$$

Then the covariance of $\underset{x}{\ddot{\mathbf{X}}}$ is,

$$\mathrm{cov}(\underset{x}{\ddot{\mathbf{X}}}, \underset{x}{\ddot{\mathbf{X}}}) = \begin{bmatrix} (Ep * \mathrm{var}(\tilde{\ddot{x}}_d))^2 & 0 & \cdots & 0 \\ 0 & (Ep * \mathrm{var}(\tilde{\ddot{x}}_d))^2 & \cdots & 0 \\ \cdots & \cdots & \cdots & \cdots \\ 0 & 0 & \cdots & (Ep * \mathrm{var}(\tilde{\ddot{x}}_d))^2 \end{bmatrix} \tag{7.31}$$

Hence Equations (7.27), (7.29) and (7.31) give the covariance matrix of all the random variables studied in this work.

7.2.5 Statistical Analysis in Damage Detection

When damage detection is performed using Equation (7.3), statistical analysis on the identified results can be performed using Equations (7.22) and (7.24). Assuming that $\boldsymbol{\alpha}_0$ corresponds to the initial set of local damage with the analytical model, the updated set of local damage, $\boldsymbol{\alpha}_1$, will be given as

$$\boldsymbol{\alpha}_1 = \boldsymbol{\alpha}_0 + \Delta\boldsymbol{\alpha}_1 \tag{7.32}$$

with an expectation value of

$$E(\boldsymbol{\alpha}_1) = E(\boldsymbol{\alpha}_0) + E(\Delta\boldsymbol{\alpha}_1) \tag{7.33}$$

and a covariance of

$$[\mathrm{cov}(\boldsymbol{\alpha}_1, \boldsymbol{\alpha}_1)]_{m\times m} = \mathrm{cov}(\boldsymbol{\alpha}_0 + \Delta\boldsymbol{\alpha}_1, \boldsymbol{\alpha}_0 + \Delta\boldsymbol{\alpha}_1)$$
$$= \mathrm{cov}(\boldsymbol{\alpha}_0, \boldsymbol{\alpha}_0) + \mathrm{cov}(\boldsymbol{\alpha}_0, \Delta\boldsymbol{\alpha}_1) + \mathrm{cov}(\Delta\boldsymbol{\alpha}_1, \boldsymbol{\alpha}_0) + \mathrm{cov}(\Delta\boldsymbol{\alpha}_1, \Delta\boldsymbol{\alpha}_1) \quad (7.34)$$

It is noted that Equations (7.33-7.34) will remain valid during the whole process of convergence of the identified results.

7.2.6 Reliability of the Identified Damage

Once the statistical properties of the estimated stiffness changes are determined, it is possible to yield an estimate on the probability of damage. There are several techniques employed to determine the probability of damage (Papadopoulas and Garcia, 1998). The probability damage quotient method (Papadopoulas and Garcia, 1998) is adopted for the assessment.

A normal probability density function (PDF) is defined as,

$$\phi(x) = \frac{1}{\sigma_x\sqrt{2\pi}}\exp[-\frac{1}{2}(\frac{x-\mu_x}{\sigma_x})^2] \qquad \text{for } -\infty < x < +\infty \quad (7.35)$$

The probability of damage is assessed by comparing the PDF of the intact structural parameter and that of the damaged parameter. Two normal PDF distributions, $\phi_u(x)$ and $\phi_d(x)$, with parameters (μ_u, σ_u) and (μ_d, σ_d), denote the distributions of the undamaged structural parameters and the damaged parameters respectively and they are shown in Figure 7.1. If the damage is a loss in the structural stiffness, it is obvious from Equation (7.33) that $\mu_u > \mu_d, \sigma_u < \sigma_d$. To find the intersection of the two distributions, distributions $\phi_u(x)$ and $\phi_d(x)$ are equated with combining terms to get the following quadratic equation,

$$\hat{a}x^2 + \hat{b}x + \hat{c} = 0 \quad (7.36)$$

where $\hat{a} = \sigma_d^2 - \sigma_u^2$, $\hat{b} = 2(\mu_d \sigma_u^2 - \mu_u \sigma_d^2)$, and $\hat{c} = \mu_u^2 \sigma_d^2 - \mu_d^2 \sigma_u^2 - 2\sigma_u^2 \sigma_d^2 \ln(\sigma_d / \sigma_u)$, with roots x_1 and x_2

$$x_1 = -\frac{1}{2\hat{a}}\left[\hat{b} + \sqrt{\hat{b}^2 - 4\hat{a}\hat{c}}\right], \qquad x_2 = -\frac{1}{2\hat{a}}\left[\hat{b} - \sqrt{\hat{b}^2 - 4\hat{a}\hat{c}}\right] \quad (7.37)$$

x_1 and x_2 are in fact the two intersection points of the two PDFs. x_1 is the point between μ_d and μ_u and x_2 is between μ_u and $+\infty$ as shown in Figure 7.1. They are used to calculate the probability damage quotient P_D, defined as,

$$P_D = 1 - \left[\Phi\left(\frac{x_1 - \mu_u}{\sigma_u}\right) + \Phi\left(\frac{x_2 - \mu_d}{\sigma_d}\right) - \Phi\left(\frac{x_1 - \mu_d}{\sigma_d}\right) + \Phi\left(\frac{\mu_u - x_2}{\sigma_u}\right)\right] \quad (7.38)$$

where $\Phi(\bullet)$ denotes the probability of a normal distribution. The reliability of the identified damage information can then be assessed with Equation (7.38) with a probability prediction.

7.3. Numerical Study

7.3.1 The Structure

A three-dimensional five-bay steel frame structure as shown in Figure 7.2 serves for the numerical study. The finite element model consists of thirty-seven three-dimensional Euler beam elements and seventeen nodes. The length of all the horizontal, vertical and diagonal tube members between the centers of two adjacent nodes is exactly 0.5m. The structure orientates horizontally and is fixed into a rigid concrete support at three nodes at one end. Table 4.8 gives a summary of the main material and geometrical properties of members of the frame structure. Each node has six DOFs, and altogether

there are 102 DOFs for the whole structure. The elastic modulus of material of all the elements is taken as unknown in the damaged state.

The translational and rotational restraints at the supports are represented by large stiffnesses of 1.5×10^{11} *kN/m* and 1.5×10^{10} *kN-m/rad* respectively in the translation and the rotational DOFs. Rayleigh damping is adopted for the system with ξ_1=0.01 and ξ_2=0.005 for the first two modes. The first tweleve natural frequencies of the structure are 9.21, 28.26, 33.71, 49.01, 49.72, 71.02, 89.80, 153.93, 194.33, 209.80, 256.51 and 274.82 *Hz* from the eigenvalue analysis of the structure. The sampling frequency is 2000 *Hz* .

7.3.2 Damage Detection

A sinusoidal excitation is applied onto the structure at the 8th node in the *z*-direction with the amplitude of 3*N* and at a frequency of 30*Hz*. The acceleration response computed at the 5th node in the *z*-direction is taken as the "measured" response and the first 500 data points are used to identify the damage. The sampling rate is 2000Hz. A damage case with 5% and 10% reduction of the flexural stiffness in the 7th member and the 26th member respectively is studied. The effect of individual type of uncertainties will be discussed as follows.

Uncertainty with the mass density

The uncertainty of mass density of material is assumed to have 1% amplitude from Equation (7.26), and damage detection is performed on the structure using the proposed approach. The mean value obtained from Equation (7.3) for all the elements in

the structure are shown in Figure 7.3(a) after the first and second iteration of computation. The standard deviations for all the elements obtained from the proposed method after the first and second iterations are shown in Figure 7.4. They are compared with the standard deviations computed from the Monte Carlo method (Robert and Casella, 1999) from 1000 samples of data. The mean values converge to the true values after four iterations. It is seen that the two sets of standard deviations are very close indicating the proposed statistical method is correct. The standard deviation from the first iteration ranges from 0.9594% to 3.3378% of the identified elastic modulus of material with only 1% amplitude in the variation of the mass density of the analytical model. This indicates that the noise amplifies the error in the identified results. The standard deviation in Figure 7.4(b) after the second iteration ranges from 1.01% to 3.77% and they are not too far away from the range after the first iteration. This indicates that the amplifying effect of the noise is not significant in the second iteration. This corresponds to the fact that the bulk of the damage vector has been updated in the first iteration.

To study the propagation of the noise effect throughout the iterations, 10 iterations are performed and the mean values and the standard deviations are shown in Figures 7.3 (b) and (c) for the damaged elements and in Figure 5 for the 7^{th}, 18^{th} and 26^{th} elements. The damage parameters converge quickly to the true values with only 4 iterations. The standard deviation in Figure 7.5 also converges quickly to a constant with increasing iterations in all the elements. This corresponds to the usual observation with stiffness identification when the error is with a non-stiffness component. The uncertainty with the mass density of the finite element model cannot be represented in the updated results, and its detrimental effect on the model updating will be carried forward to the next iteration.

The convergence criteria of the identification process are difficult to meet. Here only the noise with the amplitude of 1% is considered. As seen in Equation (7.24), the standard deviation of the damage vector is linearly related with the amplitude of noise. When the amplitudes of noise are different, the standard deviation of the damage vector can be obtained by multiplying the results from 1% noise with a corresponding coefficient. Then it is unnecessary to repeat the computation in this study. It should be noted that all the statistical analysis has the assumption that the extent of the uncertainty in finite element model or measured dynamic characteristics is small to have a valid linear approximation in Equation (7.2). When the noise is too large, the assumption of linear approximation in Equation (7.2) is not valid and it will lead to failure to solve the inverse problem.

Uncertainty with the elastic modulus of material

When 1% random noise is added to the elastic modulus of material of the initial analytical model, the mean value of the stiffness parameters are the same as shown in Figure 7.3 as they are also computed from Equation (7.3). The standard deviations are shown in Figure 6 alongside with those obtained from the Monte Carlo technique. The standard deviation of all 37 elements has a maximum value of 1.6813% after the first iteration, and it drops to 0.2605% after the second iteration. This observation shows that (a) the noise effect on the elastic modulus is comparable to that of the mass density after the first iteration, and (b) the significant reduction after the second iteration shows that the stiffness parameter, which is closely related to the elastic modulus, has been updated with the mitigation in the associated noise effect in the subsequent iterations. To study the propagation of the noise effect throughout the iterations, 10 iterations are performed

and the mean values and the standard deviations are shown in Figures 7.3 (b) and (c) for the damaged elements and in Figure 7.7 for the 7^{th}, 18^{th} and 26^{th} elements. The damage parameters converge quickly to the true values with only 4 iterations and the standard deviations for all the elements in Figure 7.7 also converge quickly to zero with about 4 iterations. It indicates that the noise effect introduced by the stiffness parameter in the finite element model can be neglected after several iterations.

Uncertainty with the excitation force

1% random noise is added into the excitation force for the dynamic analysis in the intact state. The mean value of the stiffness parameters are the same as those in Figure 7.3, and the standard deviations of all the elements after the first and second iteration are shown in Figure 7.8 alongside with those from the Monte Carlo technique. The standard deviation of all 37 elements after the first iteration has a maximum value of 3.85% which increases slightly to 4.4524% after the second iteration. The error in the damage vector has been amplified with 1% noise in the input excitation. To further investigate the propagation of this uncertainty in the identified results throughout the updating process, 10 iterations are performed and the standard deviations for 7^{th}, 18^{th} and 26^{th} elements are shown in Figure 7.9. The standard deviations for the three elements converge quickly to a constant in 4 iterations similarly as that seen in uncertainty in mass density. This observation indicates that (a) the noise effect with the excitation force is similar to that with the mass density but with larger amplitudes in the noise effect, where the stiffness parameter of the damaged element can be updated with iterations leading to a reduction in the standard deviations, while that of the undamaged element cannot be updated with

the noise effect carried forward to the subsequent iterations, and (b) the bulk of the damage vector has been updated and corresponding noise effect accounted for in the first few iterations as shown in Figure 7.9.

Uncertainty with the measured structural response

1% random noise is added into the "measured" acceleration responses from the damaged structures to simulate the measurement noise. The standard deviation of all the elements after the first iteration is shown in Figure 7.10 (a) with a maximum value of 3.7942% which increase to 4.4190% after the second iteration shown in Figure 7.10 (b). The error in the identified results has been amplified with the 1% noise in the "measured" acceleration responses. The standard deviation for the three selected elements in all the 10 iterations shown in Figure 7.11 indicates the propagation of the standard deviation similar to what has been observed with the noise effect in the mass density. The undamaged element suffers most with a drifting in the standard deviation. Other discussions are similar to those for the noise effect with the mass density and the excitation force.

As a summary to the above discussions, it can be concluded that the noise effect on the stiffness parameters in the finite element model of the structure under study is least significant and it can be mitigated with increasing iterations of model updating. The noise effect on the mass density of the finite element is more significant, and that for the excitation force and the structural response are highly significant. The last three sources of uncertainty affects more on the undamaged elements than the damaged elements, i.e. they would likely lead to false-positive in the identified results.

7.3.3 Reliability Assessment

When all the above noises (uncertainty in mass density, elastic modulus, excitation force and measured acceleration responses with the extent of 1%) are involved, the above damage case with 5% loss of stiffness in 7^{th} element and 10% loss of stiffness in 26^{th} element is studied to perform the reliability assessment. From the above studies, the updating process needs only five iterations to get some stable results. The mean values after 5 iterations are shown in Table 7.1 and the standard deviations for all elements and the PDF curves for 7^{th}, 18^{th} and 26^{th} elements are shown in Figure 7.12. From Figure 7.12 (a), the max value of the standard deviation is 7.26% at the 9^{th} member which indicates that the noise effects affect the identified results severely. The PDF curves of the three elements obviously show that due to noise effect, the distribution becomes flat and the intersection area of the two PDF curves from intact and damaged states become smaller leading to an increase in the damage probability and or false-positive. The identified damage probability for all elements are shown in Table 7.2 in which 26^{th} member has the max value of 98.8% indicating that the element is damaged. The second big value of 79.4% occurs at 7^{th} element indicating the element is possible to be damaged, at the same time, 9^{th} and 4^{th} elements have high damage possibility of 73.8% and 72.3% respectively that cause false alarm in the damage detection due to the uncertainties in the finite element and measured acceleration responses. On a whole, the proposed method can identify damage successfully with few false positive in other undamaged elements in the structures when there are uncertainties in the analytical model and the measured dynamic characteristics.

7.4. Conclusions

This chapter proposed a statistical method for damage detection in structures with uncertainties in the analytical model and measured dynamic characteristics. The analytical formula for noise effect into the structure and the identified results are given. The uncertainties from the mass density and elastic modulus, excitation force which need to be used in the analytical model and measured acceleration responses from the damaged structure are studied separately. The results show that the uncertainties in the updated stiffness parameters in the analytical model will be mitigated to zeros, while the uncertainties in other parameters will be kept in the updating process and affect the identified results. The uncertainties will propagate in the iterations for updating the system and the standard deviation does not increase when the bulk of the damage vector is obtained after the first several iterations. In the simulation study with a three-dimensional 5-bay frame structure with uncertainties, reliability assessment is performed based on the statistical analysis and the identified results show that the proposed method can identify damage successfully with few alarms in the structure with uncertainties of all types.

Table 7.1 – Identified Damage Probability and Mean Value (%)

Elements No.	1	2	3	4	5	6	7	8	9	10
Damage prob.	54.4	59.5	59.3	72.3	58.6	55.0	79.4	60.6	73.8	59.7
Mean value	0	0	0	0	0	0	5	0	0	0
Elements No.	11	12	13	14	15	16	17	18	19	20
Damage prob.	60.9	62.7	51.2	30.5	56.0	48.4	64.6	60.4	53.5	51.3
Mean value	0	0	0	0	0	0	0	0	0	0
Elements No.	21	22	23	24	25	26	27	28	29	30
Damage prob.	52.3	35.6	49.4	45.0	31.6	98.8	53.4	57.9	59.8	54.8
Mean Value	0	0	0	0	0	10	0	0	0	0
Elements No.	31	32	33	34	35	36	37			
Damage prob.	41.2	42.6	43.6	58.0	49.5	56.4	53.4			
Mean Value	0	0	0	0	0	0	0			

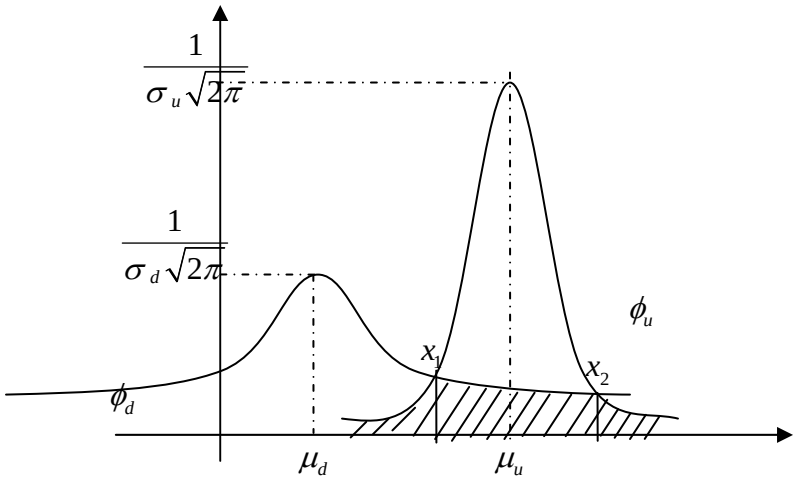

Figure 7.1- the PDFs of the structural parameter under two states

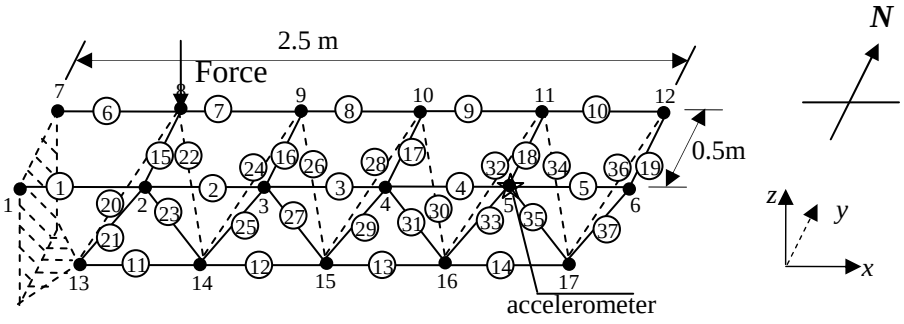

Figure 7.2 - A five-bay three-dimensional frame structure

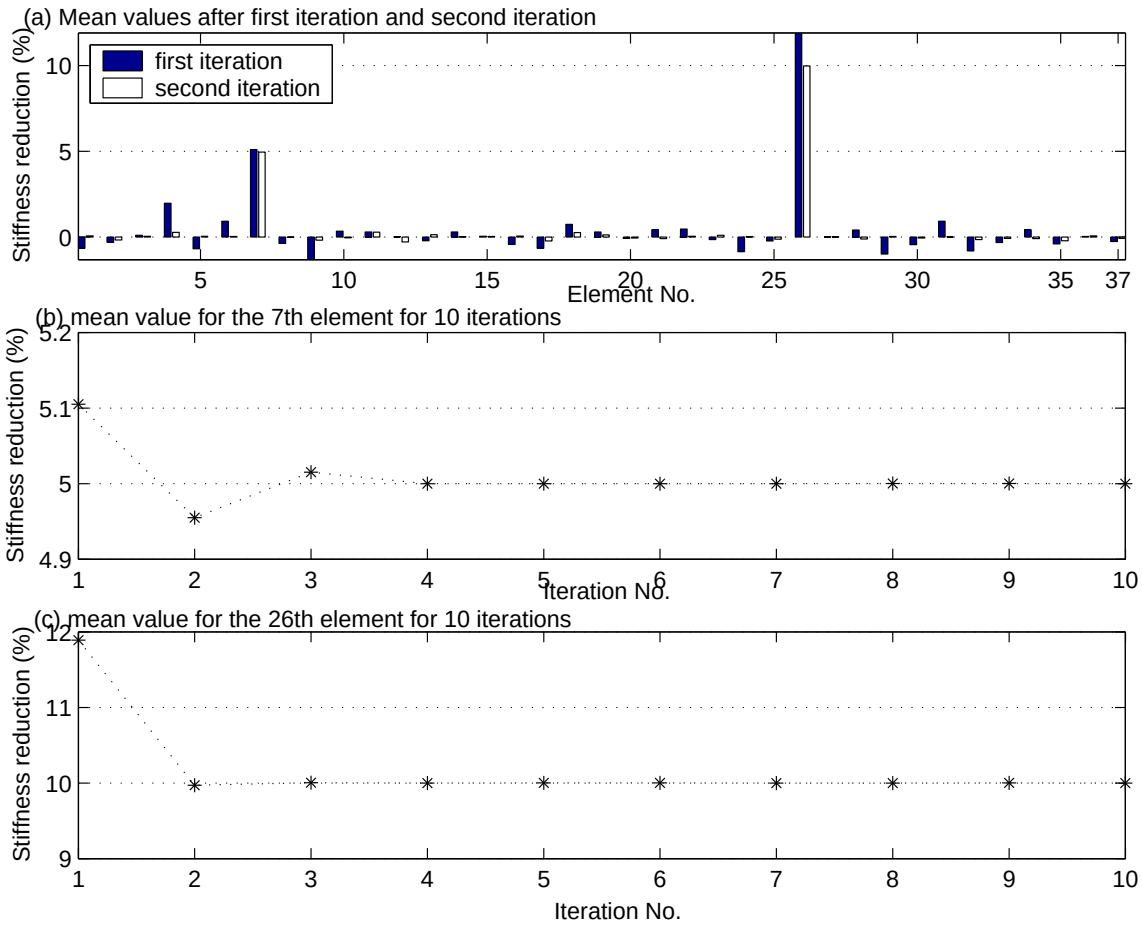

Figure 7.3 - the mean values of all elements, 7th and 26th elements for all iterations

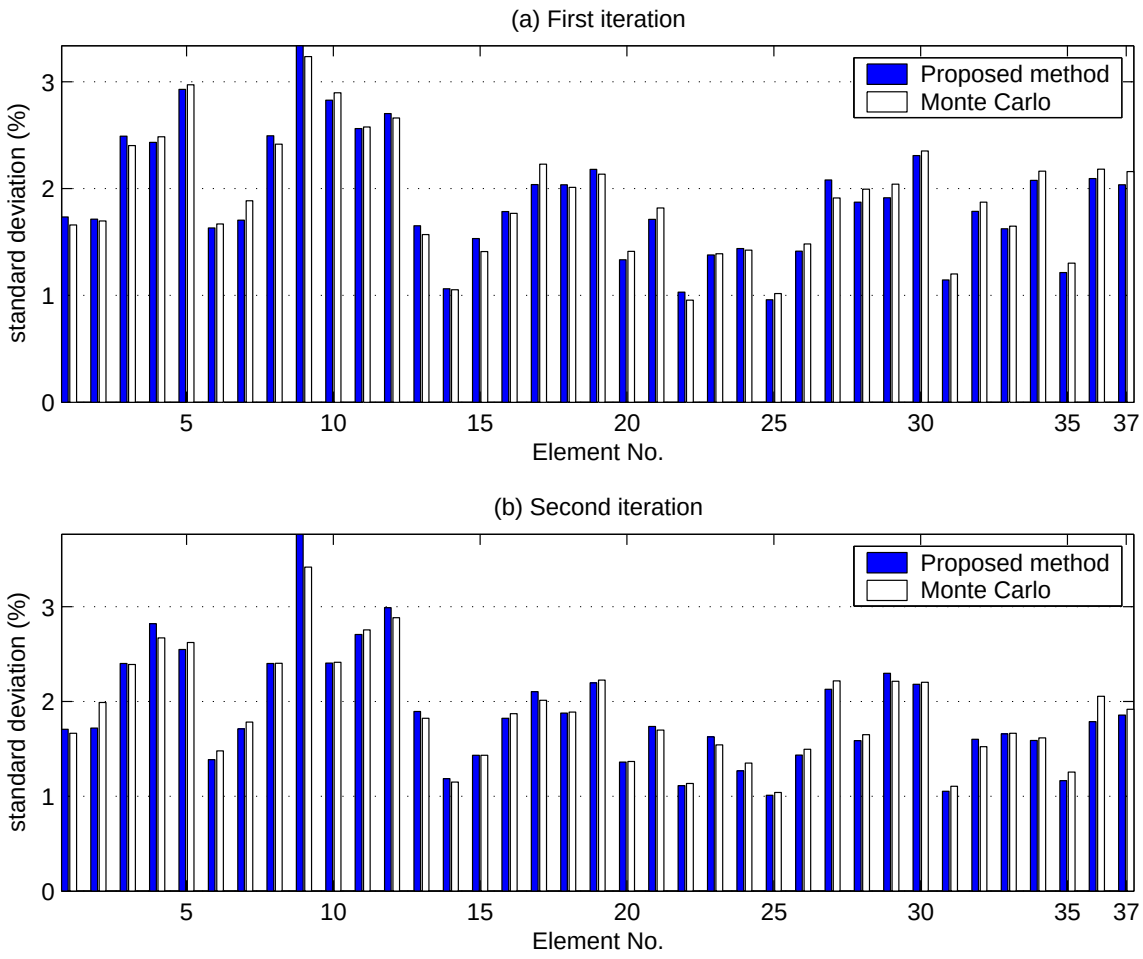

Figure 7.4 - the standard deviation of all elements due to noise in density

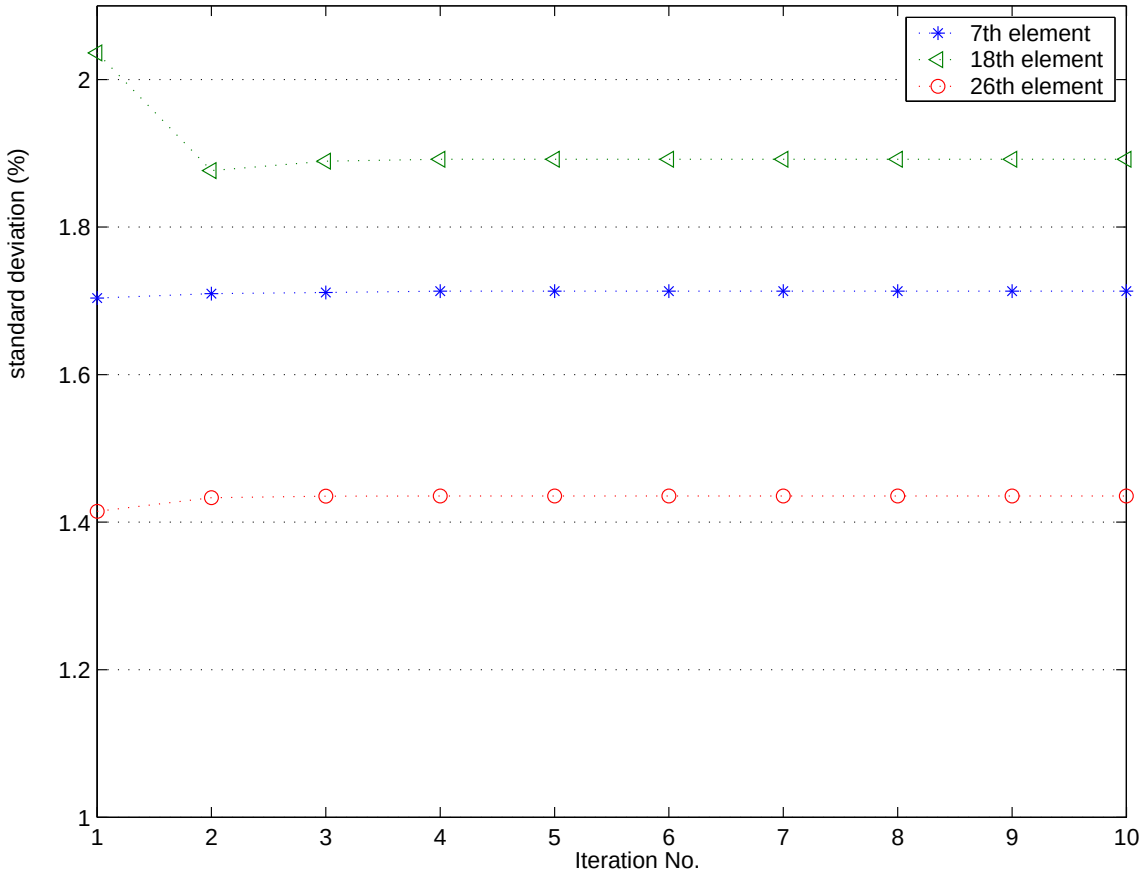

Figure 7.5 - the standard deviations for 10 iterations due to noise in mass density

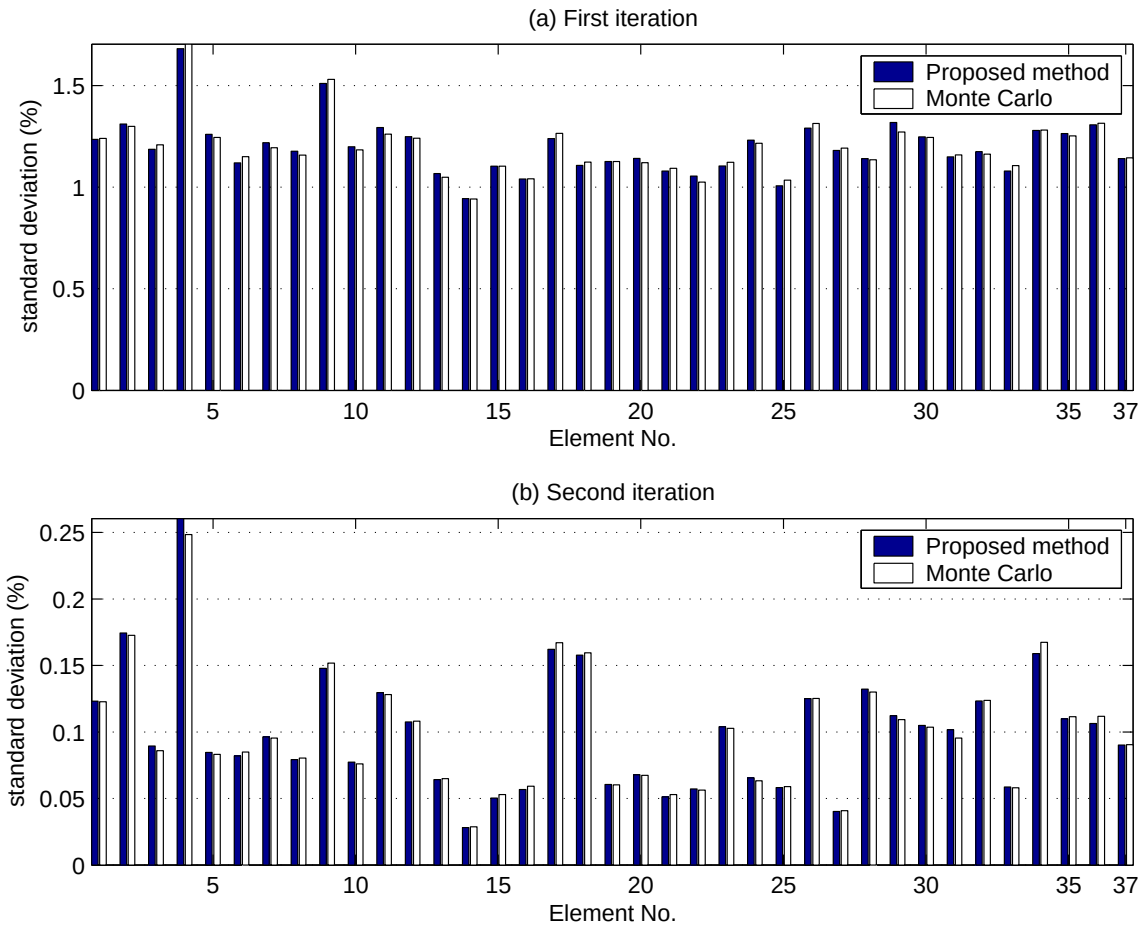

Figure 7.6 - the standard deviation of all elements due to noise in stiffness

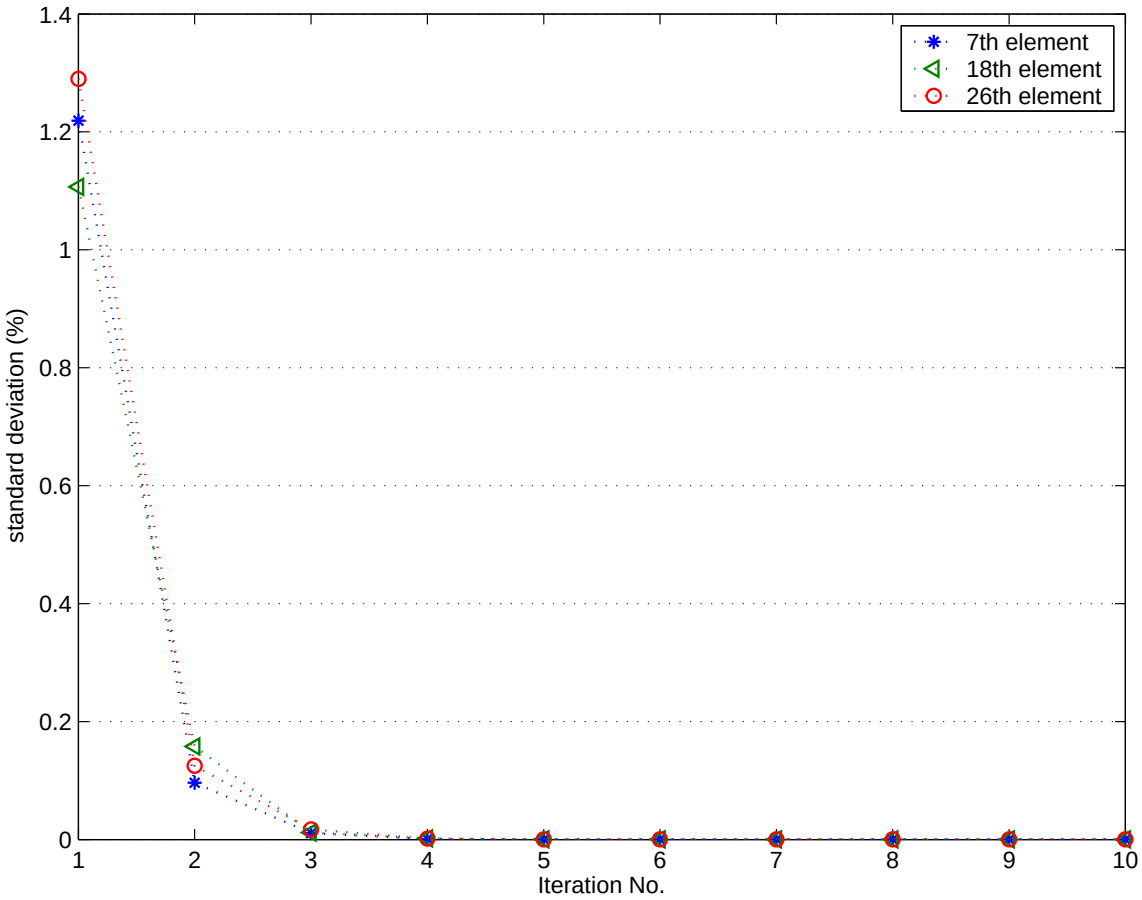

Figure 7.7 - the standard deviations for 10 iterations due to noise in stiffness

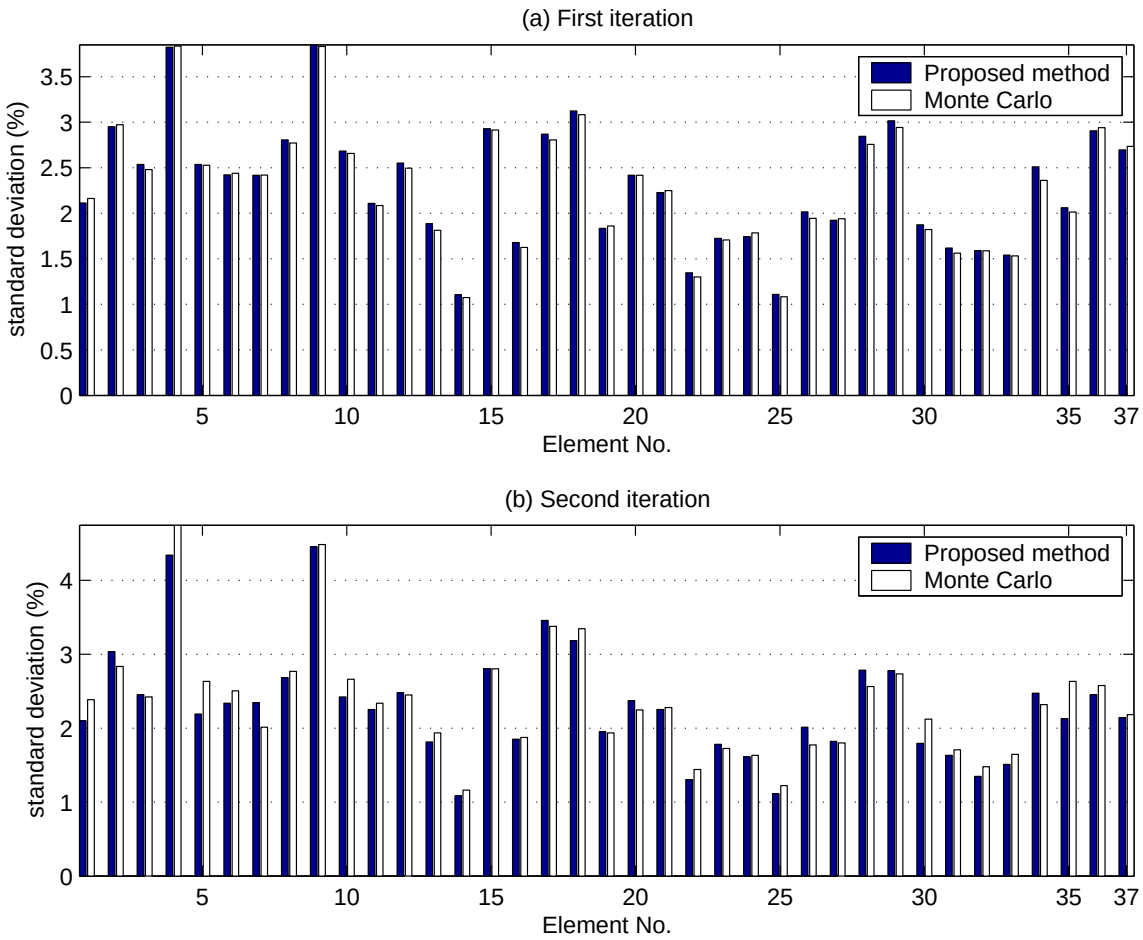

Figure 7.8 - the standard deviation of all elements due to noise in excitation

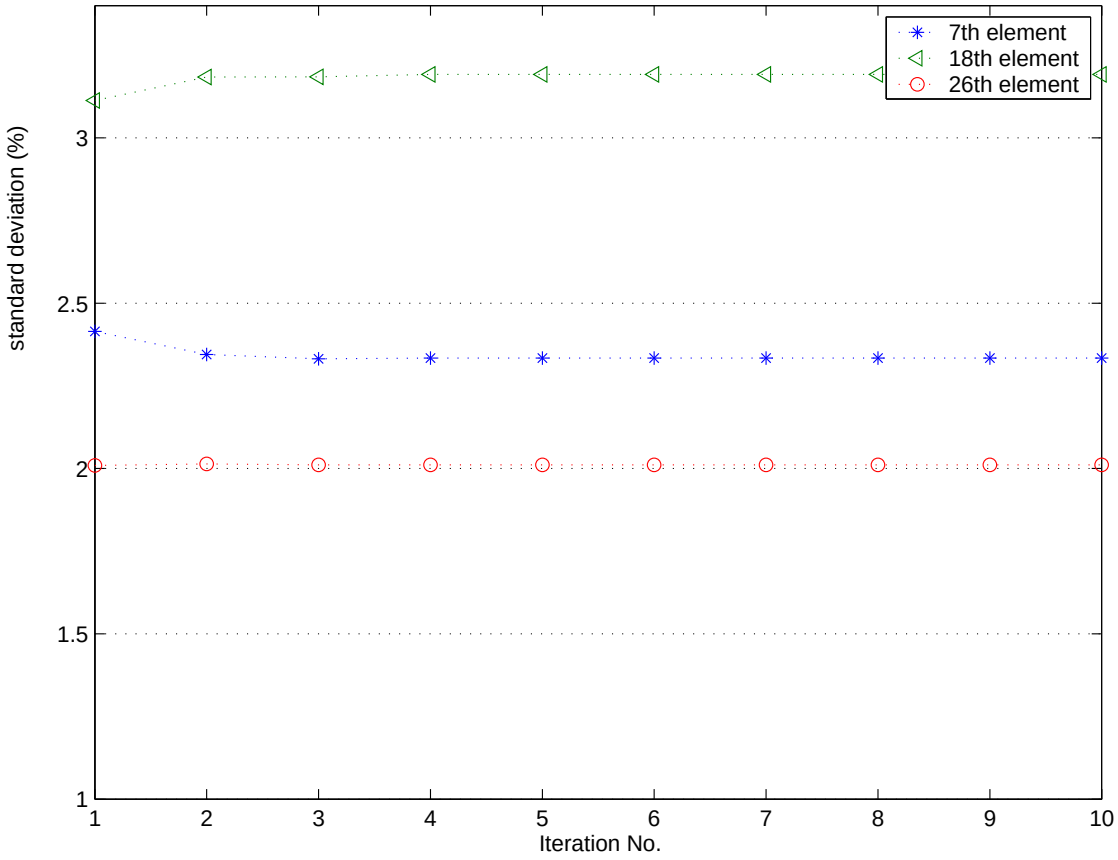

Figure 7.9 - the standard deviations for 10 iterations due to noise in measured force excitation

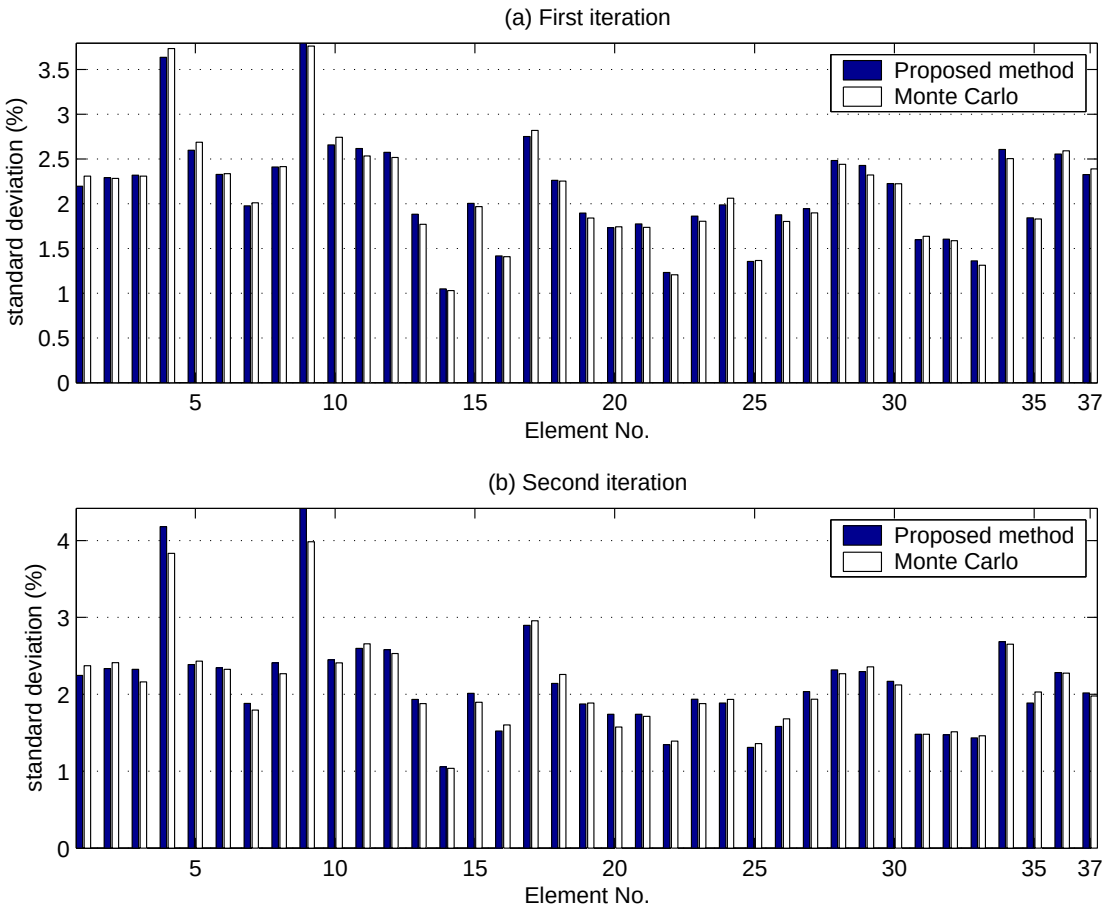

Figure 7.10 - the standard deviation of all elements due to noise in measured acceleration

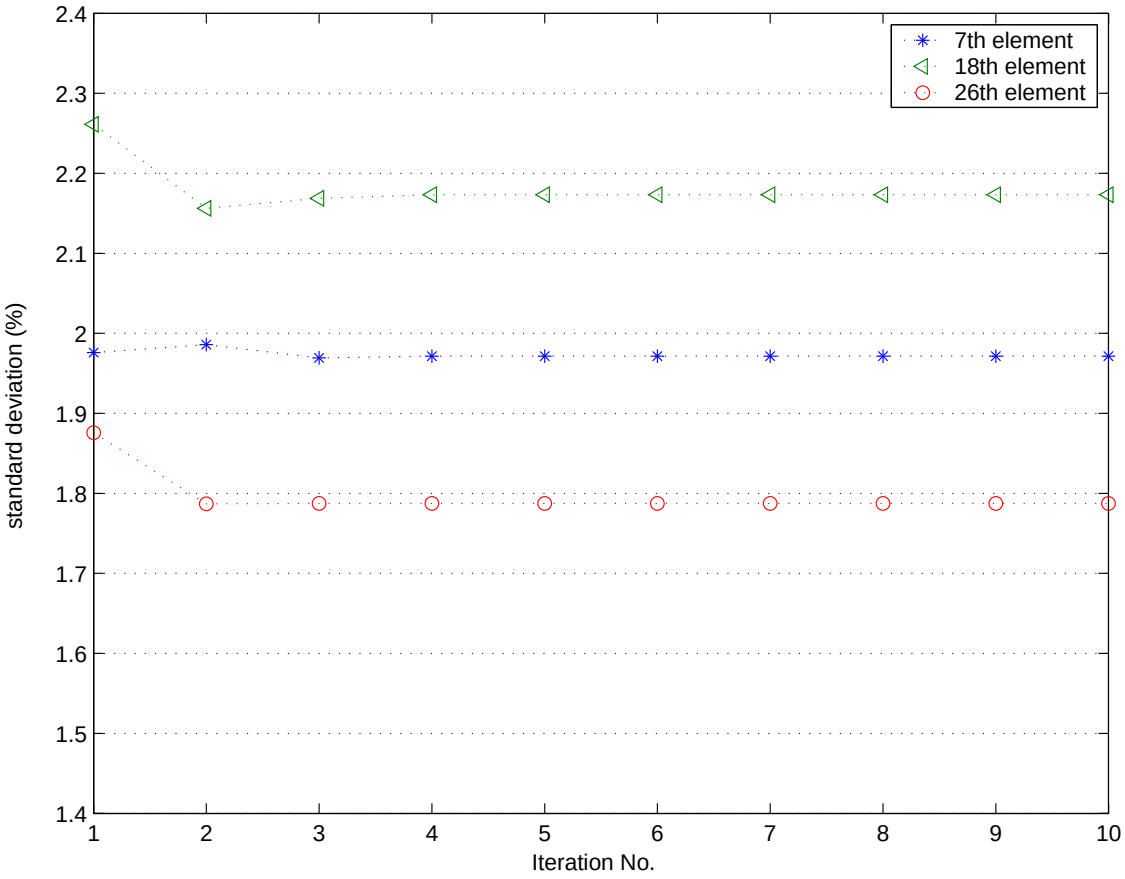

Figure 7.11 - the standard deviations for 10 iterations due to noise in measured acceleration

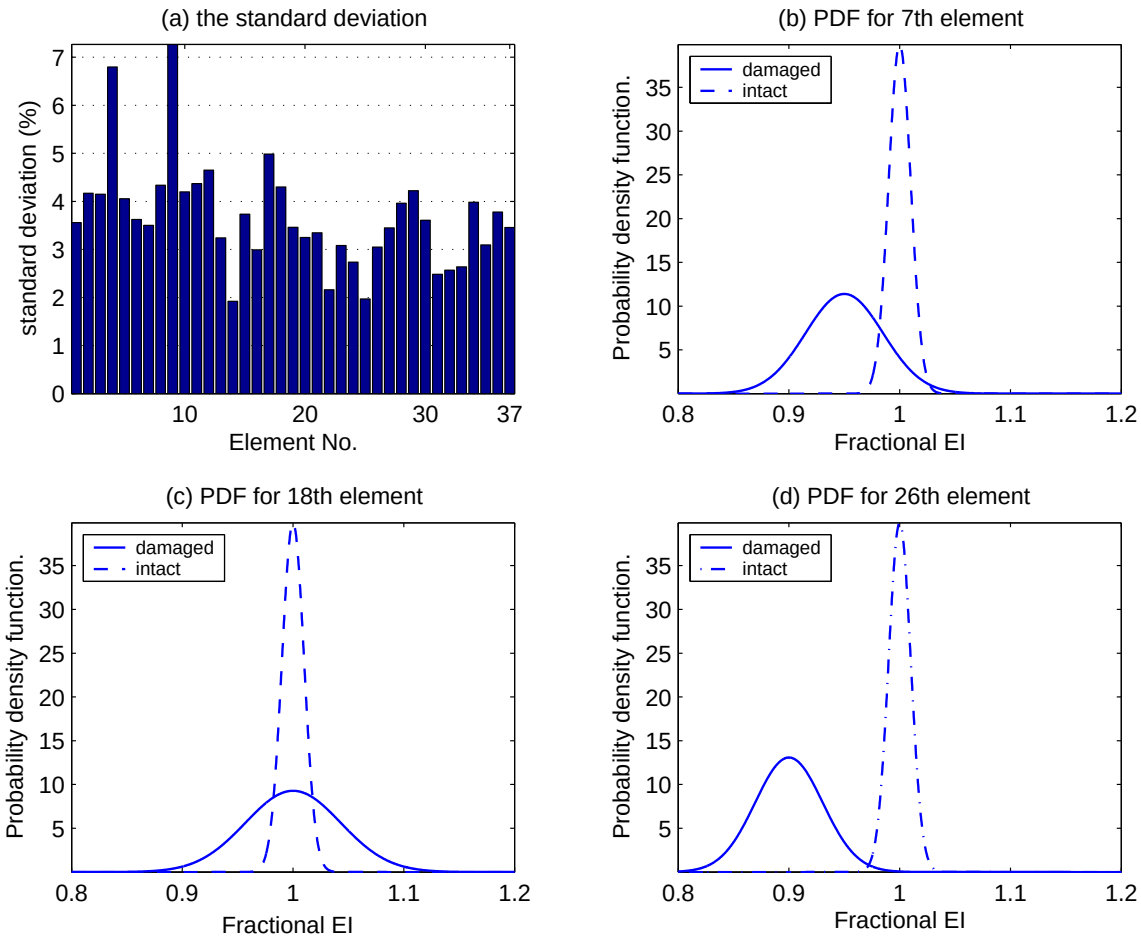

Figure 7.12 - the identified results with all types of noise

CHAPTER 8 CONCLUSIONS AND RECOMMENDATIONS

8.1 Conclusions

The subject of this study is to propose and develop damage detection methods using wavelet-based acceleration responses sensitivities and model updating techniques. The research aim has been to (a) reduce the number of sensors and make the inverse problem being over-determined in the damage detection methods based on model updating and dynamic response sensitivity. (b) reduce the dependence of the methods to the excitation such that the damage detection method is more practical. and (c) ensure the damage detection method to be more robust even with uncertainties in both the analytical model and measured vibration data.

A systematic approach for health monitoring and condition assessment has been developed in this study. This approach enables both structural damage identification and monitoring-based reliability assessment to be explored in the model updating procedure using the sensitivity of the time series data with respect to the structural parameter, and taking into account uncertainty and randomness inherent in the measurement data and structures. Though the numerical examples presented in this study are derived from bridge structures, yet most of the developed methods are general and can be used in connection with other engineering structures such as high-rise buildings and offshore platforms. The major contributions of this thesis are as follows:

(a) Investigate the direct use of acceleration responses in the damage detection via the wavelet transform when under support excitation

Acceleration responses at only the support and at limited number of locations of the structure are required for damage detection. The performance from the WPT coefficient sensitivity approach under support excitation is concluded to converge faster than the response sensitivity approach with a proper selection of the wavelet packets for a three-dimensional steel frame structure. The use of subsets of the measured response at different resampling rates would yield identified results similar to those from the full set of measured response since similar structural information is included in the subset of data. Simulation results show that the location and extent of damage of the structure can be identified accurately under the support excitation without any special artificial excitation.

(b) Damage detection using wavelet-based impulse response function in the time domain

The effect of different excitation force is removed when the impulse response functions are used instead of the acceleration response in the damage detection process. Impulse response functions are intrinsic functions of the system given the excitation location and they can be extracted from the measured response and support excitation. The analytical formulation on the sensitivity of the DWT coefficient of the impulse response function with respect to a system parameter is deduced from an analytical model based on vibration theory and Newmark method. The identification equation is solved with regularization techniques and L-curve method with some improvements.

The method on the extraction of UIRs from the accelerations of the structure and the support excitation is introduced. The sensitivity matrix of UIRs of the structure is obtained based on the finite element model and the time-stepping integral method. A two-step updating method is adopted for identifying the local damage based on the computed sensitivity matrix of UIRs from several accelerometers. Statistical analysis is included in the damage identification procedure and measurement noise is taken as an independent random variable in the UIRs from measurement. A nine-bay three-dimensional frame structure is studied numerically and experimentally with damage scenarios of multiple damages and different level of noise.

(c) Improved regularization for damage detection with noise and model errors

New techniques for improving Tikhonov regularization in an inverse structural damage detection problem with noise and model errors are proposed. The identification equation is based on the sensitivity approach with iterations. Tikhonov regularization works successfully with small noise in the system. But when the system involves both noise and model errors, the identified results often diverge after a few iterations. This arises from the fact that the signal to noise ratio decreases dramatically after a few iterations. Divergence of the regularized solution is prevented in this study by limiting the range of percentage changes with resemblance of parameter vectors from two successive iterations with the Multiple Parameter Correlation criteria. The final optimal regularization parameter λ_{opt} corresponds to a stable and converged solution satisfying the convergence criteria. Two numerical examples with a one-story plane frame and a thirty-one bar plane truss structure are studied with ten damage scenarios. Results from

different combinations of model errors and noise show that the proposed techniques could effectively improve the Tikhonov regularization method in the identification of local damages with noise and model errors in the system.

(d) Development of damage detection method based on covariance of acceleration responses of the structure when under ambient excitation

A damage detection method is proposed based on the wavelet packet energy of the covariance calculated from the measured acceleration responses of structures under ambient excitation which is assumed to be white noise distribution. To reduce the number of the unknowns involved in the inverse problem, damage localization is carried out firstly using the elemental modal strain energy. The much reduced set of potential damage element then undergoes the next state of damage quantification. The proposed damage quantification method based on the sensitivity of the WPT energy of covariance has good capability in dealing with model error and measurement noise. A five-bay three-dimensional cantilever truss structure is used to demonstrate the efficiency of the method with three damage cases, and a nine-bay three-dimensional frame structure is tested in the laboratory with the proposed method, and the identified results shows that the method is applicable to locate and quantify local damages with incomplete and noisy measurement and with initial model error.

(e) Uncertainty analysis in the damage detection method using the time domain data and model updating

A statistical method for damage detection in structures with uncertainties in the analytical model and measured dynamic characteristics is proposed. The analytical relationship between the noise effect and the identified results is given. The uncertainties from the mass density and elastic modulus, excitation force which need to be included in the analytical model and measured acceleration responses from the damaged structure are studied separately. Results show that the uncertainties in the updated parameters of the analytical model will be mitigated to zeros, while the uncertainties in other parameters will be retained in the updating process and affect the identified results. The uncertainties will propagate in the iterations when in updating the system and the standard deviation of results does not increase when the bulk of the damage vector is updated in the first several iterations. In the simulation study with a three-dimensional five-bay frame structure with uncertainties, reliability assessment is performed based on the statistical analysis and the identified results show that the proposed method can identify damage successfully with few false positives in the structure.

8.2 Recommendations

Methods for damage identification and condition assessment of bridge structures making use of acceleration responses via wavelet transform and statistical model updating have been developed. However, there are some limitations on the developed methods: (a) the inverse problem based on acceleration responses are affected largely by uncertainties in the engineering application. (b) model updating methods require an accurate model of the structure and this adds difficulty to the application of the damage detection in practice. (c) the sensitivity method based on Taylor series truncation may not

give accurate statistical model updating results in the case of high level of uncertainty; (d) the ingredients of the developed probabilistic method for bridge health monitoring and reliability assessment have been validated with numerical examples only and it still needs to be verified using the real-world data; The following recommendations are provided for further research and exploration.

1. The proposed methods in the thesis have the advantage of requiring as few as one sensor for damage detection. But computation in the simulation shows that measurements from multiple sensor combinations will result not only in a reduction in iteration steps but also an improvement in the identified results. Therefore, the issues on optimal sensor number and the optimal sensor location for the damage detection worth further research.
2. Since noise always exists in the measured data, in solving the identification equation in the inverse problem and obtaining the accurate and stable solution, the study of a more effective regularization condition and any recommendations to find the regularization parameters are desirable.
3. Only the vibration of translational degree-of-freedom is used in this thesis. Although it is still difficult to measure the vibration of rotational degree-of-freedom in most practical structures, it is suggested that both theories of vibration from rotational degree-of-freedom in a damage detection method worth further research.
4. Rayleigh damping model is used in this thesis. And the damping is assumed to remain unchanged before and after the damage occurrence. In fact, the damping

may change after the occurrence of damage, and therefore further research should identify the damping coefficients as well as the structural damage as time varies.

5. The limitation of the proposed methods includes the large computation requirement especially for large scale structures with large number of degrees-of-freedom, and a more efficient method needs to be used for computing the dynamic responses.
6. One obstacle of the proposed method which restricts general application for complex structures is the dependence on an accurate analytical model. It is necessary to reduce this dependence and to develop the method making use of ambient vibration excitation, or perform the on-line health monitoring for bridges under ambient vibration, which is in most cases, pink noise excitation.
7. Another problem is that the study of this thesis is limited to the assumption of the linearity in the structure. In practice, non-linearity often exists in the real structures, and the methods need to be developed for the nonlinear cases.
8. In this thesis, a simple damage model and finite elements are used for the study. A more detailed finite element or other numerical models can be used in the damage detection with the proposed methods and better results will be obtained. It must be noted that when the number of degrees-of-freedom increases, and computation requirement of the method will also increase.
9. It is necessary to integrate research on structural health monitoring and structural reliability analysis. The established linkage between structural health monitoring technologies and bridge inspection/maintenance exercises is still preliminary, and more thorough research is required to completely realize the potential of this

linkage to benefit bridge authorities from health monitoring technologies. This goal can be achieved by developing coordinated research programs involving participation of the researchers from both structural health monitoring and structural reliability disciplines.

REFERENCES

Abdel Wahab, M.M. (2001), "Effect of modal curvatures in damage detection using model updating", *Mechanical Systems and Signal Processing*, **15**(2), 439-445.

Abdo, M.A.B. and Hori, M. (2002), "A numerical study of structural damage detection using changes in the rotation of mode", *Journal of Sound and Vibration*, **251**(2), 227-239.

Adams, R.D., Cawley, P., Pye, C.J. and Stone, B.J. (1978), "A vibration technique for non-destructive assessing the integrity of structures", *Journal of Mechanical Engineering Science*, **20**, 93-100.

Agbabian, M. S., Masri, S. F., Miller, R. K. and Caughey, T. K. (1988), "A system identification approach to the detection of changes in structural parameters", *Structural Safety Evaluation Based on System Identification Approach*, Friedrick Vieweg & Son, Wiesbaden, 341-356.

Ahmadian, H., Mottershead, J.E. and Friswell, M.I. (1998), "Regularization methods for finite element model updating", *Mechanical Systems and Signal Processing*, **12**(1), 47-64.

Aktan, A.E., Lee, K.L., Chuntavan, C. and Aksel, T. (1994), "Modal testing for structural identification and condition assessment of constructed facilities", *Proceedings of 12th International Modal Analysis Conference*, 462-468.

Ang, A. H.S. (1988), “Seismic damage assessment and basis for damage-limiting design”, *Probabilistic Engineering Mechanics,* **3**(3), 146-150.

Ang, A.H.S. and Tang, W.H. (1975), *Probability concepts in Engineering Planning and Desing, Volume I: Basic Principles*, New York: Wiley.

Andry, A.N., Shapiro, E.Y. and Chung, J.C. (1983), “Eigenstructure Assignment for Linear Systems”, *IEEE Transactions on Aerospace and Electronic Systems*, No.**5**, pp711-729.

Araki, Y. and Hjelmstad, K.D. (2001), “Optimum sensitivity-based statistical parameters estimation from modal response”, *AIAA Journal*, **39**, 1166-1174.

Balageas, D.L. (ed.) (2002), *Proceedings of the 1st European Workshop on Structural Health Monitoring*, Cachan, France.

Bathe, K.J. (1982), *Finite Element Procedures in Engineering Analysis,* Prentice Hall, New Jersey.

Banan, M.R., Banan, M.R. and Hjelmstad, K.D. (1994a), “Parameter estimation of structures from static response I: Computational aspects”, *Journal of Structural Engineering, ASCE*, **120**, 3243-3258.

Banan, M.R., Banan, M.R. and Hjelmstad, K.D. (1994b), “Parameter estimation of structures from static response II: Numerical simulation studies”, *Journal of Structural Engineering, ASCE*, **120**, 3259-3283.

Banks, H.T., Inman, D. J., Leo, D.J. and Wang, Y. (1996), "An experimentally validated damage detection theory in smart structures", *Journal of Sound and Vibration*, **191**, 5, 859-880.

Banks, H.T. and Emeric, P. (1998), "Detection of non-symmetrical damage in smart plate-like structures", *Journal of Intelligent Material Systems and Structures*, **9** (October), 818-828.

Baruch, M. (1978), "Optimization procedure to correct stiffness and flexibility matrices using vibration tests", *AIAA Journal*, **16**(11), 1208-1210.

Beck, J.L. and Au, S.K., (2002), "Bayesian updating of structural models and reliability using Markov Chain Monte Carlo simulation", *Journal of Engineering Mechanics, ASCE* **128**, 380-391.

Bendat, J.S. and Piersol, A.G., (1980), *Engineering Applications of Correlation and Spectral Analysis*, New York: John Wiley.

Berman, A., (1979), "Comment on 'Optimal weighted orthogonalization of measured modes", *AIAA Journal*, **17**, 927-928.

Berman, A. and Flannely, W. G. (1971), "Theory of incomplete models of dynamic structures", *AIAA Journal*, **9**, 1481-1487.

Berman, A. and Nagy, E.J. (1983), "Improvement of large analytical model using test data", *AIAA Journal*, **21**(8), 1168-1173.

Biswas, M., Pandey, A.K. and Bluni, S. (1994), "Modified chain-code computer vision techniques for interrogation of vibration signatures for structural fault detection", *Journal of Sound and Vibration*, **175**(1), 89-104.

Boller, C. and Staszewski, W.J. (eds) (2004), *Proceedings of the 2nd European Workshop on Structural Health Monitoring*, Munich, Germany.

Brock, J.E. (1968), "Optimal Matrices Describing Linear Systems", *AIAA Journal*, 6(7), 1292-1296.

Busby, H.R. and TrujiUo, D.M. (1997), "Optimal Regularization of an Inverse Dynamics Problem", *Computers & Structures*, Vol. **63**. No. 2. pp. 243-248.

Cattarius, J. and Inmanm, D.J. (1997), "Time domain analysis for damage detection in smart structures", *Mechanical Systems and Signal Processing*, **11**(3), 409-423.

Cawley, P. and Adams, R.D., (1979), "The location of defects in structures from measurements of natural frequencies", *Journal of Strain Analysis*, **14**(2), 49-57.

Chalko, T.J. and Haritosn, N., (1997), "Scaling eigenvectors obtained from ambient excitation modal testing," *Proceedings of the 15th IMAC*, pp. 13 – 19.

Chance, J., Tomlinson, G.R. and Worden, K. (1994), "A simplified approach to the numerical and experimental modeling of the dynamics of a cracked beam", *Proceeding of 12th International Modal Analysis Conference*, 778-785.

Chang, C.C and Sun, Z. (2005), "Structural damage localization using spatial wavelet packet signature", *Smart Structures and Systems*, **1**(1), 29-46.

Chang, F. (ed.) (1999), *Proceedings of the 2nd International Workshop on Structural Health Monitoring*, Stanford, California.

Chang, F. (ed.) (2001), *Proceedings of the 3rd International Workshop on Structural Health Monitoring*, Stanford, California.

Chang, F. (ed.) (2003), *Proceedings of the 4th International Workshop on Structural Health Monitoring*, Standford, California.

Chaudhry, Z. and Ganino, A.J. (1994), "Damage detection using neural networks-an initial experimental study on debonded beams", *Journal of Intelligent Material Systems and Structures*, **5**, 585-589.

Chen, J. and Li, J. (2004), "Simultaneous identification of structural parameters and input time history from output-only measurements", *Computaticonal Mechanics*. **33**(5), 365-374.

Chen, J.C. and Garba, J.A. (1980), "Analytical model improvement using modal testing results", *AIAA Journal*, **18**(6), 684-690.

Chen, J.C. and Garba, J.A. (1988), "On-orbit damage assessment for large space structures", *AIAA Journal*, **26**(9), 1119-1126.

Choi, S. and Stubbs, N. (2004), "Damage identification in structures using the time-domain response", *Journal of Sound and Vibration*, **275**, 577–590.

Christides, S. and Barr, A.D.S. (1984), "One-dimensional theory of cracked Bernoulli-Euler beams", *International Journal of Mechanical Science*, **26(**11-12**)**, 639-648.

Christides, S. and Barr, A.D.S. (1986), "Torsional vibration of cracked beams of non-circular cross-section", *International Journal of Mechanical Science*, **28**, 473-490.

Cobb, R.G. and Liebst, B.S. (1997), "Structural damage identification using assigned partial eigenstructure", *AIAA Journal*, **35**(1), 152-158.

Coifman, R.R. and Wickerhauser, M.V. (1992), "Entropy-based algorithms for best basis selection", *IEEE Transaction on Information Theory*, **38**, 713-718.

Collins, J.D., Hart, G.C., Hasselman, T.K. and Kennedy, B. (1974), "Statistical identification of structures", *AIAA Journal*, **12**(2), 185-190.

Cooley, J.W. and Tukey, J.W. (1965), "An algorithm for the machine calculation of complex Fourier series", *Mathematics of Computation*, **19**, 297-301.

Crawford R. and Ward H. S. (1964), "Determination of the natural periods of buildings", *Bulletin of the Seismological Society of America*, **54**, 1743-1756.

Creed, S.G. (1987), "Assessment of large engineering structures using data collected during in-service loading", In *Structural Assessment*: *The Use of Full and Large Scale Testing* (edited by Garas, F.K., Clarke, J.K. and Armer, G.S.T.), Butterworths, London, 55-62.

D'Ambrogio, W. and Fregolent, A. (1998), "On the use of consistent and significant information to reduce ill-conditioning in dynamic model updating", *Mechanical Systems and Signal Processing*, **12**, 203-222.

Daubechies, I. (1992), *Ten lectures on wavelets*, SIAM, Philadelphia, PA.

Dawood, T.A., Sahin, M., Shenoi, R.A. and Newson, T.P. (2002), "Real-time damage detection of a composite cantilever beam using wavelet transforms", *First European Workshop on Structural Health Monitoring*, SHM 2002, Paris, France.

Desforges, M.J., Cooper, J.E. and Wright, J.R., (1995), "Spectral and modal parameter-estimation from output-only measurements", Mechanical Systems and Signal Processing, **9**(2): 169-186.

Dimarogonas, A.D. (1976), *Vibration Engineering*, West Publisher.

Doebling, S.W. (1996), "Damage detection and model refinement using elemental stiffness perturbations with constrained connectivity", *Proceedings of the AIAA/ASME/AHS Adaptive Structures Forum*, 360-370, AIAA-96-1037.

Doebling, S.W., Farrar, C.R. and Prime, M.B. (1998), "A summary review of vibration-based damage identification methods", *The Shock and Vibration Digest*, **30**(2), 91-105.

Doebling, S.W., Farrar, C.R., Prime, M.B., and Shevitz, D.W. (1996a), "Damage identification and health monitoring of structural and mechanical systems from changes in their vibration characteristics: A literature review", *Los Alamos National Laboratory Report*, LA-13070-MS.

Doebling, S.W., Peterson, L.D. and Alvin, K.F. (1996b), "Estimation of reciprocal residual flexibility from experimental modal data", *AIAA Journal*, **34**(8), 1678-1685.

Doherty, J.E. (1993), "Nondestructive evaluation", *In Handbook on Experimental Mechanics, 2nd ed.*, New York: VCH; Bethel: Society for Experimental Mechanics, 527-556.

Farrar, C.R., Baker, W.E., Bell, T.M., Cone, K.M., Darling, T.W., Duffey, T.A., Eklund, A. and Migliori, A. (1994), "Dynamic Characterization and Damage Detection in the I-40 Bridge over the Rio Grande", *Los Alamos National Laboratory, Los Alamos, New Mexico*, Report No. LA 12767-MS.

Farrar, C.R. and Doebling, S.W. (1997), "Lessons Learned from Applications of Vibration-Based Damage Identification Methods to Large Bridge Structures", In: *Proceedings of the International Workshop on Structural Health Monitoring*, Stanford, CA, pp. 351-370.

Farrar, C.R., Doebling, S.W. and Nix, D.A. (2001), "Vibration-based structural damage identification", *Philosophical Transactions of the Royal Society of London Series A-Mathematical Physical and Engineering Sciences*, **359**(1778), 131-149.

Fonseca, J.R., Friswell, M.I., Mottershead, J.E. and Lees, A.W. (2005), "Uncertainty identification by the maximum likelihood method", *Journal of Sound and Vibration*, **288**, 587-599.

Fox, C.H.J. (1992), "The location of defects in structures: a comparison of the use of natural frequency and mode shape data", *Proceeding of 10th International Modal Analysis Conference*, 522-528.

Fox, R.L. and Kapoor, M.P. (1968), "Rates of Change of eigenvalues and eigenvectors", *AIAA Journal*, **6**(12), 2426-2429.

Fregolent, A., Ambrogio, W.D., Salvini, P. and Sestieri, A. (1996), "Regularization techniques for dynamic model updating using input residual", *Inverse Problems in Engineering*, **2**, 171-200.

Friswell, M. I. and Mottershead, J. E. (1995), *Finite element model updating in structural dynamics*, Kluwer Academic Publishers.

Friswell, M.I., Mottershead, J.E. and Ahmadian, H. (2001), "Finite element model updating using experimental test data: parameterization and regularization", *Philosophical Transactions of the Royal Society of London A: Mathematical, Physical and Engineering Sciences*, **359**, 169-186.

Friswell, M.I., Penny, J.E.T. and Wilson, D.A.L. (1994), "Using vibration data and statistical measures to locate damage in structures", *Modal Analysis: The International Journal of Analytical and Experimental Modal Analysis*, **9**(4), 239-254.

Friswell, M.I. and Penny, J.E.T. (May 1997a), "The practical limits of damage detection and location using vibration data", *In 11th VPI&SU Symposium on Structural Dynamics and Control*, pp.31-40.

Friswell, M.I., and Penny, J.E.T. (1997b), "Is damage location using vibration measurements practical", *Damage Assessment of Structures Using Advanced Signal Processing Procedures: DAMAS 97*, Dulieu-Smith, J. M., Staszewski, W. J., and Worden, K. (editors), Sheffield Academic Press, Sheffield, 351-362.

Friswell, M. I., Penny, J. E. T. and Garvey, S.D. (1997), "Parameter subset selection in damage location", *Inverse Problem in Engineering* **5**(3), 115-189.

Friswell, M.L, and Mottershead, J.E. (1995), *Finite element model updating in structural dynamics*, Kluwer Academic, Norwell, MA.

Fritzen, C.P., Jennewein, D. and Kiefer, T., (1998), "Damage detection based on model updating methods", *Mechanical Systems and Signal Processing*, **12** (1), 163-186.

Gurley, K. and Kareem, A. (1999), "Applications of wavelet transforms in earthquake: wind and ocean engineering", *Engineering Structures*, **21** (2), 149-167.

Hajela, P. and Soeiro, F. (1990), "Recent Developments in Damage Detection Based on System Identification Methods", *Structural Optimization*, Vol.2, pp. 1-10.

Hall, B.M. (1970), "Linear estimation of structural parameters from dynamic test data", *Proceedings of AIAA/ASME 11th Structures, Structural Dynamics, andMaterials Conference*, 193-197.

Hansen, P.C. (1994), "Regularization tools: a MATLAB package for analysis and solution of discrete ill-posed problems", *Numerical Algorithms*, **6**, 1-35.

Hansen P.C., (1998), "Rank-deficient and Discrete Ill-posed Problems, Numerical Aspects of Linear Inversion", SIAM, Society for Industrial and Applied Mathematics, Philadelphia.

Hearn, G. and Testa, R.B. (1991), "Modal analysis for damage detection in structures", *Journal of Structural Engineering, ASCE*, **117**(10), 3042-3063.

Hemez, F.M. (1993), *Theoretical and experimental correlation between finite element models and modal tests in the context of large flexible space structures*, Ph.D. dissertation, University of Colorado, Boulder.

Hemez, F.M. and Farhat, C. (1995), "Structural damage detection via a finite element model updating methodology", Modal Analysis: The International Journal of Analytical and Experimental Modal Analysis, **10**(3), 152-166.

Hermans, L. and Auweraer, H.V., (1999), "Modal testing and analysis of structures under operational conditions: industrial application", *Mechanical Systems and Signal Processing*, **13**, 193-216.

Huynh, D., He, J. and Tran, D., (2005), "Damage location vector: a non-destructive structural damage detection technique", *Computers & Structures*, **83**(28-30), 2353-2367.

Hwang H.Y. and Kim C., (2004), "Damage detection in structures using a few frequency response measurements", *Journal of Sound and Vibration*, **270**(1-2), 1-14.

Ishak S.I., Liu G.R., Lim S.P. and Shang H.M., (2001), "Locating and sizing of delamination in composite laminates using computational and experimental methods", *Composite Part B. Engineering* Vol. 32(4), pp. 287-298.

Ishak S.I., Liu G.R., Lim S.P. and Shang, H.M., (2002), "Non-Destructive Evaluation of Crack Detection in Beams Using Transverse Impact", *Journal of Sound and Vibration*, Vol. 252 (2), pp. 343-360. Citation by others: 1.

Jahn, H.A. (1948), “Improvement of an approximate set of latent roots and modal columns of a matrix by methods akin to those of classical perturbation theory”, *Quarterly Journal of Mechanics and Applied Mathematics*, **1**, 132-144.

James, III G.H., Carne, T.G., and Lauffer, J.P., (1995), “The Natural Excitation Technique (Next) for Modal Parameters Extraction from Operating Structures”, *Modal Analysis: the International Journal of Analytical and Experimental Modal Analysis*, **10**(4), pp. 260-277.

Jin, S., Livingston, R.A. and Marzougui, D. (2000), “Energy index approach for damage detection in nonlinear highway structures”, *Proceedings of SPIE - The International Society for Optical Engineering*, v3995, *Nondestructive Evaluation of Highways, Utilities, and Pipelines IV*, Newport Beach, CA, USA, 52-63.

Jones, D.R.H. (1998). *Failure Analysis Case Studies: a sourcebook of case studies selected from the pages of Engineering failure analysis 1994-1996*, Elsevier, Amsterdam.

Jones, D.R.H. (2001), *Failure Analysis Case Studies II: a sourcebook of case studies selected from the pages of Engineering failure analysis 1997-1999*, Elsevier, Amsterdam.

Juan, C., Dyke, J.S. and Erik, A.J. (2000), “Health monitoring based on component transfer functions”, *Advances in Structural Dynamics*, Elsevier Science Ltd., Oxford, UK, 11, 997-1004.

Jung, H. and Ewins, D. J. (1992), "Error Sensitivity of the Inverse Eigensensitivity Method for Model Updating", *Proceedings of the 10th International Modal Analysis Conference*, San Diego, 992-998.

Juang, J.N. and Pappa, R.S., (1985), "An Eigensystem Realization Algorithm for Modal Parameters Identification and Model Reduction", *Journal of Guidance, Control and Dynamics*, **8**(5):620-627.

Kabe, A.M. (1985), "Stiffness matrix adjustment using mode data", *AIAA Journal*, **23**(9), 1431-1436.

Kang, J.S., Park, S.K., Shin, S. and Lee, H.S. (2005), "Structural system identification in time domain using measured acceleration", *Journal of Sound and Vibration* **288**(1-2), 215–234.

Kashangaki, T.A.L., Smith, S.W. and Lim, T.W. (1992), "Underlying modal data issues for detecting damage in truss structures", *Proceeding of the AIAA/ASME/ASCE/AHS/ASC/ 33rd Structures, Structural Dynamics, and Materials Conference*, Washington, D.C., AIAA paper 92-2264.

Katafygiotis, L.S. and Beck, J.L. (1998), "Updating models and their uncertainties II: Model identifiability", *Journal of Engineering Mechanics, ASCE*, **124**, 463-467.

Kaouk, M. and Zimmerman, D.C. (1994), "Structural damage assessment using a generalized minimum rank perturbation theory", *AIAA Journal*, **32**(4), 836-842.

Kaouk, M. and Zimmerman, D.C. (1995), "Structural health assessment using a partition model update technique", *Proceedings of 13th International Modal Analysis Conference*, 445-455.

Kirmser, P.G. (1944), "The effect of discontinuities on the natural frequency of beams", *In Proceedings of the American Society of Testing and Materials*, **44**, 897-904.

Kleiber, M. and Hien, T. D. (1992), *The stochastic finite element method*: *Basic perturbation technique and computer Implementation*, Wiley, New York.

Ko, J.M., Wong, C.W. and Lam, H.F. (1994), "Damage detection in steel framed structures by vibration measurement approach", *Proceedings of 12th International Modal Analysis Conference*, 280-286.

Koh, C.G., See, L.M. and Balendra, T. (1995), "Damage detection of buildings: numerical and experimental studies", *Journal of Structural Engineering —ASCE*, **121**(8), 1155-1160.

Kumara, S.R.T., Suh, J. and Mysore, S.P. (1999), "Machinery fault diagnosis and prognosis: applications of advanced signal processing techniques", *CIRP Annals, Manufacturing Technology*, **48**(1), 317–320.

Lancaster, J. (2000), *Engineering catastrophes: Causes and effects of major accidents*, Abington Publishing and CRC Press.

Larbi, N. and Lardies, J., (2000), "Experimental modal analysis of a structure excited by a random force," *Mechanical Systems and Signal Processing*, **14**, pp. 181 – 192.

Lardies, J., (1998), "State-space identification of vibrating systems from multi-output measurements", *Mechanical Systems and Signal Processing,* **12**, 543-558.

Law, S. S., Chan, T. H. T. and Wu, D., (2001), "Efficient numerical model for the damage detection of large scale structure", *Engineering Structures*, **23**, 436-451.

Law, S.S., Li, X.Y., Zhu, X.Q. and Chan, S.L., (2005), "Structural damage detection from wavelet packet sensitivity", *Engineering Structures,* **27**(9), 1339-1348.

Law, S.S. and Li, X.Y. (2006), "Structural Damage Detection from Wavelet Coefficient Sensitivity with Model Errors", *Journal of Engineering Mechanics*, ASCE, **132**(10), pp. 1077-1087.

Law, S.S. and Li, X.Y. (2007), Wavelet-based Sensitivity of Impulse Response Function for Damage Detection, *Journal of Applied Mechanics,* ASME, **74**(2), 375-377.

Law, S.S., Shi, Z.Y. and Zhang, L.M. (1998), "Structural damage detection from incomplete and noisy modal test data", *Journal of Engineering Mechanics*, **124**(11), 1280-1288.

Law, S.S., Waldron, P. and Taylor, C. (1992), "Damage detection of a reinforced concrete bridge deck using the frequency response function", *Proceedings of 10th International Modal Analysis Conference*, 772-778.

Zhu, X.Q. and Law, S.S. (2007), "Damage detection in simply supported concrete bridge structures under moving vehicular loads", *Journal of Vibration and Acoustics, ASME.* **129**(1), 58-65.

Learned, R.E. and Willsky, A.S. (1995), "A wavelet packet approach to transient signal classification", *Applied and Computational Harmonic Analysis*, **2**(3), 265-278.

Lieven, N.A.J. and Ewins, D.J. (1988), "Spatial correlation of mode shapes, the Coordinate Modal Assurance Criterion (COMAC)", *Proceedings of 6th International Modal Analysis Conference*, 690-695.

Lifshiz, J.M. and Rotem, A. (1969), "Determination of reinforcement unbonding of composites by a vibration technique", *Journal of Composite Materials*, **3**, 412-423.

Li, J. and Roberts, J.B. (1999a), "Stochastic structural system identification, Part 1: Mean parameter estimation", *Computational Mechanics*, **24**, 206-210.

Li, J. and Roberts, J.B. (1999b), "Stochastic structural system identification, Part 2: Variance parameter estimation", *Computational Mechanics*, **24**, 211-215.

Lim, K.B. (1992), "Method for optimal actuator and sensor placement for large flexible structures", *Journal of Guidance, Control and Dynamics*, **15**, 49-57.

Lim, T.W. (1994), "Structural damage detection of a planar truss structure using a constrained eigenstructure assignment", *Proceedings of 35thAIAA/ASME/ASCE/AHS/ASC Structures, Structural Dynamics and Materials Conference*, AIAA-94-1715-CP, 336-346.

Lim, T.W. (1995), "Structural damage detection using constrained eigenstructure assignment", *Journal of Guidance, Control and Dynamics*, **18**(3), 411-418.

Lim, T.W. and Kashangaki, T.A.L. (1994), "Structural damage detection of space truss structure using best achievable eigenvectors", *AIAA Journal*, **32**(5), 1049-1057.

Lin, R.M., Lim, M.K. and Du, H. (1995), "Improved inverse eigensensitivity method for structural analytical model updating", *Journal of vibration and Acoustics, ASME,* **117**, 192-198.

Lindner, D.K. and Goff, R. (1993), "Damage detection, location and estimation for space trusses", *SPIE Smart Structures and Intelligent Systems: Smart Structures and Materials*, 1028-1039.

Ling, X.L. and Haldar, A. (2004), "Element level system identification with unknown input with Rayleigh damping", *Journal of Engineering Mechanics*, ASCE, **130**(8), 877-885.

Liu G.R. and Chen S.C., (2001), "Flaw detection in sandwich plates based on time-harmonic response using genetic algorithm", *Computer Methods in Applied Mechanics and Engineering*, Volume 190, Issue 42, Pages 5505-5514.

Liu, P.L. (1995), "Identification and damage detection of trusses using modal data", *Journal of Structural Engineering, ASCE*, **121**, 599-608.

Livingston, R.A., Jin, S. and Marzougui, D. (2001), "Application of nonlinear dynamics analysis to damage detection and health monitoring of highway structures", *Proceedings of SPIE - The International Society for Optical Engineering*, v4337, *Health Monitoring and Management of Civil Infrastructure Systems*, Newport Beach, CA, 402-410.

Loh, C.H. and Wu, T.C. (2000), “System identification of Fei-Tsui arch dam from forced vibration and seismic response data”, *Journal of Earthquake Engineering*, **4**(4), 511-537.

Low, H.Y. and Hao, H. (2001), “Reliability analysis of reinforced concrete slabs under explosive loading”, *Structural Safety* **23**, 157-178.

Lu, Q., Ren, G. and Zhao, Y. (2002), “Multiple damage location with flexibility curvature and relative frequency change for beam structures”, *Journal of Sound and Vibration*, **253**(5), 1101-1114.

Lu, Z.R. and Law, S.S. (2007), “Features of dynamic response sensitivity and its application in damage detection”, *Journal of Sound and Vibration*. **303**(1-2), 305-329.

Lu, Y. and Gao, F. (2005), “A novel time-domain auto-regressive model for structural damage diagnosis”, *Journal of Sound and Vibration*, **283**(3-5), 1031-1049.

Luz, E., and Wallaschek, J., (1992), “Experimental modal analysis using ambient vibration”, *The International Journal of Analytical and Experimental Modal Analysis*, **7**, pp. 29 – 39.

Majumder, L. and Manohar, C.S. (2003), “A time-domain approach for damage detection in beam structures using vibration data with moving oscillator as an excitation source”, *Journal of Sound and Vibration*, **268**, 699-716.

Majumder, L. and Manohar, C.S. (2004), "Nonlinear reduced models for beam damage detection using data on moving oscillator–beam interactions", *Computers & Structures*, **82**(2-3), 301-314.

Mallat, S. (1998), *A wavelet tour of signal processing*, Academic Press, New York.

Mares, C., Friswell, M. I. and Mottershead, J. E. (2002), "Model updating using robust estimation", *Mechanical Systems and Signal Processing*, **16**, 169-183.

Mario, Paz, (1997), *Structural Dynamics Theory and Computation*, International Thomson Publishing.

Mayes, R.L. (1992), "Error localization using mode shapes: An application to a two link robot arm", *Proceedings of 10th International Modal Analysis Conference*, 886-891.

Mayes, R.L. (1995), "An experimental algorithm for detecting damage applied to the I-40 bridge over the Rio Grande", *Proceedings 13th International Modal Analysis Conference*, 219-225.

McGowan, P.E., Smith, S.W. and Javeed, M. (1990), "Experiments for locating damage members in a truss structure", *Proceedings of 2nd USAF/NASA Workshop on System Identification and Health Monitoring of Precision Space Structures*, 571-615.

McLamore V. R., Hart G. C. and Stubbs I. R. (1971), "Ambient vibration of two suspension bridges", *Proceedings of the American Society of Civil Engineers, Journal of the Structural Division*, **97**, 2567-2582.

Meirovitch, L. (1997), *Principles and Techniques of Vibrations*, Prentice Hall.

Meyer, Y. (1992), *Wavelets and operators*, Cambridge University Press, Cambridge, UK.

Messina, A., Jones, I.A. and Williams, E.J. (1996), "Damage detection and localization using natural frequency changes", *Proceedings of conference on Identification in Engineering Systems*, Swansea, U. K., 67-76.

Messina, A., Williams, E.J. and Contursi, T. (1998), "Structural damage detection by a sensitivity and statistical-based method", *Journal of Sound and Vibration*, **216**(5), 791-808.

Minas, C. and Inman, D.J. (1990), "Matching finite element models to modal data", *Journal of Vibration and Acoustics, ASME,* **112**(1), 84-92.

Morassi, A. and Rovere, N. (1997), "Localizing a notch in a steel frame from frequency measurements", *Journal of Engineering Mechanics —ASCE*, **123**(5), 422-432.

Mottershead, J.E. and Foster, C.D. (1991), "On the treatment of ill-conditioning in spatial parameter estimation from measured vibration data", *Mechanical Systems and Signal Processing*, **5**, 139-154.

Mottershead, J.E. and Shao, W., (1991), "On the tuning of analytical models by using experimental vibration data", *Proceedings of 4th International Conference on Recent Advances in Structural Dynamics*, Southampton, England, 432-443.

Mufti, A. and Ansari, F. (eds) (2004), *Proceedings of the Second International Workshop on Structural Health Monitoring of Innovative Civil Engineering Structures*, Winnipeg, Manitoba.

Natke, H.G. (1992a), "On regularisation methods applied to the error localization of mathematical models", *Proceedings of 9th International Modal Analysis Conference*, 70-73.

Natke, H.G. (1992b), "Regularization methods within system identification", *IUTAM Symposium on Inverse Problems in Engineering Mechanics*, 3-20.

Nelson, R.B. (1976), "Simplified calculations of eigenvector derivatives", *AIAA Journal*, **14**, 1201-1205.

Newland, D.E., (1993), *An introduction to Random Vibrations, Spectral & Wavelet Analysis*, 3rd Edition, Prentice Hall.

Ni, Y.Q., Zhou, X.T. and Ko, J.M., (2006), "Experimental investigation of seismic damage identification using PCA-compressed frequency response functions and neural networks", *Journal of Sound and Vibration*, **290**(1-2), 242-263.

Nwosu, D.I., Swamidas, A.S.J., Guigne, J.Y. and Olowokere, D.O. (1995), "Studies on influence of cracks on the dynamic response of tubular T-joints for nondestructive evaluation", *Proceedings of 13th International Modal Analysis Conference*, 1122-1128.

Ojalvo, I.U. and Ting, T. (1990), "Interpretation and improved solution approach for ill-conditioned linear equations", *AIAA Journal*, **28**, 1976-1979.

Pandey A.K., Biswas M. and Samman M.M. (1991), "Damage detection from changes in curvature mode shapes", *Journal of Sound and Vibration*, **145**(2), 321-332.

Pandey A.K. and Biswas M. (1994), “Damage Detection in Structures Using Changes in Flexibility”, *Journal of Sound and Vibration*, **169**(1), 3-17.

Papadopoulas, L. and Garcia, E. (1998), “Structural damage identification: a probabilistic approach”, *AIAA J.*, **36**(11), 2137–2145.

Park N.G. and Park Y.S., (2003), “Damage detection using spatially incomplete frequency response functions”, *Mechanical Systems and Signal Processing*, **17**(3), 519-532.

Parloo E., Guillaume P. and Van Overmeire M., (2003), “Damage assessment using mode shape sensitivities”, *Mechanical Systems and Signal Processing*, **17**(3), 499-518.

Pascual R., Schälchli R. and Razeto M., (2005), “Improvement of damage-assessment results using high-spatial density measurements”, *Mechanical Systems and Signal Processing*, **19**(1), 123-138.

Patsias, S. and Staszewski, W.J., (2002), “Damage detection using optical measurements and wavelets”, *Structural Health Monitoring*, **1**(1), 5-22.

Peters, B., (2000), *System Identification and Damage Detection in civil engineering*, PhD thesis, Department of Civil Engineering, K. U. Leuven.

Penny, J.E.T., Wilson, D. and Friswell, M.I. (1993), “Damage location in structures using vibration data”, *Proceedings of the 11th International Modal Analysis Conference* **1**, 861-867.

Phillips, L.D. (1962), "A technique for the numerical solution of certain integral equations of the first kind", *Journal of the Association of Computational Machining*, **9**, 84-97.

Qi, G., Barhorst, A., Hashemi, J. and Kamala, G. (1997), "Discrete wavelet decomposition of acoustic emission signals from carbon-fiber-reinforced composites", *Composites Science and Technology*, **57**(4), 389–403.

Raghavendrachar, M. and Aktan, A.E. (1992), "Flexibility by multireference impact testing for bridge diagnostics", *Journal of Structural Engineering, ASCE*, **118**, 2186-2203.

Randall, R.B., (1987), *Frequency Analysis*, 3rd Edition, Brüel and Kjær.

Ratcliffe C.P. (1997), "Damage detection using a modified laplacian operator on mode shape data", *Journal of Sound and Vibration*, **204**(3), 505-517.

Reda Taha, M. M., Noureldin, A., Lucero, J.L. and Baca, T.J., (2006), "Wavelet Transform for Structural Health Monitoring: A Compendium of Uses and Features", *Structural Health Monitoring*, **5**(3), 267-295.

Ren, W. X. (2005), "A singular value decomposition based on truncation algorithm in solving the structural damage equations", *Acta Mechanica Solida Sinica*, **18**, 181-188.

Ricles, J.M. and Kosmatka, J.B., (1992), "Damage Detection in Elastic Structures Using Vibratory Residual Forces and Weighted Sensitivity", *AIAA Journal*, **30**(9), 2310-2316.

Robert, C.P. and Casella, G. (1999), *Monte Carlo statistical methods.* New York : Springer.

Robertson, A.N., Park, K.C., Alvin, K.F. (1998a), "Extraction of Impulse Response Data via Wavelet Transform for Structural System Identification", *Journal of Vibration and Acoustics*, January 1998, Vol.**120**, 252-260.

Robertson, A.N., Park, K.C., Alvin, K.F. (1998b), "Identification of Structural Dynamics Models Using Wavelet-Generated Impulse Response Data", *Journal of Vibration and Acoustics*, January 1998, Vol.**120**, 261-266.

Rodden, W.P. (1967), "A method for deriving structural influence coefficients from ground vibration tests", *AIAA Journal*, **5**, 991-1000.

Rothwell, E. and Drachman, B. (1989), "A unified approach to solving ill conditioned matrix problems", *International Journal for Numerical Methods in Engineering*, **28**, 609-620.

Rus, G., Castro, E., Gallego, A., Pe′ rez-Aparicio, J.L. and Garcı′ a-Herna′ ndez, T. (2004), "Detection and location of damage in rods using wavelets of vibration simulated by the NSM and FEM." In: Boller, C. and Staszewski, W.J. (eds), *Proceedings of the 2nd European Workshop on Structural Health Monitoring, Munich*, Germany, pp. 465–473.

Rytter, A. (1993), "Vibration based inspection of civil engineering structures, Doctoral Dissertation", *Department of Building Technology and Structural Engineer*ing, University of Aalborg.

Salawu, O.S. (1997a), "Detection of structural damage through changes in frequency: A review", *Engineering Structures*, **19**(9), 718-723.

Salawu, O.S. (1997b), "An integrity index method for structural assessment of engineering structures using modal testing", *Insight: The journal of the British Institute of Non-Destructive Testing*, **39**(1).

Samman, M.M., Biswas, M. and Pandey, A.K., (1991), "Employing pattern recognition for detecting cracks in a bridge model", *Modal Analysis: The International Journal of Analytical and Experimental Modal Analysis*, **6**(1), 35-44.

Sanayei, M. and Saletnik, M.J. (1996a), "Parameter estimation of structures from static strain measurements, Part I: Formulation", *Journal of Structural Engineering, ASCE*, **122**(5), 555-562.

Sanayei, M. and Saletnik, M.J. (1996b), "Parameter estimation of structures from static strain measurements, Part II: Error sensitivity analysis", *Journal of Structural Engineering, ASCE*, **122**(5), 563-572.

Schultz, M.J., Pai, P.F. and Abdelnaser, A.S. (1996), "Frequency response function assignment technique for structural damage identification", *Proceedings of 14thInternational Modal Analysis Conference*, 105-111.

Seibold, S. and Weinert, K. (1996), "A time domain method for the localization of cracks in rotors", *Journal of Sound and Vibration*, **195**(1), 57-73.

Shen F., Zheng M., Shi D.F. and Xu F., (2003), "Using the Cross-correlation Technique to Extract Modal Parameters on Response-only Data", *Journal of Sound and Vibration*, **259**(5), pp. 1163-1179.

Shi, T.H., Jones, N.P. and Ellis, J.H. (2000), "Simultaneous estimation of system and input parameters from output measurements", *Journal of Engineering Mechanics*, ASCE, **126**(7), 746-753.

Shi, Z.Y., Law, S.S. and Zhang, L.M. (1998), "Structural damage localization from modal strain energy change", *Journal of Sound and Vibration*, **218**(5), 825-844.

Shi, Z.Y., Law, S.S. and Zhang, L.M. (2000a), "Damage location by directly using incomplete mode shapes", *Journal of Engineering Mechanics*, *ASCE*, **126**(6), 656-660.

Shi, Z.Y., Law, S.S. and Zhang, L.M. (2000b), "Structural damage detection from modal strain energy change", *Journal of Engineering Mechanics*, **126**(12), 1216-1223.

Shi, Z.Y., Law, S.S. and Zhang, L.M. (2002), "Improved damage quantification from elemental modal strain energy change", *Journal of Engineering Mechanics*, **128**(5), 521-529.

Skjaeraek, P.S., Nielsen, S.R.K., and Cakmak, A.S. (1996), "Identification of damage in reinforced concrete structures from earthquake records: Optimal location of sensors", *Soil Dynamics and Earthquake Engineering*, **15**(6), 347-358.

Smith, S.W. and Beattie, C.A. (1991), "Model correlation and damage location for large space truss structures: Secant method development and evaluation", *NASA Report NASA-CR-188102*.

Smith, S.W. (1992), "Iterative use of direct matrix updates: connectivity and convergence", *Proceedings of 33rd AIAA Structures, Structural Dynamics and Materials Conference*, 1797-1806.

Smyth, A. W., Masri, S. F., Caughey, T. K. and Hunter, N. F. (2000), "Surveillance of mechanical systems on the basis of vibration signature analysis", *Journal of Applied Mechanics, ASME*, **67**, 540-551.

Sohn, H. and Farrar, C.R. (2000), "Statistical process control and projection techniques for damage detection", *European COST F3 Conference on System Identification and Structural Health Monitoring*, Madrid, Spain, 105-114.

Sohn, H., Park, G., Wait, J.R. and Limback, N.P. (2003), "Wavelet based analysis for detecting delamination in composite plates", In: Chang, F.-K. (ed.), *Proceedings of 4th Int. Workshop on Structural Health Monitoring*, Stanford, CA, USA, pp. 567–574.

Sophia, H. and Garrett, D.J. (1995), "Identification of stiffness reduction using natural frequencies", *Journal of Engineering Mechanics, ASCE*, **121**, 1106-1113.

Staszewski, W.J. and Tomlinson, G.R. (1997), "Application of the wavelet transform to fault detection in spur gear", *Mechanics System and Signal Processing*, **8**(3), 289-307.

Stubbs, N. and Osegueda, R. (1990), "Global damage detection in solids: Experimental verification", *Modal analysis: The International Journal of Analytical and Experimental Modal Analysis*, **5**(2), 81-97.

Stubbs, N. and Kim, J.T. (1996), "Damage localization in structures without baseline modal parameters", *AIAA journal*, **34**(8), 1644-1649.

Stubbs, N., Kim, J.T. and Topole, K. (1992), "An efficient and robust algorithm for damage localization in offshore platforms", *Proceedings of the ASCE 10th Structures Congress*, 543-546.

Sun, Z. and Chang, C.C. (2002a), "Structural damage assessment based on wavelet packet transform", *Journal of Structural Engineering, ASCE*, **130**(7), 1055-1062.

Sun, Z. and Chang, C.C., (2002b), "Wavelet Packet Signature: A Novel Structure Condition Index", China-Japan Workshop on Vibration Control and Health Monitoring of Structures and Third Chinese *Symposium on Structural Vibration Control*, Shanghai, China, Dec.

Tavares, R., Kosmatka, J.B., Ricles, J.M. and Wicks, A., (April 1993), "Using Experimental Modal Data to Detect Damage in a Space Truss", Proceedings of the AIAA/ASME/ASCE/AHS/ASC 34th Structures, *Structural Dynamics and Materials Conference*, AIAA, Washington, DC, pp. 1556-1564.

Thomson, A.S. (1949), "Vibration of slender bars with discontinuities in stiffness", *Journal of Applied Mechanics*, **17**, 203-207.

Thyagarajan, S. K., Schulz, M. J., Pai, P. F. and Chung, J. (1998), "Detecting Structural Damage Using Frequency Response Functions", *Journal of Sound and Vibration*, **210**(1), 162-170.

Tikhonov, A.M., (1963), "On the solution of ill-posed problems and the method of regularization", *Soviet Mathematics*, **4**, 1035-1038.

Tikhonov, A.N. and Arsenin, V.Y. (1977), *Solutions of ill-posed problems*, John Wiley & Sons, New York.

Ting, T. (1992), "Accelerated subspace iteration for eigenvector derivatives", *AIAA Journal*, **30**(8), 2114-2118.

Toksoy, T. and Aktan, A.E. (1995), "Bridge-condition assessment by modal flexibility", *Workshop on Instrumentation and Vibration Analysis of Highway Bridges*, University of Cincinati, Ohio.

Topole, K.G. and Stubbs, N. (1995), "Nondestructive damage evaluation of structure from limited modal parameters", *Earthquake Engineering and Structural Dynamics*, **24**(11), 1427-1436.

Topole, K.G. and Tzvetkova, G. (1996), "Damage detection of highly nonlinear structures from response measurements", *Proceedings of SPIE (V2719): Smart Structures and Materials 1996: Smart Systems for Bridges, Structures, and Highways*, San Diego, CA, USA, 170-179.

Torkamani, M. A. M., and Ahmadi, A. K. (1988), "Stiffness identification of frames using simulated ground excitations", *Journal of Engineering Mechanics*, ASCE, **114**, 753-776.

Trujillo, D.M. and Busby, H.R. (1989), "Optimal regularization of the inverse heat-conduction problem", *AIAA J. Thermophys. Heat Transfer* 3(4) 423427.

Vandiver, J.K. (1975), "Detection of structural failure on fixed platforms by measurement of dynamic response", *Proceedings of 7th Annual Offshore Technology Conference*, 243-252.

Vandiver, J.K. (1977), "Detection of structural failure on fixed platforms by measurement of dynamic response", *Journal of Petroleum Technology*, **3**, 305-310.

Varah, J.M. (1983), "Pitfalls in solution of linear ill-posed problems", *SIAM Journal of Scientific and Statistical Computation*, **4**,164-176.

Wang, J.H. and Liou, C.M. (1991), "Experimental identification of mechanical joint parameters", *Journal of Vibration and Acoustics, ASME*, **113**, 28-36.

Wang, Q. and Deng, X. (1999), "Damage detection with spatial wavelets", *International Journal of Solids and Structures*, **36**(23), 3443-3468.

Wang, W. and Zhang, A. (1987), "Sensitivity analysis in fault vibration diagnosis of structures", *Proceedings of the 5th International Modal Analysis Conference*, 496-501.

Wang W.J. and McFadden P.D. (1995), "Application of orthogonal wavelets to early gear damage detection", *Mechanical Systems and Signal Processing*, **9**(5), 497-507.

West, W.M. (1984), “Illustration of the use of modal assurance criterion to detect structural changes in an orbiter test specimen”, *Proceedings of the Air Force Conference on Aircraft Structural Integrity*, 1-6.

Williams, E.J., Contursi, T. and Messina, A. (1996), “Damage detection and localization using natural frequencies sensitivity”, *Proceedings of Conference on Identification in Engineering Systems*, Swansea, U. K., 368-376.

Wojnarowski, M.E., Stiansen, S.G., and Reddy, N.E. (1977), “Structural integrity evaluation of a fixed platform using vibration criteria”, *Proceedings of 9thAnnual Offshore Technical Conference*, 247-256.

Wong, L.A. and Chen, J.C. (2001), “Nonlinear and chaotic behavior of structural system investigated by wavelet transform techniques”, *International Journal of Non-linear Mechanics*, **36**, 221-235.

Worden, K., Farrar, C.R., Manson, G. and Park, G. (2005), “Fundamental axioms of structural health monitoring”, *Structural Health Monitoring 2005: Advancements and Challenges for Implementation*, Chang, F. K. (editor), DEStech Publications, Lancaster, Pennsylvania, 26-41.

Wu, D., and Law, S.S., (2004a), “Anisotropic damage model for an inclined crack in thick plate and sensitivity study for its detection”, *International Journal of Solids and Structures*, **41**(16-17), 4321-4336.

Wu, D. and Law, S.S. (2004b), “Damage localization in plate structures from uniform load surface curvature”, *Journal of Sound and Vibration*, **276**(1-2), 227-244.

Wu, Y. and Du, R. (1996), "Feature extraction and assessment using wavelet packets for monitoring of machining processes", *Mechanics Systems and Signal Processing*, **10**(1), 29-53.

Wu, Z.S., and Abe, Masat., (eds) (2003), *Proceedings of the First International Conference on Structural Health Monitoring and Intelligent Infrastructure,* Tokyo, Japan.

Xia, Y. and Hao, H. (2000), "Measurement selection for vibration-based structural damage identification", *Journal of Sound and Vibration,* **236**(1), 89-104.

Xia, Y., Hao, H., Brownjohn, J.M.W. and Xia, P.Q. (2002), "Damage identification of structures with uncertain frequency and mode shape data", *Earthquake Engineering and Structural Dynamics*, **31**, 1053-1066.

Xia, Y. and Hao, H. (2003), "Statistical damage identification of structures with frequency changes", *Journal of Sound and Vibration,* **263(**4), 853-870.

Xu, B., Wu, Z.S., Chen G.D. and Yokoyama K., (2004), "Direct identification of structural parameters from dynamic responses with neural networks", *Engineering Applications of Artificial Intelligence,* **17**(8), 931-943.

Yagola, A.G., Leonov, A.S. and Titarenko, V.N., (2002), "Data errors and an error estimation for ill-posed problems", *Inverse Problems in Engineering*, **10**(2), 117-129.

Yan Y.J., Hao H.N. and Yam L.H. (2004), "Vibration-based construction and extraction of structural damage feature index", *International Journal of Solids and Structures*, **41**(24-25), 6661-6676.

Yan, Y.J. and Yam, L.H. (2004), "Detection of delamination in composite plates using energy spectrum of structural dynamic responses decomposed by wavelet analysis", *Computers and Structures*, **82**, 347–358.

Yeo, I., Shin, S., Lee, H.S. and Chang, S.P. (2000), "Statistical damage assessment of framed structures from static responses", *Journal of Engineering Mechanics, ASCE*, **126**(4), 414-421.

Yuen, K.V. and Katafygiotis, L.S. (2005), "Model updating using noisy response measurements without knowledge of the input spectrum", *Earthquake Engineering and Structural Dynamics*, **34**, 167-187.

Yuen, M.M.F. (1985), "A numerical study of the eigen-parameters of a damaged cantilever", *Journal of Sound and Vibration*, **103**, 301-310.

Zhang, Q., Lallement, G., Fillod, R. and Piranda, J. (1987), "A Complete Procedure for the Adjustment of a Mathematical Model from the Identified Complex Modes", *Proceedings of the 5th International Modal Analysis Conference*, London, U.K., 1183-1190.

Zhang, Z. and Aktan, A.E. (1995), "The damage indices for constructed facilities", *Proceedings of 13th International Modal Analysis Conference*, 1520-1529.

Zhang, Z. and Aktan, A.E. (1998), “Application of modal flexibility and its derivatives in structural identification”, *Research in Nondestructive Evaluation*, **10**(1), 43-61.

Zhao, J. and Dewolf, J.T. (1999), “Sensitivity study for vibrational parameters used in damage detection”, *Journal of Structural Engineering, ASCE*, **125**(4), 410-416.

Zhou, J., Feng, X. and Fan, Y. F. (2003), “A probabilistic method for structural damage identification using uncertain data”, *Structural Health Monitoring and Intelligent Infrastructure*, Wu, Z. S., and Abe, M. (editors), A.A. Balkma, Lisse, 487-492,

Ziaei-Rad, S. (1997), *Methods for updating numerical models in structural dynamics*, Ph.D. Thesis, Imperial College, University of London.

Ziaei-Rad, S. and Imregun, M. (1996), “On the accuracy required of experimental data for finite element model updating”, *Journal of Sound and Vibration*, **196**(3), 323-336.

Ziaei-Rad, S. and Imregun, M. (1999), “On the use of regularization techniques for finite element model updating”, *Inverse Problems in Engineering*, **7**, 471-503.

Zimmerman, D.C. (2006), “Statistical confidence using minimum rank perturbation theory”, *Mechanical Systems and Signal Processing*, **20**, 1155-1172.

Zimmerman, D.C. and Smith, S.W. (1992), “Model refinement and damage location for intelligent structures”, *Intelligent Structural Systems*, Kluwer Academic Publishers, 403-452.

Zimmerman, D.C. and Kaouk, M. (1994), “Structural damage detection using a minimum rank update theory”, *Journal of Vibration and Acoustics, ASME*, **116**, 222-230.

Zimmerman, D.C. and Kaouk, M. (1992), "Eigenstructure assignment approach for structural damage detection", *AIAA Journal*, **30**(7), 1848-1855.

Zimmerman, D.C. and Widengren, M. (1990), "Correcting finite element models using a symmetric eigenstructure assignment technique", *AIAA Journal*, **28**(9), 1670-1676.